SHEAR CAPACITY OF DRY-CAST EXTRUDED PRECAST/PRESTRESSED HOLLOW-CORE SLABS

by

KARL AXEL TRUDERUNG, P.Eng.

A Thesis submitted to the Faculty of Graduate Studies of

The University of Manitoba

in partial fulfillment of the requirements of the degree of

Master of Science

Department of Civil Engineering

University of Manitoba

Winnipeg, Manitoba, Canada

Copyright © 2011 by Karl A. Truderung, P.Eng.

ABSTRACT

Based on previous testing and analysis, it is believed that North American concrete design codes yield conservative shear designs for precast/prestressed hollow-core slabs in the 203 to 305 mm depth range. The objective of this research program is to calibrate the Canadian code shear equations to precast/prestressed hollow-core slabs, through testing a series of full-scale slabs to failure in shear. A total of twelve hollow-core slabs from one slab producer, using two types of extruders were tested in shear. Test variables include the bearing length and the prestressing level. Results are presented in terms of experimental to predicted capacity using the Canadian and American concrete design codes, the failure mode, crack profiles, and the critical section location for shear. It was concluded that the Canadian code shear equations are inappropriate for use with hollow-core slabs with low prestressing levels in the 203 to 305 mm depth range.

Acknowledgements

The author would like to express his sincere gratitude to his supervisor, Professor Ehab El-Salakawy, Ph.D., P.Eng., Canada Research Chair in Advanced Composite Materials and Monitoring of Civil Infrastructures in the Department of Civil Engineering at the University of Manitoba, for his guidance and direction throughout the development and implementation of this research program.

The author is very grateful for funding and technical support provided by:

- The Canadian Precast/Prestressed Concrete Institute (CPCI) and the CPCI Technical Committee.
- The University of Manitoba Grants Research Program (URGP).
- The Natural Science and Engineering Research Council of Canada (NSERC), through Canada Research Chairs program.
- The equipment provided by Canada Foundation for Innovation (CFI) grant.
- The hollow-core slab producers and the hollow-core extruder suppliers who contributed towards this research project.
- The technical staff of the McQuade Heavy Structural Laboratory in the Department of Civil Engineering at the University of Manitoba.
- Dave Marshall at Black Mint Software.
- Dr. Matti Pajari – VTT Technical Research Centre of Finland.

In addition, the author would like to sincerely thank Dr. Amr El-Ragaby for his help and guidance with the laboratory testing of this research project.

To my parents, I would like to express my deepest gratitude for inspiring me to live out my dream to be a Structural Engineer. Finally, to Naomi, Abigail, Victoria, and Nathan, I am especially grateful for your patience, support and encouragement during the time of my studies; God has truly blessed me through each of you.

Table of Contents

List of Tables

List of Figures

List of Notations

a shear span, *mm*

a_g specified nominal maximum size of coarse aggregate, *mm*

A area of the whole cross-section, mm^2

A_c area of the concrete cross-section, mm^2

A_{cp} area above critical point, mm^2

A_{ct} area of concrete on flexural tension side of member, mm^2

$A_c(y)$ area above height y, mm^2

A_E effective shear area, $in.^2$

A_i fictive cross-section surface, mm^2

A_p area of prestressing tendons, mm^2

A_s area of longitudinal reinforcement on the flexural tension side of the member, mm^2

$A_{s\ell}$ area of tensile reinforcement, mm^2

$b(z_{cp})$ total web width of hollow-core slab, *mm*

b_w minimum effective web width, smallest width of the cross-section in the tensile area, width of the cross-section at the centroidal axis, total web width of all webs at the smallest section, *mm, in.*

$b_w(y)$ web width at height y, *mm*

c distance from a point to the neutral axis, *mm*

$Cp_t(y)$ factor taking into account the position of the considered tendon layer

d distance from extreme compression fibre to centroid of longitudinal tension reinforcement, *mm, in.*

d_b strand diameter, *mm, in.*

d_p distance from extreme compression fibre to centroid of prestressing steel, *in.*

dN_p/dx gradient of effective prestress force in strands, *N/mm*

d_v effective shear depth, *mm*

e vertical distance between centroid of prestressed strands and centroid of whole cross-section, *mm, in.*

E_p modulus of elasticity of prestressing tendons, *MPa*

E_s modulus of elasticity of non-prestressed reinforcement, *MPa*

f_c compressive strength of concrete, *MPa*

f_c': specified compressive strength of concrete, *MPa, psi*

f_{cd} design value of concrete compressive strength, *MPa*

f_{ck} characteristic compressive cylinder strength of concrete at 28 days, *MPa*

f_{cp} average compressive stress in concrete due to effective prestress force only (after allowance for all prestress losses) , *MPa*

f_{ct} concrete tensile strength, characteristic tensile strength of concrete, *MPa*

f_{ctd} design value of concrete tensile strength, *MPa*

f_{ctk} characteristic axial tensile strength of concrete, *MPa*

f_d stress due to unfactored dead load at the extreme section fibre, where tensile stress is caused by externally applied loads, *psi*

f_{pc} compressive stress in concrete (after allowance for all prestress losses) at the centroid of the cross-section resisting externally applied loads, or at the junction of the web and flange, when the centroid lies within the flange, *psi*

f_{pe} compressive stress in concrete due to effective prestress forces only (after allowance for all prestress losses) at the extreme section fibre, where tensile stress is caused by externally applied loads, *MPa*, *psi*

f_{po} stress in prestressing tendons when strain in the surrounding concrete is zero, *MPa*

f_{px} stress at the member centroid due to prestress at section *x*, *psi*

f_{se} effective stress in the prestressing tendons after allowance for all prestressing losses, *psi*

f_t principal tension at the member centroid, *psi*

h overall thickness or height of member, *mm, in.*

I moment of inertia of section about centroidal axis, second moment of area of cross-section, mm^4, $in.^4$

I_y moment of inertia of section, mm^4

L_b span of beam, *mm*

ℓ_d development length of prestressing strands, *mm, in.*

ℓ_t transfer length of prestressing strands, *mm, in.*

ℓ_x distance of section considered from the starting point of the transmission length, distance of the considered point on the line of failure from the starting point of the transmission length (=*x*) , *mm*

ℓ_{pt2} upper bound value of the transmission length of the prestressing element, *mm*

M ultimate moment, *in.-lb*

M_{cr} cracking moment, *kN-m, in.-lb*

M_{cre} moment causing flexural cracking at section due to externally applied loads, *in.-lb*

M_{Ed} bending moment due to vertical load, *N-mm*

M_f moment due to factored loads, *kN-m*

M_{max} maximum factored moment at section due to externally applied loads, *in.-lb*

M_o decompression moment, *N-mm*

M_x flexural moment at distance *x* from bearing, *N-mm*

N_{Ed} axial force in the cross-section due to the loading or prestressing, *N*

N_f factored axial load normal to the cross-section occurring simultaneously with V_f, including effects of tension due to creep and shrinkage, *kN*

N_p effective prestress force in strands, *N*

n number of tendon layers

$P_t(\ell_x)$ prestressing force in the considered tendon layer at distance l_x, *N*

S first moment of area above and about the centroidal axis, mm^3

S_{cp} first area moment above critical point, mm^3

$S_c(y)$ first moment of area above height *y* and about the centroidal axis, mm^3

s_z crack spacing parameter dependent on crack control characteristics of longitudinal reinforcement, *mm*

s_{ze} equivalent value of s_z that allows for influence of aggregate size, *mm*

T_f factored tensile force in the reinforcement, *kN*

T_r factored tensile resistance of the reinforcement, *kN*

V_c shear resistance attributed to the concrete, nominal shear strength provided by the concrete, *kN, lb*

V_{ccd} design value of the shear component of the force in the compression area, in the case of an inclined compression chord, *N*

V_{ci} nominal shear strength provided by concrete when diagonal cracking results from combined shear and moment, *lb*

V_{cw} web-shear resistance of the concrete, nominal shear strength provided by concrete when diagonal cracking results from high principal tensile stress in web, *kN, lb*

V_d shear force at section due to unfactored dead load, *lb*

V_{Ed} design value of the shear force, *N*

V_f factored shear force, *kN*

V_i factored shear force at a section due to externally applied loads occurring simultaneously with M_{max}, *lb*

V_n nominal shear strength, *lb*

V_p component in the direction of the applied shear of the effective prestressing force, vertical component of effective prestress force at section, *kN, lb*

V_r factored shear resistance, *kN*

V_{Rd} shear resistance of a member without shear reinforcement, *N*

$V_{Rd,c}$ design value for the shear resistance of a member without shear reinforcement, *N*

$V_{Rd,s}$ design value of the shear force that can be sustained by the yielding shear reinforcement, *N*

$V_{Rd,12}$ design shear strength in regions un-cracked in flexure, *N*

V_s shear resistance provided by shear reinforcement, nominal shear strength provided by shear reinforcement *kN, lb*

V_{td} design value of the shear component of the force in the tensile reinforcement, in the case of an inclined tensile chord, *N*

V_{test} experimental value of shear force at failure, *kN*

V_u factored shear force, *lb*

$V_{(x)}$ theoretical shear force at distance *x* from slab end due to test load and slab self weight, *kN*

v_{cw} nominal shear stress at the centroid of a member, *psi*

v_{min} minimum value of shear stress resistance for concrete, *MPa*

x_{cp} horizontal distance between critical point and centre of support, *mm*

Y_c height of the centroidal axis, *mm*

Yp_t height of the position of the considered tendon layer, *mm*

y height of the critical point on the line of failure, *mm*

y_b centroidal distance from the bottom face of the slab, *mm*

y_t distance from centroidal axis of gross section, neglecting reinforcement, to tension face, *in.*

z_{cp} z-coordinate of critical point, *mm*

α fraction of the prestressing at the section considered, reduction factor due to parabolic distribution of prestressing force transfer

β factor accounting for shear resistance of cracked concrete, angle (*degrees*), ratio or coefficient, angle between bottom surface of hollow-core slab and line from centre of support to critical point, *degrees*

γ_c partial factor for concrete

ε_x longitudinal strain at mid-depth of the member due to factored loads

θ angle of inclination of diagonal compressive stresses to the longitudinal axis of the member, *degrees*

λ factor to account for low-density concrete

ν strength reduction factor for concrete cracked in shear

ρ_o reinforcement percentage

σ_{cp} compressive stress in the concrete from axial load or prestressing, *MPa*

$\sigma_{cp}(y)$ concrete compressive stress at height *y* and distance l_x, *MPa*

σ_N average concrete compressive stress in the cross-section, average stress due to fully transferred prestressing force in the ultimate state, *MPa*

σ_p stress in the prestressing strands, *MPa*

τ shear stress, *MPa*

$\tau_{cp}(y)$ concrete shear stress due to transmission of prestress at height *y* and distance l_x, *MPa*

ϕ strength reduction factor

ϕ_c resistance factor for concrete

ϕ_p resistance factor for prestressing tendons

ϕ_s resistance factor for non-prestressed reinforcing bars

CHAPTER 1 INTRODUCTION

1.1 BACKGROUND

A common structural engineering challenge involves the design of a floor or roof system, to maximize the span, minimize the overall floor or roof thickness, and restrict the deflections under service loads to acceptable limits. Precast, prestressed hollow-core slabs offer the designer an economical solution to meet these challenges.

Precast hollow-core slabs are structurally efficient, since they combine the beneficial effects of prestressing together with a structurally efficient cross-section. For a given slab thickness, prestressing alone would extend the maximum serviceable span of a solid concrete slab section beyond the limits of conventionally reinforced concrete slabs. By placing continuous voids into the slab cross-section or removing the structurally-ineffective concrete, the weight of the slabs is reduced in comparison to a solid slab, which results in a further increase in span lengths compared to a solid prestressed slab.

An additional benefit of precast hollow-core slabs is that a large area of floor or roof can be produced in advance at the precast supplier's facility, allowing the site contractor more lead time to prepare the supporting structure and shorten the overall project schedule. Precast manufacturers also operate on a one-day production cycle, by accelerating the curing process to provide a one-day turn-around time on product manufacturing. The accelerated curing process, which uses steam-applied heat to rapidly increase the concrete strength gain after casting, typically results in concrete strengths at 28-days on the order of 35-60 MPa, which further enhances the benefits the hollow-core slab system noted above.

It is estimated by the Canadian Precast Concrete Institute (CPCI) that each year the approximate total area of hollow-core slabs that is produced and erected is on the order of 1.67 million m^2 (approx. 18 million square feet) in Canada, and 14.9 million m^2 (approx. 160 million square feet) in the United States (CPCI 2011).

In North America, hollow-core slabs are most often used for floor areas supporting uniformly distributed loads such as office, school and residential occupancies, or snow drift loads on roofs – however in some cases larger uniform or concentrated loads are encountered, typically in industrial, warehouse and parking structure applications, where heavy storage or equipment loads may dictate the design. In these cases, hollow-core slabs can also be used by taking advantage of prestressing together with high-strength concrete and an efficient cross-section to support these larger loads in a relatively shallow floor depth. In some cases, the designer may also consider adding a site-cast structural concrete topping onto the surface of the hollow-core slabs, which becomes composite with the hollow-core slabs after curing, thereby extending the spans even further than in the un-topped condition.

Hollow-core slabs in North America are typically produced in one of two ways; either as part of a wet-cast system (where the slabs are slip-formed, using normal-slump concrete) or as part of a dry-cast system (where the slabs are extruded, using very low-slump concrete). In either case, the maximum economy in the use of hollow-core slabs is fully realized when the slabs can be cast, cured, saw-cut and sent to the job-site without any further modification, as shown in Figure 1.1.

Figure 1.1: Precast Hollow-core Slabs (Saw-cut and Ready for Shipment to Project Site)

However, in some cases the designer encounters situations where the nominal shear capacity of the slabs is exceeded; typically when large concentrated point or line loads are present. In these cases, the voids of the slabs are typically opened up immediately after extrusion and filled with additional wet-cast concrete, thereby bringing the overall shear capacity of the slabs to the required strength level. Unfortunately, any additional work required to modify hollow-core slabs from the finished product (as-cast) adds cost to the system. Therefore, an accurate assessment of the shear capacity of hollow-core slabs is necessary in order to take full advantage of the economy of the hollow-core system.

1.2 PROBLEM DEFINITION

For the design of a prestressed concrete member in Canada, the previous edition of the Canadian code, CSA A23.3-94 (CSA 1994) followed the methodology of the American code (ACI 1989), by considering two types of shear failures. The first type, considered to be a "flexure-shear" failure mode, originates when a flexural crack begins to propagate diagonally towards the

compression flange of the member. The second type of shear failure occurs when the elastic diagonal principal tensile stress in the web of the member exceeds the tensile capacity of the concrete. Once the diagonal tensile capacity of the webs is reached, an inclined crack typically forms at or near the elastic neutral axis, which then propagates rapidly towards the compression and tension flanges of the member – referred to as a "web-shear" crack.

The expression for evaluating the flexure-shear capacity of a prestressed member in the previous edition of the Canadian code (CSA 1994) was given by:

$$V_c = 0.06\lambda\phi_c\sqrt{f_c'}\, b_w d + \frac{V_f}{M_f} M_{cr} \qquad [1.1]$$

The expression for evaluating the web-shear capacity of a prestressed member in the previous edition of the Canadian code (CSA 1994) was given by:

$$V_{cw} = 0.4\lambda\phi_c\sqrt{f_c'}\sqrt{1+\frac{\phi_p f_{cp}}{0.4\lambda\phi_c\sqrt{f_c'}}}\, b_w d + \phi_p V_p \qquad [1.2]$$

An explanation on the background and derivation of the equations for flexure-shear and web-shear is provided in Chapters 2 and 4. To evaluate the shear capacity of a prestressed member, the least of either the flexure-shear capacity, V_c, or the web-shear capacity, V_{cw}, was taken as the governing shear capacity of the member. With the changes to the Canadian code in 2004 (CSA 2004), there is currently only one set of equations for the shear design of prestressed members, based on the post-cracking shear capacity; the independent equation used for evaluating the elastic web-shear capacity of the member, V_{cw}, was eliminated from the 2004-edition of the Canadian code (CSA 2004).

The current Canadian concrete design code, CSA A23.3-04 (CSA 2004), utilizes an analytical model for the shear design of prestressed concrete members, based on the Modified Compression Field Theory, MCFT, (*Vecchio and Collins* 1986), which predicts the load-deformation response of a section loaded in shear and flexure. The MCFT model for shear design is based on the assumption that the member can continue to carry load after the formation of initial shear cracks; however hollow-core slabs with high shear stresses near the member end will typically fail immediately after the formation of the first diagonal web-shear cracks, with little-to-no post-cracking shear strength.

During the preparation of hollow-core load capacity charts for a local precast supplier, the author has noted that the predicted shear capacities of hollow-core slabs using the current edition of the Canadian code (CSA 2004) with low to intermediate levels of prestressing have a dramatic drop, compared to the previous edition of the Canadian code (CSA 1994). In addition, Clause 11.3.9.5 of the Canadian code (CSA 2004) requires the designer to check the tensile anchorage capacity of the strands in the bearing region of the member, due to the potential formation of a diagonal crack adjacent to the face of the support, as shown in Figure 1.2 (CSA 2004).

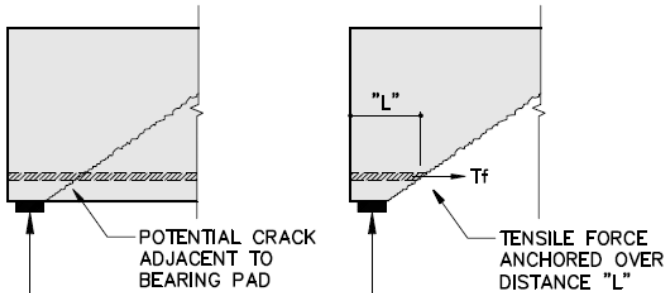

Figure 1.2: Anchorage of Longitudinal Reinforcement at End Supports, (Reproduced from CSA A23.3-04)

The intent of this design check is to provide post-cracking strength and ductility for simply-supported members, in the event that a diagonal crack forms near the end of the member. For low-to-mid levels of prestressing commonly used in hollow-core slabs, analysis using the Canadian code equations (CSA 2004) indicates that the post-cracking anchorage capacity near the member end is typically less than required by the code.

This lower capacity is due to the small length of bearing commonly used in hollow-core slabs, resulting in a very short anchorage length for the strands. Therefore, hollow-core slabs that are shear-critical in the end region will typically fail in a sudden and brittle manner once shear cracks form, unless supplemental reinforcing is grouted into the voids to satisfy the ductility requirements of Clause 11.3.9.5, which adds cost to the hollow-core slab system.

1.3 SCOPE OF WORK

Since shear failure of a concrete member without stirrups is typically sudden and brittle in nature, it is critical that the actual behaviour of such members is understood and accurately predicted in cases where shear strength governs the design. In addition, the appearance of a dramatic drop in the code-predicted (CSA 2004) capacities of hollow-core slabs with low to intermediate levels of prestressing needs to be confirmed by testing. The scope of this study is to test a series of full-scale hollow-core slabs to failure in shear and compare the test results with the predicted capacities based on the current editions of the Canadian and American concrete design codes (CSA 2004, ACI 2008). Specific variables considered in the testing program include the length of bearing (to check for the possibility of an anchorage failure, due to the formation of a bearing or shear crack adjacent to the bearing pad) and the level of prestressing.

1.4 RESEARCH OBJECTIVES

Since the shear capacity of hollow-core slabs is a very specific case that is not explicitly covered by the Canadian or American codes (CSA 2004, ACI 2008), calibration of the current codes to the observed behaviour of hollow-core slabs in shear is necessary. The main objectives of this research are to:

- Verify the experimental to predicted capacities of hollow-core slabs in the 203, 254 and 305 mm range of slab depths, according to the current Canadian and American concrete design codes (CSA 2004, ACI 2008).

- Confirm the observed modes of failure and compare them with those predicted by the codes.

- Verify the effect on the hollow-core slab shear capacity of the length of bearing over the support region and the level of prestressing.

- Verify the effect on the hollow-core slab shear capacity of the level of prestressing, ranging from the lowest to the highest amount of prestressing used by a local hollow-core slab producer.

1.5 WORK METHODOLOGY AND ORIGINALITY

A total of twelve full-scale hollow-core slabs were tested, using the standardized hollow-core shear test, found in Annex J, of European Product Standard EN-1168 (EN-1168 2008) as a guideline. This standardized shear test is used as a quality-assurance check for hollow-core slab

designers and producers, to verify that the European code-predicted (EC2 2004) shear capacities of hollow-core slabs are able to be achieved.

In previous research performed on the shear capacity of hollow-core slabs, variables that have been tested include the level of prestressing, the slab depth, and the geometry of the cross section. To the author's knowledge, no one has yet verified the effect of the length of bearing at the supports on the shear capacity of hollow-core slabs. In some cases, due to an accumulation of production and construction tolerances, hollow-core slabs are erected with less than the detailed length of slab bearing at the support, leaving the designer with a difficult decision regarding whether the slabs have adequate capacity. Part of the intent of this research is to confirm through load testing if there is an effect on either the member shear capacity or the mode of failure, due to a reduced amount of bearing over the supports.

Finally, a detailed review of the shear failure profiles observed in each of the hollow-core test slabs was conducted as part of this research; previous research has included photographs of the observed failure modes, however, to the author's knowledge no one has measured and plotted in detail the failure profiles of each of the webs in relation to the end of the slab. It is expected that these detailed failure profiles will supplement previous research, by helping to locate the experimental critical section of the slabs for shear, as compared to the code-predicted locations of the critical section for shear resistance.

1.6 THESIS STRUCTURE

This thesis consists of six chapters. The contents of each chapter are as follows:

- Chapter one presents a brief introduction on hollow-core slabs, as well as the problem definition, scope of work and research objectives and the followed methodology.
- Chapter two outlines the code provisions for evaluating the shear capacity of a prestressed member using the Canadian, American and European concrete design codes (CSA 2004, ACI 2008, EC2 2004, EN-1168 2008). In addition, an extensive literature review of the previous research conducted in the last 35 years on the shear capacity of hollow-core slabs in North America and in Europe is presented. Finally, the concerns with the application of current Canadian code (CSA 2004) provisions to the design of prestressed hollow-core slabs for shear are reviewed.
- Chapter three provides details of the experimental research program; the main factors affecting the shear strength of members without web reinforcement, test specimen geometric and structural properties, material properties, test set-up and loading procedure, and instrumentation.
- Chapter four outlines the code-predicted shear resistance of each test-slab, based on analysis using the current Canadian and American concrete design codes (CSA 2004, ACI 2008). Differences between code methods and shear-capacity predictions are noted.
- Chapter five provides the test observations, failure modes and experimental shear capacities for all test specimens. In addition, the code-predicted shear capacities and those obtained experimentally are compared. The effect of the bearing length and level of prestressing on the experimental shear capacities is also presented. Finally, the

failure profiles for the slabs are reviewed in comparison with the code-predicted critical sections for shear.

- Chapter six outlines the conclusions obtained from this research and highlights future research work that would supplement the research conducted in this thesis project.

CHAPTER 2 LITERATURE REVIEW

2.1 BACKGROUND

The shear capacity of hollow core slabs is a very specific case that is not explicitly covered by the Canadian or American codes (CSA 2004, ACI 2008). During the development of the precast/prestressed concrete industry, many hollow-core slab producers performed unpublished in-house tests to verify slab shear capacities in comparison to the code equations. In early testing performed in North America and published by the Precast Concrete Institute (PCI) - *Becker and Buettner* (1985), it was shown that the ACI code equations ACI 318-83 (1983) for shear were thought to be conservative for dry-cast extruded hollow-core slabs in the 203 to 254 mm depth range. However, more recently *Hawkins and Ghosh* (2006) raised concerns regarding testing performed on slab depths greater than 300 mm, which showed that the ACI code equations for web-shear were thought to be un-conservative, for hollow-core slab depths greater than 300 mm.

In Europe, research has also been performed on hollow-core slabs and shear. *Pajari* (2009) noted that it has been known since the early nineteen-eighties that the traditional European design method for the web-shear capacity of prestressed members was un-conservative for numerous hollow-core slab types. Pajari also summarized the developments that led to the design procedure used for evaluating the web-shear capacity of hollow-core slabs, found in the current European Product Standard for hollow-core slabs, EN1168 (EN-1168 2008).

A summary of the current code provisions for shear in Europe (EC2 2004, EN-1168 2008), Canada (CSA 2004), and the United States (ACI 2008), are outlined in Sections 2.2, 4.2 and 4.3,

while Section 2.3 presents a historical summary of previous research performed on the shear resistance of prestressed members, with a specific focus on shear testing of hollow-core slabs.

2.2 CODE PROVISIONS FOR EVALUATION OF SHEAR CAPACITY

2.2.1 Introduction

A detailed review of the Canadian code (CSA 2004) and American code (ACI 2008) shear equations and their specific use for evaluating the shear capacity of hollow-core slabs is presented in Chapter 4. The development of the current European code expressions for the shear capacity of prestressed members, including hollow-core slabs is presented in Section 2.3.2. For reference, a summary of the shear provisions found in the current European codes (EC2 2004, EN-1168 2008) are outlined below.

2.2.2 European Code (EC2 2004, EN-1168 2008) Shear Equations

The shear resistance of a prestressed member is calculated from the following expression, found in Clause 6.2.1 of the Euro-code (EC2 2004):

$$V_{Rd} = V_{Rd,s} + V_{ccd} + V_{td} \qquad [2.1]$$

Where V_{Rd} is the shear resistance of a member with shear reinforcement, $V_{Rd,s}$ is the design value of the shear force that can be sustained by the yielding shear reinforcement, V_{ccd} is the design value of the shear component of the force in the compression area, in the case of an inclined compression chord and V_{td} is the design value of the shear component of the force in the tensile reinforcement, in the case of an inclined tensile chord.

The design value for the shear resistance of a member without shear reinforcement, $V_{Rd,c}$ is given by:

$$V_{Rd,c} = \left[C_{Rd,c} k (100 \rho_l f_{ck})^{1/3} + k_1 \sigma_{cp}\right] b_w d \geq (v_{\min} + k_1 \sigma_{cp}) b_w d \qquad [2.2]$$

where the recommended value for $C_{Rd,c}$ is taken as $0.18/\gamma_c$ (γ_c = partial factor for concrete) and the recommended value for k_1 is taken as 0.15. In the above expression, f_{ck} is the characteristic compressive cylinder strength of concrete at 28 days, and

$$k = 1 + \sqrt{\frac{200}{d}} \leq 2.0 \qquad [2.3] \qquad \rho_l = \frac{A_{sl}}{b_w d} \leq 0.02 \qquad [2.4]$$

where A_{sl} is the area of the tensile reinforcement, and b_w is the smallest width of the cross-section in the tensile area. In Equation 2.2, v_{min} is calculated from the following expression:

$$v_{min} = 0.035 k^{3/2} f_{ck}^{1/2} \qquad [2.5]$$

Finally, σ_{cp}, the compressive stress in the concrete from axial load or prestressing is taken as:

$$\sigma_{cp} = N_{Ed} / A_c < 0.2 f_{cd} \qquad [2.6]$$

where f_{cd} is the design value of concrete compressive strength. N_{Ed} is the axial force in the cross-section due to the loading or prestressing (N_{Ed} is positive for compression) and A_c is the area of the concrete cross-section.

It is worth mentioning that in Equation 2.2, $V_{Rd,c}$ is not dependent on the applied moment and shear forces, unlike shear capacity expressions in the Canadian code (CSA 2004) or American code (ACI 2008).

Clause 6.2.2 specifies that for prestressed single-span members without shear reinforcement, the shear resistance of regions cracked in bending may be calculated according to Equation 2.2. In regions un-cracked in bending, the shear resistance should be limited by the tensile strength of the concrete. In these regions the shear resistance is given by:

$$V_{Rd,c} = \frac{Ib_w}{S}\sqrt{\left(f_{ctd}\right)^2 + \alpha_\ell \sigma_{cp} f_{ctd}} \qquad [2.7]$$

where I is the second moment of area, b_w is the width of the cross-section at the centroidal axis, S is the first moment of area above and about the centroidal axis, f_{ctd} is the design value of concrete tensile strength, $\alpha_\ell = \ell_x / \ell_{pt2} \leq 1.0$ for pre-tensioned tendons, ℓ_x is the distance of section considered from the starting point of the transmission length, and ℓ_{pt2} is the upper bound value of the transmission length of the prestressing element. Note that the Euro-code (EC2 2004) uses the tensile strength in the code expression for web-shear, f_{ctd} , while the American code (ACI 318-08) uses the compressive strength, f_c', in the code expression for web-shear.

An upper limit is placed on the design value of the shear force, V_{Ed}, as follows:

The shear force, V_{Ed}, calculated without reduction by β should always satisfy the following condition:

$$V_{Ed} \leq 0.5 b_w d \upsilon f_{cd} \qquad [2.8]$$

where the recommended value for the strength reduction factor for concrete cracked in shear, υ is calculated using:

$$\upsilon = 0.6\left[1 - \frac{f_{ck}}{250}\right] \qquad [2.9]$$

Clause 4.3.3.2.2.1 of European Product Standard EN-1168 (EN-1168 2008), provides a specific set of equations that are to be followed for the shear design of hollow-core slabs. The expressions developed in Clause 4.3.3.2.2.1, which are derived from research performed by *Yang* (1994) and *Pajari* (2005) are listed below.

For hollow-core slabs without shear reinforcement, the shear resistance of the regions cracked by bending shall be calculated using Equation 2.2, from the Euro-code (EC2 2004). However, for prestressed single-span hollow-core members without shear reinforcement, the shear resistance of the regions un-cracked by bending, should be calculated with the following expression:

$$V_{Rd,c} = \frac{I b_w(y)}{S_c(y)}\left(\sqrt{(f_{ctd})^2 + \sigma_{cp}(y) f_{ctd}} - \tau_{cp}(y)\right) \qquad [2.10]$$

where $\sigma_{cp}(y)$ (positive if compressive) is evaluated from:

$$\sigma_{cp}(y) = \sum_{t=1}^{n}\left\{\left[\frac{1}{A_i} + \frac{(Y_c - y)(Y_c - Yp_t)}{I}\right] P_t(\ell_x)\right\} - \frac{M_{Ed}}{I}(Y_c - y) \qquad [2.11]$$

And

$$\tau_{cp}(y) = \frac{1}{b_w(y)} \sum_{t=1}^{n} \left\{ \left[\frac{A_c(y)}{A_i} - \frac{S_c(y)(Y_c - Yp_t)}{I} + Cp_t(y) \right] \frac{dP_t(\ell_x)}{dx} \right\} \qquad [2.12]$$

Equation 2.10 is to be evaluated with reference to the critical points of a straight line of failure rising from the edge of the support with an angle $\beta = 35°$ with respect to the horizontal axis. The critical point is taken as the point on the above line where the result of the expression of $V_{Rd,c}$ is lowest.

The definitions for the terms in the above equations are provided below:

- I is the second moment of area of the cross-section;
- $b_w(y)$ is the web-width at height y;
- Y_c is the height of the centroidal axis;
- $S_c(y)$ is the first moment of the area above height y and about the centroidal axis;
- y is the height of the critical point on the line of failure;
- ℓ_x is the distance of the considered point on the line of failure from the starting point of the transmission length (= x);
- $\sigma_{cp}(y)$ is the concrete compressive stress at height y and distance ℓ_x;
- n is the number of tendon layers;

- A_i is the fictive cross-section surface;
- $P_t(\ell_x)$ is the prestressing force in the considered tendon layer at distance ℓ_x;
- M_{Ed} is the bending moment due to the vertical load, for this expression the bending moment may be ignored ($M_{Ed} = 0$);
- $\tau_{cp}(y)$ is the concrete shear stress due to the transmission of prestress at height y and distance ℓ_x – Note: in Equation 2.10, $\tau_{cp}(y)$ generally causes a reduction in shear capacity due to the prestressing, which is not recognized in the Canadian code (CSA 2004), American code (ACI 2008) or the Euro-code (EC2 2004);
- $A_c(y)$ is the area above height y;
- $Cp_t(y)$ is a factor taking into account the position of the considered tendon layer;
    - $Cp_t = -1$, when $y \leq Yp_t$
    - $Cp_t = 0$, when $y > Yp_t$
- Yp_t is the height of the position of the considered tendon layer.

According to Clause 4.3.3.2.2.1 of EN-1168 (EN-1168 2008), for hollow-core slabs deeper than 450 mm the shear strength, both for regions cracked or un-cracked by bending, shall be reduced by 0.90 with respect to Equations 2.2 and 2.10. Sections between the edge of a support and the section at a distance 0.5h from this edge need not be checked for shear. Finally, in case of

flexible supports, the reducing effect of transversal shear stresses on the shear capacity shall be taken into account.

2.3 RESEARCH ON PRESTRESSED MEMBER SHEAR CAPACITY

2.3.1 North American Research

Anderson (1976) published a report on the shear strength of prestressed concrete beams, noting that the shear capacities of precast prestressed concrete beams are sometimes considerably higher than the predicted ACI code design strengths ACI 318-71 (ACI 1971). Anderson conducted a series of full-scale shear tests on several types of prestressed beams, including double tee beams with varying top flange widths, rectangular beams and decked bulb tees.

Anderson noted that shear failures of prestressed concrete beams involve many different and complex mechanisms. Based on the load tests performed on the prestressed beams, it was found that the ACI design provisions for shear ACI 318-71 (ACI 1971) appeared to be reasonable and conservative for a typical prestressed concrete beam. However, Anderson noted that for several standard precast products, code design provisions could be refined to obtain greater efficiency.

The full-scale testing also revealed that the shape and dimensions of the compression flange can have a significant effect on the member shear strength. Thick flanges increased the shear strength and thin flanges tended to decrease the shear strength. Anderson observed that prestressed members such as decked bulb-tees (Figure 2.1) appeared to be significantly stronger than the ACI code predictions (ACI 1971), the principal reason being the wide, thick compression flange. Finally, Anderson concluded that hollow-core slabs warranted further testing, as they are also characterized by a wide, thick compression flange.

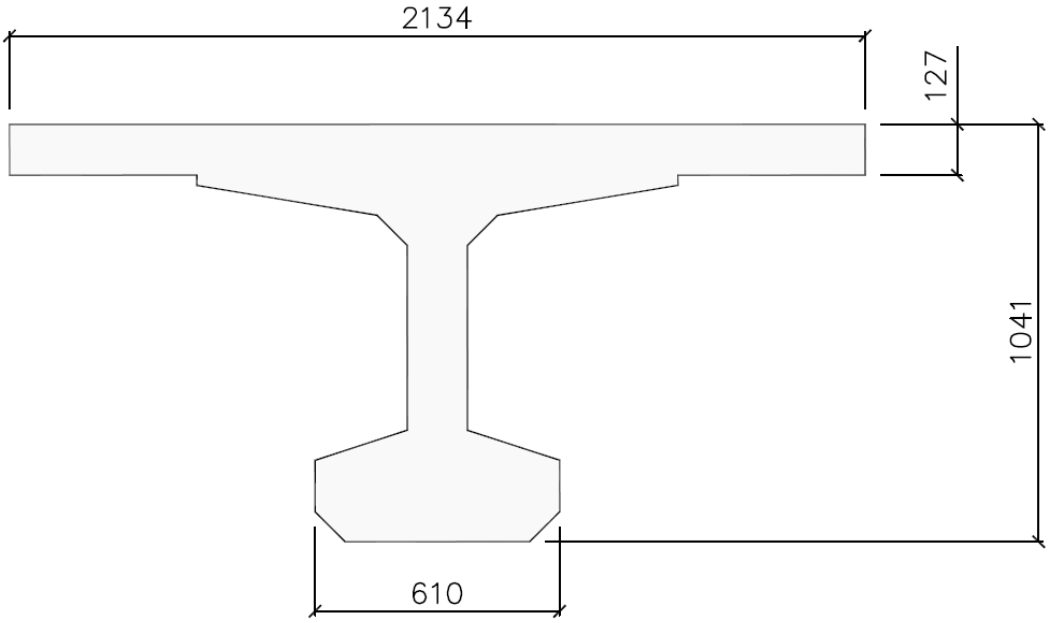

Figure 2.1: Decked Bulb Tee Test Specimens (Reproduced from CTA-76-B11/B12)

Anderson (1978) investigated the shear strength of hollow-core slabs by comparing the experimental capacities to the ACI 318-77 (ACI 1977) code-predicted capacities, using the minimum web-width for the code based shear calculations.

For reference, the shear strength provisions of ACI 318-77 (ACI 1977) are repeated below (all units in imperial):

The expression for evaluating the flexure-shear capacity of a prestressed member was given by:

$$V_{ci} = 0.6\sqrt{f_c^{'}}\, b_w d + V_d + \frac{V_i M_{cr}}{M_{\max}} \qquad [2.13]$$

Anderson explained the derivation of the above expression as follows (CTA-76-B11/B12, CTA-78-B1):

In the above expression, the flexure-shear capacity, V_{ci} is a function of the 28-day concrete strength, f_c', the minimum web-width within the height of the section, b_w, the depth to the prestressing strands, d, and the shear at flexural cracking which is the sum of the last two terms in Equation 2.13.

The first term in Equation 2.13 represents the increment of shear necessary to transform a flexural crack into an inclined crack, which is independent of the loading. In addition, the 0.6 factor in the first term of Equation 2.13 is an empirically derived value selected as a lower bound from test data. The second term, V_d, represents the shear-force due to un-factored dead load and the last term represents the additional applied shear to cause a flexural crack at the critical section. In addition, the last term of Equation 2.13 indicates that the flexure-shear resistance, V_{ci}, is a function of the shear-to-moment ratio at any section along the member span. Finally, it is important to note that the flexure-shear resistance, V_{ci}, is much more sensitive to the moment than is V_c, the reinforced concrete shear resistance, because of the relatively low post-cracking strength.

The expression for evaluating the web-shear capacity of a prestressed member in the ACI 318-77 code (ACI 1977) was given by:

$$V_{cw} = (3.5\sqrt{f_c'} + 0.3 f_{pe}) b_w d + V_p \qquad [2.14]$$

Anderson explained the derivation of the above expression as follows (CTA-76-B11/B12, CTA-78-B1):

The above equation is a simplification of a constraint on the principal tension at the centroid of the cross-section, due to the combined stresses from the shear-force and the prestressing force. The principal tension can be computed by elastic analysis since for web-shear cracking, no flexural cracks exist at the critical section prior to the formation of inclined cracks.

Equation 2.14 can be derived in the following manner: Let f_t be the principal tension at the centroid. Ignoring any vertical stresses at the centroid, the principal tension depends only on the shear stress, v_{cw}, and the axial stress due to prestressing at the centroid, f_{pc}.

$$f_t = \sqrt{v_{cw}^{\ 2} + \left(\frac{f_{pc}}{2}\right)^2} - f_{pc}/2 \qquad [2.15]$$

Solving for v_{cw} results in the following equation:

$$v_{cw} = f_t\sqrt{1 + \frac{f_{pc}}{f_t}} \qquad [2.16]$$

Web shear cracking occurs when the principal tension at the centroid exceeds $4\sqrt{f_c'}$. The allowable value of f_t is set at $3.5\sqrt{f_c'}$ rather than the value $4\sqrt{f_c'}$ indicated by tests because v_{cw} is only the nominal shear stress at the centroid rather than the actual shear stress. For evaluation of the web-shear capacity of a hollow-core member (Equation 2.14), Anderson

suggested that since the shape of the compression zone has little effect on the principal tension at the centroid, it would be appropriate to use the minimum web width for web-shear calculations.

In addition, Anderson noted that for evaluation of the flexure-shear capacity of a hollow-core member (Equation 2.13), a value for the web width, b_w, must also be determined. Since the width of the webs of most hollow-core products is not constant, it is not clear what the appropriate value of b_w should be for flexure-shear calculations, where the shape of the compression zone may have an effect on the shear capacity. To validate the theory that the ACI code equation for flexure-shear was overly conservative ACI 318-77 (ACI 1977), full-scale shear tests were performed on hollow-core slabs from several different manufacturers with depths ranging from 152 to 368 mm. The geometry of the cross-sections and the amount of prestressing were varied, along with the moment-to-shear ratio. The hollow-core slabs were tested as simply-supported beams subjected to a single concentrated load, applied through a steel beam running across the full width of the slabs. The shear span, a, which is the distance from the centreline of the load to the centreline of the nearest support was also varied in the testing.

Test results indicated that it was nearly impossible to obtain an experimental flexure-shear failure of a hollow-core slab, even though a flexure-shear failure was predicted using the ACI 318-77 code equations (ACI 1977). In addition, it was found that using the minimum web-width for the evaluation of the flexure-shear capacity of hollow-core slabs is too conservative. To correlate the experimental results with the ACI code equations (ACI 1977), Anderson proposed that an "effective shear area" based on the slab geometry was more suitable for use in evaluating the flexure-shear capacity of hollow-core slabs, rather than use the minimum web width within the slab depth, as outlined in Figure 2.2.

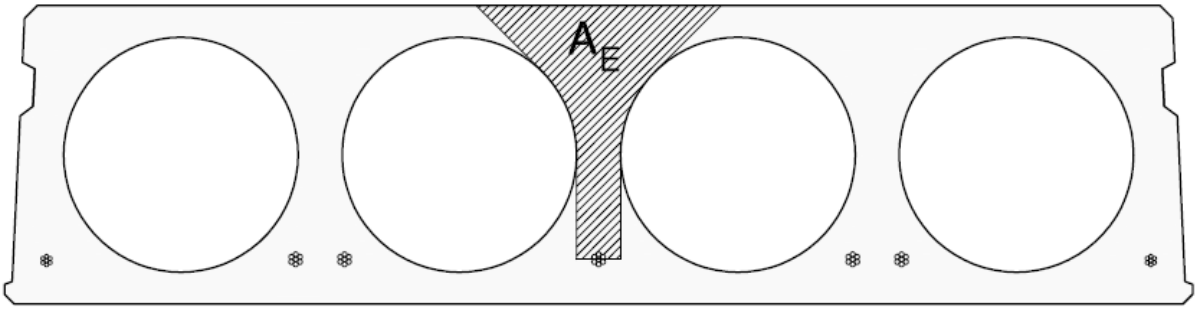

Figure 2.2: Example of Effective Shear Area for a Typical Web within a Hollow-Core Slab with Circular Voids (Reproduced from CTA-78-B1)

The following equation for the flexure-shear capacity of a hollow-core slab was proposed, in lieu of Equation 2.13:

$$V_{ci} = K\sqrt{f_c'}\ A_E + V_d + \frac{V_i M_{cr}}{M_{max}} \qquad [2.17]$$

Where:

K = 0.6, unless a higher value is justified by tests. Testing of slabs from two separate manufacturers indicated values for K ranging from 0.75 to 1.0, depending on the moment-to-shear ratio.

A_E = the effective shear area defined as the portion of the cross-section above the centroid of the prestressing steel enclosed by lines that follow the contour of the cross section, but never exceed a 45 degree angle with respect to the vertical.

Becker and Buettner (1985) performed a series of shear tests on dry-cast hollow-core slabs to determine the applicability of the ACI-318 code provisions (ACI 1983) for prestressed concrete to the design of hollow-core slabs. An additional objective was to determine whether the web reinforcement exemption for slabs is valid for zero-slump, extruded hollow-core slabs. Finally, the code equations ACI 318-83 (ACI 1983) for development length, (the length from the end of a member required to fully transfer the prestressing strand force to the concrete section through bond) were verified for extruded hollow-core slabs.

The variables studied in the test program were loading conditions, span length and amount of prestressing. Concrete strength was not considered as a variable in the testing program. A series of 203 mm depth (8-inch) slabs and 254 mm depth (10-inch) slabs were tested for shear strength characteristics, using two-point loading and a shear span of 760 mm (2-foot 6-inches) and 1140 mm (3-foot 9-inches). The test results confirmed that the tested shear capacity of the hollow-core slabs exceeded the capacity predicted by the ACI-318 code equations (ACI 1983). In addition, it was demonstrated that the minimum shear reinforcement exemption allowed by the ACI code (ACI 1983) is valid for extruded hollow-core slabs. Finally, it was shown that the ACI code (ACI 1983) development length provisions are conservative.

Anderson (1987) derived an alternate method to calculate the web-shear strength of a prestressed concrete member, in lieu of the simplified ACI 318 equation for web-shear (ACI 1983), resulting in an increase in web-shear capacity ranging from 10 to 20%.

Anderson noted that the role of principal tension in determining the shear strength of prestressed concrete members is explicitly noted in ACI 318-83 (ACI 1983), Section 11.4.2.2 as follows:

Alternatively, V_{cw} may be computed as the shear force corresponding to dead load plus live load that results in a principal tensile stress of $4\sqrt{f_c'}$ at centroidal axis of member, or at intersection of flange and web when centroidal axis is in the flange. In composite members, principal tensile stress shall be computed using the cross section that resists live load.

Using elastic stress analysis and the Mohr's circle, Anderson derived an alternate expression for the evaluation of the web-shear capacity, as permitted by the ACI code (ACI 1983) noted above. In the derivation of the alternate expression for web-shear, Anderson noted that strictly speaking, local shearing stresses are introduced in the vicinity of the transfer zone near the member ends; however they were neglected in the derivation of the alternate equation. The alternate equation for the web-shear capacity of a prestressed member is listed below (in imperial units):

$$V_{cw} = \sqrt{(0.016) f_c' + (0.1265)\sqrt{f_c'}\,(f_{px} - \sum Mc / I)}\; b_w d \qquad [2.18]$$

Anderson also commented on the location of the critical section for use of the above expression (Figure 2.3).

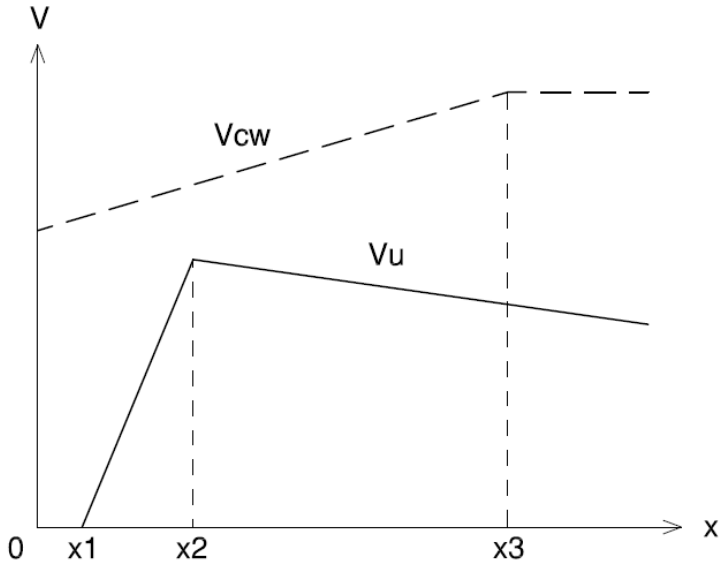

Figure 2.3: Variation of Shear Near Support (Reproduced from CTA-85-B1)

In Figure 2.3, the web-shear resistance, V_{cw}, increases from the member end up to a maximum value at the end of the strand transfer length, x_3. The edges of the bearing pad are located at x_1 and x_2, (the reaction is assumed to be applied over a finite distance near the end of the member, extending from x_1 to x_2) and the end of the member is at $x = 0$. V_u represents the applied shear force along the member, based on a uniformly distributed in this case.

Anderson observed that it is apparent that V_u assumes its maximum value at x_2. He also noted that in the vast majority of cases involving simply supported precast-prestressed members, x_2 will occur in a region of increasing V_{cw}, between $x = 0$ and $x = x_3$. It therefore follows that the critical value of x, namely the value at which (V_{cw} - V_u) is a minimum, is x_2. Anderson recommended that designers using Equation 2.18 not use the reduced value of V_u described in Section 11.1.2.2 of ACI 318-83 (ACI 1983), because the effects of the reaction referred to in the code have been explicitly neglected in the analysis.

The alternate equation for web-shear proposed by Anderson (Equation 2.18) was compared with testing performed on five different types of hollow-core slabs, and a single tee. The hollow-core slabs and the single tee were tested as simply supported beams subjected to a single concentrated load, applied at a distance *a,* from the centreline of bearing. The test results indicated that using the proposed alternate expression for web-shear strength of prestressed members was justified, since the test values of shear strength exceeded predictions in nearly every case, often by large margins.

Anderson noted that the average test value was 20% higher than the predicted value, even though many tests did not result in shear failure of the specimen. He concluded that this additional 20% of experimental shear capacity reflects the fact that the true strength of concrete in direct tension is probably considerably higher than $4\sqrt{f_c'}$. Finally, Anderson noted that ignoring the beneficial effect of upward thrust of the reaction at the end of a simply supported beam is another conservative factor, which would explain why observed strengths are higher than predicted, especially in members such as hollow-core.

Hawkins and Ghosh (2006) highlighted a recent concern regarding the shear capacity of hollow-core slabs with depths larger than 320 mm (12.5-inches).

The nominal web-shear strength for a prestressed member, V_{cw}, is given in ACI 318-05 (ACI 2005) by the following equation:

$$V_{cw} = (3.5\sqrt{f_c'} + 0.3 f_{pe}) b_w d_p + V_p \qquad [2.19]$$

Note that the above equation has remained unchanged from previous ACI codes (ACI 1977), except for a minor change in terminology in using "d_p" in lieu of "d". *Hawkins and Ghosh* noted that the shear strength of a reinforced concrete member is given in ACI 318-05 (ACI 2005) by the following equation:

$$V_c = 2\sqrt{f_c'}\, b_w d \qquad [2.20]$$

In addition, they noted that there is a discontinuity in concept between the evaluation of the web-shear strength of prestressed members in comparison with the shear strength of reinforced members; as f_{pc} decreases along the transfer length. Therefore, it is reasonable to assume that the strength for a prestressed concrete beam should approach that of a reinforced concrete beam. Values from the two equations are not consistent with that assumption.

It appears from limited testing of slabs with depths greater than 320 mm (12.5-inches) from three different hollow-core slab suppliers, that the ratio of the tested web-shear strengths to the calculated web-shear strengths becomes less than unity, when using ACI-318 code equations (ACI 2005). Hawkins and Ghosh noted that the $V_{test}/b_w d$ values for the 16-inch (406 mm) slabs provided by one of the suppliers averaged only $2.66\sqrt{f_c'}$. Therefore, for these members the shear strength was more like that of a reinforced concrete member than a prestressed member. The principal tensile stress in the concrete at the centroidal axis of those units was clearly less than $4\sqrt{f_c'}$ at time of failure.

It was also observed in the testing of the slabs that in all cases where the web-shear cracks resulted in failure, the cracks seemed to initiate in the units close to the face of the support. In the units tested from one supplier, horizontal cracking appeared along the junction of the webs and lower flange often appeared to be a part of the shear failure mechanism. In general, the results also indicated that if bond-slip of the strand occurred, it was after the formation of the web-shear crack.

Hawkins and Ghosh also noted that none of the tests showed flexure-shear cracking strengths less than those calculated by ACI 318-05 (ACI 2005). In some of the tests, flexure-shear cracks developed but they did not result in failure and they occurred at shear values consistent with those predicted using the flexure-shear equation in ACI 318-05 (ACI 2005). From the test results, they concluded that it appears that the reduction in the web-shear cracking with depth is related to the spread of the prestressing force into the section and associated with a combination of effects due to shear lag, anchorage bond, prestress location, and the geometry of the cross-section of the unit.

Finally, *Hawkins and Ghosh* examined European research on the shear-testing of hollow-core slabs (summarized in Section 2.3.2). They concluded by noting that more research was needed to study the web-shear strength of hollow-core slabs, and they recommended that a reduction be applied to the calculated web-shear capacity when using the ACI expression (ACI 2005) for hollow-core members deeper than 12.5 inches (320 mm).

Palmer and Schultz (2010) studied the main parameters affecting the web-shear capacities of hollow-core units as demonstrated by previous and current research. These parameters that were studied included the member depth, cross-sectional geometry, transverse distribution of load

between webs, axial stress due to prestress, tensile strength of web concrete, the shear lag of the prestressing force, and the shear span-to-depth ratio, a/d.

They also compared the web-shear capacities of hollow-core units produced by two U.S. manufacturers (Supplier A and Supplier B) using ACI 318-05 (ACI 2005), the Euro-code (EC2 2004), the Modified Compression Field Theory (*Vecchio and Collins* 1986), the American Association of State Highway Transportation Officials' AASHTO LRFD Bridge Design Specifications (AASHTO 2004), and Yang's method (*Yang* 1994).

For the analysis of the web-shear capacities of the test slabs produced by the two U.S. manufacturers, a specified compressive strength of 6,000 psi (41.4 MPa) was used along with the nominal web widths for Supplier A. However, Supplier B performed two cylinder tests from the concrete batch used for each unit and also measured the web widths for each unit. The a/d ratios for the test slabs from each supplier were all greater than or equal to 2.4, therefore the effects of arching action were ignored.

The authors concluded the following, regarding the factors affecting the web-shear capacity of deep hollow-core units:

- Analysis of 198 hollow-core units failing in shear found in the literature revealed that there is no clear evidence of a size effect in shear for units up to 19.7 in. (500 mm) in depth, due in part to the large scatter of the web-shear strength data.

- There is a possibility that the tensile strength of the web concrete varies between the units from the two manufacturers considered for the study, which may be the reason for a disparity in performance between the two suppliers.

- *Yang* (1994) demonstrated that the geometry of the cross-section can have an impact on the shear capacity of hollow-core units. The void geometry affects the location of the maximum principal tensile stress in the slabs, which affects the critical point for shear resistance.

- Theoretically, the relative stiffness of the individual webs may affect the distribution of shear across the section. This, coupled with the shear lag of the prestressing force across the width, may tend to further reduce the shear capacity of hollow-core units.

- An accurate estimate of the prestressing force at the critical point requires an accurate estimate of the transfer length and transfer-stress distribution of the strands. It is unclear whether a transfer length of 50 db, as recommended by ACI 318-08 (ACI 2008) and ACI 318-05 (ACI 2005) is applicable to extruded hollow-core units because no transfer-length experiments of U.S. manufactured units have been reported.

- Given the disparity in predicted shear capacities of the units from Suppliers A and B, none of the prediction methods considered in the study were able to provide uniform reliability in shear-strength prediction. However, the AASHTO method (AASHTO 2004), followed by Yang's method (*Yang* 1994), performed better than ACI 318-05 (ACI 2005), the Euro-code (EC2 2004), and the modified compression field theory (*Vecchio and Collins* 1986).

Finally, *Palmer and Schultz* (2010) concluded that more research was needed to resolve the question regarding the most applicable shear-prediction method for deep hollow-core units and

to develop a more rational and logical revision than an overall reduction factor to the web-shear predictions based on ACI 318-08 (ACI 2008).

Cheng and Wang (2010) studied the impact of the interaction between adjacent webs on the shear strength of prestressed concrete hollow-core units. For the research program, both experimental tests and 3-D non-linear finite-element models were developed to simulate the behaviour of prestressed concrete hollow-core units and I-shaped beams.

For the experimental tests, two groups of specimens were used in the study. The first group included four identical I-shaped, prestressed concrete beams (single-web strips cut from a hollow-core unit), while the second set of specimens included four identical full-sized hollow-core units (multi-web). All test specimens had a depth of 203 mm (8 in.). A specified concrete strength of 6,000 psi (41.4 MPa) was used for the analysis of the test specimens and the shear span-to-depth ratio, *a/d*, was varied for the tests from 2.5 to 4.3.

Two types of shear failures were observed during the testing, one web-shear failure occurred for the I-section with an *a/d* ratio of 3.0, while all remaining shear failures were observed to be flexure-shear failures.

Chen and Wang (2010) concluded that the finite-element models developed in the study were able to accurately simulate the shear behaviour of I-shaped concrete beams and prestressed hollow-core units. For the case of single-web hollow-core units where web-interaction from adjacent webs does not exist, they found that the empirical equations in ACI 318-05 (ACI 2005) can provide satisfactory a prediction. However, for the case of full-sized prestressed concrete

hollow-core units, where multiple webs exist, the ACI 318-05 (ACI 2005) prediction of the shear strength is conservative, when using only the sum of the minimum web widths for the slab.

A possible explanation is that ACI 318-05 (ACI 2005) ignores the interaction between the adjacent webs and their contribution to the shear capacity, which leads to a more conservative prediction.

2.3.2 European Research

Walraven and Mercx (1983) performed extensive testing on hollow-core slabs to determine the failure modes for various load configurations. In Series I of the testing program, twelve tests were performed on 200-mm deep single hollow-core slabs subjected to line loads with variable load span-to-depth ratios (*a/d* ranging from 2.3 to 11.2), and on double slabs coupled by filling the longitudinal joint between the slabs, which were subjected to eccentric line and concentrated loads. In the Series I tests, only flexural failures were observed.

In order to verify the shear failure modes, a second series of thirty tests were performed (Series II) on hollow-core slabs with varying cross-section, depth and prestressing steel, which were subjected to line loads with varying load span-to-depth ratios (*a/d* ranging from 2.0 to 6.67) . The shear testing comprised 20 specimens, ranging in cross-section and in depth (from 255 mm to 300 mm). *Walraven and Mercx* (1983) noted that as far as the behaviour in shear is concerned two failure modes can occur. A shear crack can develop from a flexural crack and reduce the compression area to such an extent that it fails (a shear-compression failure). A general empirical formula was derived for the shear-compression failure mode:

$$V_{uk} = 0.068 b_w d \xi (1 + 0.5\rho_o)\sqrt{f_c} + \frac{M_x}{V_x} M_o \qquad [2.21]$$

where b_w is the total web width of all webs at the smallest section, d is the effective depth (to prestressing strands), f_c is the concrete cylinder compressive strength, M_x and V_x are the moment and shear force at distance x from the bearing, M_o is the decompression moment, and:

$$\xi = 1.6 - d \geq 1 \qquad \text{(where } d \text{ is in metres)} \qquad [2.22]$$

$$\rho_o = \frac{100 A_p}{b_w d} \qquad [2.23]$$

In addition, shear failure can also occur in the region un-cracked in flexure if the concrete tensile strength, at about mid-depth of the webs is reached (a shear-tension failure). The equation for web-shear strength was derived by setting the principal tensile stress equal to the tensile strength of the concrete, f_{ct}:

$$V_u = \frac{I b_w}{S}\sqrt{f_{ct}^2 + \alpha \frac{A_p}{A_c}\sigma_p f_{ct}} \qquad [2.24]$$

where b_w is the total web width of all webs at the smallest section, I is the moment of inertia, S is the first area moment of the cross-section, α is the fraction of the prestressing at the section considered, A_p and A_c are the cross-sectional areas of the prestressing strand and the concrete section, and σ_p is the stress in the prestressing strands. Note that the term $(A_p/A_c)\ \sigma_p$ can be

replaced by σ_N , which is the average concrete compressive stress in the cross-section. Equation 2.24 can then be rewritten as:

$$V_{uk} = \frac{Ib_w}{S}\sqrt{f_{ct}^2 + \alpha\sigma_N f_{ct}} \qquad [2.25]$$

A review of the shear tension failures indicated that an average value of $V_{u,exp}/V_{u,th}$ of 0.91 was obtained, with a standard deviation of 0.10. To correct the over-prediction made by Equation 2.25, *Walraven and Mercx* (1983) recommended that the web-shear capacity equation be multiplied by a correction factor of 0.75:

$$V_{uk} = 0.75\frac{Ib_w}{S}\sqrt{f_{ct}^2 + \alpha\sigma_N f_{ct}} \qquad [2.26]$$

Finally, *Walraven and Mercx* (1983) found that the equation for shear-compression failure could be used for design, based on the shear-test results.

Pisanty (1992) investigated the shear strength of extruded prestressed, precast hollow-core slabs both analytically and experimentally. *Pisanty* (1992) addressed the concerns regarding the design of hollow-core slabs for shear in Europe by reviewing the shear strength assessment according to the codes that were applicable at the time the research was conducted; BS-8110 (BS 1985) ACI 318-89 (ACI 1989) and the FIP recommendations (FIP 1988).

For reference, the FIP equation in the 1988 code (FIP 1988) used for evaluation of the shear capacity in cracked regions (often referred to as a shear-compression failure mode), similar in form to Equation 2.21, developed by *Walraven and Mercx* (1983) is presented below:

$$V_{Rd11} = 0.068 b_w d (1 + \frac{50 A_p}{b_w d}) \left(\frac{f_c}{\gamma_c} \right)^{1/2} + M_o \frac{M_x}{V_x} \qquad [2.27]$$

In the above equation, V_{Rd11} is the design shear strength in regions cracked in flexure.

The FIP equation for web-shear in the 1988 FIP Recommendations (FIP 1988), similar in form to Equation 2.24, developed by *Walraven and Mercx* (1983) is presented below:

$$V_{Rd12} = \frac{I b_w}{S} (f^2_{ctd} + 0.9 \alpha \sigma_{cp} f_{ctd})^{1/2} \qquad [2.28]$$

In the above equation, V_{Rd12} is the design shear strength in regions un-cracked in flexure.

For the assessment of the shear capacity in un-cracked regions, the main considerations made by *Pisanty* (1992) were as follows:

- What is the actual concrete tensile strength relevant for this assessment?
- What will be the appropriate compressive stress due to prestressing, to be accounted for in combination with the concrete tensile strength?
- At what section should this assessment be carried out?
- Is there any justification for an overall reduction factor (0.75 by *Walraven and Mercx* (1983)? and if yes, what should it be?

Pisanty (1992) found that based on tests carried out on concrete samples taken from extruded hollow-core webs, the flexural tensile strengths were of the expected order of magnitude, but

were rather low. In addition he noted that the concrete in the web is in a biaxial state of stress (principal tension and transverse principal compression) and the question arises as to whether a reduced uniaxial tensile strength should not be applied for assessment of the shear strength capacity – the average splitting strength may be too high.

Regarding the compressive stress due to prestressing and the location of the critical section, *Pisanty* (1992) noted that, as acknowledged by *Walraven and Mercx* (1983), the most probable section where shear cracks initiate is at a distance y_b (the centroidal distance from the bottom face of the slab) from the inner edge of the support (where the most unfavourable shear crack is projected under a very conservative assumption of 45° inclination) as shown in Figure 2.4.

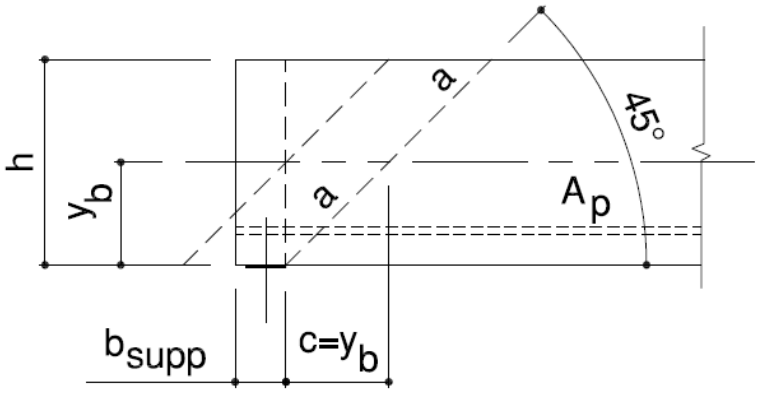

Figure 2.4: Section for Verification of Shear Capacity at Distance *c* from Support Edge

(Reproduced from *Pisanty* (1992))

For the transfer of prestressing force, *Pisanty* (1992) stated that a parabolic distribution with some overall reduction is believed to reflect reasonably well the stress state in the transfer area.

For the experimental investigation, *Pisanty* (1992) tested ten specimens, all from extruded hollow-core slabs, 300 mm thick. Four of the slab specimens were 900 mm wide (full slab widths). In addition, six specimens were obtained by dividing two full-width slabs into three parts each, leaving two side specimens and one central specimen, taken from one full-width slab.

The concrete characteristic compressive strength was tested at 47 MPa and the prestressing level was varied between specimens, with the central specimens having top and bottom strands. The clear span was set at 1930 mm and all specimens were loaded by a point load at mid-span. All specimens failed in shear, with four of the slabs failing in a shear-compression mode and six of the specimens failing in a shear-tension mode.

Based on the analysis and experimental results, *Pisanty* (1992) made the following conclusions:

- For shear-compression failure (shear in flexural-cracked regions), it was found that the British code, BS-8110 (BS 1985) underestimated the shear capacity considerably, while those of ACI 318-89 (ACI 1989), the FIP recommendations (FIP 1988), and *Walraven and Mercx* (1983) approximated the capacity more closely (in spite of some scatter in the results).

- For shear-tension (shear in un-cracked regions) the parameters involved should be at their realistic values: for concrete tensile strengths, 55% of the flexural tensile strength, or $f_{ctk,min}$ (both render close results) is suggested; for the compression stress, a prestressing force transfer in parabolic distribution, with a reduction factor due to possible slip. The relevant section for shear capacity verification is at a distance from the inner face of the support approximated as y_b.

- *Pisanty* (1992) suggested a modified version of the equation proposed by *Walraven and Mercx* (1983), (Equation 2.26) be considered:

$$V_{uk} = 0.75 \frac{I \sum b_w}{S} (f^2_{ctk,min} + 0.8\alpha\sigma_N f_{ctk,min})^{1/2} \qquad [2.29]$$

Pisanty (1992) stated that Equation 2.29 is preferred because of the simple and clear expression for the concrete tensile strength. In the above equation, $f_{ctk,min}$ is according to CEB-FIP (1978), α is a reduction factor due to parabolic distribution of the prestressing force transfer, and σ_N is the average stress due to fully transferred prestressing force in the ultimate state. Finally, *Pisanty* (1992) concluded that the need for an additional factor exists and it should be 0.75, to reduce the predicted capacity by a single safety factor to obtain a design value.

Yang (1994) developed a design procedure to determine the capacity against shear failure of webs of prestressed hollow-core slabs. The main consideration differentiating Yang's work from previous research was that Yang took into account the presence of additional shear stresses in the webs due to the build up of prestressing force in the transfer region of the slabs. In addition, Yang derived his expressions for the web shear capacity following equilibrium of forces for shear stresses and normal stresses.

According to traditional expressions used for evaluating the web-shear capacity of prestressed members in Europe and North America, the higher the prestressing level in the concrete, the higher the capacity against shear failure of the web. However, Yang found that according to 3D finite-element analysis, this assumption is not correct and the critical point is not always close to the centroidal axis either, especially for slabs with non-circular voids.

Calculations by *Yang* (1994) showed that the differences between the results from 3D finite-element analysis and traditional methods could be as large as 40%. Rather than attempt to apply correction factors to the predicted slab capacities, as done in previous research by *Walraven and Mercx* (1983) and *Pisanty* (1992), Yang chose to revisit the derivation for the traditional web-shear capacity expression, using an equilibrium approach to improve the web-shear capacity predictions.

Yang's expression for the capacity against web-shear failure is presented below:

$$V_t = V_{z,max} = \frac{bI_y}{S_{cp}} \left\{ \begin{array}{l} \frac{b}{2S_{cp}} f_{ct} x_{cp} z_{cp} + \frac{S_{cp}}{b}\left(\frac{e}{I_y} - \frac{A_{cp}}{AS_{cp}}\right)\frac{dN_p}{dx} \\ + \left[\left(\frac{b}{2S_{cp}} f_{ct} x_{cp} z_{cp}\right)^2 + \left(\frac{e}{I_y} - \frac{A_{cp}}{AS_{cp}}\right) f_{ct} x_{cp} z_{cp} + \left(\frac{1}{A} - \frac{z_{cp} e}{I_y}\right) N_p f_{ct} + f_{ct}^{\,2}\right]^{1/2} \end{array} \right\} \qquad [2.30]$$

The above expression enables an evaluation of the critical section location to be made, based on shear stresses throughout the depth and length of the member, in conjunction with a reduction of the web-shear capacity due to the horizontal shear stresses caused by the prestressing force gradient the transfer zone, by the term dN_p/dx. Note however that the zone of the slab in which the pressure due to the support reaction affects the principal stresses is excluded from the calculations, as the effect on the principal stresses are not taken into account in the above expression. The above equation is similar in form to the current web-shear expression (Equation 2.10), found in Clause 4.3.3.2.2.1 of EN-1168 (EN-1168 2008).

Yang (1994) found that the coordinate of the critical point (x_{cp}, z_{cp}), can be predicted as the intersection of the narrowest web width of the hollow-core slab and the line from the centre of the support at an angle $\beta = 35°$ with respect to the bottom surface of the hollow-core slab, which is again similar to the requirements of Clause 4.3.3.2.2.1 of EN-1168 (EN-1168 2008).

Yang (1994) compared the prediction of Equation 2.30 with 3D finite-element analysis and with a large number of extruded hollow-core slab shear tests performed at the Technical Research Centre of Finland (VTT) conducted during the period from 1978 to 1987. Yang found that Equation 2.30 was in good agreement with 3D finite-element analysis and the test results from VTT. In addition, Equation 2.30 was more consistent in predicting the web-shear capacities of all types of hollow-core slabs, than the traditional web-shear equations used in Europe, including the FIP Recommendations (FIP 1988).

Pajari and Koukkari (1998) conducted ten full-scale tests on floor systems made up of 265 mm deep and 400 mm deep hollow-core slabs supported on various types of steel and precast beams. Their tests demonstrated that the shear resistance of prestressed hollow-core slabs is considerably reduced due to deflection of the supporting beams, typically by 23 to 60%. In all of the load tests, the failure mode was web-shear at the slab ends. They also found that a deflection of the beams as small as L_b/1000 to L_b/300 could cause considerable reduction in the shear resistance of the slabs, even in cases with strengthened slab ends or with reinforced concrete topping. *Pajari and Koukkari* (1998) also noted that deflection of the beams alone cannot qualitatively account for the reduction in web-shear capacity.

Pajari and Koukkari (1998) concluded that the reduction in shear resistance is attributable to the transverse (shear) deformation of the ends of the slabs. In addition, they noted that the

magnitude of the transverse deformation and hence the reduction, depends not only on the deflection of the beam but also on the interaction between the slab ends and the beams. Factors enhancing the shear resistance are weak bond at the bottom of the slabs, better bond at the mid-depth or on top of the slabs, reinforced concrete topping on the floor, filling of the voids at the slabs ends for a relatively long distance, and continuity of the beams.

Finally, they noted that the design of the slab cross-section plays an important role; cross-sections with large voids and thin webs are susceptible to a strong reduction in capacity. This reduction in capacity is so large that it cannot be ignored in design. *Pajari* (1998) addressed this concern, by developing a simple calculation method for analysis and design of hollow-core slabs on beams.

Pajari (2005) examined 49 shear tests performed at the Technical Research Centre of Finland (VTT) on extruded hollow-core slabs specimens in the 200-500 mm depth range, to evaluate the European code, (EC2 2004) and Yang's method, *Yang* (1994). All 49 shear tests selected for review, taken from VTT's extensive shear testing data-base, had ended in a shear-tension failure. According to the 2005 edition of EN-1168 (EN-1168 2005), the web-shear equation found in the Euro-code (EC2 2004) was to be used for assessing the web-shear capacity of hollow-core slabs; however hollow-core slab manufacturers in Europe were required to verify that the web-shear capacities predicted by the Euro-code method (EC2 2004) were in accordance with the results of a standard full-scale shear test found in Annex J, of European Product Standard EN-1168 (EN-1168 2005).

Based on analysis and testing, *Pajari* found that the Euro-code (EC2 2004) method for evaluation of web-shear capacity overestimated the mean shear resistance of all tested slabs. For

200 mm slabs and slabs with flat webs, the overestimation was tens of percent. When the characteristic values of experimental and theoretical resistance were compared, the fit was better but there was still a considerable overestimation for 200 mm slabs and for slabs with flat webs. On the other hand, the Euro-code method (EC2 2004) was over-conservative for 265 mm and 320 mm slabs with circular voids.

Pajari noted that the Euro-code (EC2 2004) method ignores the shear stresses due to the transfer of prestressing force. When these additional shear stresses were taken into account by applying Yang's method, *Yang* (1994), the accuracy for 265 mm and 320 mm slabs with circular voids was the same as the Euro-code (EC2 2004), but much better for the other slabs. Pajari concluded that Yang's method should replace the method in the Euro-code (EC2 2004) for evaluation of the web-shear capacity of hollow-core slabs. In addition, Pajari concluded that the Euro-code method (EC2 2004) should not be used for hollow-core slabs with flat webs without a reduction factor, and it's applicability for use with other types of slabs should be verified either numerically or experimentally prior to use. Finally, Pajari extended Yang's theory to include cases where a layer of strands was above the considered section (in the vertical direction).

Fellinger and Breunese (2005) performed 39 standard shear tests on hollow-core slabs according to Annex J, of European Product Standard EN-1168 (EN-1168 2005). The slab depths varied from 260 mm to 400 mm in depth and the slab specimens were derived from several different manufacturers and therefore had varying cross-sections. The nominal cross-sectional properties were used for the analysis, using the Euro-code (EC2 2004) web-shear equation.

Test results show that all specimens had a shear-tension failure. In addition, *Fellinger and Breunese* (2005) demonstrated that on average, the ratio between the experimental shear-tension

capacity and the design shear-tension capacity was 1.51, with a coefficient of variation (COV) of 24.5%. They also found a large range in the ratio of experimental/predicted shear capacities between the different slab types ranging from 1.12 to 1.93. The COV within one slab type, cast in one batch was much smaller than the entire population, in the range of 1.0 to 9.5%.

Fellinger and Breunese (2005) also noted that the differences in average experimental/predicted load ratio per slab type cannot be explained by a different concrete strength, since the ratio between the estimated actual tensile strength and the design tensile strength used in the calculations of the design shear-tension capacity varied between 2.11 and 2.41. On the contrary, the highest strength ratio of 2.41 corresponds to the slab type with the lowest experimental/predicted load ratio of 1.15. *Fellinger and Breunese* (2005) pointed out that the production process plays an important role on the experimental/predicted load ratio, as the load ratios are fairly consistent for different slab types of the same producer.

Fellinger and Breunese (2005) concluded that modifications to the calculation method for the design shear-tension capacity cannot eliminate the differences in the load ratios between the producers. Notably, the cross-sections and concrete properties of the 400 mm deep slab of *Betonson and Dycore* are very similar, yet the shear-tension capacities were 390 kN and 547 kN respectively. Finally, *Fellinger and Breunese* (2005) noted that sometimes cracks occurred in either the thinnest section of the outer webs, or through the upper flange of the outer hollow-core web. They pointed out that it is expected that both types of cracks have a detrimental effect on the load-bearing capacity.

Pajari (2009) described the procedure which resulted in the design rules adopted in the European Product Standard for hollow-core slabs, EN-1168 (EN-1168 2008). In his article, Pajari

demonstrated that the traditional European design method for web-shear failure can be inaccurate and un-conservative, due to the incorrect assumption that the critical location for web-shear failure exists at the centroid of the webs, and due to the fact that traditional European web-shear design methods ignore the reduction in capacity caused by the horizontal shear stresses, caused by the transfer of the prestressing force into the hollow-core slabs.

Pajari pointed out that one might expect that everyone who agrees that the classic expression for shear stress, $\tau = (VS)/(Ib_w)$ is based on an assumption of constant axial force, would immediately accept Yang's formula for τ , *Yang* (1994), because both are derived in exactly the same way and because there were many who recognized prior to Yang's work the role of the transfer of prestressing on predicting the web-shear capacity. However, Pajari noted that this has not been the case; after publication of Yang's method in 1994, it took more than ten years to include it to product standard EN-1168 (EN-1168 2008).

Pajari added that the traditional European design method for web-shear failure is still present in the Euro-code (EC2 2004). Pajari noted that *Bertagnoli and Mancinci* (2009) have recently shown that the Euro-code (EC2 2004) gives satisfactory results when compared with a great number of shear test results. *Pajari* explained that this seems odd, but it can be explained by the following – In the Euro-code (EC2 2004), the design model for shear-compression failure, which is completely different from web-shear failure, is over-conservative. This model often predicts a lower resistance than the model for web-shear failure. When this lower value is applied to cases in which the actual failure mode is web-shear failure, a safe design is obtained.

Pajari summarized the above observation by stating that in the Euro-code (EC2 2004), the design model for shear-compression failure is over-conservative near the support and un-

conservative in the span, while the model for web-shear failure is un-conservative near the support where it is supposed to be used. Pajari stated that it is obvious that the shear design method for members without shear reinforcement needs to be reconsidered in Europe.

Finally, *Pajari* added that in Finland, separate equations for shear-compression have been published for hollow-core slabs as an SFS standard, that solve the problem of shear-compression model used in the Euro-code (EC2 2004). Pajari concluded by saying that when a formula becomes too familiar, there is a risk that we forget where it comes from and apply it to cases where it should not be applied. This risk was realized when $\tau = (VS)/(Ib_w)$ was applied to the ends of hollow-core slabs. As in all science, to know it is not enough; to correctly apply the knowledge, we must know how the knowledge has been acquired.

2.4 CONCERNS WITH CANADIAN CODE PROVISIONS (CSA 2004)

To the author's knowledge, the current Canadian code shear provisions (CSA 2004) have not been calibrated against an extensive set of shear test data performed on hollow-core slabs. This may be due to the fact that the number of shear tests performed on hollow-core slabs is somewhat limited in comparison to the extensive number of shear tests that have been performed on reinforced and prestressed concrete members in general.

Based on the review of current codes and research performed in North America and in Europe, presented in Sections 2.2, 4.2 and 4.3, it seems clear that the current equations for shear in the Canadian code (CSA 2004) are not appropriate for use in predicting the shear capacity of hollow-core slabs for several reasons. The first reason is that the Canadian shear equations do

not have a separate expression for evaluation of the elastic web-shear capacity of a member that is vulnerable to a shear-tension failure, such as a hollow-core slab.

The second reason is that the current method for shear design in the Canadian code (CSA 2004) attempts to ensure a ductile shear failure in a member, which is easy to achieve for members that are cast with plastic concrete, and in which shear reinforcement can be easily added.

However, vertical shear reinforcement cannot be added to members that are extruded such as hollow-core slabs; the only way to provide ductility in shear for hollow-core slabs is to cast plastic concrete inside the voids, together with additional longitudinal reinforcement that is properly anchored into the supports, which is not practical for the short bearing lengths commonly used with hollow-core slabs, and which adds costs to the product that have not been required in the past.

As noted by *Pajari* (2009), when a formula becomes too familiar, there is a risk that we forget where it comes from and apply it to cases where it should not be applied. In this case, shear testing of full-scale hollow-core slabs is necessary to further calibrate the Canadian code equations (CSA 2004) for shear, and verify if they are indeed being incorrectly applied to hollow-core slabs.

CHAPTER 3 EXPERIMENTAL PROGRAM

3.1 INTRODUCTION

In order to verify the as-cast shear capacity of prestressed hollow-core slabs, a suitable test set-up must be designed to take into account all variables which may contribute either negatively or positively to the shear capacity of the slabs.

Bartlett and MacGregor (2000) list the main factors affecting the shear strength of beams without web reinforcement as: the tensile strength of the concrete, the longitudinal reinforcement ratio, the shear span-to-depth ratio, *a/d*, the size (depth) of the beam, and the presence of axial forces. The two main variables that can be easily controlled in the design of a test set-up for evaluating the shear capacity of hollow-core slabs include the shear span-to-depth ratio and the presence of axial forces in the member. *Bartlett and MacGregor* (2000) note that axial tensile forces tend to decrease the inclined cracking load, whereas the presence of axial compressive forces tends to increase it. In the design of a shear test, a pin and roller support system can be used, to provide relief of any potential axial tensile or compressive forces on the hollow-core slabs during the test.

Bartlett and MacGregor (2000) suggest that ratio of the shear span, *a*, to the reinforcement depth, *d*, can be divided into four types: very short, short, slender and very slender. The term *deep beam* is also used to describe beams with very short and short shear spans. Very short shear spans are categorized by an *a*/*d* ratio from 0.0 to 1.0, where inclined cracks will form joining the load and the support. These cracks, in effect destroy the horizontal shear flow from the longitudinal steel to the compression zone and the behaviour changes from beam action to

arch action, where the reinforcement serves as the tension tie of a tied arch and has a uniform tensile force from support to support. The most common mode of failure in such a beam is an anchorage failure at the ends of the tension tie.

They also note that short shear spans, *a/d* from 1.0 to 2.5, develop inclined cracks and, after a redistribution of internal forces, are able to carry additional load, in part by arch action. The final failure of such beams will be caused by a bond failure, a splitting failure, or a dowel failure along the tension reinforcement, or by crushing of the compression zone over the crack, *a shear-compression failure*. Because the inclined crack generally extends higher into the beam than a flexural crack, failure occurs at less than the flexural moment capacity.

Finally, they mention that in slender shear spans, *a/d* from about 2.5 to about 6.0, the inclined cracks disrupt equilibrium to such an extent that the beam fails at the inclined cracking load, while very slender shear spans with an *a/d* ratio larger than about 6.0 will fail in flexure prior to the formation of inclined cracks.

Therefore, the location of the test load in relation to the support is critical – placing the load too close to the support will permit a large portion of the test load to be carried directly to the support through a compression strut between the load and the support, rather than through shear forces. Moving the load too far from the support will result in a flexural failure, rather than a shear failure.

The selection of the type of load used for a shear test (uniform or concentrated) can also have an effect on the member behaviour. A common approach for shear testing is to use a concentrated point load, resulting in shear forces that are essentially constant between the load and the support

reaction. Since the shear resistance of a prestressed hollow-core slab would theoretically be less near the support, compared to the resistance further from the end of the slab (due to the strand transfer length), this type of loading is generally considered to be more critical in nature than the load effects resulting from a uniformly distributed load, where the shear forces drop as the distance from the support is increased.

As there are no guidelines to date in the Canadian (CSA 2004) or the American codes (ACI 2008) on full-scale shear testing of precast/prestressed hollow-core slabs, the load tests in this research program closely followed the guidelines of the standard hollow-core shear test found in Annex J, of European Product Standard EN-1168 (EN-1168 2008). This standardized test is used in Europe as a quality control measure for hollow-core slab producers to verify the shear capacity of their slabs in relation to the code-predicted (EC2 2004) shear resistance.

3.2 DETAILS OF THE EXPERIMENTAL PROGRAM

3.2.1 Test specimens

The hollow-core test slabs were cast as part of the manufacturer's regular production, using a long-line automated slab extrusion process. In this process, the manufacturer casts approximately 150 metres of slab per line of form, using a hollow-core extruder. The slabs are cast using zero-slump concrete, covered with an insulated tarp and steam cured and saw-cut after the concrete has reached the strength required to cut the strands, typically 18 hours later.

For the testing program, a total of 12 hollow-core slabs, provided by one supplier, were cast in three depths 203, 254 and 305 mm, with four slabs each. The slabs were labelled according to their nominal depth, strand code and length of bearing. The local hollow-core slab manufacturer

that supplied the test specimens uses strand codes, to designate various strand patterns for use in the slabs; the higher the strand code number, the higher the level of prestressing (Appendix A). Slabs that shared a common depth and a common strand code were cast successively on the same line of production to ensure that uniformity in the concrete was achieved for each slab. A summary of the slab identification is listed in Table 3.1.

The slabs were divided into three series based on the slab thickness. Each series consists of four slabs; Series-200 (203 mm thick), Series-250 (254 mm thick) and Series-300 (305 mm thick). The slabs were named such that the first three digits denote the nominal slab thickness, the following two digits denote the strand code used by the manufacturer for the selected strand pattern, and the letter designates the length of bearing at the loaded end of the slab ("A": represents full bearing length (63 mm), "B" represents reduced bearing length (38 mm)). For example, slab 200-01A indicates a 203-mm thick slab, with strand code 01, and 63 mm of bearing at the loaded end, while slab 200-01B indicates a 203-mm thick slab, with strand code 01, and 38 mm of bearing at the loaded end.

3.2.1.1 *Slab Geometry*

The geometry of the slabs varies depending on the type of extruder machinery used in the slab extrusion process. Some extruders produce a cross-section that utilizes round voids, whereas other extruders use a combination of straight and curved profiles to establish the geometry of the voids. Figures 3.1 to 3.3 outline the nominal cross-sections for all test specimens. However, due to production tolerances, and variations in mix consistency, there can sometimes be differences between the nominal and as-cast geometry. To ensure that a high level of accuracy could be achieved in the calculation of predicted slab shear capacities, the as-cast geometry was traced at

the loaded end of all test slabs. For reference, detailed measurements and drawings for each of the as-cast slab geometries have been included in Appendix A.

Table 3.1: Slab Identification

Series	Slab ID	Nominal Slab Depth (mm)	Strand Code	Bearing Length (mm)	Prestress Force/Slab Area at Jacking (MPa)
Series-200	200-01A	203	01	63	2.18
	200-01B			38	
	200-20A		20	63	8.93
	200-20B			38	
Series-250	250-01A	254	01	63	1.97
	250-01B			38	
	250-20A		20	63	8.08
	250-20B			38	
Series-300	300-06A	305	06	63	3.61
	300-06B			38	
	300-18A		18	63	10.21
	300-18B			38	

3.2.1.2 *Slab Properties*

Figures 3.4 to 3.6 outline the nominal section properties for all test specimens. For reference, the as-cast slab section properties have been included in Appendix B. A summary comparison of the geometric and section properties for the nominal and as-cast test slabs is presented in Table 3.2.

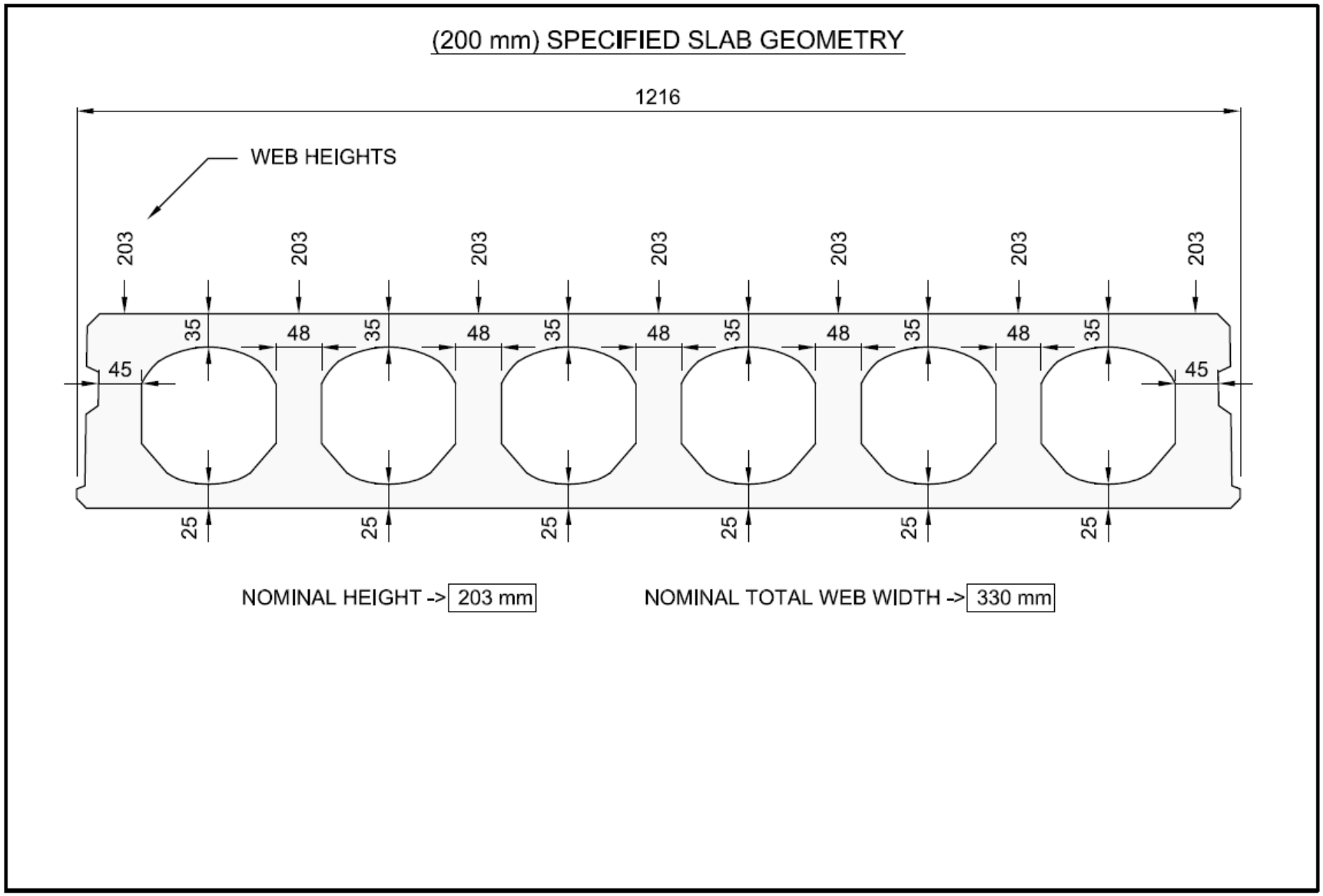

Figure 3.1: Series-200 Specified Slab Geometry

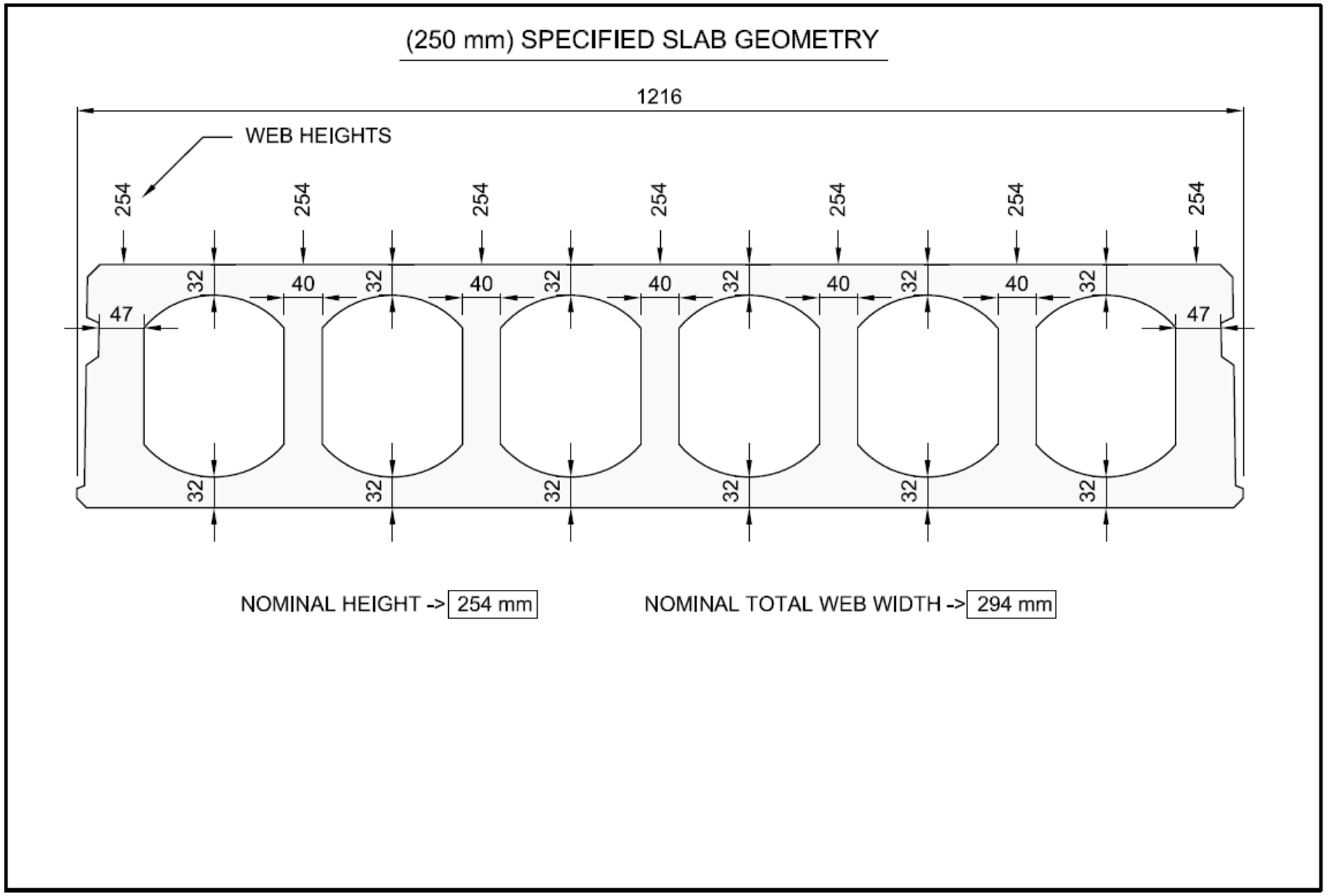

Figure 3.2: Series-250 Specified Slab Geometry

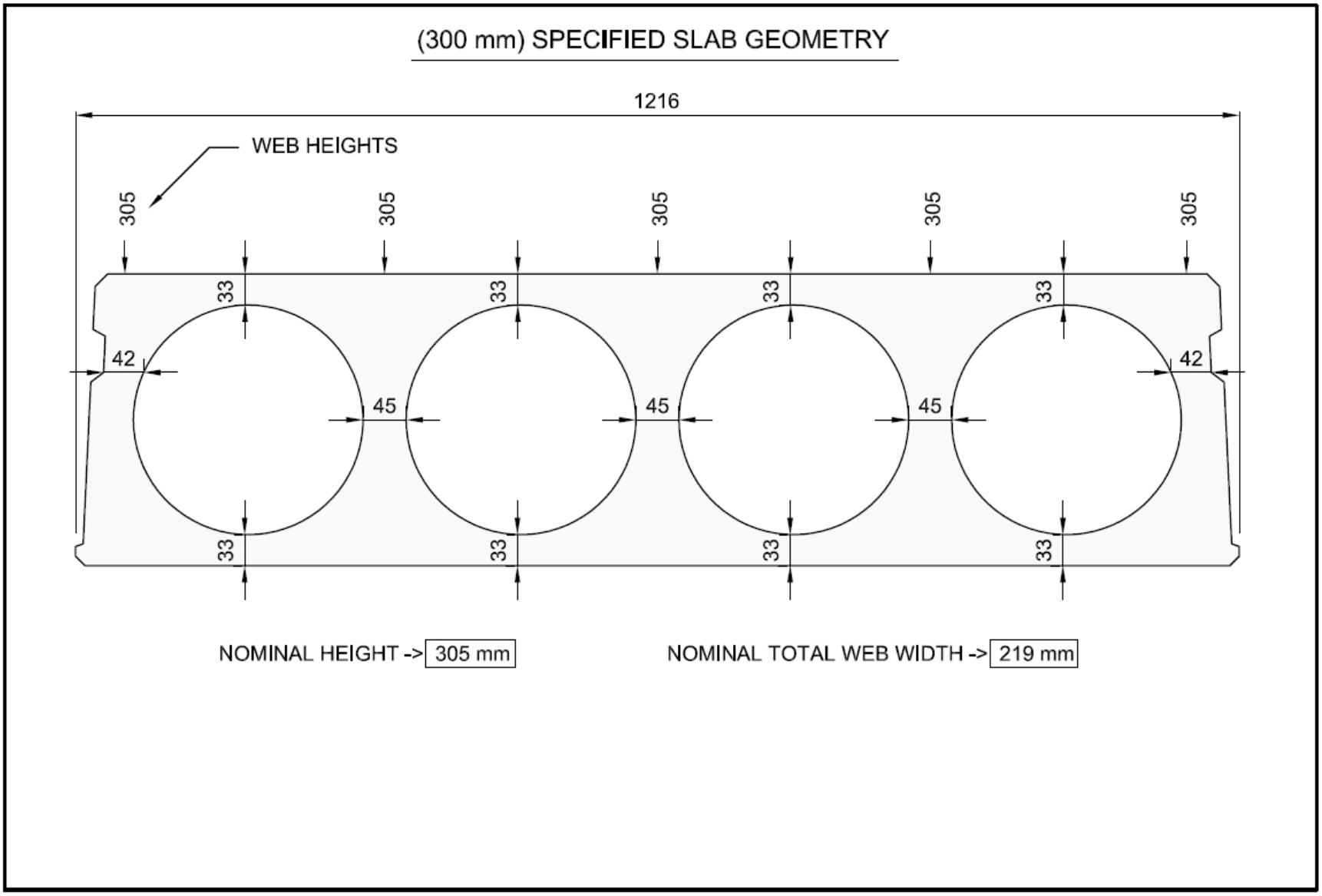

Figure 3.3: Series-300 Specified Slab Geometry

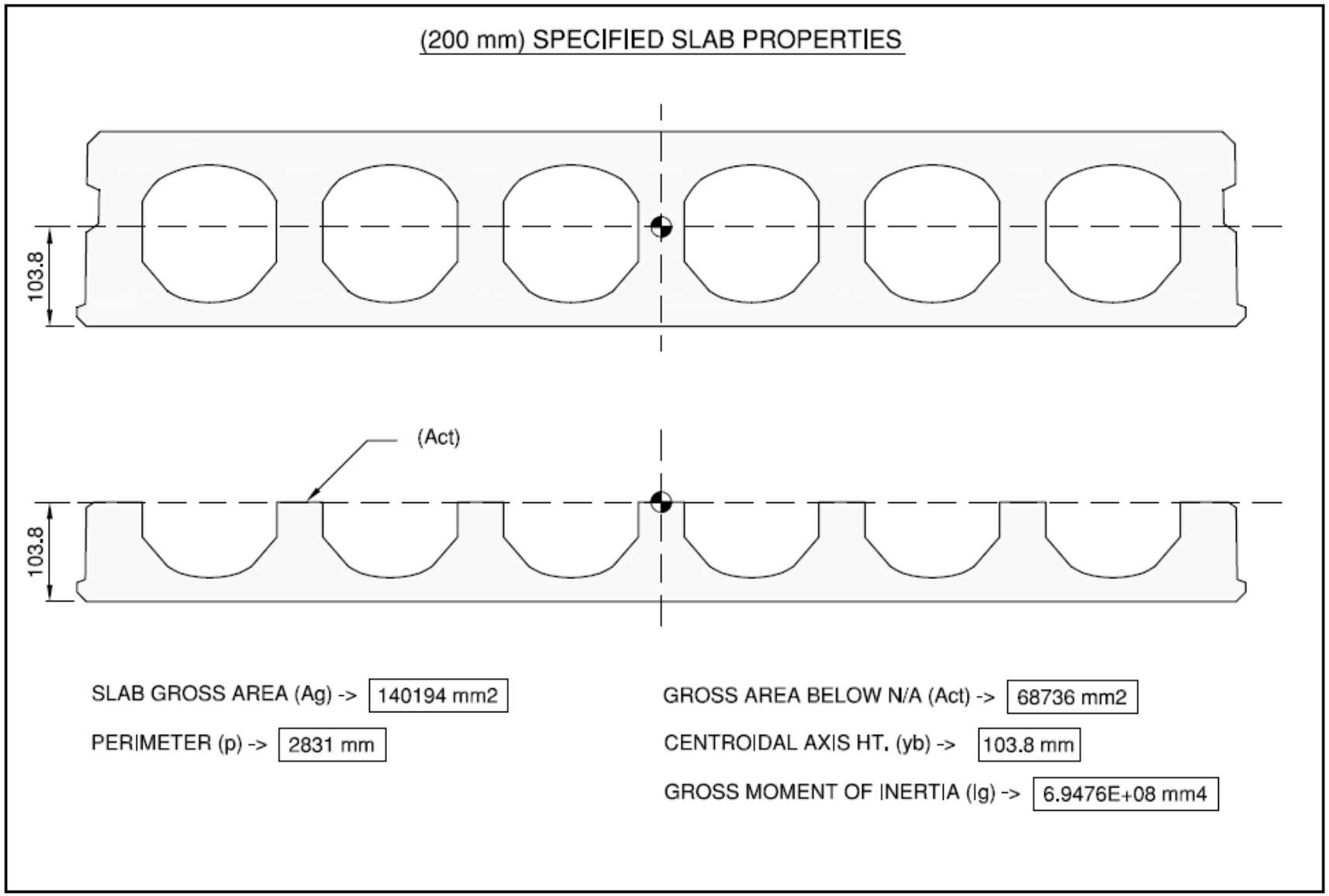

Figure 3.4: Series-200 Specified Slab Properties

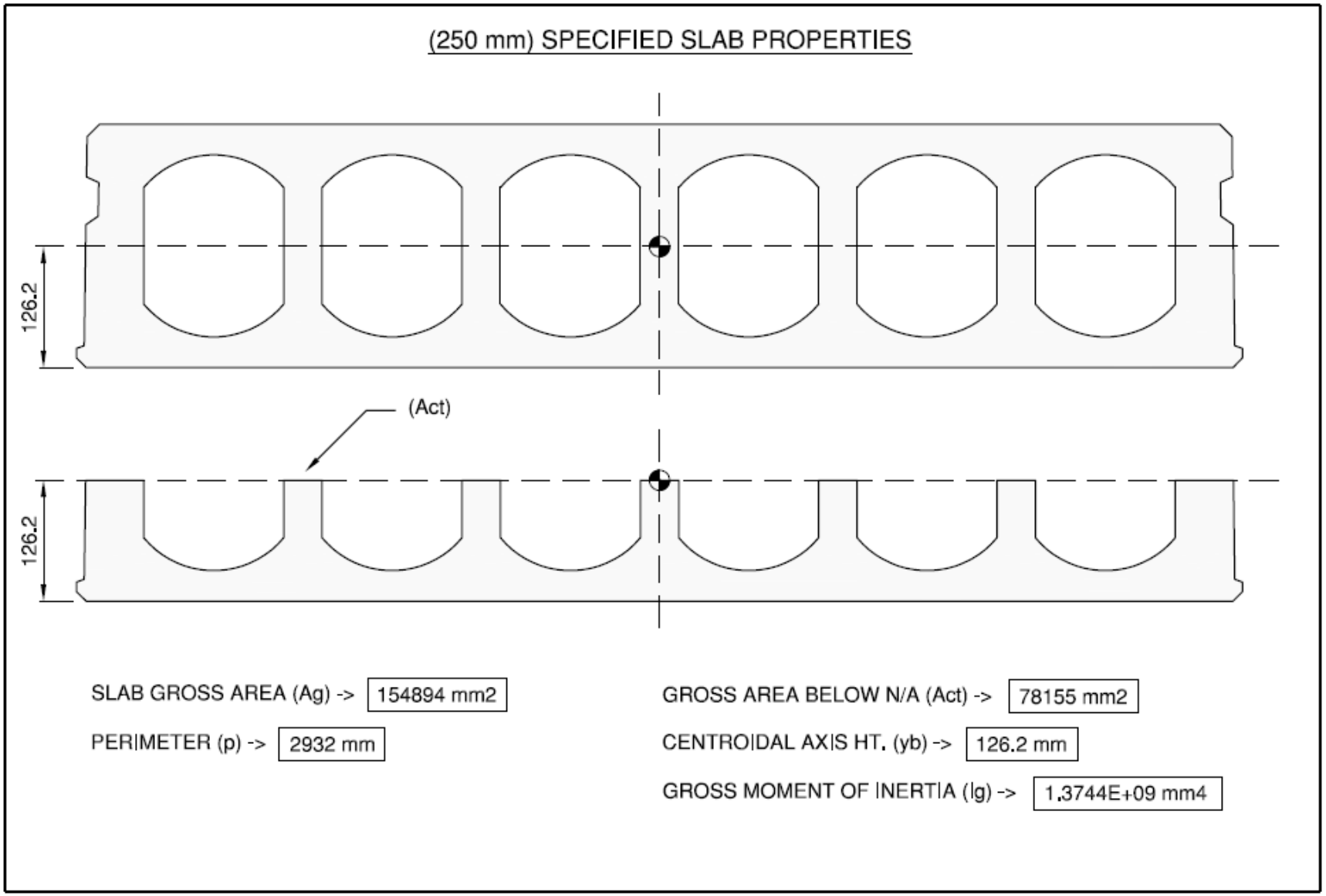

Figure 3.5: Series-250 Specified Slab Properties

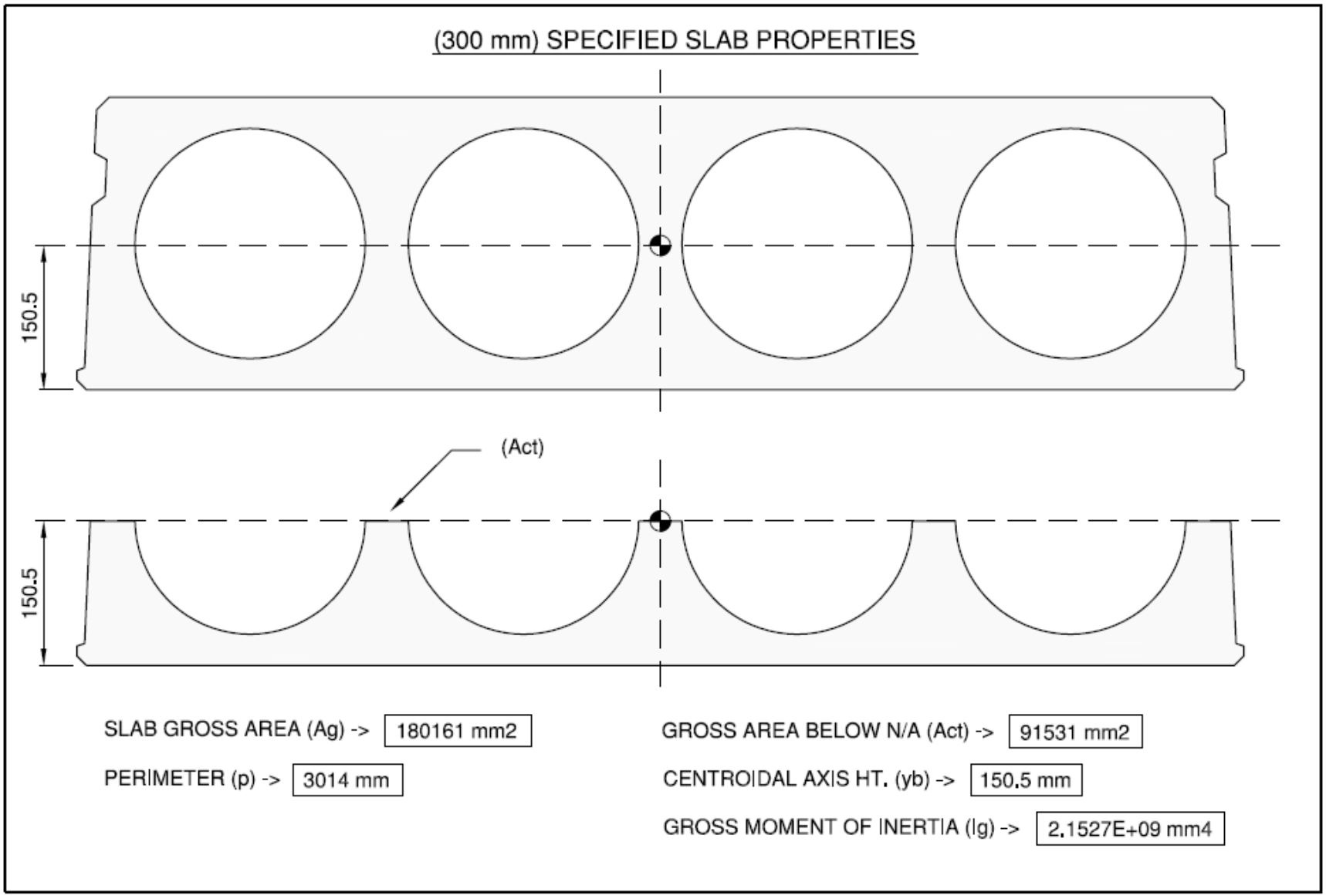

Figure 3.6: Series-300 Specified Slab Properties

Table 3.2: Nominal vs. Experimental Slab Geometry & Section Properties

Slab ID	Average. Height (mm)	Total Web Width (mm)	Slab Gross Area (mm^2)	Flexural Tension Area, A_{ct} (mm^2)	Perimeter (mm)	Centre of Gravity Height-y_{bot} (mm)	Gross Moment of Inertia - I_g (mm^4)
Series-200							
200 (Nominal)	*203.0*	*330*	*140194*	*68736*	*2831*	*103.8*	*6.9476E+08*
200-01A	202.3	341	142385	72378	2806	99.7	6.8825E+08
200-01B	202.0	345	142173	72197	2807	99.8	6.8304E+08
200-20A	202.1	345	143922	72539	2812	100.5	6.9064E+08
200-20B	201.1	346	142305	71942	2800	99.7	6.8008E+08
Series-250							
250 (Nominal)	*254.0*	*294*	*154894*	*78155*	*2932*	*126.2*	*1.3744E+09*
250-01A	253.4	346	180374	88235	2897	128.3	1.3561E+09
250-01B	253.6	340	179201	88898	2892	126.9	1.3556E+09
250-20A	253.3	319	173363	86632	2903	126.1	1.3417E+09
250-20B	253.4	319	173285	86582	2899	126.5	1.3473E+09
Series-300							
300 (Nominal)	*305.0*	*219*	*180161*	*91531*	*3014*	*150.5*	*2.1527E+09*
300-06A	304.8	244	200800	98389	3009	153.3	2.2798E+09
300-06B	305.2	242	200128	98620	3005	153.4	2.2949E+09
300-18A	303.2	257	211552	103542	3024	152.7	2.3403E+09
300-18B	304.6	247	208379	102547	3009	153.4	2.3526E+09

3.2.2 Material Properties

3.2.2.1 *Concrete*

For each set of two slabs sharing a common strand pattern, a total of twelve cylinders were cast; four were tested at one day, four were tested at 28 days and four were tested on the slab test date. In addition, several 150 mm long slab wafers were cut from the slabs on either side of the test slabs for making core samples. A total of twelve 50-mm diameter by 100-mm long cores were made; four were tested at one day, four were tested at 28 days and four were tested on the slab test date. Each core was drilled from the top flange right at a web location, in the direction of the slab length to ensure the cores would be representative of the type of compaction achieved in the same direction of the applied compressive stresses during the load test.

The design concrete strength for the slabs produced by the manufacturers was 28 MPa at 18 hours and 45 MPa at 28 days. The aggregates used for the test slabs were crushed limestone, using a nominal maximum aggregate size of 20 mm for the concrete mix. The angular surface profile of the crushed limestone aggregate provides a very strong interlock between the aggregates and the cement paste, enabling the use of high-strength concrete for the typical hollow-core slab mix. A summary of all concrete strength parameters for each test slab can be found in Appendix C.

It should be noted that in some cases the cylinder strengths on the day of the test were quite low in comparison to core tests, or to the cylinder strengths achieved at 28 days. There may be some variability in the way in which the cylinders are cast, compared to the actual compaction achieved from the extrusion process. Occasionally a cylinder may be cast improperly due to the difficulty in making consistent cylinders with zero-slump concrete, leading to a lower strength value.

When testing cores, the largest core diameter that can be taken from the slabs is limited to 50 mm, due to the web and flange geometry. When assessing concrete strength from the 50 mm diameter cores, there may be an effect on the measured core strength versus the in-place slab concrete strength, due to the small core size in comparison to the 20 mm nominal maximum aggregate size. A review of the concrete test data shows that the core strengths compare reasonably well to the cylinder strengths at release (within 8% on average), and at 28 days (within 5% on average). Therefore, it can be assumed that the core strengths represent a reasonably accurate assessment of the concrete compressive strength of the as-cast hollow-core slabs, especially in cases where the cylinder strengths appear too low.

It was noted during the testing of the cores taken from individual webs, that the concrete strength varied both along the length of the slab and also from web to web. This is likely due to the way the slabs are extruded, since some webs receive more compaction than others during the extrusion process. Depending on the length of the slab, the concrete within the slab may also be from two separate concrete batches.

Due to the fact that there is some scatter in the as-cast concrete strengths of the test specimens (see Appendix C), for analysis, it would be more appropriate to consider a range of concrete

strengths when comparing failure loads to predicted capacities. In addition, varying the concrete strength over a range of values allows for an evaluation of the sensitivity of the concrete strength in the shear equations for each code. For the code analysis calculations performed in Chapter 4, the concrete compressive strength was varied in increments of 5 MPa, from 65 MPa up to a maximum of 90 MPa. In practice, for design a single value for the 28-day compressive strength is selected based on a statistical analysis of cylinder and core samples, using standard mix designs.

3.2.2.2 *Reinforcement*

The strands used for the test slabs were 9 mm, 13 mm, or 15 mm seven-wire, 1860 MPa low-relaxation strands. Strand from the same reels was intended to be used for all twelve test slabs, to ensure uniformity of strand strength and bond characteristics. However, due to production constraints, two of the 254 mm test slabs were cast using different strand. A summary of the strand properties is given in Appendix D.

3.2.3 Test Set-Up and Procedure

The load test set-up used in this research program closely followed the guidelines of the standard hollow-core shear test found in Annex J, of European Product Standard EN-1168 (EN-1168 2008). A schematic elevation of the typical test set-up is outlined in Figure 3.7. The test slabs were made up of full-width elements with a nominal slab length of 4000 mm for both the 203 and 254 mm deep slabs, and a nominal slab length of 4575 mm for the 305 mm slabs. A detailed set of elevation sketches showing the as-cast slab lengths, location of test load and bearing lengths are included in Appendix E for reference.

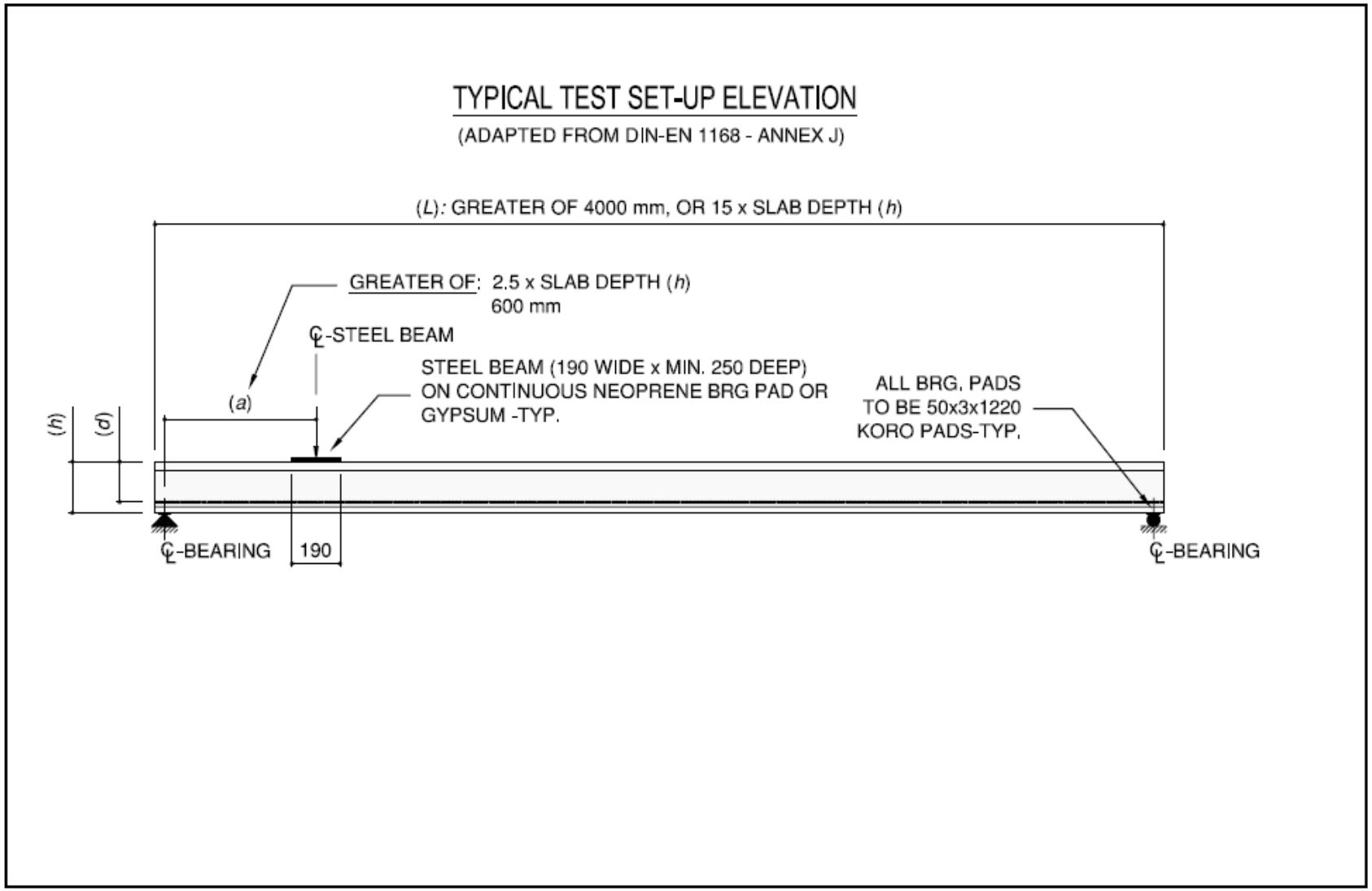

Figure 3.7: Elevation of Typical Test Set-Up for Full Scale Shear Test

As noted in Section 3.1, slender shear spans with an *a/d* ratio between 2.5 and 6.0, typically fail in shear at the inclined cracking load. To ensure the observed test loads at failure are not falsely increased by the beneficial effects of arching action between the load and the support, an *a/d* ratio larger than 2.5 should be used for the test set-up. A summary of the *a/d* ratios selected for testing of each of the nominal slab depths, with the full bearing length at the loaded end of the slabs is presented in Table 3.3.

Table 3.3: Ratio of *a/d* for Nominal Test Slab Depths with Full Bearing Length at Loaded End

Nominal Slab Height, *h* (mm)	Slab Bearing Length at Test End (mm)	* Nominal Depth to Strands, *d* (mm)	Shear Span, *a* (mm)	Shear Span-to-Depth Ratio *(a/d)*	Shear Span-to-Height Ratio *(a/h)*
203	63	158	600	3.80	2.96
254	63	209	635	3.04	2.50
305	63	260	763	2.93	2.50
305	63	250	763	3.05	2.50

***** *Note: 305 mm slabs have either one or two layers of strands*

The length of bearing (defined as the distance from the end of the slab to the face of the bearing pad) at the loaded end was 63 mm for slabs in series "A" (to represent the standard detailed bearing length) and 38 mm for slabs in series "B" (to represent potential reduced bearing on-site), as shown in Figure 3.8. The length of bearing at the opposite end of the test load was 63 mm for all test slabs.

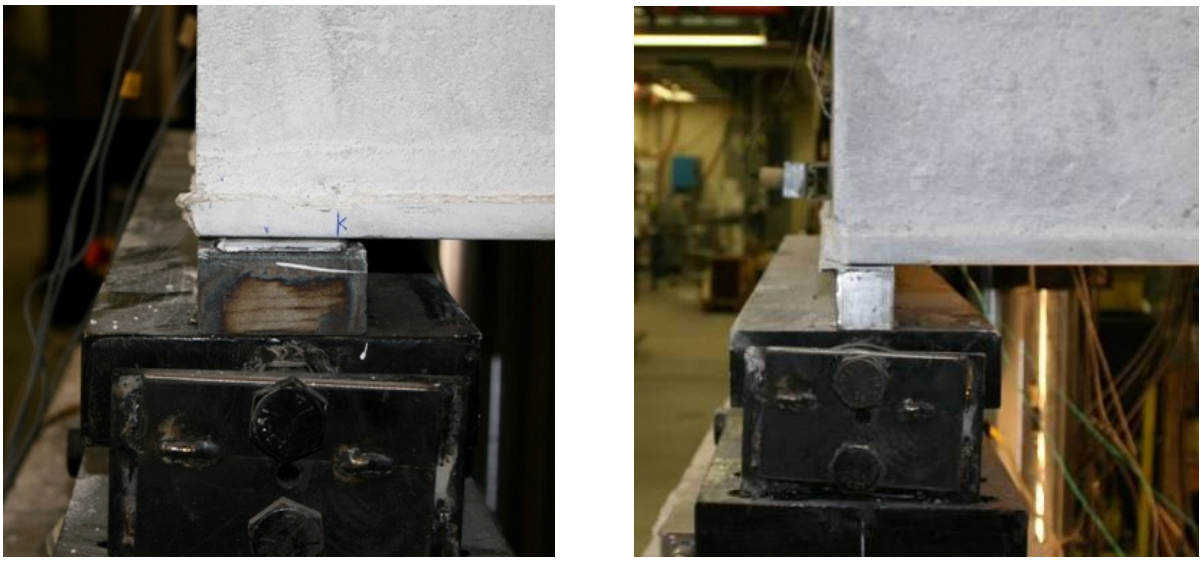

Figure 3.8: Tested End of Slab with 63 and 38 mm Bearing

The support conditions emulated a pin at the loaded end of the slab and a roller at the opposite end, to eliminate any axial forces that may have been caused by rotation and restraint of the element at the supports (Figures 3.9 to 3.11).

Figure 3.9: Pin Assembly at Loaded End of Test Slab

Figure 3.10: Elevation of Pin Assembly at Loaded End of Test Slab

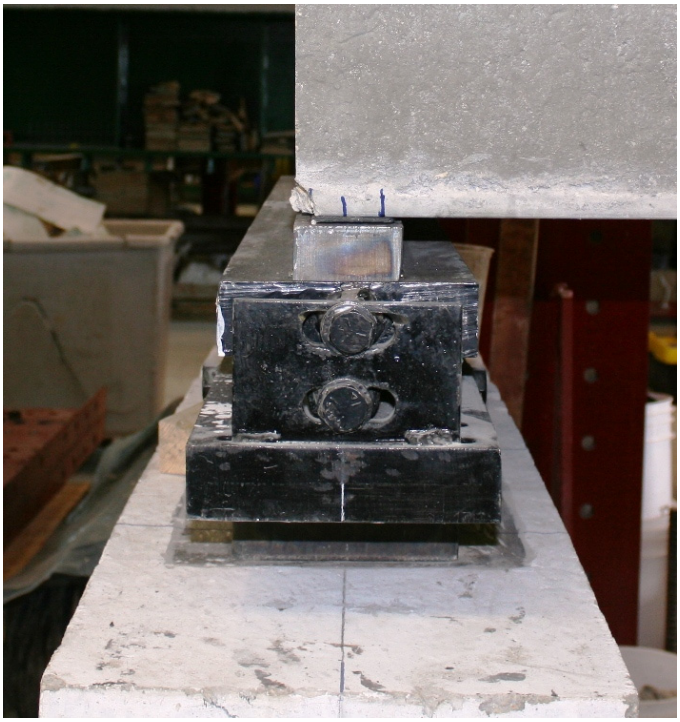

Figure 3.11: Roller Assembly at Opposite End of Test Slab

The slabs were loaded with a stiffened 254-mm deep I-Section steel beam across the full width of the cross-section, with the load applied at a specific distance from the end of the slabs as shown in the test elevations in Appendix E.

A neoprene pad or a layer of plaster was placed between the slab and the steel beam, to prevent load concentrations and ensure the load was uniformly distributed across all webs during loading. A 190-mm wide continuous steel plate was welded to the bottom flange of the steel loading beam, to emulate the width of a load-bearing concrete masonry wall – a common condition in the local region for slabs with high shear loads. A photograph of the typical test set up is shown in Figure 3.12.

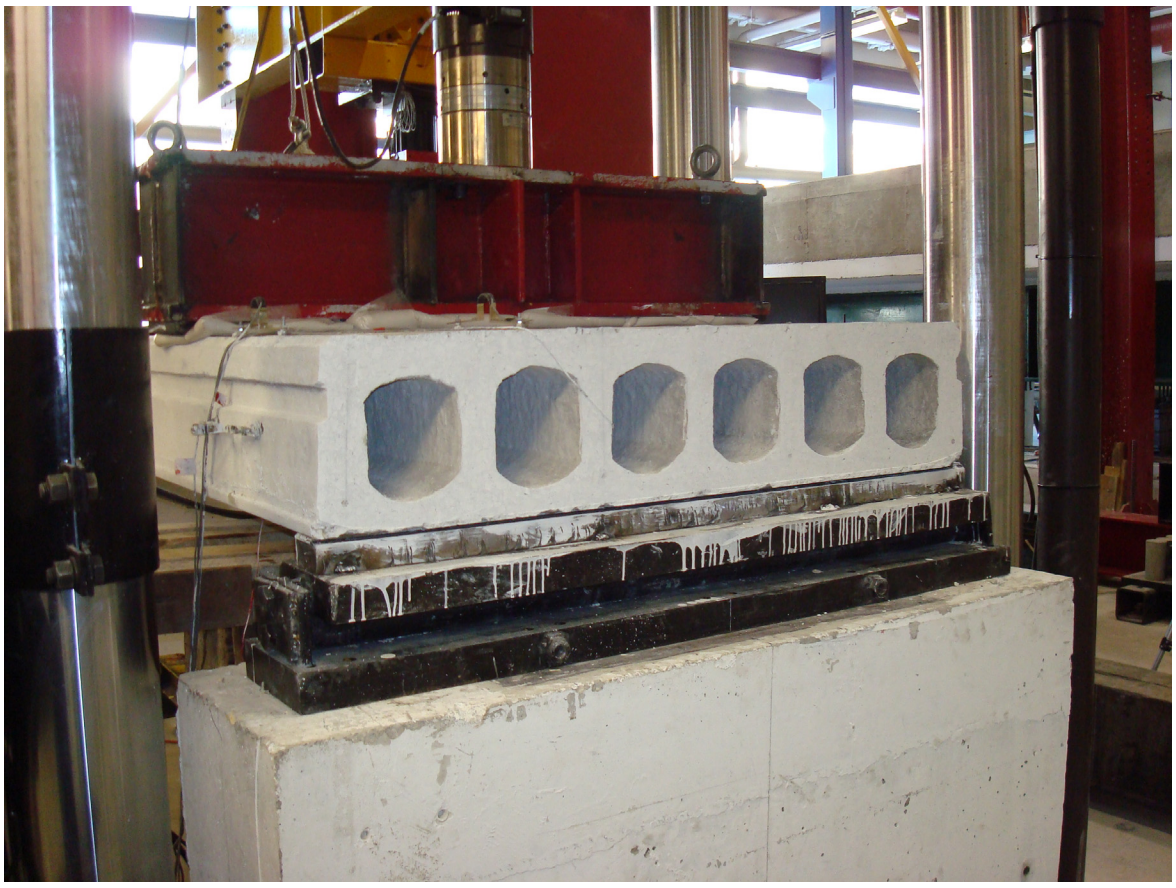

Figure 3.12: Typical Set-up and Instrumentation for Hollow-Core Slab Shear Tests

The guidelines of the standard hollow-core shear test in Annex J, of European Product Standard EN-1168 (EN-1168 2008), require that the test load be applied as repeated loading in two cycles – the amplitude of the loading in the first cycle should be at least 70% of the predicted failure load. In the second load cycle, the load should be increased until failure is reached. The speed of the loading of the element should not exceed the following:

- For the first cycle:
    - Two steps of equal amplitude in one minute each and subsequent withdrawal of the load.
- For the second cycle:
    - A first step up to 50% of the calculated ultimate load in one minute.
    - A second step up to 75% of the calculated ultimate load in one minute.
    - A subsequent increase of the test load with speed not exceeding 10% of the calculated ultimate load per minute.

The test slabs for this research project were initially loaded up to 70% of the predicted failure load for two successive cycles (one additional cycle than specified), while the load was increased up to failure during the third (final) cycle. A 5000-kN MTS testing machine was used to apply the load under a load-controlled rate of 20 kN/min.

3.2.4 Instrumentation

Each slab was instrumented at the loaded end, with strain gauges on several strands (installed by drilling through the concrete cover and bonding the gauges directly onto the bottom surface of the strands). PI-gauges were installed onto the side of selected webs and on the top surface of the same webs. Also, two linear variable displacement transducers (LVDTs) were installed on the slabs; one to measure mid-span deflection and the second to measure end slippage of one of the strands at the loaded end. In addition, two load cells were placed at the bearing plate (support) close to the loaded end of the slab for the first few test slabs to verify the reactions were in agreement with the applied test loads.

The data collected from all gauges and instrumentation will be reviewed and analyzed in conjunction with predicted strains from a detailed finite element analysis in a subsequent research project. The bearing details, slab instrumentation and failure profiles at the underside of each of the test slabs are outlined in Appendix F; all shown at the tested end of the slabs.

CHAPTER 4 ANALYSIS USING CODE PROVISIONS

4.1 BACKGROUND

Prior to casting of the test specimens, in order to arrive at a lower-bound level of prestressing, the nominally specified slab cross sections were initially analyzed using the software program "Concise Beam" (*Black Mint Software* 2010), assuming a concrete compressive strength equivalent to the specified 28-day design strength of 45 MPa. In each case, a shear failure mode was predicted by the Canadian code (CSA 2004) for the selected prestressing levels used in each of the test slabs. For the analysis, the test load was modelled as a 190 mm-long line load across the full slab width and was increased until the maximum shear force reached the shear capacity of the slabs between the end of the slab and the test load.

4.2 CSA A23.3-04 (CSA 2004) CODE-PREDICTED SHEAR RESISTANCE

Each of the twelve test specimens were analyzed with the Canadian code (CSA 2004) using the as-cast material, geometric and section properties, as outlined in Chapter 3. To assist in the analysis procedure, a spreadsheet was written to perform a complete analysis of the predicted shear resistance of each specimen, using the relevant provisions of the Canadian code (CSA 2004). For reference, the following is an outline of the procedure used for assessing the shear capacity of a prestressed hollow-core slab, according to the CSA A23.3-04 Canadian code (CSA 2004).

4.2.1 Critical Section for Shear

Clause 11.3.2 permits sections located less than a distance d_v from the face of the support to be designed for the same shear, V_f, as that computed at a distance d_v, provided that:

(a) The reaction force in the direction of applied shear introduces compression into the member; and

(b) No concentrated load that causes a shear force greater than $0.3\lambda\phi_c\sqrt{f_c'}b_w d_v$ is applied within the distance d_v from the face of the support.

The above clause relates to the critical section for shear force; the critical section for shear resistance (which is also considered by the code to be at a distance d_v from the face of the support) is highlighted in Section 4.2.3.

4.2.2 Strand Transfer Length and Prestressing Losses

The transfer length can be defined as the distance from the end of the member to the point where the force in the prestressing strands is fully transferred to the concrete through bond. Clause 11.2.11 of the code states:

In pre-tensioned members, the reduction in prestress in the transfer length of prestressing tendons shall be considered when computing V_p, f_{po}, and the tensile force that can be resisted by the longitudinal reinforcement. The prestress force may be assumed to vary linearly from zero at the point at which bonding commences to a maximum at a distance from the end of the tendon

equal to the transfer length, assumed to be 50 diameters for strand and 100 diameters for a single wire.

Clause 12.9.1 of the code defines the development length, ℓ_d of prestressing strands as:

$$\ell_d = 0.145\ (f_{pr} - 0.67 f_{pe})\ d_b \qquad [4.1]$$

In lieu of using a fixed value of 50 strand diameters for the transfer length, the code commentary for Clause 12.9.1 derives an expression for the transfer length based on the effective stress in the prestressing tendons after allowance for all prestressing losses, f_{pe}, and the strand diameter, d_b, as follows:

$$\ell_t = 0.0048\ f_{pe}\ d_b \qquad [4.2]$$

A value of ℓ_t was calculated based on each of the strand diameters present in the test slabs, using Equation 4.2. For the slabs tested with a reduced amount of bearing, the predicted shear capacity was slightly lower as compared to the slabs with full bearing, since the critical section for shear (taken at d_v from the face of the bearing pad) would move closer to the slab end resulting in slightly less prestressing force in the strands at the critical section.

Regarding the calculation of the prestress losses, the detailed method for calculating losses found in the CPCI Design Manual (CPCI 2007) was used to assess the reduction of prestressing force, for the analysis using the Canadian code. The mix designs from the supplier were used to evaluate the factors in the loss equations, and zero-slump concrete was assumed as one of the parameters.

4.2.3 Shear Resistance Equations

The factored shear resistance for a prestressed hollow-core slab is calculated based on the following expression, found in Clause 11.3.3:

$$V_r = V_c + V_s + V_p \qquad [4.3]$$

Where V_r is the factored shear resistance of the member, V_c is the concrete contribution to shear resistance, based on tensile stresses transmitted across cracks via aggregate interlock (factored by ϕ_c), V_s is the shear resistance provided by shear reinforcement (factored by ϕ_s), and V_p is the component in the direction of the applied shear of the effective prestressing force (factored by ϕ_p). For a hollow-core slab, there is no shear reinforcement and the strand profile is horizontal, therefore V_s and V_p both equal zero. Therefore, for a hollow-core slab the shear resistance is simply based on the concrete contribution alone:

$$V_r = V_c \qquad [4.4]$$

To evaluate V_c, the following expression from Clause 11.3.4 is used:

$$V_c = \phi_c \lambda \beta \sqrt{f_c'} b_w d_v \qquad [4.5]$$

For design, the material resistance factor, ϕ_c is taken as 0.70 for products manufactured in a certified plant, however for the analysis of the hollow-core test slabs, a value of 1.0 was used for ϕ_c. The term λ is a factor that accounts for low-density concrete, which does not apply to any of the test slabs, therefore a value of 1.0 was used for λ. Equation 4.5 then reduces to:

$$V_c = \beta\sqrt{f_c'}\,b_w d_v \quad [4.6]$$

In the above expression, the concrete strength for shear calculations is limited to a maximum of 64 MPa, which is implied by the requirement found in Clause 11.3.4: *In the determination of V_c, the term $\sqrt{f_c'}$ shall not be taken greater than 8 MPa*. This limit has been set because aggregate interlock is less effective for higher strength concretes.

In the case of the hollow-core test slabs, the 64 MPa limit on f_c' was removed and the concrete compressive strength was varied from 65 MPa up to a maximum of 90 MPa in increments of 5 MPa, to evaluate the effect of concrete strength on the predicted slab shear capacity and to account for the variability of the tested concrete strengths in each slab. The range of concrete strength was selected to reflect the observed strengths obtained from core and cylinder tests for the test specimens, which turned out to be much higher than the initially assumed 28-day strength of 45 MPa (Appendix C).

In Equation 4.6, b_w represents the minimum effective web width. Clause 11.2.10.4 permits a slight increase for b_w, for members with tapering webs – however, since the permissible increase in web width is very marginal for a hollow-core slab, b_w was simply taken as the sum of the minimum web widths across the slab width, based on the as-cast geometry (Appendix A). The term d_v is defined as the effective shear depth, taken as the greater of $0.9d$, or $0.72h$.

The value of β in Equation 4.6 is determined using Clause 11.3.6.4 as follows:

$$\beta = \frac{0.40}{(1+1500\varepsilon_x)} \bullet \frac{1300}{(1000+s_{ze})} \quad [4.7]$$

Where ε_x is the longitudinal strain at mid-depth of the member due to factored loads (positive when tensile) and s_{ze} represents an equivalent value of s_z, which allows for the influence of aggregate size. s_z is a crack spacing parameter, that is dependent on the crack control characteristics of the longitudinal reinforcement. The equations for s_{ze} and s_z that are applicable to hollow-core slabs are outlined below:

$$s_{ze} = \frac{35 s_z}{(15 + a_g)} \geq 0.85 s_z \quad [4.8] \qquad\qquad s_z = d_v \quad [4.9]$$

In Equation 4.8, a_g is the specified nominal maximum size of the coarse aggregate. Clause 11.3.6.4 requires that the value of a_g be reduced to zero, if f_c' exceeds 70 MPa. In addition, a_g shall be linearly reduced to zero, as f_c' goes from 60 to 70 MPa. For the analysis of the test slabs using the Canadian code, the above reduction factors were applied to a_g, as required.

The angle of inclination, θ, of the diagonal compressive stresses is calculated with the following expression:

$$\theta = 29 + 7000 \varepsilon_x \quad [4.10]$$

As a conservative simplification to the detailed calculations of Clause 11.3.6.4, Clause 11.3.6.2 permits the use of a value for β equal to 0.21 for slabs or footings, with an overall thickness not greater than 350 mm (for which the hollow-core test slabs would qualify). For the analysis of the test slabs, all calculations were performed using the detailed method in Clause 11.3.6.4; however, for reference the predicted shear capacity using Clause 11.3.6.2 was calculated for

comparison with the values calculated with the detailed method. A plot of each of these shear capacity curves is presented in Section 4.2.5.

The variable ε_x is evaluated using clause 11.3.6.4, based on the following expression:

$$\varepsilon_x = \frac{M_f / d_v + V_f - V_p + 0.5N_f - A_p f_{po}}{2(E_s A_s + E_p A_p)} \qquad [4.11]$$

In the numerator of Equation 4.11, M_f equals the moment due to factored loads at the considered section, d_v is the effective shear depth, V_f is the factored shear force at the considered section and V_p is the component in the direction of the applied shear of the effective prestressing force. N_f is the factored axial load normal to the cross-section occurring simultaneously with V_f, including the effects of tension due to creep and shrinkage (positive for tension).

Finally, A_p is the total area of tendons on the flexural tension side of the member (A_p is constant along the member length) and f_{po} is the stress in the prestressing tendons when the strain in the surrounding concrete is zero (may be taken as $0.70f_{pu}$ for bonded tendons outside the transfer length, where f_{pu} equals the specified tensile strength of the prestressing tendons = 1860 MPa, per Clause 2.3). For the analysis of the test specimens, f_{po} was calculated using a value of 0.70 f_{pu}, and f_{po} was varied from zero at the end of the slab, to a maximum value at the transfer point.

Recalling Equation 4.11:

$$\varepsilon_x = \frac{M_f / d_v + V_f - V_p + 0.5N_f - A_p f_{po}}{2(E_s A_s + E_p A_p)} \qquad [4.11]$$

The denominator of the above expression represents the axial stiffness of a member with tensile strains, which assumes that the axial stiffness of the cracked concrete is essentially zero. The terms E_s and E_p are the modulus of elasticity of the non-prestressed and prestressed reinforcement, respectively. While, the terms A_s and A_p are the total areas of the non-prestressed and prestressed reinforcement, respectively.

For hollow-core slabs, only prestressing strands are used as reinforcement - therefore $A_s = 0$. In addition, the strands are horizontal - therefore $V_p = 0$ and finally in the tested condition, there is no axial tensile restraint - therefore $N_f = 0$. Equation 4.11 becomes:

$$\varepsilon_x = \frac{M_f / d_v + V_f - A_p f_{po}}{2(E_p A_p)} \qquad [4.12]$$

Clause 11.3.6.4 lists a number of conditions that apply to Equation 4.12. The applicable conditions pertaining to hollow-core slabs are listed below:

(a) V_f and M_f are positive quantities, and M_f shall not be taken less than $(V_f - V_p)\, d_v = V_f\, d_v$.

(b) If the value of ε_x calculated from Equation 4.12 is negative (compressive strain), it shall be taken as zero, or the value shall be recalculated with the denominator replaced as shown below (Equation 4.13), however ε_x shall not be taken as less than -0.20×10^{-3}:

$$\varepsilon_x = \frac{M_f / d_v + V_f - A_p f_{po}}{2(E_p A_p + E_c A_{ct})} \qquad [4.13]$$

In Equation 4.13, A_{ct} is defined as the area of concrete on the flexural tension side of the member. For the analysis of the test slabs, Equation 4.13 was used to re-evaluate the calculated strain, ε_x, in cases where the initial evaluation of strain by Equation 4.12 yielded a compressive strain.

(c) For sections located closer than d_v to the face of the support, the value of ε_x calculated at d_v from the face of the support may be used in evaluating β and θ. This implies that the critical section for shear-resistance is at d_v from the face of the support.

(d) ε_x shall not be taken greater than 3.0×10^{-3} (maximum permitted tensile strain).

4.2.4 Tensile Anchorage Check at Supports

Clause 11.3.9.5 requires a specific anchorage check of the longitudinal reinforcement at exterior direct bearing supports. Since hollow-core slabs have no shear reinforcement, the strands must be capable of resisting the tension across a potential shear crack adjacent to the support, to ensure a ductile shear failure.

According to the code, the longitudinal reinforcement on the flexural tension side of the member shall be capable of resisting a tensile force, T_f, of:

$$T_f = (V_f - 0.5\ V_s - V_p)\ \cot\theta + 0.5\ N_f \qquad [4.14]$$

Where θ is as specified in Clause 11.3.6 (Equation 4.10). The tension force in the reinforcement shall be developed at the point where a line inclined at an angle θ to the

longitudinal axis and extending from the inside edge of the bearing area intersects the centroid of the reinforcement (Figure 4.1).

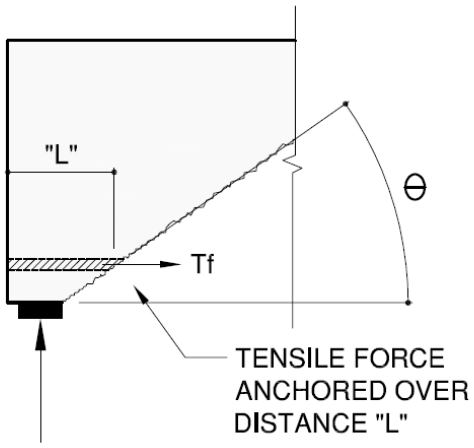

Figure 4.1: Anchorage of Strands at End Supports (Reproduced from CSA A23.3-04)

For the test slabs, V_s, V_p and N_f are all zero, which reduces the anchorage equation to the following:

$$T_f = (V_f)\cot\theta \qquad [4.15]$$

The tensile resistance of the strands, T_r, was found by pro-rating the stress in the strands at the distance "L" from the end of the slabs with the full value of the effective prestressing force at the transfer point. The results of these calculations are presented in Chapter 5, in comparison with the predicted and experimental failure loads.

4.2.5 Shear Resistance Diagrams

For reference, the shear-force and code-predicted shear-resistance diagrams using the Canadian code (CSA 2004) are shown for all test slabs in Figures 4.2 to 4.13 for a concrete compressive strength of 65 MPa, to reflect the approximate point at which limits on concrete strength for shear begin to apply in the Canadian code.

However, as noted in Section 4.2.3 the analysis was performed for the full range of concrete compressive strengths from 65 MPa to 90 MPa (in increments of 5 MPa), to evaluate the effect of the concrete strength on the predicted slab shear capacity and to account for the variability of the tested concrete strengths in each slab.

The shear-force and shear-resistance diagrams presented in Section 4.2.5 include the following information:

- $V_{(x)}$ represents the theoretical (factored) shear force, V_f, due to the effects of the test load and the member self weight, that would initiate a shear failure based on the code equations.

- V_c is the predicted shear resistance using the detailed shear method of Clause 11.3.6.4.

- The location of the critical section (at $x = d_v$ from the face of the support) is also plotted on the shear-resistance diagrams for each test slab.

- Finally, values for the predicted shear resistance using the simplified shear method as per Clause 11.3.6.2 of the Canadian code (CSA 2004) have been plotted on the shear-resistance diagrams for reference *(V_c-Simplified)*.

For a given concrete strength, the typical shear-resistance curves, V_c, calculated using the Canadian code (CSA 2004) derive their shape based the value of β in Equation 4.7, which is inversely proportional to the longitudinal strain demand, ε_x, on the member. As the longitudinal strain in the member approaches tensile values, there is a steep drop in the value of β, which sharply reduces the member shear capacity, V_c. However, as ε_x approaches the code maximum permitted tensile strain of 3.0×10^{-3}, the drop in β occurs at a lesser rate.

Peaks in the shear resistance curves result from increasing longitudinal compression strains (or moving away from tensile strains), which rapidly increases the value of β, and therefore the member shear capacity, V_c. Additional factors affecting the shape of the shear-capacity curves derived from the Canadian code (CSA 2004) for hollow-core slabs include the variables listed in Equations 4.8, 4.12 and 4.13 as well as the conditions listed in Clause 11.3.6.4, that are applied to Equation 4.12 (Section 4.2.3).

Based on the analysis of the test slabs, there is a marginal difference in the code-predicted capacities for the slabs with the reduced bearing in comparison with those with the full bearing, due to the location of the critical section along the transfer length in relation to the end of the slabs. Slabs with reduced bearing typically had slightly lower predicted shear capacities. It should be noted that there are also some differences in predicted capacities between slabs cast on the same production line, due to the use of the as-cast geometric and section properties for each of the test slabs.

The following sections outline the predicted shear-resistance for each series of test slabs using the Canadian code (CSA 2004).

4.2.5.1 *Shear Resistance Diagrams for Series-200 Hollow-Core Slabs*

The shear-resistance diagrams for slabs 200-01A, 200-01B, 200-20A and 200-20B are outlined in Figures 4.2 to 4.5. It is evident from the figures that the code-predicted shear capacities for slabs 200-01A and 200-01B (slabs with the least amount of prestressing) are only about half the values of slabs 200-20A and 200-20B. The predicted capacities for slabs 200-01A and 200-01B using the detailed method of Clause 11.3.6.4 are even lower than the conservative values assumed in Clause 11.3.6.2 (V_c-*Simplified*). However, the shear-resistance curves for slabs 200-20A and 200-20B are well above the V_c-*Simplified* capacity curve, since the strain demand on these slabs is less due to the high level of prestressing.

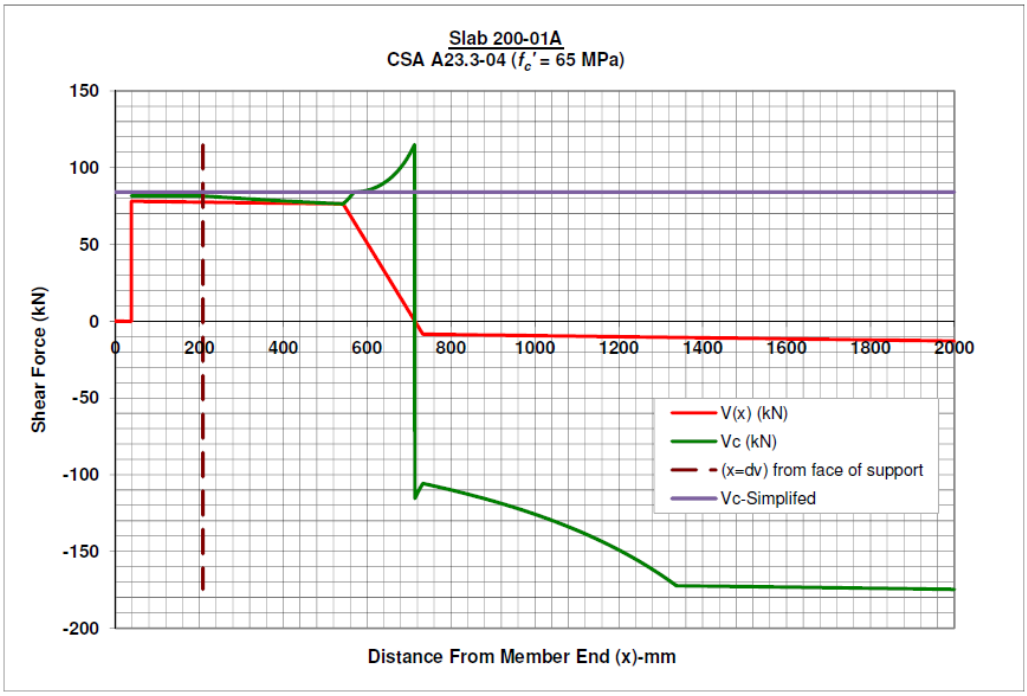

Figure 4.2: Slab 200-01A - CSA A23.3-04 Predicted Shear Resistance at f_c' = 65 MPa

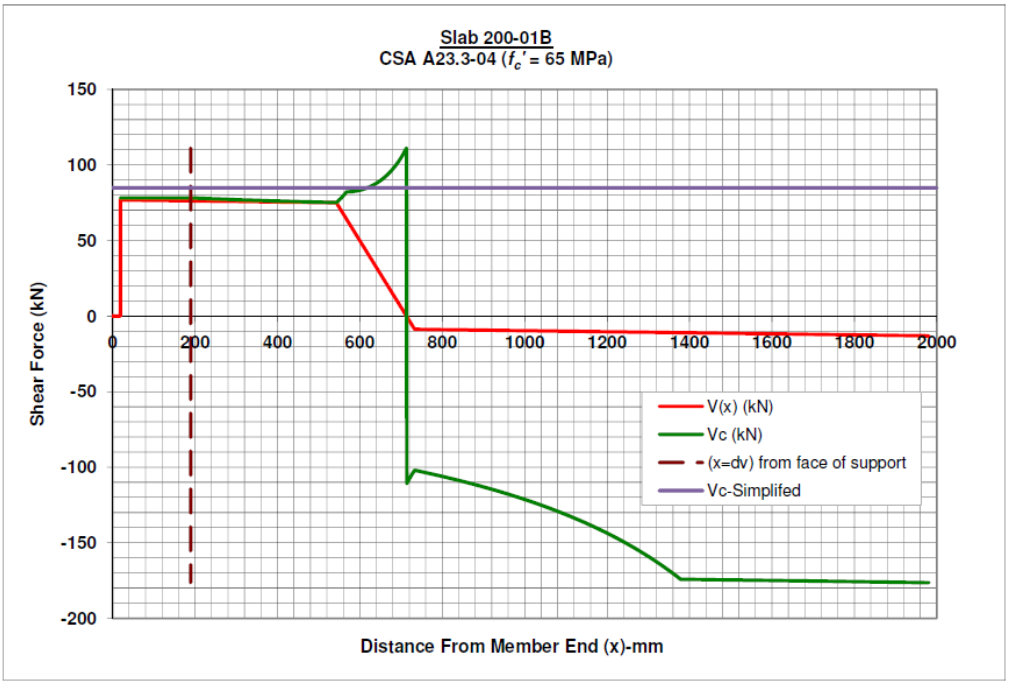

Figure 4.3: Slab 200-01B - CSA A23.3-04 Predicted Shear Resistance at f_c' = 65 MPa

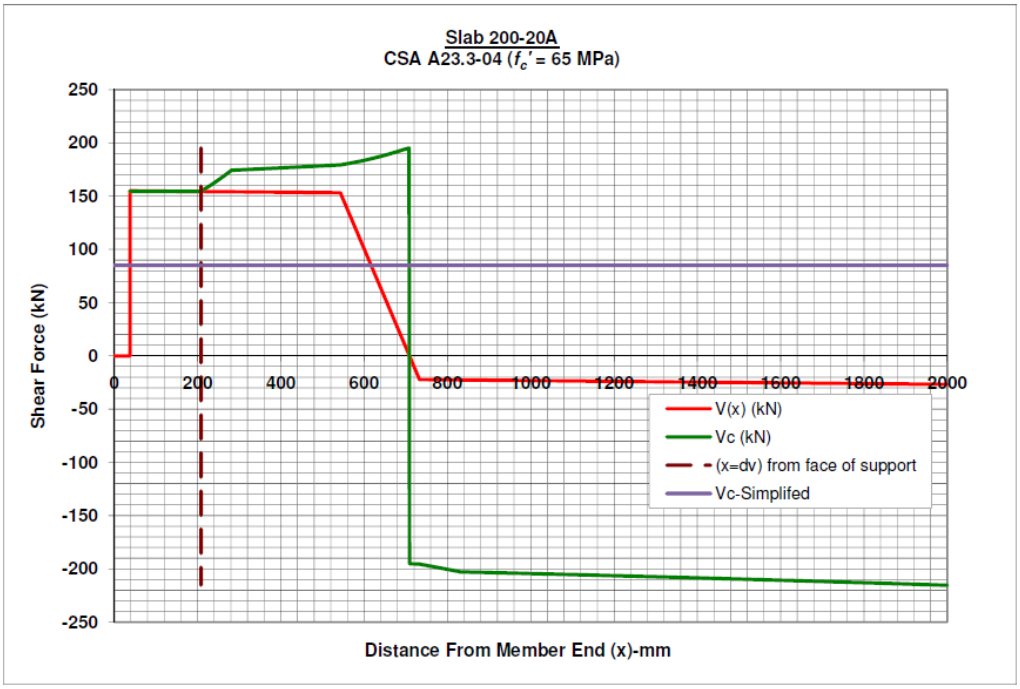

Figure 4.4: Slab 200-20A - CSA A23.3-04 Predicted Shear Resistance at f_c' = 65 MPa

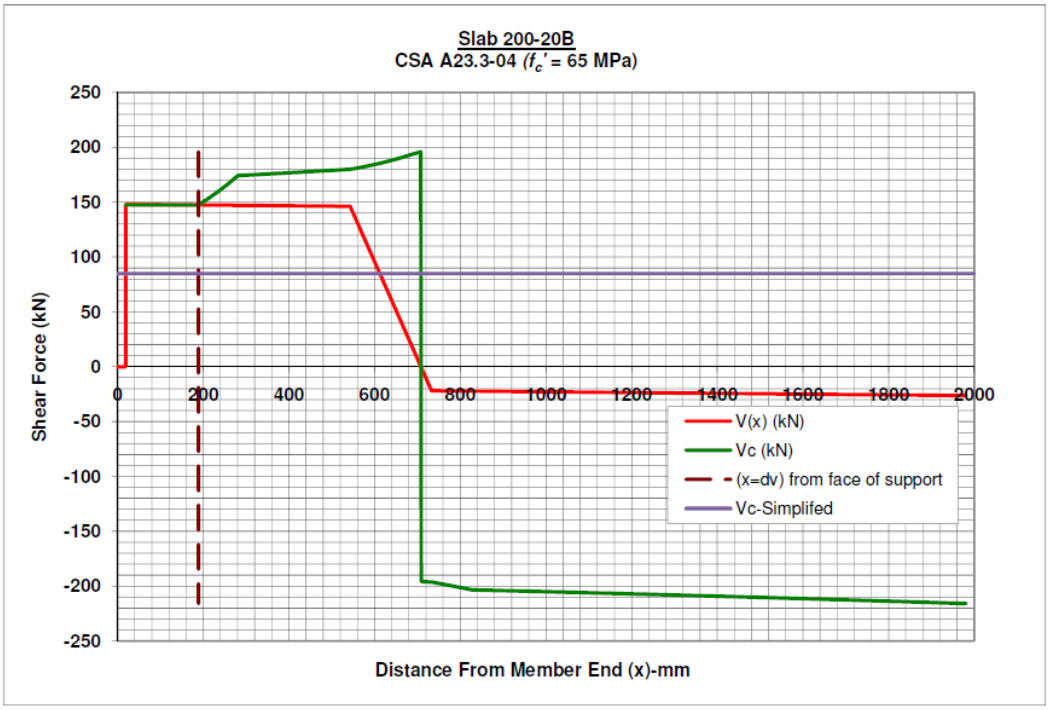

Figure 4.5: Slab 200-20B - CSA A23.3-04 Predicted Shear Resistance at f_c' = 65 MPa

4.2.5.2 *Shear Resistance Diagrams for Series-250 Hollow-Core Slabs*

The shear-resistance diagrams for slabs 250-01A, 250-01B, 250-20A and 250-20B are outlined in Figures 4.6 to 4.9. Again, it is evident from the figures that the code-predicted shear capacities for slabs 250-01A and 250-01B (slabs with the least amount of prestressing) are only about half the values of slabs 250-20A and 250-20B. The predicted capacities for slabs 250-01A and 250-01B using the detailed method of Clause 11.3.6.4 are also lower than the conservative values assumed in Clause 11.3.6.2 (V_c-*Simplified*). In this case, the prediction of shear-resistance values using the detailed shear method are only 85% of the values predicted using the simplified shear method. However, the shear-resistance curves for slabs 250-20A and 250-20B are well

above the V_c-*Simplified* capacity curve, since the strain demand on these slabs is less due to the high level of prestressing.

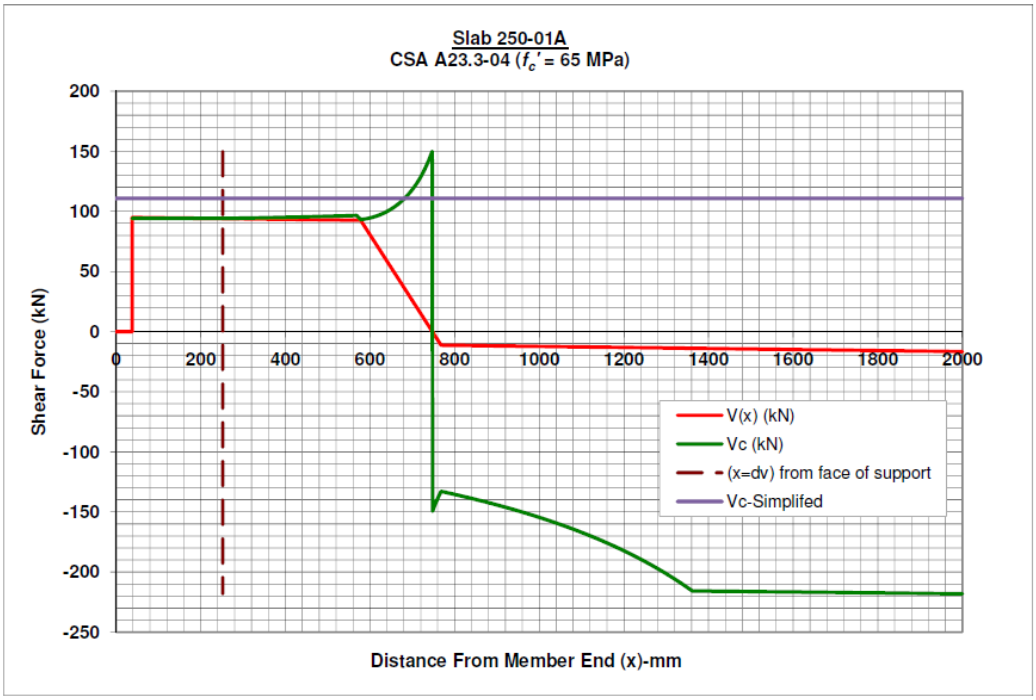

Figure 4.6: Slab 250-01A - CSA A23.3-04 Predicted Shear Resistance at f_c' = 65 MPa

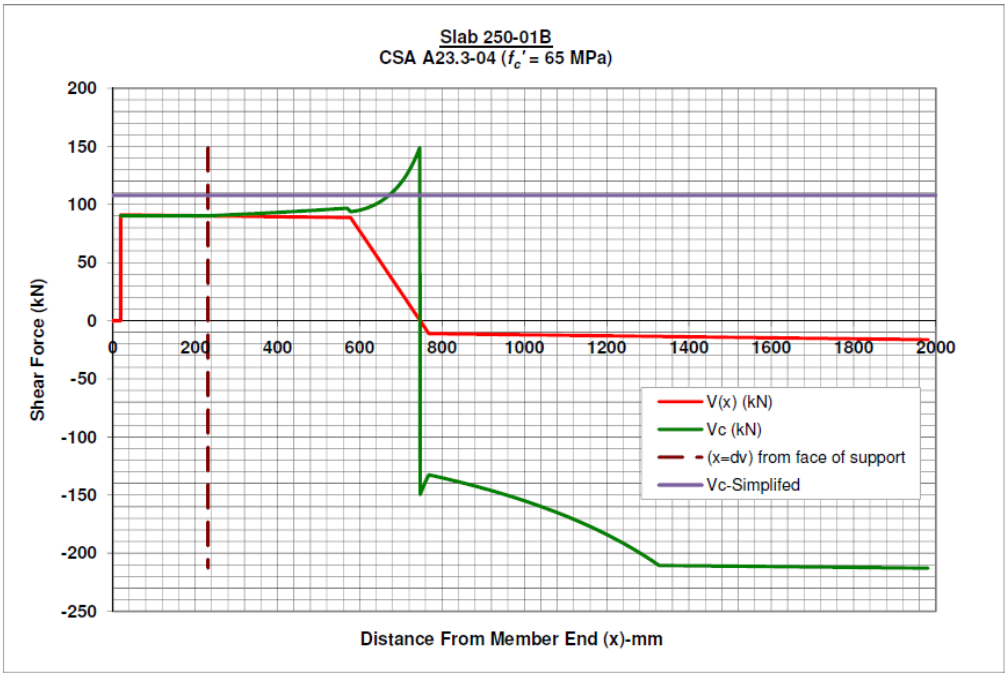

Figure 4.7: Slab 250-01B - CSA A23.3-04 Predicted Shear Resistance at f_c' = 65 MPa

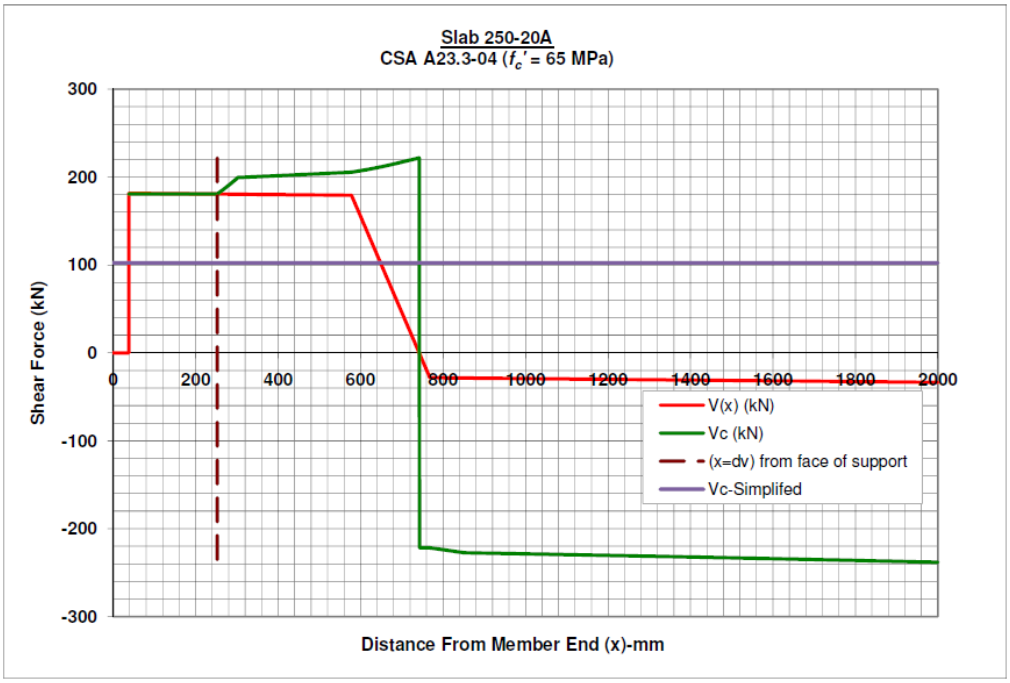

Figure 4.8: Slab 250-20A - CSA A23.3-04 Predicted Shear Resistance at f_c' = 65 MPa

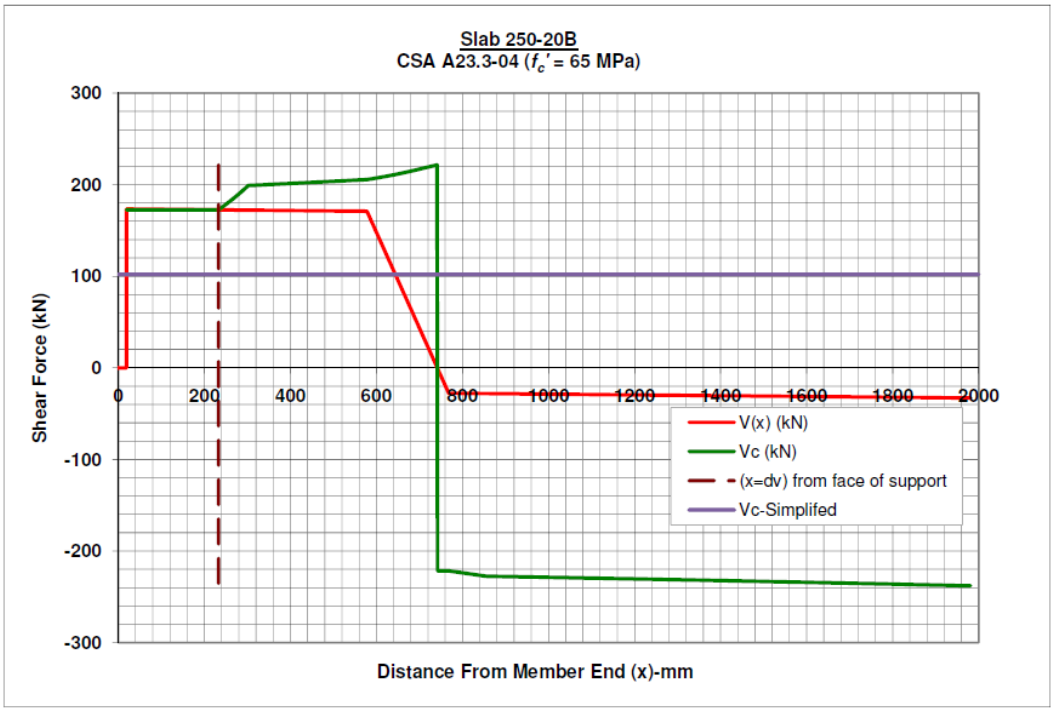

Figure 4.9: Slab 250-20B - CSA A23.3-04 Predicted Shear Resistance at f_c' = 65 MPa

4.2.5.3 *Shear Resistance Diagrams for Series-300 Hollow-Core Slabs*

The shear-resistance diagrams for slabs 300-06A, 300-06B, 300-18A and 300-18B are outlined in Figures 4.10 to 4.13. In this case, the code-predicted shear capacities for slabs 300-06A and 300-06B (slabs with the least amount of prestressing) are about 0.8 times the value calculated for slabs 300-18A and 300-18B. However, the level of prestressing for slabs 300-06A and 300-06B is comparatively higher than for slabs 200-01A, 200-01B, 250-01A and 250-01B - therefore the difference between predicted shear-capacities between slabs with low and high levels of prestressing is not as dramatic as for the Series-200 and Series-250 slabs. In addition, the predicted capacities for slabs 300-06A and 300-06B using the detailed method of Clause 11.3.6.4 are significantly higher than the conservative values assumed in Clause 11.3.6.2 (V_c-*Simplified*).

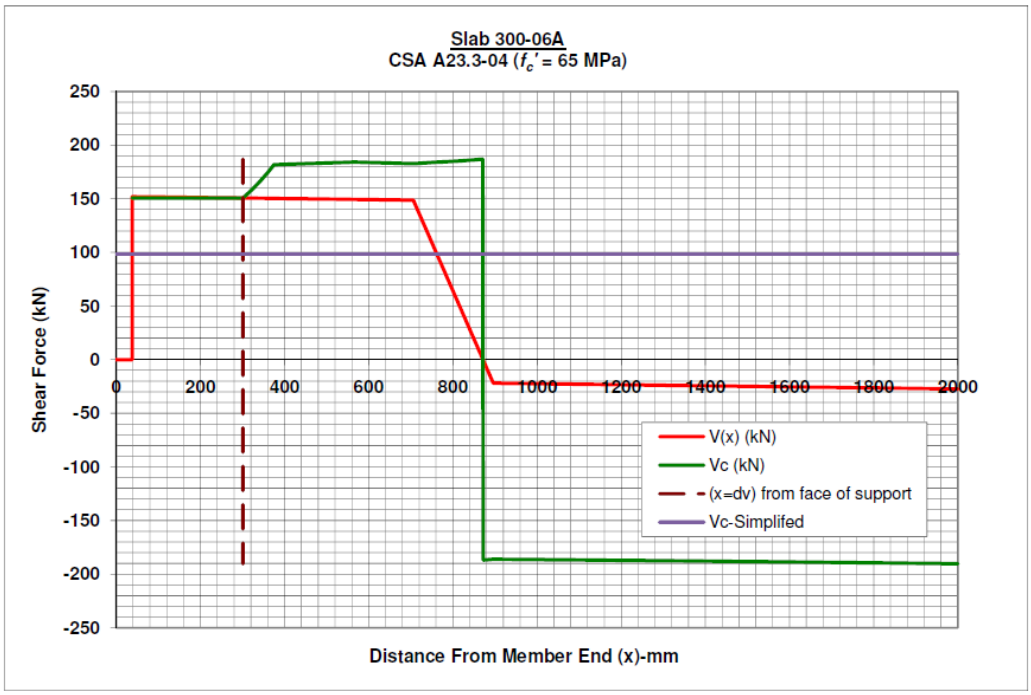

Figure 4.10: Slab 300-06A - CSA A23.3-04 Predicted Shear Resistance at f_c' = 65 MPa

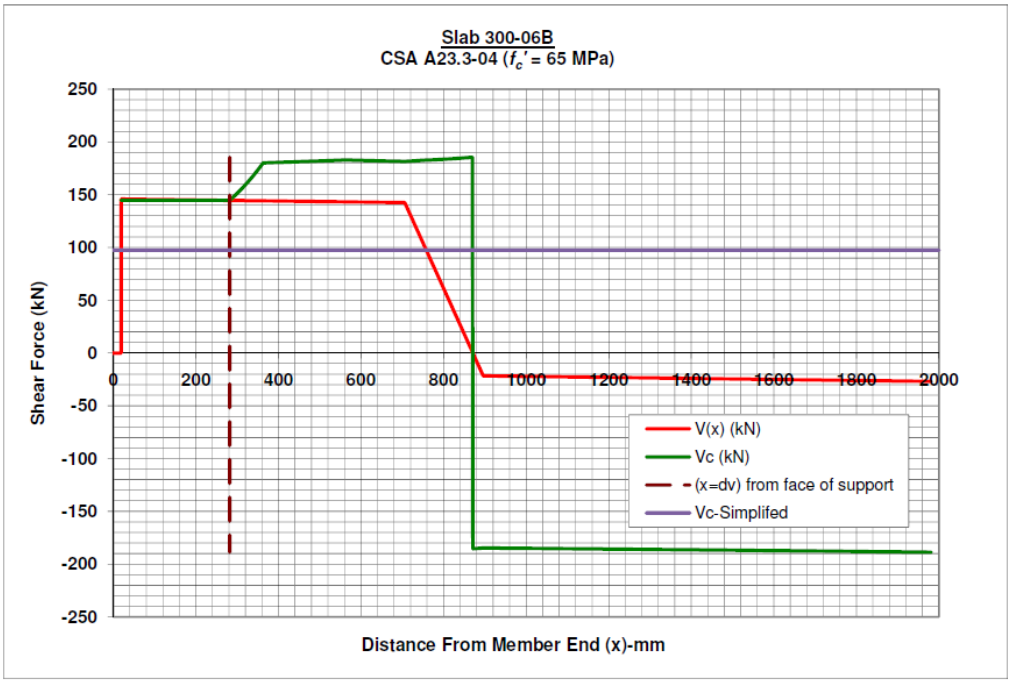

Figure 4.11: Slab 300-06B - CSA A23.3-04 Predicted Shear Resistance at f_c' = 65 MPa

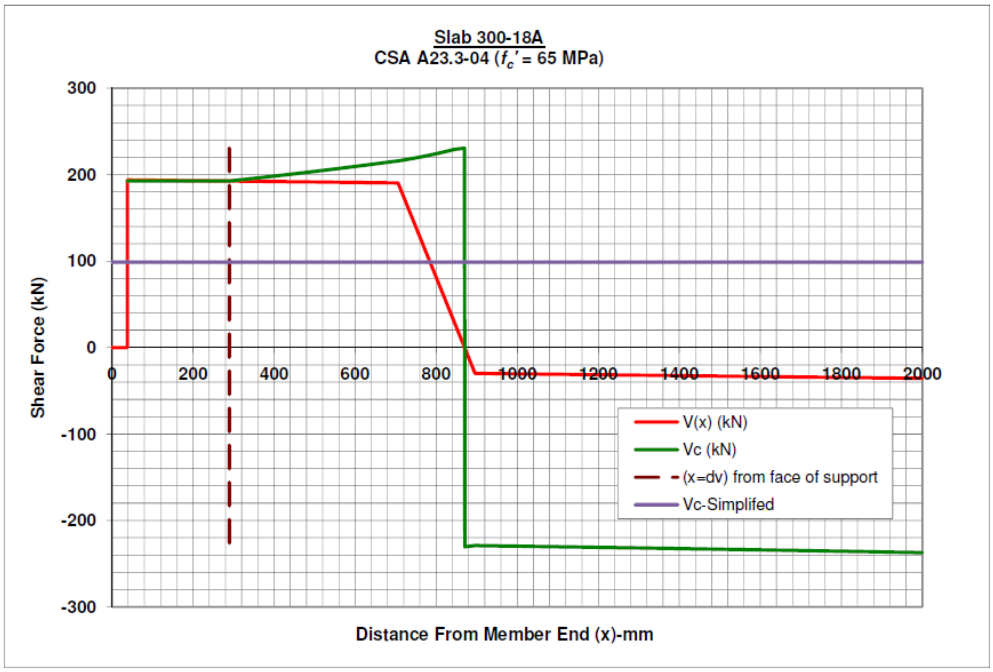

Figure 4.12: Slab 300-18A - CSA A23.3-04 Predicted Shear Resistance at f_c' = 65 MPa

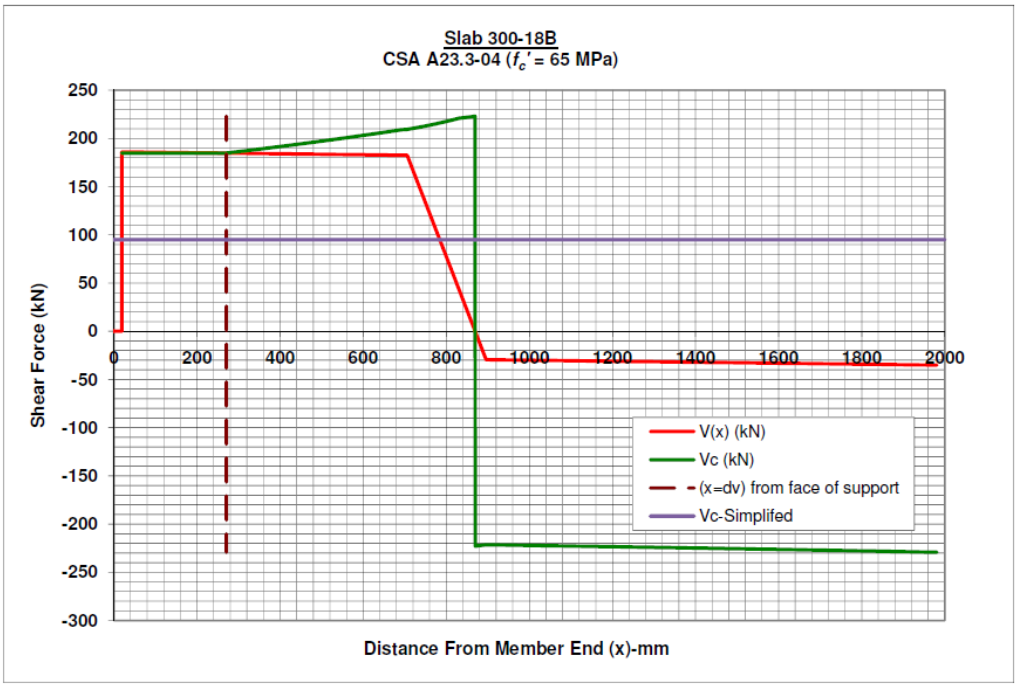

Figure 4.13: Slab 300-18B - CSA A23.3-04 Predicted Shear Resistance at f_c' = 65 MPa

4.3 ACI 318-08 (ACI 2008) CODE-PREDICTED SHEAR RESISTANCE

Each of the twelve test slabs were also analyzed with the American code (ACI 2008) using the as-cast material, geometric and section properties, as outlined in Chapter 3. To assist in the analysis procedure, a spreadsheet was developed to perform a complete analysis of the predicted shear resistance of each specimen, using the relevant provisions of the American code (ACI 2008). To ensure accuracy with the calculations, imperial units were substituted into each of the appropriate equations, and the resulting numbers were converted to metric units. For reference, the following is an outline of the procedure used for assessing the shear capacity of a prestressed hollow-core slab, according to the ACI 318-08 American code (ACI 2008).

4.3.1 Critical Section for Shear

Clause 11.1.3.2 permits sections located less than a distance *h/2* from the face of the support (where *h* is the overall height of the member) to be designed for the same shear, V_u (the factored shear force), as that computed at a distance *h/2*, provided that all of the following conditions are met (Clause 11.1.3):

(a) The support reaction, in the direction of applied shear, introduces compression into the end regions of the member.

(b) Loads are applied at or near the top of the member.

(c) No concentrated load applies between the face of the support and the location of the critical section defined in Clause 11.1.3.2.

The commentary to the code notes that since the depth to the prestressing strands, *d*, frequently varies in prestressed members, the location of the critical section has arbitrarily been taken as *h/2* from the face of the support.

The above clauses relate to the critical section for shear force; however the code does not appear to explicitly allow the designer to assume that the critical section for shear resistance also occurs at the same location of *h*/2 from the face of the support (ACI 2008). From a rational perspective, with the beneficial effect of the vertical compressive stresses imposed by the support reaction, it is highly unlikely that a web-shear failure would originate immediately above and adjacent to the bearing pad, and evaluation of the web-shear resistance at *h*/2 makes more sense, than at the face of the bearing pad.

A review of the PCI Design Handbook (PCI 2004) indicates that for calculation of the shear resistance of a hollow-core member, the critical section for shear resistance is taken at a distance *h*/2 from the face of the bearing pad. Therefore, the critical section for shear force and for shear resistance was assumed to be at *h*/2 from the edge of the bearing pad for the ACI code equations.

4.3.2 Strand Transfer Length and Prestressing Losses

Similar to the Canadian code (CSA 2004), the transfer length is defined in the American code (ACI 2008) as the length of embedded pre-tensioned strand required to transfer the effective prestress to the concrete. Clause 11.3.4 of the code states:

In a pre-tensioned member in which the section at a distance h/2 from the face of the support is closer to the end of the member than the transfer length of the prestressing steel, the reduced

prestress shall be considered when computing V_{cw}. The prestress force shall be assumed to vary linearly from zero at the end of the prestressing steel, to a maximum at a distance from the end of the prestressing steel equal to the transfer length, assumed to be 50 diameters for strand and 100 diameters for a single wire.

Clause 12.9.1 of the code defines the development length, ℓ_d of prestressing strands as:

$$\ell_d = \left(\frac{f_{se}}{3000}\right)d_b + \left(\frac{f_{ps} - f_{se}}{1000}\right)d_b \qquad [4.16]$$

In lieu of using a fixed value of 50 strand diameters for the transfer length, the code commentary for Clause 12.9.1 derives an expression for the transfer length based on the effective stress in the prestressing tendons after allowance for all prestressing losses, f_{se}, and the strand diameter, d_b, as follows:

$$\ell_t = \left(f_{se}/3000\right)d_b \qquad [4.17]$$

A value of ℓ_t was calculated based on each of the strand diameters present in the test slabs, using Equation 4.17. For the slabs tested with a reduced amount of bearing, the predicted shear capacity was slightly lower as compared to the slabs with full bearing, since the critical section for shear (taken at *h/2* from the face of the bearing pad) would result in slightly less prestressing force in the strands at the critical section.

Regarding the calculation of the prestressed losses, the method for calculating losses found in the *"Notes on ACI 318-08 Building Code Requirements for Structural Concrete"* (PCA 2008) was used to assess the reduction of prestressing force, for the analysis using the American code (ACI

2008). The mix designs from the supplier were used to evaluate the factors in the loss equations, and zero-slump concrete was assumed as one of the parameters.

4.3.3 Shear Resistance Equations

The nominal shear strength for a prestressed hollow-core slab is calculated from the following expression, found in Clause 11.1.1:

$$V_n = V_c + V_s \qquad [4.18]$$

Where V_n is the nominal shear strength of the member, V_c is the nominal shear strength provided by concrete calculated in accordance with Clause 11.3 (shear strength of prestressed concrete members) and V_s is the nominal shear strength provided by shear reinforcement. For a hollow-core slab, there is no shear reinforcement, therefore V_s is equal to zero. Therefore, for a hollow-core slab the nominal shear strength is simply based on the concrete contribution alone:

$$V_n = V_c \qquad [4.19]$$

For design, the nominal shear strength is multiplied by a strength reduction factor, ϕ, (which is taken as 0.75 for shear), to obtain the design shear resistance of the member. However, for the analysis of the hollow-core test specimens, a value of 1.0 was used for ϕ.

In the code expressions for V_c, the concrete strength for shear calculations is limited to a maximum of 10,000 psi (69 MPa), which is implied by the requirement found in Clause 11.1.2: *The values of* $\sqrt{f_c'}$ *used in this chapter shall not exceed 100 psi except as allowed in 11.1.2.1.*

This limit has been set due to a lack of test data and practical experience with concretes having compressive strengths greater than 10,000 psi.

Similar to the note in Section 4.2.3, for the hollow-core test slabs the 69 MPa limit on f_c' was removed, and the concrete compressive strength was varied from 65 MPa up to a maximum of 90 MPa in increments of 5 MPa, to review the effect of concrete strength on the predicted slab shear capacity and to account for the variability of the tested concrete strengths in each slab. The range of concrete strength was selected to reflect the observed strengths obtained from core and cylinder tests for the test specimens, which turned out to be much higher than the initially assumed 28-day strength of 45 MPa (Appendix C).

V_c, is taken as the lesser of V_{ci} (flexure-shear) or V_{cw} (web-shear). According to the code commentary, flexure-shear cracking is initiated by flexural cracking. When flexural cracking occurs, the shear stresses in the concrete above the crack are increased. The flexure-shear crack develops when the combined shear and tensile stress exceeds the tensile strength of the concrete. The equation used to evaluate the nominal capacity for flexure-shear, V_{ci}, is specified in Clause 11.3.3.1 as follows:

$$V_{ci} = 0.6\lambda\sqrt{f_c'}\, b_w d_p + V_d + \frac{V_i M_{cre}}{M_{max}} \qquad [4.20]$$

The term λ is a factor that accounts for low-density concrete, which does not apply to any of the test slabs, therefore a value of 1.0 was used for λ . The term b_w was taken as the sum of the minimum web widths across the slab width, based on the as-cast geometry (Appendix A). In the above equation, d_p, the distance from the extreme compression fibre to the centroid of the

prestressing steel, need not be taken as less than 0.80h. V_d is the shear force at a section due to unfactored dead load, and V_i is the factored shear force at a section due to externally applied loads occurring simultaneously with M_{max}.

Finally, the term M_{cre} represents the moment causing flexural cracking at a section due to externally applied loads, calculated as:

$$M_{cre} = (I / y_t)(6\lambda\sqrt{f_c'} + f_{pe} - f_d) \qquad [4.21]$$

In the above expression, I / y_t is equivalent to the section modulus, and f_{pe} is the compressive stress in the concrete due to the effective prestress forces only (after allowance for all prestress losses) at the extreme section fibre, where tensile stress is caused by externally applied loads. Finally, f_d is the stress due to unfactored dead load at the extreme section fibre, where tensile stress is caused by externally applied loads. As per Clause 11.3.3.1, V_{ci} need not be taken less than $1.7\lambda\sqrt{f_c'}b_w d$.

According to the code commentary, web-shear cracking begins from an interior point in a member when the principal tensile stresses exceed the tensile strength of the concrete. The equation used to evaluate the nominal capacity for web-shear, V_{cw}, is specified in Clause 11.3.3.2 as follows:

$$V_{cw} = (3.5\lambda\sqrt{f_c'} + 0.3f_{pc})b_w d_p + V_p \qquad [4.22]$$

In the above expression, all terms are the same as in Equation 4.20, except as follows – f_{pc} is the compressive stress in the concrete (after allowance for all prestress losses) at the centroid of the

cross section resisting externally applied loads, or at the junction of the web and flange, when the centroid lies within the flange. Finally, V_p is the vertical component of the effective prestressing force at a section, which for a hollow-core slab with horizontal strands is equal to zero.

Alternatively, the code permits V_{cw} to be computed as the shear force corresponding to the dead load plus live load resulting in a principal tensile stress of $4\lambda\sqrt{f_c'}$ at the centroidal axis of the member, or at the intersection of flange and web when the centroidal axis is in the flange. For the analysis of the test slabs, Equation 4.22 was used to evaluate the web-shear capacity of the slabs, V_{cw}.

Regarding the analysis of the hollow-core test specimens, according to Clause 11.3.2, in the calculation of the nominal shear strength of a prestressed concrete member, V_c need not be taken less than $2\lambda\sqrt{f_c'}b_w d$. However, in addition, V_c shall not be taken greater than $5\lambda\sqrt{f_c'}b_w d$, or the value given in Clause 11.3.4 (the value of V_{cw}, with consideration of the reduction of prestressing force within the transfer length).

4.3.4 Shear Resistance Diagrams

For reference, the shear-force and code-predicted shear-resistance diagrams for the American code (ACI 2008) are shown for all test slabs in Figures 4.14 to 4.25 for a concrete compressive strength of 65 MPa, to allow comparisons with the Canadian code (CSA 2004).

However, as noted in Section 4.3.3, the analysis was performed for the full range of concrete compressive strengths from 65 MPa to 90 MPa (in increments of 5 MPa), to review the effect of

the concrete strength on the predicted slab shear capacity and to account for the variability of the tested concrete strengths in each slab.

The shear-force and shear-resistance diagrams presented in Section 4.3.4 include the following information:

- $V_{(x)}$ represents the theoretical (factored) shear force, V_f, due to the effects of the test load and the member self weight, that would initiate a shear failure based on the code equations.

- V_c is the predicted shear resistance using the governing value of the web-shear and flexure-shear equations, as outlined in Section 4.3.3.

- The location of the critical section (at $x = h/2$ from the face of the support) is also plotted on the shear-resistance diagrams for each test slab.

For a given concrete strength, the typical shear-resistance curves, V_c, calculated using the American code (ACI 2008) derive their shape based the lesser of the flexure-shear capacity (Equation 4.20) or the web-shear capacity (Equation 4.22). The linear diagonal line from the bearing region to the peak shear capacity for the member is a straight line relationship, based on the web-shear capacity and a maximum permitted capacity for shear. The diagonal line typically intercepts the flexure-shear capacity curve, which rapidly increases as the shear force increases, but the moment approaches zero near the support region (Equation 4.20).

Based on the analysis of the test slabs, there is a marginal difference in the code-predicted capacities for the slabs with the reduced bearing in comparison with those with the full bearing,

due to the location of the critical section along the transfer length in relation to the end of the slabs – slabs with reduced bearing typically had slightly lower predicted shear capacities. Note that there are also some differences in predicted capacities between slabs cast on the same production line, due to the use of the as-cast geometric and section properties for each of the test slabs.

The following sections outline the predicted shear-resistance for each series of test slabs using the American code (ACI 2008).

4.3.4.1 *Shear Resistance Diagrams for Series-200 Hollow-Core Slabs*

The shear-resistance diagrams for slabs 200-01A, 200-01B, 200-20A and 200-20B are outlined in Figures 4.14 to 4.17. Unlike the Canadian code (CSA 2004), the American code-predicted shear capacities for slabs 200-01A and 200-01B (slabs with the least amount of prestressing) are much closer in comparison with those for slabs 200-20A and 200-20B (using the American code). Slabs 200-01A and 200-01B had predicted shear capacities in the order of 0.8 times the values predicted for slabs 200-20A and 200-20B using the American code (ACI 2008).

In addition, the American code-predicted capacities for slabs 200-01A and 200-01B are far-greater than the capacities predicted by the Canadian code (approximately 1.7 times larger). However, for slabs 200-20A and 200-20B, the predicted capacities using the Canadian code and the American code are relatively close to each other (within 5 %).

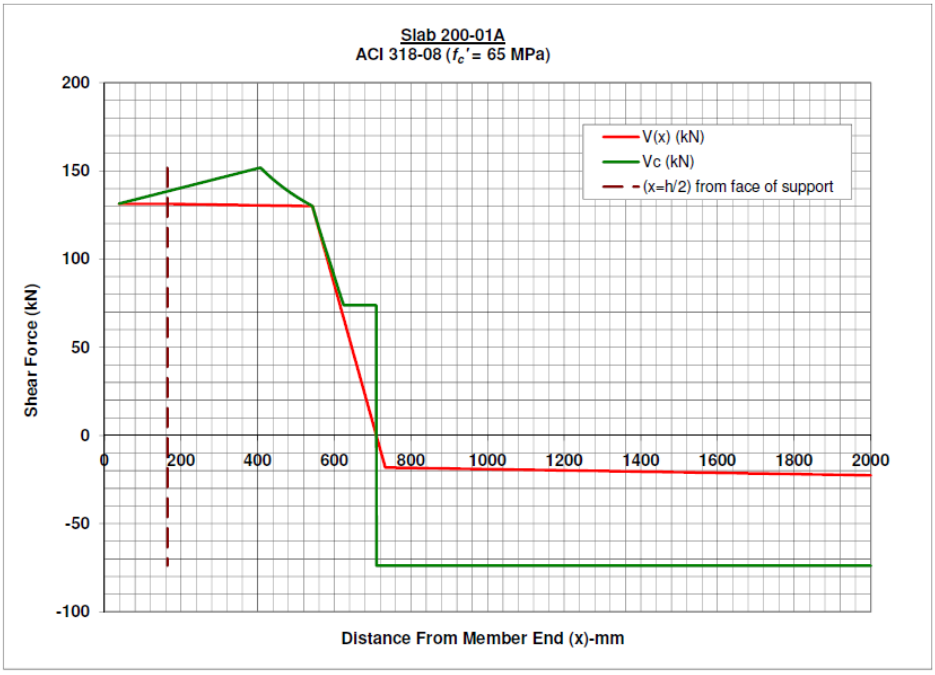

Figure 4.14: Slab 200-01A - ACI 318-08 Predicted Shear Resistance at f_c' = 65 MPa

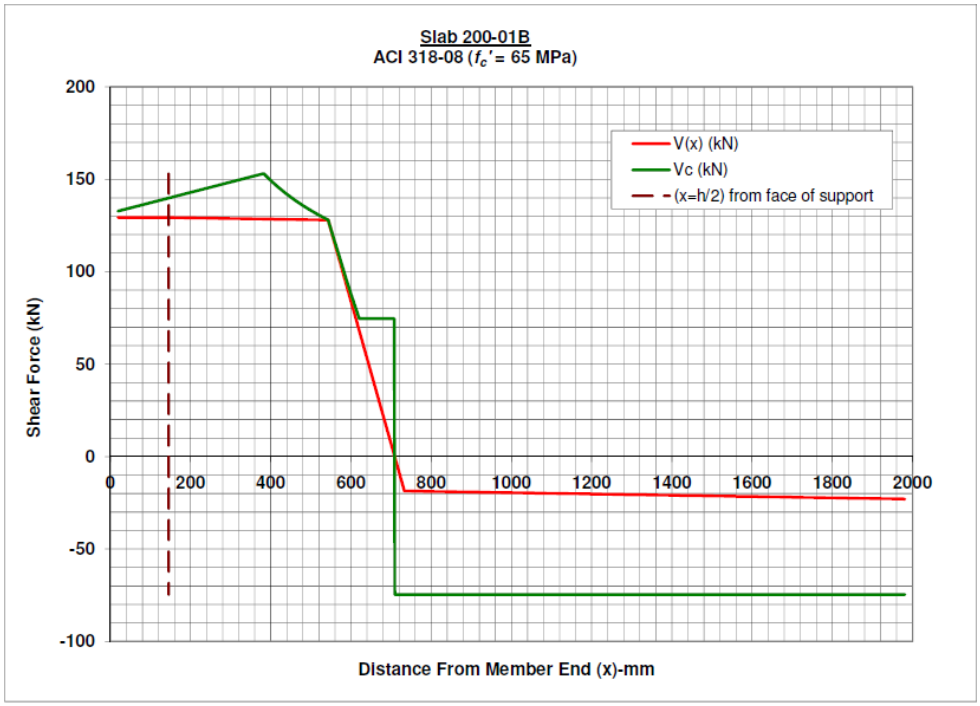

Figure 4.15: Slab 200-01B - ACI 318-08 Predicted Shear Resistance at f_c' = 65 MPa

Figure 4.16: Slab 200-20A - ACI 318-08 Predicted Shear Resistance at f_c' = 65 MPa

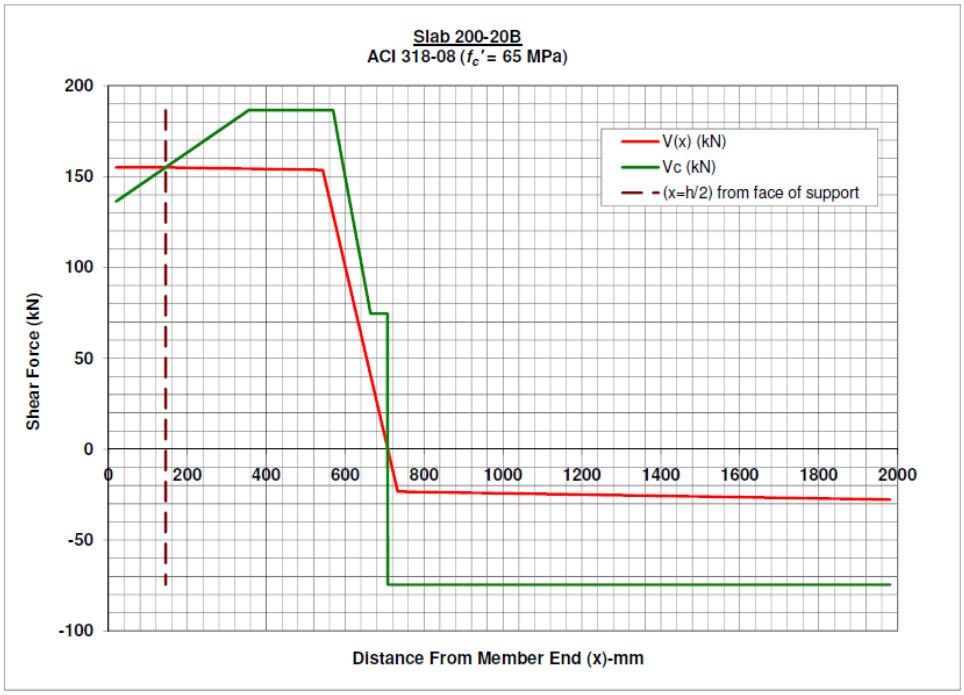

Figure 4.17: Slab 200-20B - ACI 318-08 Predicted Shear Resistance at f_c' = 65 MPa

4.3.4.2 *Shear Resistance Diagrams for Series-250 Hollow-Core Slabs*

The shear-resistance diagrams for slabs 250-01A, 250-01B, 250-20A and 250-20B are outlined in Figures 4.18 to 4.21. Unlike the Canadian code (CSA 2004), the American code-predicted shear capacities for slabs 250-01A and 250-01B (slabs with the least amount of prestressing) are much closer in comparison with those for slabs 250-20A and 250-20B (using the American code). Slabs 250-01A and 250-01B had predicted shear capacities within 3 to 16% of the values predicted for slabs 250-20A and 250-20B using the American code (ACI 2008).

In addition, the American code-predicted capacities for slabs 250-01A and 250-01B are far-greater than the capacities predicted by the Canadian code (approximately 1.7 to 1.9 times larger). However, for slabs 250-20A and 250-20B, the predicted capacities using the Canadian code and the American code are relatively close to each other (within 3 to 7 %).

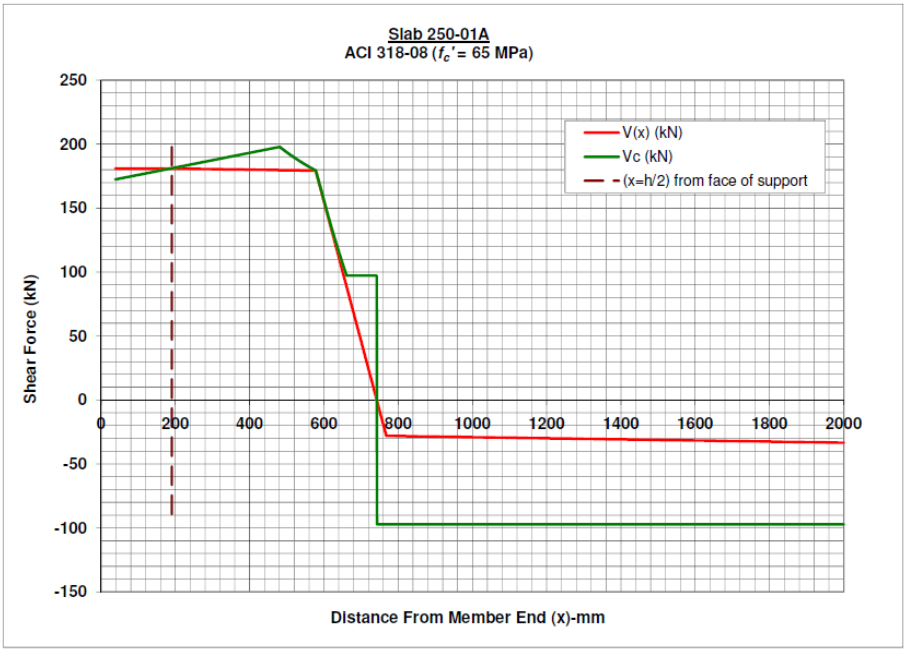

Figure 4.18: Slab 250-01A - ACI 318-08 Predicted Shear Resistance at f_c' = 65 MPa

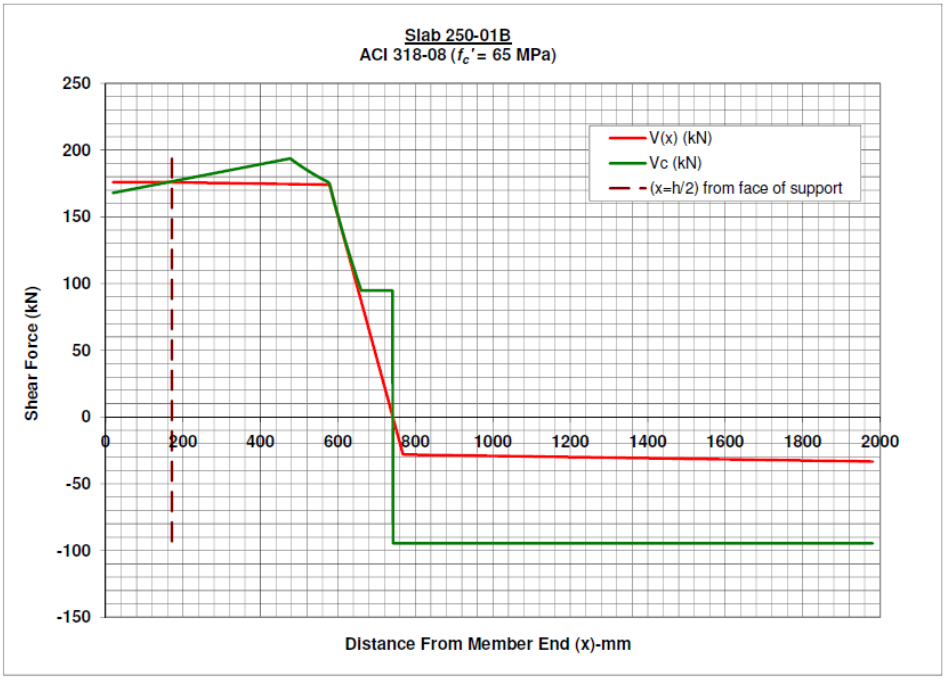

Figure 4.19: Slab 250-01B - ACI 318-08 Predicted Shear Resistance at f_c' = 65 MPa

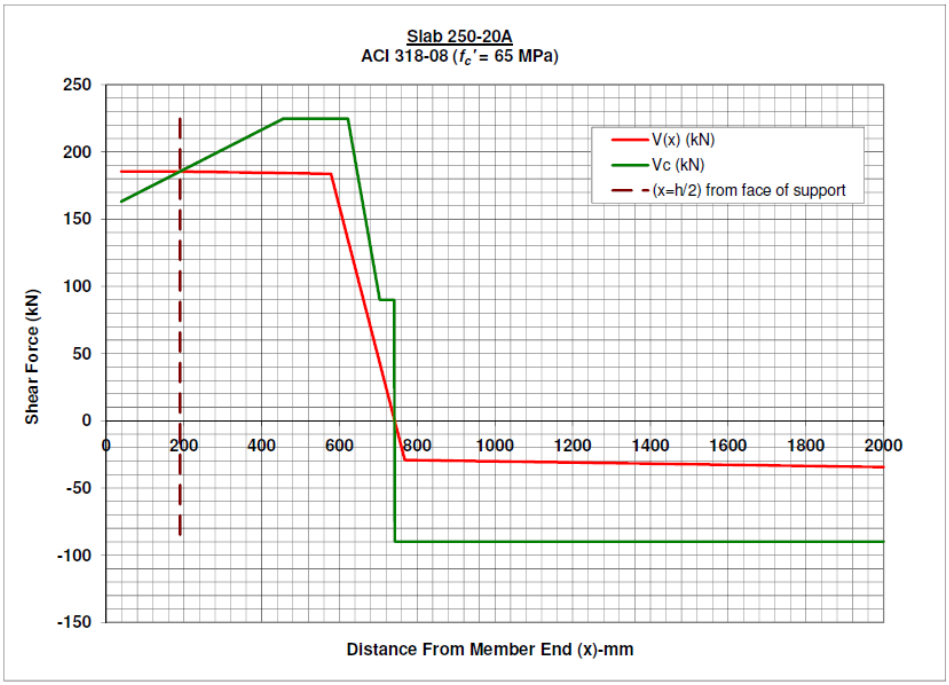

Figure 4.20: Slab 250-20A - ACI 318-08 Predicted Shear Resistance at f_c' = 65 MPa

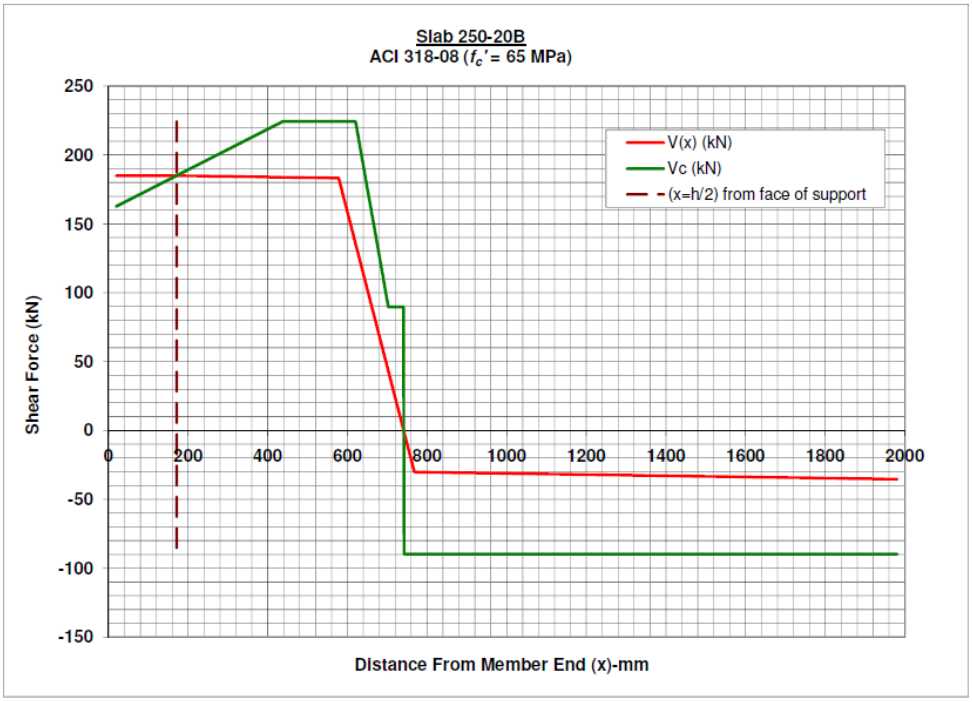

Figure 4.21: Slab 250-20B - ACI 318-08 Predicted Shear Resistance at f_c' = 65 MPa

4.3.4.3 *Shear Resistance Diagrams for Series-300 Hollow-Core Slabs*

The shear-resistance diagrams for slabs 300-06A, 300-06B, 300-18A and 300-18B are outlined in Figures 4.22 to 4.25. The American code-predicted shear capacities for slabs 300-06A and 300-06B (slabs with the least amount of prestressing) are lower than the predicted capacities for slabs 300-18A and 300-18B. In this case, the Canadian code-predicted capacities for slabs 300-06A and 300-06B (CSA 2004) were closer to the American code-predicted capacities (within 9 to 12%); nevertheless, the American code-predicted values were still higher than the Canadian code-predicted values.

However, for slabs 300-18A and 300-18B, the predicted capacities using the Canadian code and the American code are much closer to each other (within 1%).

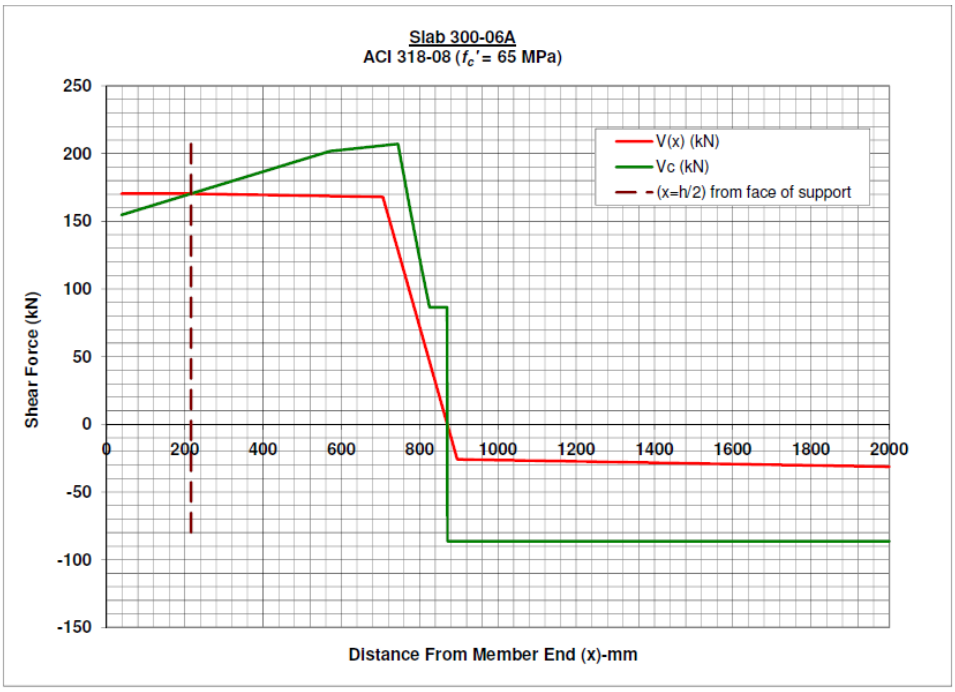

Figure 4.22: Slab 300-06A - ACI 318-08 Predicted Shear Resistance at f_c' = 65 MPa

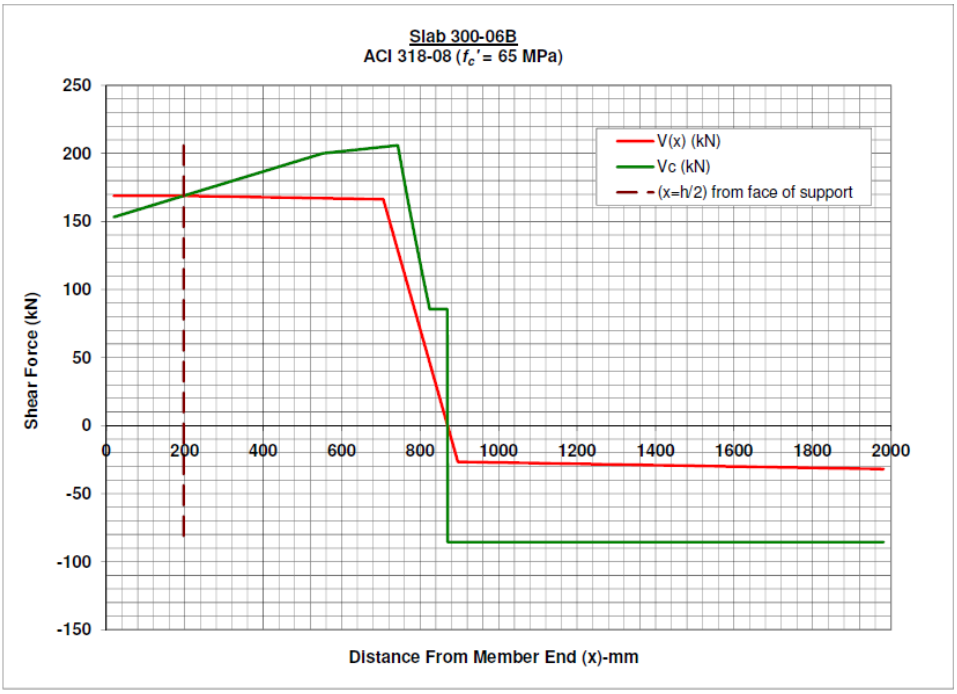

Figure 4.23: Slab 300-06B - ACI 318-08 Predicted Shear Resistance at f_c' = 65 MPa

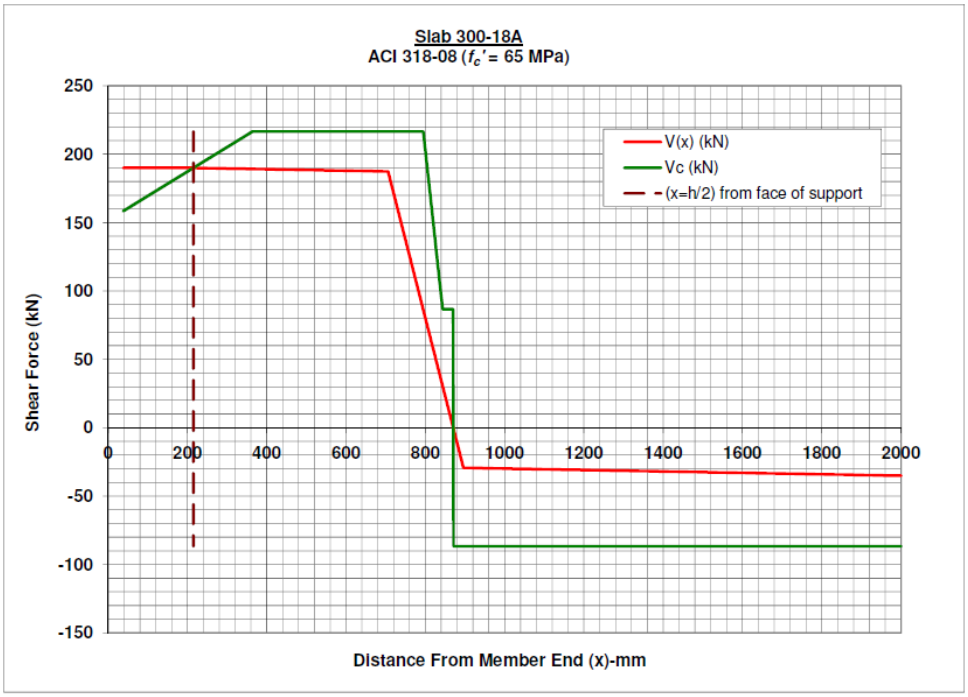

Figure 4.24: Slab 300-18A - ACI 318-08 Predicted Shear Resistance at f_c' = 65 MPa

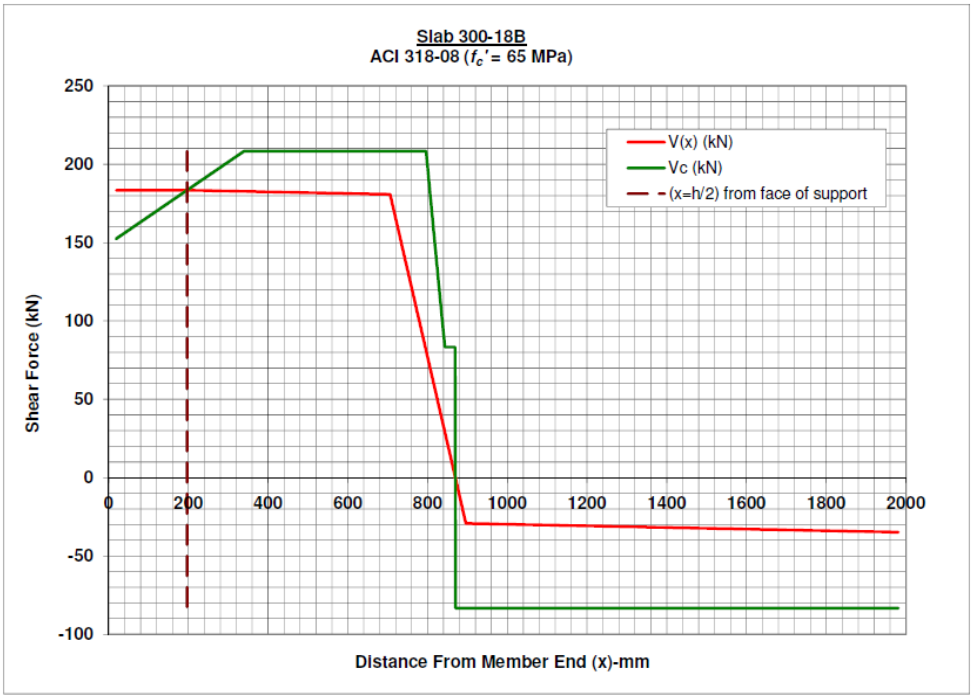

Figure 4.25: Slab 300-18B - ACI 318-08 Predicted Shear Resistance at f_c' = 65 MPa

CHAPTER 5 TEST RESULTS AND DISCUSSION

5.1 INTRODUCTION

The results obtained from Series-200, 250 and 300 test slabs are presented below in terms of the test observations, modes of failure and experimental shear capacities. In addition, the code-predicted shear capacities and the experimental shear capacities are compared. The effect of the bearing length and the level of prestressing on the experimental shear capacities are presented. Finally, the failure profiles for all slabs are reviewed in comparison with the code-predicted critical sections for shear.

The test observations are summarized in detail for each of the twelve test slabs, for reference in Appendix G. Each test summary includes test notes, the observed loads at first cracking and at failure, the observed failure modes and photos of the slabs during the test and after failure.

5.2 FAILURE LOAD AND MODE OF FAILURE

Sections 5.2.1 to 5.2.3 provide a summary of the predicted and experimental failure loads for each series of slabs in the 203 mm, 254 mm and 305 mm depth range. Each section notes the following information for each of the test slabs:

- f_c' - *Estimated* (MPa) – represents the average value or range of values for the estimated concrete compressive strengths of each test slab. The values presented in the tables are derived from the core and cylinder strengths found in Appendix C.

- *P-Exp* (kN) – represents the peak test load that was achieved at failure of the test slab.

- *P-Anchor* (kN) – is the theoretical maximum test load at which the tensile anchorage resistance of the strands adjacent to the support, T_r, would just meet the tensile anchorage force required by the code, T_f, from Clause 11.3.9.5 of the Canadian code (CSA 2004).

- *Exp/Anchor* – is equal to *P-Exp* divided by *P-Anchor*. A value greater than one indicates that the tensile anchorage requirement of Clause 11.3.9.5 of the Canadian code (CSA 2004) cannot be met at the experimental failure load.

- *Failure Mode* – is the observed failure mode for each test slab. In many cases, at the failure of the slab there was no single type of failure mode, but rather a combination of two distinct modes of failure.

- f_c' (MPa) – represents the range of concrete compressive strengths used for the analysis of each test slab. The code-predicted shear capacities were calculated by ranging f_c' from 65 to 90 MPa, in increments of 5 MPa to evaluate the effect of the concrete compressive strength on the predicted shear capacity and to allow for a comparison with the estimated compressive strength of each slab.

- *Predicted Failure Location CSA 2004* (mm) – is the location, measured from the end of the test slab to the point where the Canadian code (CSA 2004) predicted the slab would fail in shear, for the given concrete strength.

- V_c-*Predict CSA 2004* (kN) – is the predicted shear capacity of the test slab at the predicted failure location, according to the Canadian code (CSA 2004).

- *V-Exp CSA 2004* (kN) – is the shear force due to the experimental test load, *P-Exp*, at the predicted failure location, according to the Canadian code (CSA 2004).

- *Predicted Failure Location ACI 2008* (mm) – is the location, measured from the end of the test slab to the point where the American code (ACI 2008) predicted the slab would fail in shear, for the given concrete strength.

- *Predicted Failure Mode ACI 2008* – is the shear-failure mode predicted by the American code (ACI 2008), for the given concrete strength. The predicted shear-failure mode is either web-shear or flexure-shear. Note that the Canadian code (CSA 2004) does not have specific failure modes for shear.

- *V_c-Predict ACI 2008* (kN) – is the predicted shear capacity of the test slab at the predicted failure location, according to the American code (ACI 2008).

- *V-Exp ACI 2008* (kN) – is the shear force due to the experimental test load, *P-Exp*, at the predicted failure location, according to the American code (ACI 2008).

- *V-Exp/V_c-Predict CSA 2004* – is the ratio of *V-Exp/V_c-Predict*, according to the Canadian code (CSA 2004). Values less than one indicate an un-conservative shear capacity prediction by the code, while values greater than one indicate a conservative shear-capacity prediction by the code.

- *V-Exp/V_c-Predict ACI 2008* – is the ratio of *V-Exp/V_c-Predict*, according to the American code (ACI 2008). Values less than one indicate an un-conservative shear capacity

prediction by the code, while values greater than one indicate a conservative shear-capacity prediction by the code.

Based on the initial design of the test slabs, shear-failures were predicted by the Canadian code (CSA 2004) for all cases, with an assumed concrete compressive strength of 45 MPa. However, since the as-cast compressive strength of the slabs ranged between 80 and 90 MPa on the test-date, some of the slabs with low amounts of prestressing exhibited a flexural failure, or a combined shear and flexural failure as noted in the sections below.

5.2.1 Series-200 Test Slabs

The results of the code-predicted and experimental failure loads and modes of failure for slabs 200-01A, 200-01B, 200-20A and 200-20B are listed in Tables 5.1 and 5.2. Recall that slabs 200-01A and 200-01B had the least amount of prestressing and slabs 200-20A and 200-20B had the highest level of prestressing. Slabs 200-01A and 200-20A had 63 mm of bearing at the loaded end of the slab, while slabs 200-01B and 200-20B had 38 mm of bearing at the loaded end of the slab.

Table 5.1: Predicted and Experimental Failure Loads –Test Slabs 200-01A, 200-01B

Slab 200-01A

f_c'-Estimated (MPa)	P-Exp (kN)	P-Anchor (kN)	Exp/Anchor
88	158.4	24.8	6.39

Failure Mode: *Flexure-Shear and Flexural Failure*

f_c' (MPa)	* Predicted Failure Location CSA 2004	V_c-Predict (kN) CSA 2004	V-Exp (kN) CSA 2004	* Predicted Failure Location ACI 2008	Predicted Failure Mode ACI 2008	V_c-Predict (kN) ACI 2008	V-Exp (kN) ACI 2008	V-Exp/V_c-Predict CSA 2004	V-Exp/V_c-Predict ACI 2008
65	543 mm	76.4	139.2	543 mm	Flex-Shear	130.0	139.2	1.82	1.07
70	543 mm	75.2	139.2	543 mm	Flex-Shear	132.9	139.2	1.85	1.05
75	543 mm	75.7	139.2	543 mm	Flex-Shear	135.7	139.2	1.84	1.03
80	543 mm	76.4	139.2	543 mm	Flex-Shear	138.5	139.2	1.82	1.01
85	543 mm	77.2	139.2	543 mm	Flex-Shear	141.1	139.2	1.80	0.99
90	543 mm	77.7	139.2	543 mm	Flex-Shear	143.7	139.2	1.79	0.97

** Predicted Failure Location measured from end of slab*

Slab 200-01B

f_c'-Estimated (MPa)	P-Exp (kN)	P-Anchor (kN)	Exp/Anchor
88	136.7	19.3	7.08

Failure Mode: *Flexure-Shear and Flexural Failure*

f_c' (MPa)	* Predicted Failure Location CSA 2004	V_c-Predict (kN) CSA 2004	V-Exp (kN) CSA 2004	* Predicted Failure Location ACI 2008	Predicted Failure Mode ACI 2008	V_c-Predict (kN) ACI 2008	V-Exp (kN) ACI 2008	V-Exp/V_c-Predict CSA 2004	V-Exp/V_c-Predict ACI 2008
65	543 mm	75.1	120.2	543 mm	Flex-Shear	128.0	120.2	1.60	0.94
70	543 mm	73.7	120.2	543 mm	Flex-Shear	130.9	120.2	1.63	0.92
75	543 mm	74.5	120.2	543 mm	Flex-Shear	133.6	120.2	1.61	0.90
80	543 mm	75.2	120.2	543 mm	Flex-Shear	136.2	120.2	1.60	0.88
85	543 mm	75.9	120.2	543 mm	Flex-Shear	138.8	120.2	1.58	0.87
90	543 mm	76.4	120.2	543 mm	Flex-Shear	141.3	120.2	1.57	0.85

** Predicted Failure Location measured from end of slab*

Table 5.2: Predicted and Experimental Failure Loads –Test Slabs 200-20A, 200-20B

Slab 200-20A

f_c'-Estimated (MPa)	P-Exp (kN)	P-Anchor (kN)	Exp/Anchor
84	178.1	77.4	2.30

Failure Mode: *Web-Shear-Tension Failure*

f_c' (MPa)	* Predicted Failure Location CSA 2004	V_c-Predict (kN) CSA 2004	V-Exp (kN) CSA 2004	* Predicted Failure Location ACI 2008	Predicted Failure Mode ACI 2008	V_c-Predict (kN) ACI 2008	V-Exp (kN) ACI 2008	V-Exp/V_c-Predict CSA 2004	V-Exp/V_c-Predict ACI 2008
65	208 mm	154.6	157.2	164 mm	Web-Shear	155.0	157.3	1.02	1.01
70	208 mm	150.1	157.2	164 mm	Web-Shear	159.9	157.3	1.05	0.98
75	208 mm	152.4	157.2	164 mm	Web-Shear	164.7	157.3	1.03	0.96
80	208 mm	154.5	157.2	164 mm	Web-Shear	169.3	157.3	1.02	0.93
85	208 mm	156.6	157.2	164 mm	Web-Shear	173.7	157.3	1.00	0.91
90	208 mm	158.6	157.2	164 mm	Web-Shear	178.1	157.3	0.99	0.88

** Predicted Failure Location measured from end of slab*

Slab 200-20B

f_c'-Estimated (MPa)	P-Exp (kN)	P-Anchor (kN)	Exp/Anchor
85-90	166.5	62.9	2.65

Failure Mode: *Web-Shear-Tension Failure*

f_c' (MPa)	* Predicted Failure Location CSA 2004	V_c-Predict (kN) CSA 2004	V-Exp (kN) CSA 2004	* Predicted Failure Location ACI 2008	Predicted Failure Mode ACI 2008	V_c-Predict (kN) ACI 2008	V-Exp (kN) ACI 2008	V-Exp/V_c-Predict CSA 2004	V-Exp/V_c-Predict ACI 2008
65	189 mm	147.5	146.6	145 mm	Web-Shear	155.1	146.8	0.99	0.95
70	189 mm	143.1	146.6	145 mm	Web-Shear	160.0	146.8	1.02	0.92
75	189 mm	145.4	146.6	145 mm	Web-Shear	164.8	146.8	1.01	0.89
80	189 mm	147.6	146.6	145 mm	Web-Shear	169.3	146.8	0.99	0.87
85	189 mm	149.7	146.6	145 mm	Web-Shear	173.8	146.8	0.98	0.84
90	189 mm	151.6	146.6	145 mm	Web-Shear	178.1	146.8	0.97	0.82

** Predicted Failure Location measured from end of slab*

5.2.1.1 *Experimental and Code-Predicted Capacities*

For slabs 200-01A and 200-01B, the Canadian code (CSA 2004) and American code (ACI 2008) both predicted the same failure location, at 543 mm from the end of the slab. If the Canadian code limit on the concrete compressive strength for shear calculations was followed (approximately 65MPa) then the experimental-to-predicted shear capacity is 1.82 for slab 200-01A and 1.60 for slab 200-01B, which indicates a high level of conservatism for each case. If the estimated concrete compressive strength of 88 MPa is used for the Canadian code predictions, then the experimental-to-predicted shear capacity changes only slightly. Varying the concrete strength from 65 to 90 MPa changed the code-predicted capacities by less than 2%.

The reason for the small variation in shear capacities above 65 MPa is due to the aggregate reduction factor in Clause 11.3.6.4 of the Canadian code (CSA 2004), in which the nominal aggregate size, a_g, is linearly reduced from the specified nominal size at a concrete compressive strength of 60 MPa, down to a value of zero for concrete compressive strengths exceeding 70 MPa.

It is quite evident that the tensile anchorage requirement of the strands near the support in Clause 11.3.9.5 of the Canadian code (CSA 2004) could not be met at the failure load for slabs 200-01A and 200-01B, with the experimental failure load being 6.39 to 7.08 times larger than what the strands are capable of resisting in tension adjacent to the support.

If the American code limit on the concrete compressive strength for shear calculations was followed (approximately 70 MPa) then the experimental-to-predicted shear capacity is 1.05 for slab 200-01A and 0.92 for slab 200-01B, which is much closer to a value of 1.0, compared to the

Canadian code. If the estimated concrete compressive strength of 88 MPa is used for the American code predictions, then the experimental-to-predicted shear capacity reduces to 0.97 for slab 200-01A and 0.85 for slab 200-01B. The American code-predicted shear capacity is therefore very close to the experimental shear capacity for slab 200-01A, but is un-conservative for slab 200-01B. Varying the concrete strength from 65 to 90 MPa changed the code-predicted capacities by approximately 11%.

For slabs 200-20A and 200-20B, the Canadian code (CSA 2004) and American code (ACI 2008) both predicted different failure locations from the end of the slab. If the Canadian code limit on the concrete compressive strength for shear calculations was followed (approximately 65 MPa) then the experimental-to-predicted shear capacity is 1.02 for slab 200-20A and 0.99 for slab 200-20B, which is very close to a value of 1.0. If the estimated concrete compressive strength of 84 MPa is used for the Canadian code prediction for slab 200-20A, then the experimental-to-predicted shear capacity becomes 1.0 and if the estimated strength of 85-90 MPa was applied to slab 200-20B, the experimental-to-predicted shear capacity ranges from 0.97 to 0.98, still very close to 1.0. Varying the concrete strength from 65 to 90 MPa changed the code-predicted capacities by less than 3%.

Again, it is evident that the tensile anchorage requirement of the strands near the support in Clause 11.3.9.5 of the Canadian code (CSA 2004) could not be met at the failure load for slabs 200-20A or 200-20B, with the experimental failure load being 2.30 to 2.65 times larger than what the strands are capable of resisting in tension adjacent to the support.

If the American code limit on the concrete compressive strength for shear calculations was followed (approximately 70 MPa) then the experimental-to-predicted shear capacity is 0.98 for

slab 200-20A and 0.92 for slab 200-20B, which is fairly close to a value of 1.0. If the estimated concrete compressive strength of 84 MPa is used for the American code prediction for slab 200-20A, then the experimental-to-predicted shear capacity becomes 0.91 and if the estimated strength of 85-90 MPa was applied to slab 200-20B, the experimental-to-predicted shear capacity ranges from 0.82 to 0.84, which are further from a value of 1.0 as compared to the Canadian code. The American code-predicted shear capacity is slightly on the un-conservative side for slab 200-20A, but more so for slab 200-20B. Varying the concrete strength from 65 to 90 MPa changed the code-predicted capacities by approximately 15%.

5.2.1.2 *Modes of Failure*

The American code (ACI 2008) predicted a flexure-shear failure for slabs 200-01A and 200-01B, which was the observed mode of failure. The American code (ACI 2008) predicted a web-shear failure for slabs 200-20A and 200-20B. This was in agreement with the observed mode of failure, which was a web-shear failure for slabs 200-20A and 200-20B. Recall that the Canadian code (CSA 2004) does not have separate failure modes for shear.

5.2.1.3 *Effect of Length of Bearing*

Slab 200-01A, which had 63 mm of bearing failed at a test load of 158.4 kN, while slab 200-01B, which had 38 mm of bearing failed at a test load of 136.7 kN, indicating that the smaller bearing length reduced the failure load by approximately 14%. Note that slab 200-01A had a total web width of 341 mm, while slab 200-01B had a total web width of 345 mm (Appendix A) – therefore the web-widths were within 1% of each other.

Slab 200-20A, which had 63 mm of bearing failed at a test load of 178.1 kN, while slab 200-20B, which had 38 mm of bearing failed at a test load of 166.5 kN, indicating that the smaller bearing length reduced the failure load by approximately 7%. Note that slab 200-20A had a total web width of 345 mm, while slab 200-20B had a total web width of 346 mm (Appendix A) – therefore the web-widths were essentially the same.

5.2.1.4 *Effect of Prestressing Level*

The level of prestressing appears to have a much larger effect on the Canadian code (CSA 2004) predictions compared to the American code (ACI 2008) predictions, based on the dramatic difference in the predicted shear capacities. In terms of the observed failure loads, increasing the area of prestressing by a factor of approximately 4 (from slabs 200-01A and 200-01B to slabs 200-20A and 200-20B) increased the failure loads by approximately 12% for slabs with 63 mm of bearing and by about 22% for slabs with 38 mm of bearing.

5.2.2 Series-250 Test Slabs

The results of the code-predicted and experimental failure loads and modes of failure for slabs 250-01A, 250-01B, 250-20A and 250-20B are listed in Tables 5.3 and 5.4. Recall that slabs 250-01A and 250-01B had the least amount of prestressing and slabs 250-20A and 250-20B had the highest level of prestressing. Slabs 250-01A and 250-20A had 63 mm of bearing at the loaded end of the slab, while slabs 250-01B and 250-20B had 38 mm of bearing at the loaded end of the slab.

Table 5.3: Predicted and Experimental Failure Loads –Test Slabs 250-01A, 250-01B

Slab 250-01A

f_c'-Estimated (MPa)	P-Exp (kN)	P-Anchor (kN)	Exp/Anchor
85-90	211.9	25.8	8.21

Failure Mode: *Flexure-Shear and Flexural Failure*

f_c' (MPa)	* Predicted Failure Location CSA 2004	V_c-Predict (kN) CSA 2004	V-Exp (kN) CSA 2004	* Predicted Failure Location ACI 2008	Predicted Failure Mode ACI 2008	V_c-Predict (kN) ACI 2008	V-Exp (kN) ACI 2008	V-Exp/V_c-Predict CSA 2004	V-Exp/V_c-Predict ACI 2008
65	252 mm	94.1	185.2	578 mm	Flex-Shear	179.4	183.8	1.97	1.02
70	252 mm	90.8	185.2	578 mm	Flex-Shear	183.4	183.8	2.04	1.00
75	252 mm	92.1	185.2	578 mm	Flex-Shear	187.4	183.8	2.01	0.98
80	252 mm	93.3	185.2	578 mm	Flex-Shear	191.2	183.8	1.98	0.96
85	252 mm	94.5	185.2	578 mm	Flex-Shear	194.8	183.8	1.96	0.94
90	252 mm	95.5	185.2	578 mm	Flex-Shear	198.4	183.8	1.94	0.93

** Predicted Failure Location measured from end of slab*

Slab 250-01B

f_c'-Estimated (MPa)	P-Exp (kN)	P-Anchor (kN)	Exp/Anchor
85-90	205.5	20.8	9.88

Failure Mode: *Flexural Failure*

f_c' (MPa)	* Predicted Failure Location CSA 2004	V_c-Predict (kN) CSA 2004	V-Exp (kN) CSA 2004	* Predicted Failure Location ACI 2008	Predicted Failure Mode ACI 2008	V_c-Predict (kN) ACI 2008	V-Exp (kN) ACI 2008	V-Exp/V_c-Predict CSA 2004	V-Exp/V_c-Predict ACI 2008
65	231 mm	90.2	179.0	595 mm	Flex-Shear	156.1	159.1	1.98	1.02
70	231 mm	87.1	179.0	594 mm	Flex-Shear	160.8	160.1	2.06	1.00
75	231 mm	88.3	179.0	593 mm	Flex-Shear	165.4	161.2	2.03	0.97
80	231 mm	89.5	179.0	593 mm	Flex-Shear	168.8	161.2	2.00	0.95
85	231 mm	90.5	179.0	592 mm	Flex-Shear	173.3	162.3	1.98	0.94
90	231 mm	91.6	179.0	592 mm	Flex-Shear	176.5	162.3	1.95	0.92

** Predicted Failure Location measured from end of slab*

Table 5.4: Predicted and Experimental Failure Loads –Test Slabs 250-20A, 250-20B

Slab 250-20A

f_c'-Estimated (MPa)	P-Exp (kN)	P-Anchor (kN)	Exp/Anchor
85-90	294.2	84.0	3.50

Failure Mode: *Web-Shear-Tension Failure*

f_c' (MPa)	* Predicted Failure Location CSA 2004	V_c-Predict (kN) CSA 2004	V-Exp (kN) CSA 2004	* Predicted Failure Location ACI 2008	Predicted Failure Mode ACI 2008	V_c-Predict (kN) ACI 2008	V-Exp (kN) ACI 2008	V-Exp/V_c-Predict CSA 2004	V-Exp/V_c-Predict ACI 2008
65	252 mm	180.8	253.9	190 mm	Web-Shear	185.5	254.2	1.40	1.37
70	252 mm	174.4	253.9	190 mm	Web-Shear	191.4	254.2	1.46	1.33
75	252 mm	176.9	253.9	190 mm	Web-Shear	197.1	254.2	1.44	1.29
80	252 mm	179.1	253.9	190 mm	Web-Shear	202.7	254.2	1.42	1.25
85	252 mm	181.3	253.9	190 mm	Web-Shear	208.1	254.2	1.40	1.22
90	252 mm	183.4	253.9	190 mm	Web-Shear	213.3	254.2	1.38	1.19

** Predicted Failure Location measured from end of slab*

Slab 250-20B

f_c'-Estimated (MPa)	P-Exp (kN)	P-Anchor (kN)	Exp/Anchor
85-90	273.5	69.4	3.94

Failure Mode: *Web-Shear-Tension Failure*

f_c' (MPa)	* Predicted Failure Location CSA 2004	V_c-Predict (kN) CSA 2004	V-Exp (kN) CSA 2004	* Predicted Failure Location ACI 2008	Predicted Failure Mode ACI 2008	V_c-Predict (kN) ACI 2008	V-Exp (kN) ACI 2008	V-Exp/V_c-Predict CSA 2004	V-Exp/V_c-Predict ACI 2008
65	233 mm	172.6	235.5	171 mm	Web-Shear	185.0	235.7	1.36	1.27
70	233 mm	166.2	235.5	171 mm	Web-Shear	190.9	235.7	1.42	1.23
75	233 mm	168.6	235.5	171 mm	Web-Shear	196.6	235.7	1.40	1.20
80	233 mm	170.9	235.5	171 mm	Web-Shear	202.2	235.7	1.38	1.17
85	233 mm	173.1	235.5	171 mm	Web-Shear	207.5	235.7	1.36	1.14
90	233 mm	175.3	235.5	171 mm	Web-Shear	212.7	235.7	1.34	1.11

** Predicted Failure Location measured from end of slab*

5.2.2.1 *Experimental and Code-Predicted Capacities*

For slabs 250-01A and 250-01B, the Canadian code (CSA 2004) and American code (ACI 2008) predicted different failure locations from the end of the slab. Note that slab 250-01B failed in flexure; therefore the experimental-to-predicted shear resistance would be higher than the values listed in Table 5.3.

If the Canadian code limit on the concrete compressive strength for shear calculations was followed (approximately 65MPa) then the experimental-to-predicted shear capacity was 1.97 for slab 250-01A and 1.98 for slab 250-01B, which indicates a very high level of conservatism for each case. If the estimated concrete compressive strength of 85 to 90 MPa is used for the Canadian code predictions, then the experimental-to-predicted shear capacity changed only slightly. Varying the concrete strength from 65 to 90 MPa changed the code-predicted capacities by less than 2%.

It is quite evident that the tensile anchorage requirement of the strands near the support in Clause 11.3.9.5 of the Canadian code (CSA 2004) could not be met at the failure load for slabs 250-01A and 250-01B, with the experimental failure load being 8.21 to 9.88 times larger than what the strands are capable of resisting in tension adjacent to the support.

If the American code limit on the concrete compressive strength for shear calculations was followed (approximately 70 MPa) then the experimental-to-predicted shear capacity was 1.0 for slab 250-01A and 1.0 for slab 250-01B, which is exactly in agreement with the observed failure load. If the estimated concrete compressive strength of 85 to 90 MPa is used for the American code predictions, then the experimental-to-predicted shear capacity ranged from 0.93 to 0.94 for

slab 250-01A and 0.92 to 0.94 for slab 250-01B. The American code-predicted shear capacity is therefore very close to the experimental shear capacity for slabs 250-01A and 250-01B. Varying the concrete strength from 65 to 90 MPa changed the code-predicted capacities by approximately 11 to 13%.

For slabs 250-20A and 250-20B, the Canadian code (CSA 2004) and American code (ACI 2008) both predicted different failure locations from the end of the slab. If the Canadian code limit on the concrete compressive strength for shear calculations was followed (approximately 65MPa) then the experimental-to-predicted shear capacity was 1.40 for slab 250-20A and 1.36 for slab 250-20B, which is conservative compared to a value of 1.0. If the estimated concrete compressive strength of 85 to 90 MPa is used for the Canadian code prediction for slab 250-20A and 250-20B, then the experimental-to-predicted shear capacities changed only slightly. Varying the concrete strength from 65 to 90 MPa changed the code-predicted capacities by less than 2%.

Again, it is evident that the tensile anchorage requirement of the strands near the support in Clause 11.3.9.5 of the Canadian code (CSA 2004) could not be met at the failure load for slabs 250-20A or 250-20B, with the experimental failure load being 3.50 to 3.94 times larger than what the strands are capable of resisting in tension adjacent to the support.

If the American code limit on the concrete compressive strength for shear calculations was followed (approximately 70 MPa) then the experimental-to-predicted shear capacity was 1.33 for slab 250-20A and 1.23 for slab 250-20B, which is conservative and closer to a value of 1.0 than the Canadian code. If the estimated concrete compressive strength of 85 to 90 MPa is used for the American code prediction for slab 250-20A, then the experimental-to-predicted shear capacity ranged between 1.19 and 1.22, and if the estimated strength of 85-90 MPa was applied

to slab 250-20B, the experimental-to-predicted shear capacity ranged from 1.11 to 1.14, which is closer to a value of 1.0 as compared to the Canadian code. Varying the concrete strength from 65 to 90 MPa changed the code-predicted capacities by approximately 15%.

5.2.2.2 *Modes of Failure*

The American code (ACI 2008) predicted a flexure-shear failure for slabs 250-01A and 250-01B, which was the observed failure mode for slab 250-01A, however a flexural failure was observed for slab 250-01B. The American code (ACI 2008) predicted a web-shear failure for slabs 250-20A and 250-20B. This was in agreement with the observed failure mode, which was a web-shear failure for slabs 250-20A and 250-20B.

5.2.2.3 *Effect of Length of Bearing*

Slab 250-01A, which had 63 mm of bearing failed at a test load of 211.9 kN, while slab 250-01B, which had 38 mm of bearing failed at a test load of 205.5 kN, indicating that the smaller bearing length reduced the failure load by approximately 3%. Note that slab 250-01A had a total web width of 346 mm, while slab 250-01B had a total web width of 340 mm (Appendix A) – therefore the web-widths were within 2% of each other.

Slab 250-20A, which had 63 mm of bearing failed at a test load of 294.2 kN, while slab 250-20B, which had 38 mm of bearing failed at a test load of 273.5 kN, indicating that the smaller bearing length reduced the failure load by approximately 7%. Note that slab 250-20A had a total web width of 319 mm, while slab 250-20B had a total web width of 319 mm (Appendix A) – therefore the web-widths were the same in each slab.

5.2.2.4 *Effect of Prestressing Level*

The level of prestressing appears to have a much larger effect on the Canadian code (CSA 2004) predictions compared to the American code (ACI 2008) predictions, based on the dramatic difference in the predicted shear capacities. In terms of the observed failure loads, increasing the area of prestressing by a factor of approximately 4 (from slabs 250-01A and 250-01B to slabs 250-20A and 250-20B) increased the failure loads by approximately 39% for slabs with 63 mm of bearing and by about 33% for slabs with 38 mm of bearing.

5.2.3 Series-300 Test Slabs

The results of the code-predicted and experimental failure loads and modes of failure for slabs 300-06A, 300-06B, 300-18A and 300-18B are listed in Tables 5.5 and 5.6. Recall that slabs 300-06A and 300-06B had the least amount of prestressing and slabs 300-18A and 300-18B had the highest level of prestressing. Slabs 300-06A and 300-18A had 63 mm of bearing at the loaded end of the slab, while slabs 300-06B and 300-18B had 38 mm of bearing at the loaded end of the slab**.**

Table 5.5: Predicted and Experimental Failure Loads –Test Slabs 300-06A, 300-06B

Slab 300-06A

f_c'-Estimated (MPa)	P-Exp (kN)	P-Anchor (kN)	Exp/Anchor
80	199.5	57.0	3.50

Failure Mode: *Web-Shear-Tension Failure*

f_c' (MPa)	* Predicted Failure Location CSA 2004	V_c-Predict (kN) CSA 2004	V-Exp (kN) CSA 2004	* Predicted Failure Location ACI 2008	Predicted Failure Mode ACI 2008	V_c-Predict (kN) ACI 2008	V-Exp (kN) ACI 2008	V-Exp/V_c-Predict CSA 2004	V-Exp/V_c-Predict ACI 2008
65	301 mm	150.7	175.4	216 mm	Web-Shear	170.4	175.8	1.16	1.03
70	301 mm	145.5	175.4	216 mm	Web-Shear	176.1	175.8	1.21	1.00
75	301 mm	147.1	175.4	216 mm	Web-Shear	181.6	175.8	1.19	0.97
80	301 mm	148.6	175.4	216 mm	Web-Shear	187.0	175.8	1.18	0.94
85	301 mm	150.1	175.4	216 mm	Web-Shear	192.1	175.8	1.17	0.92
90	301 mm	151.4	175.4	216 mm	Web-Shear	197.1	175.8	1.16	0.89

** Predicted Failure Location measured from end of slab*

Slab 300-06B

f_c'-Estimated (MPa)	P-Exp (kN)	P-Anchor (kN)	Exp/Anchor
80-85	228.7	45.7	5.00

Failure Mode: *Web-Shear-Tension Failure*

f_c' (MPa)	* Predicted Failure Location CSA 2004	V_c-Predict (kN) CSA 2004	V-Exp (kN) CSA 2004	* Predicted Failure Location ACI 2008	Predicted Failure Mode ACI 2008	V_c-Predict (kN) ACI 2008	V-Exp (kN) ACI 2008	V-Exp/V_c-Predict CSA 2004	V-Exp/V_c-Predict ACI 2008
65	282 mm	144.7	198.7	197 mm	Web-Shear	168.8	199.1	1.37	1.18
70	282 mm	139.5	198.7	197 mm	Web-Shear	174.5	199.1	1.42	1.14
75	282 mm	141.1	198.7	197 mm	Web-Shear	180.0	199.1	1.41	1.11
80	282 mm	142.5	198.7	197 mm	Web-Shear	185.2	199.1	1.39	1.08
85	282 mm	144.1	198.7	197 mm	Web-Shear	190.4	199.1	1.38	1.05
90	282 mm	145.4	198.7	197 mm	Web-Shear	195.3	199.1	1.37	1.02

** Predicted Failure Location measured from end of slab*

Table 5.6: Predicted and Experimental Failure Loads –Test Slabs 300-18A, 300-18B

Slab 300-18A

f_c'-Estimated (MPa)	P-Exp (kN)	P-Anchor (kN)	Exp/Anchor
81	213.7	147.9	1.44

Failure Mode: *Web-Shear-Tension Failure*

f_c' (MPa)	* Predicted Failure Location CSA 2004	V_c-Predict (kN) CSA 2004	V-Exp (kN) CSA 2004	* Predicted Failure Location ACI 2008	Predicted Failure Mode ACI 2008	V_c-Predict (kN) ACI 2008	V-Exp (kN) ACI 2008	V-Exp/V_c-Predict CSA 2004	V-Exp/V_c-Predict ACI 2008
65	290 mm	192.6	187.9	215 mm	Web-Shear	190.0	188.3	0.98	0.99
70	290 mm	174.1	187.9	215 mm	Web-Shear	195.7	188.3	1.08	0.96
75	290 mm	179.6	187.9	215 mm	Web-Shear	201.2	188.3	1.05	0.94
80	290 mm	185.0	187.9	215 mm	Web-Shear	206.6	188.3	1.02	0.91
85	290 mm	190.1	187.9	215 mm	Web-Shear	211.8	188.3	0.99	0.89
90	290 mm	195.1	187.9	215 mm	Web-Shear	216.8	188.3	0.96	0.87

** Predicted Failure Location measured from end of slab*

Slab 300-18B

f_c'-Estimated (MPa)	P-Exp (kN)	P-Anchor (kN)	Exp/Anchor
85-90	212.6	126.2	1.68

Failure Mode: *Web-Shear-Tension Failure*

f_c' (MPa)	* Predicted Failure Location CSA 2004	V_c-Predict (kN) CSA 2004	V-Exp (kN) CSA 2004	* Predicted Failure Location ACI 2008	Predicted Failure Mode ACI 2008	V_c-Predict (kN) ACI 2008	V-Exp (kN) ACI 2008	V-Exp/V_c-Predict CSA 2004	V-Exp/V_c-Predict ACI 2008
65	271 mm	184.7	186.0	197 mm	Web-Shear	183.5	186.4	1.01	1.02
70	271 mm	167.0	186.0	197 mm	Web-Shear	189.0	186.4	1.11	0.99
75	271 mm	172.3	186.0	197 mm	Web-Shear	194.3	186.4	1.08	0.96
80	271 mm	177.4	186.0	197 mm	Web-Shear	199.4	186.4	1.05	0.93
85	271 mm	182.4	186.0	197 mm	Web-Shear	204.4	186.4	1.02	0.91
90	271 mm	187.2	186.0	197 mm	Web-Shear	209.3	186.4	0.99	0.89

** Predicted Failure Location measured from end of slab*

5.2.3.1 *Experimental and Code-Predicted Capacities*

For slabs 300-06A and 300-06B, the Canadian code (CSA 2004) and American code (ACI 2008) predicted different failure locations from the end of the slab. If the Canadian code limit on the concrete compressive strength for shear calculations was followed (approximately 65MPa) then the experimental-to-predicted shear capacity was 1.16 for slab 300-06A and 1.37 for slab 300-06B, which indicates conservatism for each case. If the estimated concrete compressive strength of 80 MPa is used for slab 300-06A, and if the estimated range from 80 to 85 MPa is used for slab 300-06B for the Canadian code predictions, then the experimental-to-predicted shear capacity changed only slightly. Varying the concrete strength from 65 to 90 MPa changed the code-predicted capacities by less than 1%.

It is quite evident that the tensile anchorage requirement of the strands near the support in Clause 11.3.9.5 of the Canadian code (CSA 2004) could not be met at the failure load for slabs 300-06A and 300-06B, with the experimental failure load being 3.50 to 5.00 times larger than what the strands are capable of resisting in tension adjacent to the support.

If the American code limit on the concrete compressive strength for shear calculations was followed (approximately 70MPa) then the experimental-to-predicted shear capacity was 1.0 for slab 300-06A and 1.14 for slab 300-06B, which is in close agreement with the observed failure load. If the estimated concrete compressive strength of 80 MPa is used for slab 300-06A for the American code predictions, then the experimental-to-predicted shear capacity reduced to 0.94. If the estimated concrete compressive strength of 80 to 85 MPa is used for the American code prediction for slab 300-06B, then the experimental-to-predicted shear capacity ranged between 1.05 and 1.08. The American code-predicted shear capacity is therefore very close to the

experimental shear capacity for slabs 300-06A and 300-06B. Varying the concrete strength from 65 to 90 MPa changed the code-predicted capacities by approximately 16%.

For slabs 300-18A and 300-18B, the Canadian code (CSA 2004) and American code (ACI 2008) both predicted different failure locations from the end of the slab. If the Canadian code limit on the concrete compressive strength for shear calculations was followed (approximately 65MPa) then the experimental-to-predicted shear capacity was 0.98 for slab 300-18A and 1.01 for slab 300-18B, which is very close to a value of 1.0. If the estimated concrete compressive strength of 81 MPa is used for slab 300-18A, and if the estimated range from 85 to 90 MPa is used for slab 300-18B for the Canadian code predictions, then the experimental-to-predicted shear capacity changed only slightly. Varying the concrete strength from 65 to 90 MPa changed the code-predicted capacities by less than 2%.

Again, it is evident that the tensile anchorage requirement of the strands near the support in Clause 11.3.9.5 of the Canadian code (CSA 2004) could not be met at the failure load for slabs 300-06A or 300-06B, with the experimental failure load being 1.44 to 1.68 times larger than what the strands are capable of resisting in tension adjacent to the support.

If the American code limit on the concrete compressive strength for shear calculations was followed (approximately 70MPa) then the experimental-to-predicted shear capacity was 0.96 for slab 300-18A and 0.99 for slab 300-18B, which is very close to a value of 1.0. If the estimated concrete compressive strength of 81 MPa is used for the American code prediction for slab 300-18A, then the experimental-to-predicted shear capacity reduced to 0.91, and if the estimated strength of 85-90 MPa was applied to slab 300-18B, the experimental-to-predicted shear capacity ranged from 0.89 to 0.91, which is un-conservative compared to a value of 1.0, and compared to

the Canadian code. Varying the concrete strength from 65 to 90 MPa changed the code-predicted capacities by approximately 14%.

5.2.3.2 *Modes of Failure*

The American code (ACI 2008) predicted a web-shear failure for slabs 300-06A, 300-06B, 300-18A and 300-18B. This was in agreement with the observed failure mode, which was a web-shear failure for slabs 300-06A, 300-06B, 300-18A and 300-18B.

5.2.3.3 *Effect of Length of Bearing*

Slab 300-06A, which had 63 mm of bearing failed at a test load of 199.5 kN, while slab 300-06B, which had 38 mm of bearing failed at a test load of 228.7 kN, indicating that the smaller bearing length surprisingly increased the failure load by approximately 15%. Note that slab 300-06A had a total web width of 244 mm, while slab 300-06B had a total web width of 242 mm (Appendix A) – therefore the web-widths were within 1% of each other.

Slab 300-18A, which had 63 mm of bearing failed at a test load of 213.7 kN, while slab 300-18B, which had 38 mm of bearing failed at a test load of 212.6 kN, indicating that the smaller bearing length reduced the failure load by less than 1%. Note that slab 300-18A had a total web width of 257 mm, while slab 300-18B had a total web width of 247 mm (Appendix A) – a difference of about 4%.

5.2.3.4 *Effect of Prestressing Level*

The level of prestressing appears to have a larger effect on the Canadian code (CSA 2004) predictions compared to the American code (ACI 2008) predictions, based on the difference in

the predicted shear capacities. In terms of the observed failure loads, increasing the area of prestressing by a factor of approximately 2.80 (from slabs 300-06A and 300-06B to slabs 300-18A and 300-18B) increased the failure load by approximately 7% for slabs with 63 mm of bearing but reduced the failure load by about 7% for slabs with 38 mm of bearing.

5.3 CRACK PROFILES AND CRITICAL SECTION LOCATION FOR SHEAR

5.3.1 Predicted and Experimental Locations of Critical Section

As outlined in Chapter 4, the Canadian code (CSA 2004) considers the critical section for shear at "d_v" from the face of the support, whereas the American code (ACI 2008) considers the critical section for shear at "h/2" from the face of the support, resulting in a different location of the critical section from the end of the member for each code.

The critical section for shear resistance was typically located further from the member end for the Canadian Code (CSA 2004) than for the American code (ACI 2008). Since the strands are assumed to linearly develop over an approximate distance of 50 strand diameters, this difference in the location for critical shear resistance would have some theoretical effect on the shear resistance of the slabs.

Tables 5.1 to 5.6 indicate the predicted shear failure locations for each slab according to the Canadian code (CSA 2004) and the American code (ACI 2008). These predicted failure

locations have been plotted for the three series; 200, 250 and 300 test slabs, together with the observed web-crack profiles for each individual web in Figures 5.1 to 5.3.

For reference, the location of d_v, and $h/2$ are also included in Figures 5.1 to 5.3. Furthermore, the critical section for web-shear in the European Product Standard EN-1168 (EN-1168 2008) is assumed to occur along a line that extends from the face of the bearing pad, at an angle of 35 degrees to the horizontal; this line has also been included in the failure profile drawings for reference. Finally, detailed crack profiles and measured crack angles have been plotted for each individual web in Appendix H, for all slabs except slabs 200-01A and 250-01B, which did not have cracked surfaces that were available for measurement due to the mode of failure.

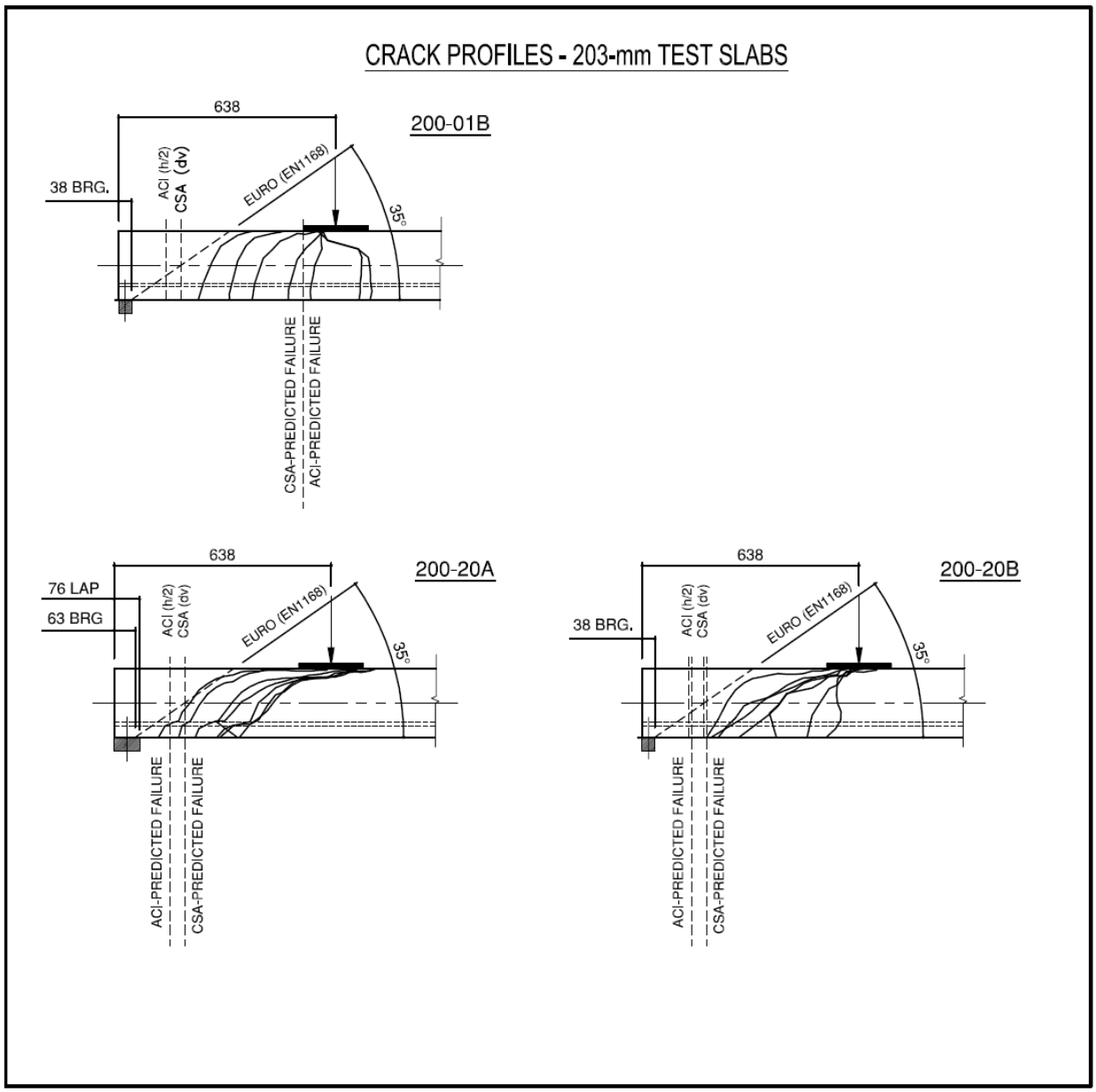

Figure 5.1: Crack Profiles and Predicted Locations of Shear Failure for CSA and ACI Codes – Series-200 Test Slabs

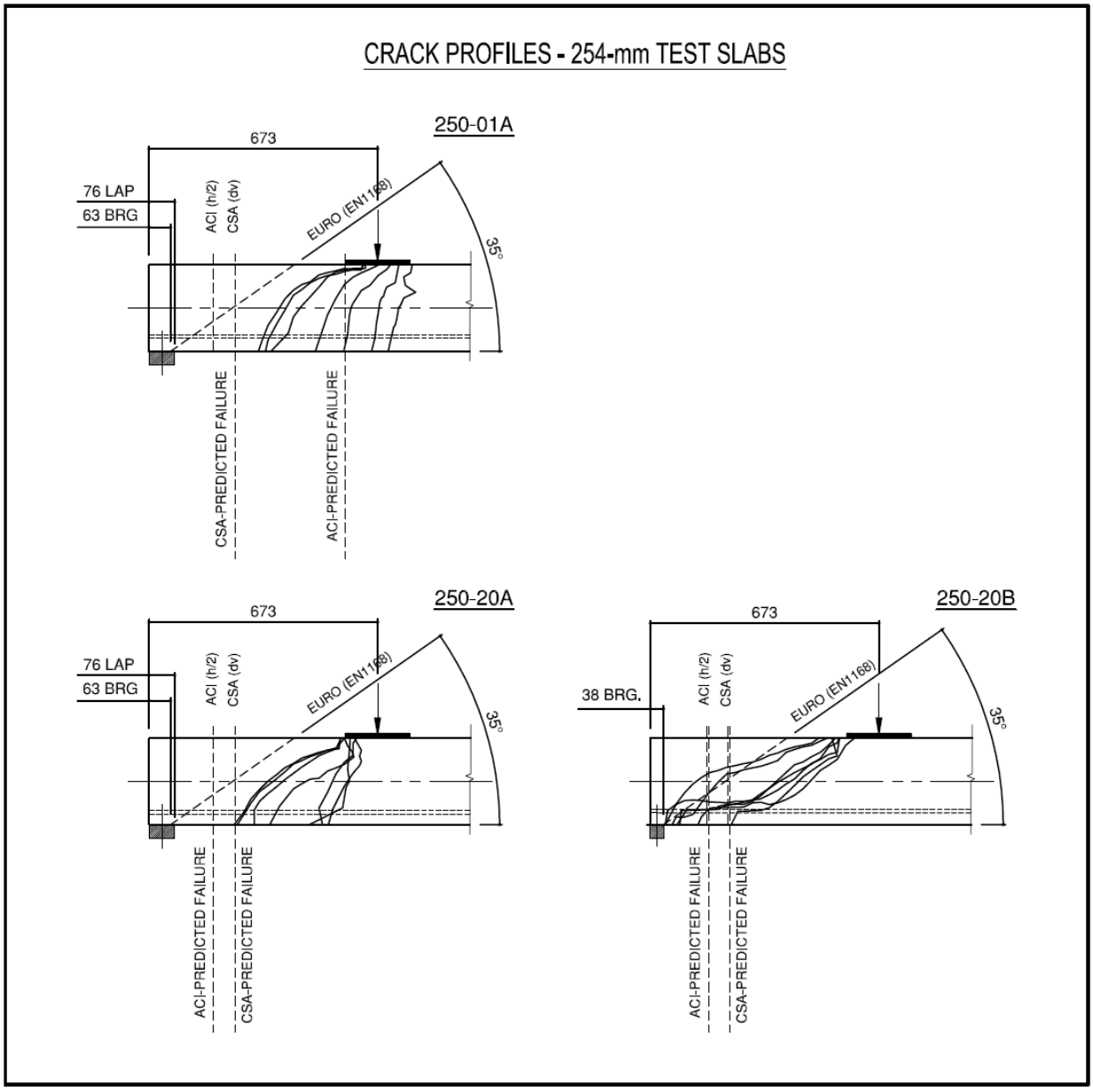

Figure 5.2: Crack Profiles and Predicted Locations of Shear Failure for CSA and ACI Codes – Series-250 Test Slabs

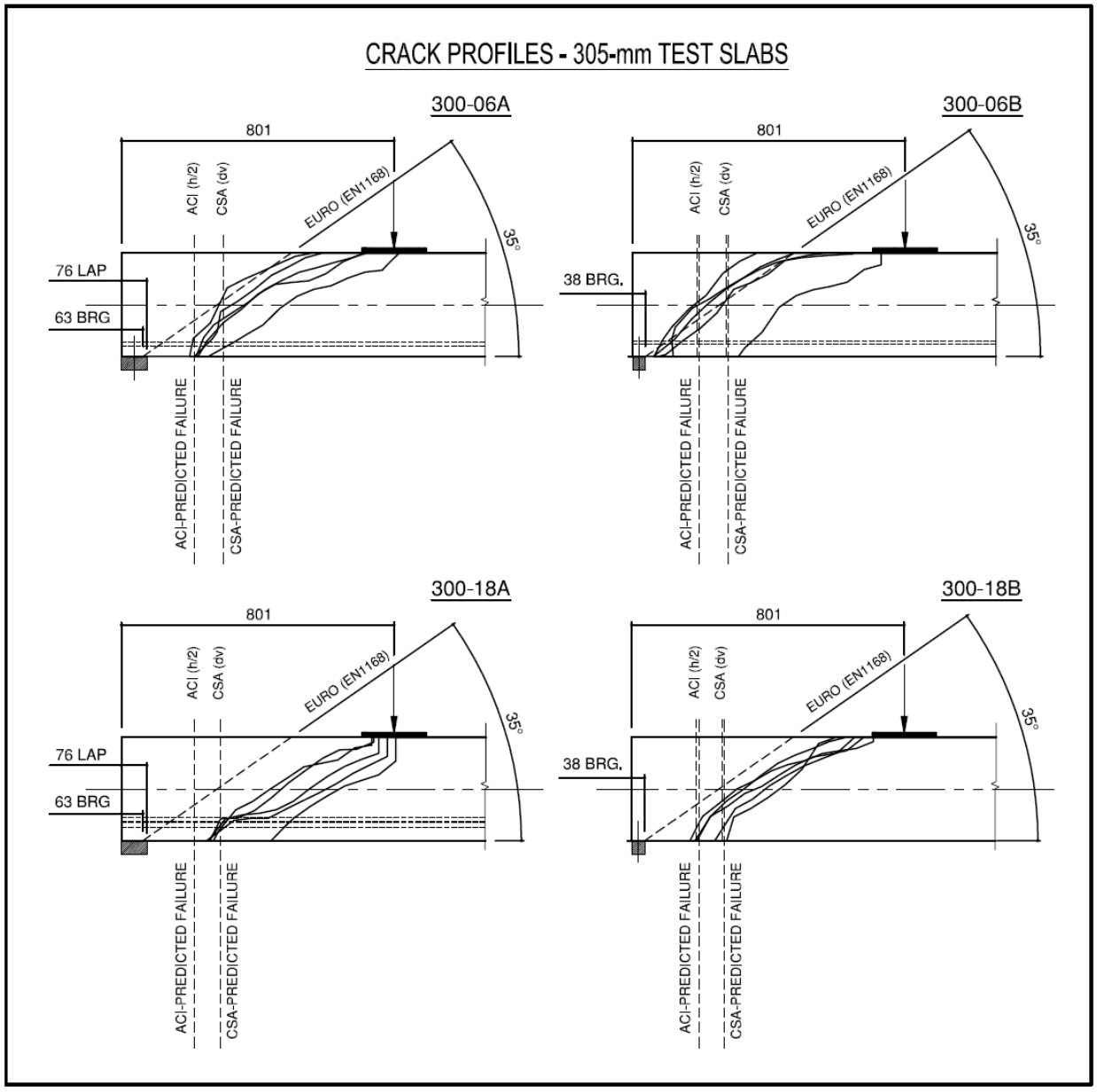

Figure 5.3: Crack Profiles and Predicted Locations of Shear Failure for CSA and ACI Codes – Series-300 Test Slabs

For slab 200-01B, the Canadian code and American code predicted the shear failure location to be adjacent to the load, which appears to be reasonable compared to the observed web cracks. However, the European Product Standard predicted a shear failure much closer to the support. For slabs 200-20A and 200-20B the observed web cracks are all between the load and the

support and not at the American code, Canadian code or European Product Standard predicted locations, with the exception of two of the web cracks in slab 200-20A which are relatively close to the European Product Standard predicted location.

For slab 250-01A, the American code predicted the shear failure location to be adjacent to the load, which appears to be reasonable compared to the observed web cracks. However, the Canadian code and European Product Standard predicted a shear failure much closer to the support. For slab 250-20A many of the cracks are adjacent to the load and are not near the failure locations predicted by the American code, Canadian code and the European Product Standard. Finally, for slab 250-20B the observed web cracks are all between the load and the support and not at the American code, Canadian code or European Product Standard predicted locations, with the exception of two of the web cracks in slab 250-20B which are relatively close to the European Product Standard predicted location.

For slab 300-06A the Canadian code, and European Product Standard predicted shear failure locations appear to be reasonable compared to the observed web cracks. For slab 300-06B all three codes have a reasonable agreement with the observed web cracks. However, for slabs 300-18A and 300-18B the observed web cracks are all between the load and the support and not at the American code, Canadian code or European Product Standard predicted locations.

To review the effect of the level of prestressing and the length of bearing on the web crack profile locations, the failure profiles for each slab have been superimposed together in Figures 5.4 to 5.6.

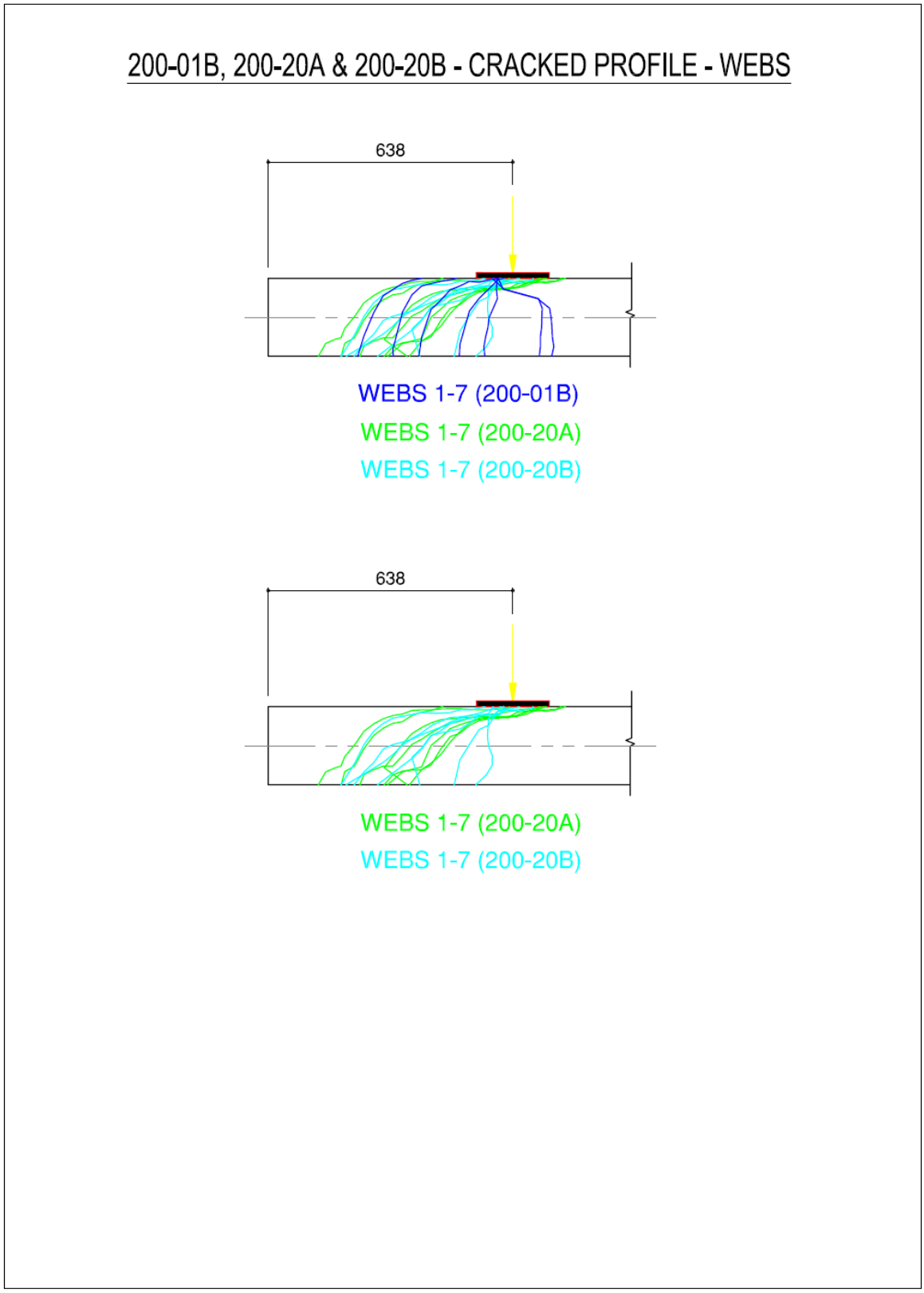

Figure 5.4: Slabs 200-01B, 200-20A and 200-20B Cracked Profile - Webs

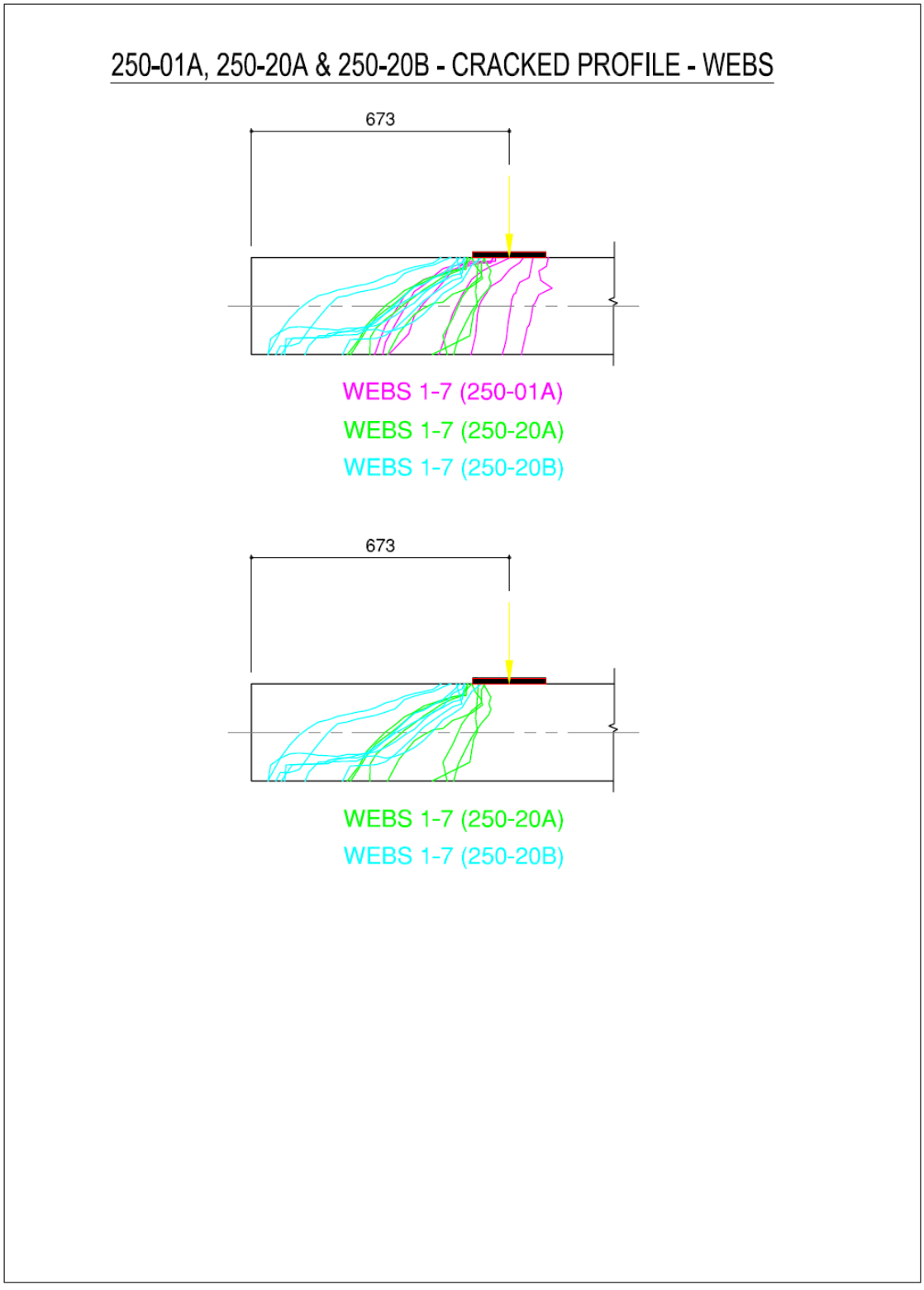

Figure 5.5: Slabs 250-01A, 250-20A and 250-20B Cracked Profile - Webs

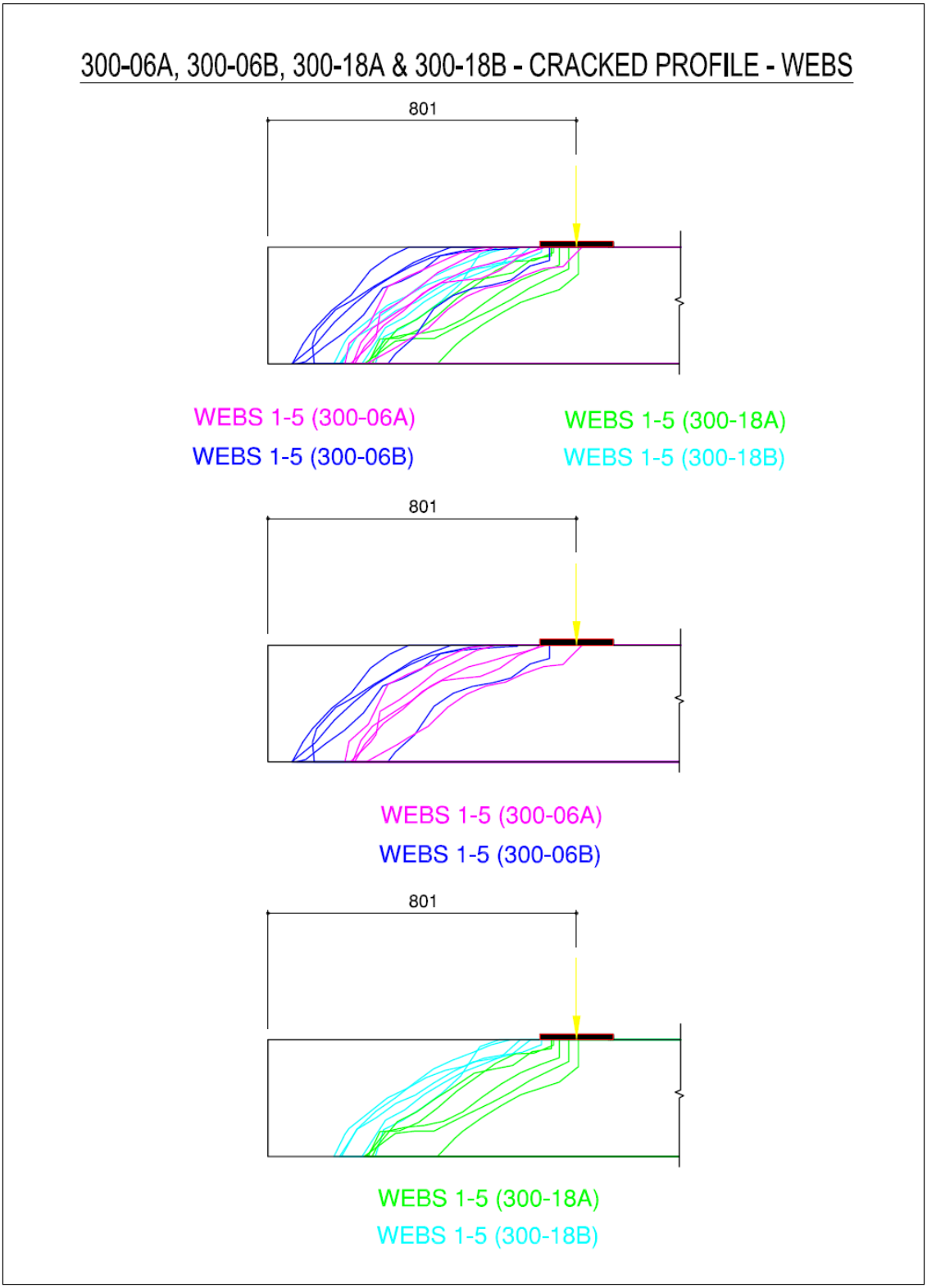

Figure 5.6: Slabs 300-06A, 300-06B, 300-18A and 300-18B Cracked Profile - Webs

5.3.2 Effect of Length of Bearing on Failure Locations

In general, the length of bearing appears to shift the location of the failure profiles. In Series-250, comparing slabs 250-20A and 250-20B indicates a notable difference in the location of failure profiles, with those for slab 250-20B (reduced bearing) shifting closer to the end of the slab. Similarly, comparing Series-300 slabs indicates that slabs with reduced bearing had their shear failure profiles shifted closer to the end of the slab, for both low and high levels of prestressing. However, the one exception is found in comparing slabs 200-20A and 200-20B, where the failure profiles for 200-20A and 200-20B are in the same general region. In this case, the two failure-cracks for 200-20B that appear adjacent to and under the load have a very steep angle and may be more flexural in nature.

5.3.3 Effect of Level of Prestressing on Failure Locations

The level of prestressing affected the failure profiles in several ways. Slabs with low levels of prestressing (200-01A, 200-01B, 250-01A, 250-01B) exhibited a combined flexure-shear and flexural failure, with much steeper slopes in the failure profiles. In addition, for these slabs the failure profiles were concentrated near the load. However, for Series-300 slabs, the effect of lowering the level of prestressing was a shift in the failure profiles away from the load and closer to the end of the slab.

5.4 SHEAR CRACK ANGLES

5.4.1 Predicted and Experimental Shear Crack Angles

The Canadian code (CSA 2004) defines *"θ"* as the angle of inclination of diagonal compressive stresses to the longitudinal axis of the member. Shear cracks are expected to form at these theoretical angles, as the principal tensile stresses perpendicular to the angle "*θ*" exceed the tensile capacity of the concrete in the webs. A summary of the predicted "*θ*" angles for all slabs at the code-predicted critical section is presented in Table 5.7.

Table 5.7: Predicted Shear Crack Angles (CSA)

Slab ID	CSA Predicted Shear Failure Angles (degrees)	Average Experimental Shear Failure Angles (degrees)
200-01A	35	N/A
200-01B	35-36	71
200-20A	30	54
200-20B	29-30	50
250-01A	35	68
250-01B	35-36	N/A
250-20A	30	48
250-20B	30	39
300-06A	30	41
300-06B	30	40
300-18A	29	34
300-18B	29	35

***** *Failure angle measured at slab mid-depth for all slabs*

It can be seen that the experimental crack angles were significantly higher than predicted for slabs with a shallower depth and also for slabs with low levels of prestressing. However, it should be noted that the observed failure profiles are not one continuous angle, but rather a variable angle along each crack. In addition, it is very difficult to single out which web was the

one that triggered the failure and some of the variation in the angles and locations of the failure profiles may be due to the very rapid re-distribution of load to other undamaged webs, or possibly some differential warping between the end supports prior to loading.

Further study of the crack angles could be done using either a strut-and-tie model and/or a finite element analysis to determine the expected compressive strut angles within the zone between the support and the load. In addition, this type of analysis could be supplemented by the strains recorded in the test program.

CHAPTER 6 CONCLUSIONS AND FUTURE WORK

6.1 SUMMARY AND CONCLUSIONS

The scope of this study was to verify the experimental-to-predicted shear capacities of 203, 254 and 305 mm deep hollow-core slabs (Series-200, -250 and -300, respectively), according to the current Canadian and American concrete design codes (CSA 2004, ACI 2008) through shear tests performed on twelve full-scale hollow-core slabs. An additional objective was to confirm the observed modes of failure and compare them with those predicted by the codes. Finally, the the effect on the hollow-core slab shear capacity of the length of bearing over the support region and the level of prestressing were studied.

Shear tests were performed using the European standardized hollow-core shear test (Annex J, EN-1168 2008); used as a quality-assurance check for hollow-core slab designers and producers to verify the European code-predicted (EC2 2004) shear capacities through testing. Analysis of the test slabs for the load configuration of the standardized shear test indicated that for Series-200 and Series-250 slabs with low levels of prestressing, the American code-predicted shear capacities (ACI 2008) are approximately 1.7 to 1.9 times larger than the shear capacities predicted by the Canadian code (CSA 2004). However, for slabs with high levels of prestressing, the difference in the predicted shear capacities between each code is much closer, ranging from 2.0 to 21.0% for all slab depths.

A summary of the experimental results and conclusions are outlined below:

1. The Canadian code (CSA 2004) shear equations are appropriate for ductile shear failures, where vertical shear reinforcement or adequate anchorage of longitudinal reinforcement ensure that members can sustain additional loading beyond that causing the formation of initial shear cracks. Due to production constraints, hollow-core slabs have no vertical shear reinforcement. In addition, the longitudinal prestressing reinforcement cast into the hollow-core slabs does not typically provide adequate anchorage to develop a ductile shear failure, when the failure occurs near the slab ends.

   This was observed in the shear failures of the slabs when shear cracks formed between the load and support. The sudden tensile demand on the strands after cracking consistently proved to be greater than the resistance, and the slabs failed immediately following the formation of shear cracks across the full slab width. Therefore, it is unlikely that a ductile shear failure can be achieved for hollow-core slabs through strand anchorage alone for shear cracks that occur near the bearing zone.

   Additional reinforcement that is properly anchored over a relatively short bearing length (which can be difficult to achieve in practice) would be required, to satisfy the ductility anchorage requirements of Clause 11.3.9.5 in the Canadian code (CSA 2004) for hollow-core slabs. This requirement for additional slab tensile anchorage reinforcing adversely affects both the simplicity and economy of prestressed hollow-core slabs.

2. Regarding the effect of the prestressing on the predicted-to-experimental shear capacities; in general the level of prestressing has a much larger effect on the predictions of the Canadian code (CSA 2004) compared to those of the American code (ACI 2008). The

Canadian code (CSA 2004) heavily penalizes the shear capacity of members with low levels of prestressing. Slabs in the 203 and 254 mm depth range, with the lowest levels of prestressing had the highest experimental-to-predicted capacities - on the order of 1.6 to 2.0, indicating a high level of conservatism. However, the experimental-to-predicted capacities improved for slabs with maximum levels of prestressing - on the order of 1.0 for the 203 and 305 mm deep slabs, and 1.4 for the 254 mm deep test slabs.

In general, there is a fundamental error in applying the post-cracking shear method in the Canadian code (CSA 2004) to hollow-core slabs that are prone to fail in web-shear - an elastic principal stress analysis is more suitable for these cases. However, considering that the slabs with the highest level of conservatism in the Canadian code (CSA 2004) experienced either a flexure-shear failure, or a flexural failure, there is still a large difference between the predicted and experimental shear capacities for hollow-core slabs, even when web-shear is not the observed failure mode.

3. The American code (ACI 2008) flexure-shear and web-shear equations predicted the failure loads with more consistency than the Canadian code (CSA 2004) over the range of tested slab depths, prestressing levels and bearing lengths. The experimental-to-predicted capacities ranged from 0.9 to 1.2 for slabs with the lowest level of prestressing and from 0.8 to 1.4 for slabs with the highest level of prestressing. However, there is a concern in applying the American code (ACI 2008) shear equations to hollow-core slabs greater than 320 mm in depth, since the predicted-to-experimental capacities have been shown to be un-conservative for slabs deeper than 320 mm.

4. Experimental-to-predicted shear capacities less than one indicate an over-prediction of shear capacity by the code (un-conservative). The aggregate size factor in the shear equations of the Canadian code (CSA 2004) prevents over-prediction of the shear capacity in comparison to cases where the experimental-to-predicted capacities were less than unity for the ACI code.

5. The Canadian code (CSA 2004) does not have separate equations predicting shear failure modes; however the American code (ACI 2008) has expressions to evaluate the shear capacity due to web-shear failure and flexure-shear failure. Regarding the predicted and observed modes of failure, the American code (ACI 2008) correctly predicted the failure mode for all slabs, except for one case in which a flexural failure occurred prior to a shear failure.

6. All slabs were able to reach their full shear capacity with as little as 38 mm of bearing. Based on the observed failures, reducing the length of bearing from 63 mm to 38 mm had only a small effect on the experimental slab shear capacities – the typical reduction in shear capacity ranged from 1.0 to 14.0%. However in one case, a 305-mm deep slab with reduced bearing had an experimental failure load that was 15.0% higher than the companion slab with 63-mm of bearing, even though the web-widths were within 1.0% of each other. In general, reducing the length of bearing shifted the shear-failure profiles closer to the support.

7. In general, slabs with low levels of prestressing exhibited shear-failure profiles that had steeper slopes compared to slabs with higher levels of prestressing. Finally, there was a wide range in locations between the code-predicted critical sections for shear and the observed shear-crack profile locations; none of the codes (CSA 2004, ACI 2008, EN-1168 2008) consistently predicted the observed shear failure locations.

8. To address the difficulty in achieving a ductile shear failure in hollow-core slabs, a single shear-capacity reduction factor should be considered for hollow-core slabs that fail in shear near the support, where the strands cannot achieve the required tensile anchorage strength after shear failure of the webs.

6.2 FUTURE WORK

Ideally, design codes should accurately predict both the failure mode and ultimate capacity of a member, for the full range of expected loads that the member will experience in its design life. However, applying code equations to situations that are not in agreement with the original assumptions made in the derivation of these equations results in inaccurate predictions of the member capacity. In the case of hollow-core slabs in the 203 to 254 mm depth range, applying the Canadian code (CSA 2004) equations for shear to slabs with low levels of prestressing results in over-conservative predictions by a factor of 1.6 to 2.0, without the application of any load or material-resistance factors, which is excessive.

It is clear that a separate web-shear equation is required for hollow-core slabs in the next edition of the Canadian code, to accurately predict the web-shear capacity of hollow-core slabs. In Europe, extensive testing has been performed to validate an elastic stress analysis method based

on equilibrium of forces that accurately predicts the web-shear capacity of hollow-core slabs (EN-1168 2008) – a version of this method should be considered for adoption in the next edition of the Canadian code. For the cases where a flexure-shear failure was observed, the Canadian code did not accurately predict the experimental shear capacity, in spite of using a post-cracking shear model. This should also be addressed in the shear equations for the next edition of the Canadian code.

The Canadian Precast/Prestressed Concrete Institute (CPCI) is funding research for a second phase of shear testing to be performed on an additional twelve full-scale hollow-core slabs, of which six slabs are from the same supplier as the current research project, while the remaining six slabs are from another local supplier. In the second phase of testing, a level of prestressing will be selected that is approximately halfway between the lower and upper bounds of prestressing used in the current research project, to further study the effects of the level of prestressing.

In addition, the data collected from the instrumentation in both phases of the testing program will be used in conjunction with finite element analysis to study further the behaviour of hollow-core slabs in shear. Detailed calculations will be performed for slabs tested in each phase using the European Codes (EC2 2004, EN-1168: 2008) to compare the experimental-to-predicted values with those of the North American codes (CSA 2004, ACI 2008). Finally, specific equations for use in the evaluation of the shear capacity of hollow-core slabs will be developed and proposed for consideration in the 2014 edition of the Canadian code.

REFERENCES

1. ACI Committee 318. (1971). "Building Code Requirements for Reinforced Concrete (ACI 318-71) and Commentary (ACI 318R-71)," *American Concrete Institute*, Farmington Hills, Michigan.
2. ACI Committee 318. (1977). "Building Code Requirements for Reinforced Concrete (ACI 318-83) and Commentary (ACI 318R-77)," *American Concrete Institute*, Farmington Hills, Michigan.
3. ACI Committee 318. (1983). "Building Code Requirements for Reinforced Concrete (ACI 318-83) and Commentary (ACI 318R-83)," *American Concrete Institute*, Farmington Hills, Michigan.
4. ACI Committee 318. (1989). "Building Code Requirements for Structural Concrete (ACI 318-89) and Commentary (ACI 318R-89)," *American Concrete Institute*, Farmington Hills, Michigan.
5. ACI Committee 318. (2005). "Building Code Requirements for Structural Concrete (ACI 318-89) and Commentary (ACI 318R-05)," *American Concrete Institute*, Farmington Hills, Michigan.
6. ACI Committee 318. (2008). "Building Code Requirements for Structural Concrete (ACI 318-08) and Commentary (ACI 318R-08)," *American Concrete Institute*, Farmington Hills, Michigan.
7. American Association of State Highway and Transportation Officials (AASHTO). (2004). "LRFD Bridge Design Specifications," 3rd Edition, Washington DC: AASHTO.
8. Anderson, A. R. (1976). "Shear Strength of Prestressed Concrete Beams," Technical Bulletin 76-B11/B12, *Concrete Technology Associates*, Tacoma, WA, Nov., 45 p.

9. Anderson, A. R. (1978). "Shear Strength of Hollow Core Members," Technical Bulletin 78-B1, *Concrete Technology Associates*, Tacoma, WA, April, 33 p.
10. Anderson, R. G. (1987). "Web Shear Strength of Prestressed Concrete Members," Technical Bulletin 85-B1, *Concrete Technology Associates*, Tacoma, WA, March, 38 p.
11. Becker, R. J. and Buettner, D. R. (1985). "Shear Tests of Extruded Hollow Core Slabs," *PCI Journal,* Vol. 30, No.2, pp. 40-54.
12. Bertagnoli, G. and Mancini, G. (2009). "Failure Analysis of Hollow-Core Slabs Tested in Shear," Lausanne, *fib, Structural Concrete, Journal of the fib,* Vol. 10, No.3, September, pp. 139-152.
13. Black Mint Software. (2010). "Concise Beam," Version 4, copyright 2002-2010, Black Mint Software, Ottawa, ON.
14. British Standards Institution. (1985). "Structural Use of Concrete, Part 1, Code of Practice for Design and Construction," BS 8110, *British Standards Institution*, London, UK.
15. Canadian Precast/Prestressed Concrete Institute (CPCI). (2007). "Design Manual," 4th Edition, *Canadian Precast/Prestressed Concrete Institute*, Ottawa, ON, Canada.
16. Canadian Standard Association (CSA). (1994). "Design of Concrete Structures," CAN/CSA-A23.3-94, *Canadian Standards Association*, Rexdale, ON, Canada.
17. Canadian Standard Association (CSA). (2004). "Design of Concrete Structures," CAN/CSA-A23.3-04, *Canadian Standards Association*, Rexdale, ON, Canada.
18. CEB-FIP. (1978). "Model Code for Concrete Structures," *CEB Bulletin d'Information*, No. 124/125.

19. Cheng, S. and Wang, X. (2010). "Impact of Interaction between Adjacent Webs on the Shear Strength of Prestressed Concrete Hollow-Core Units", *PCI Journal*, Vol. 55, No. 3, pp. 46-63.
20. Deutsche Norm. (2004). "Eurocode 2: Design of Concrete Structures – Part 1-1: General Rules and Rules for Buildings," DIN EN 1992-1-1-04, *CEN-European Committee for Standardization*, Brussels, Belgium.
21. Deutsche Norm. (2008). "Precast Concrete Products–Hollow Core Slabs (includes Amendment A1:2008)." DIN EN 1168-08, *CEN-European Committee for Standardization*, Brussels, Belgium.
22. Deutsche Norm. (2005). "Precast Concrete Products–Hollow Core Slabs." DIN EN 1168-05, *CEN-European Committee for Standardization*, Brussels, Belgium.
23. Fellinger, J. H. H. and Breunese, A. J. (2005). "TNO Report: Standard Shear Tests on Prestressed Hollow Core Slabs According to EN 1168: 2005, *TNO Building and Construction Research*, Delft, the Netherlands, Nov., 47 p.
24. FIP Recommendations (1988), "Precast Prestressed Hollow-Core Floors," London: Thomas Telford, 1988, 31p.
25. Hawkins, N. M. and Ghosh, S. K. (2006). "Shear Strength of Hollow-Core Slabs", *PCI Journal*, Vol. 51, No. 1, pp. 110-114.
26. Macgregor, J. G. and Bartlett, F. M. (2000). "Reinforced Concrete Mechanics and Design," First Canadian Edition, *Prentice Hall Canada Inc.,* Toronto, ON, Canada.
27. Micallef, P. (2005). "Assessment of Shear Capacity of Pre-stressed Hollow Core Floor Units in the Local Construction Industry," Faculty of Architecture and Civil Engineering, University of Malta, June, 7 p.

28. Pajari, M. (2005). "Resistance of Prestressed Hollow Core Slabs Against Web Shear Failure," *Research Notes 2292*, VTT Building and Transport, Kemistintie, Finland, April, 69 p.

29. Pajari, M. and Koukkari, H. (1998). "Shear Resistance of PCH Slabs Supported on Beams I: Tests," *Journal of Structural Engineering*, Sept., pp. 1062-1061.

30. Pajari, M. (1998). "Shear Resistance of PCH Slabs Supported on Beams II: Analysis," *Journal of Structural Engineering*, Sept., pp. 1050-1073.

31. Pajari, M. (2009). "Web Shear Failure in Prestressed Hollow Core Slabs," *Rakenteiden Mekaniikka (Journal of Structural Mechanics)*, Vol. 42, No. 4, pp. 207-217.

32. Palmer, K. D. and Schultz, A. E. (2010). "Factors Affecting Web-Shear Capacity of Deep Hollow-Core Units", *PCI Journal*, Vol. 55, No. 2, pp. 123-146.

33. Pisanty, A. (1992). "The Shear Strength of Extruded Hollow-Core Slabs", *Materials and Structures*, RILEM, France, V. 25, pp. 224-230.

34. Portland Cement Association (PCA). (2008). "Notes on ACI 318-08 Building Code Requirements for Structural Concrete," *Portland Cement Association*, Skokie, IL.

35. Precast/Prestressed Concrete Institute (PCI). (2004). "Design Handbook," 6th Edition, *Precast/Prestressed Concrete Institute*, Chicago, IL.

36. Vecchio, F. J., and Collins, M. P. (1986). "The Modified Compression Field Theory for Reinforced Concrete Elements Subjected to Shear," *Journal of the American Concrete Institute,* V. 83, No. 2 (March-April), pp. 219-231.

37. Vecchio, F. J., and Collins, M. P. (1988). "Predicting the Response of Reinforced Concrete Beams Subjected to Shear Using Modified Compression Field Theory," *ACI Structural Journal,* V. 85, No. 3 (May-June), pp. 258-268.

38. Walraven, J. C. and Mercx, W. P. M. (1983). "The Bearing Capacity of Prestressed Hollow Core Slabs," *Heron*, Vol. 28, No. 3, pp. 1-46 p.

39. Yang, L. (1994). "Design of Prestressed Hollow Core Slabs with Reference to Web Shear Failure," *Journal of Structural Engineering,* ASCE, V. 120, No. 9, pp. 2675-2696.

APPENDICES

APPENDIX A

AS-CAST SLAB GEOMETRY

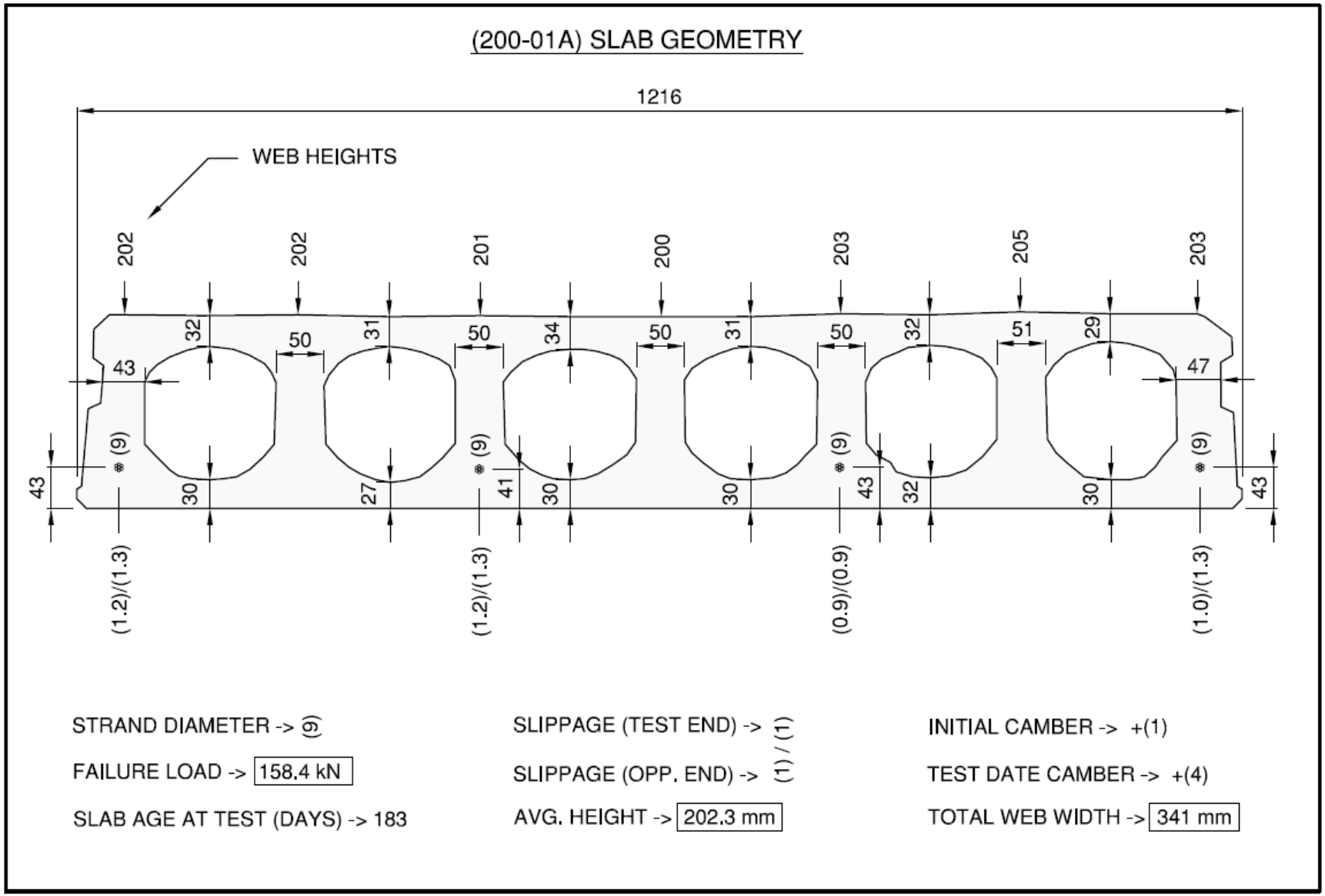

Figure A1: 200-01A Slab Geometry

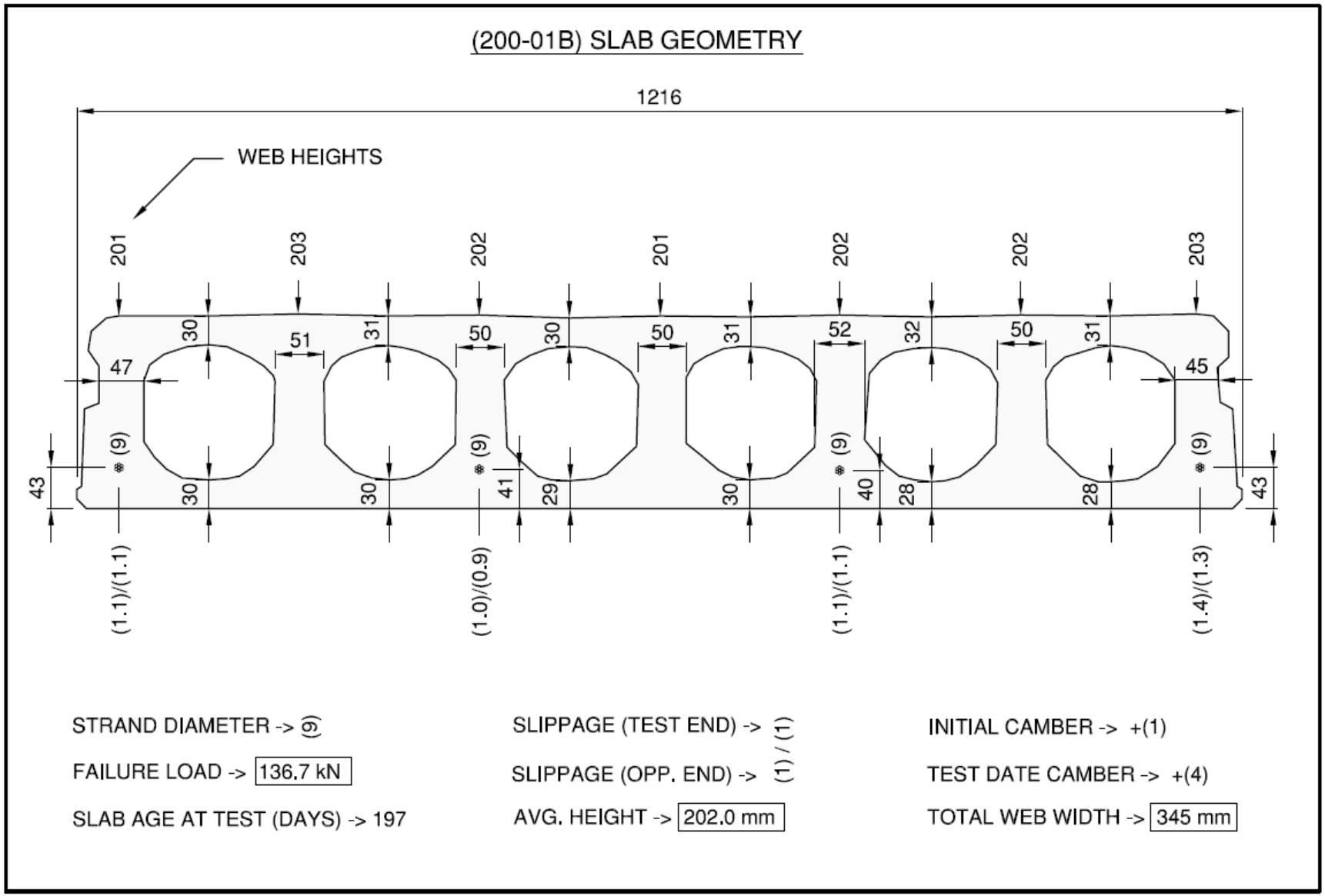

Figure A2: 200-01B Slab Geometry

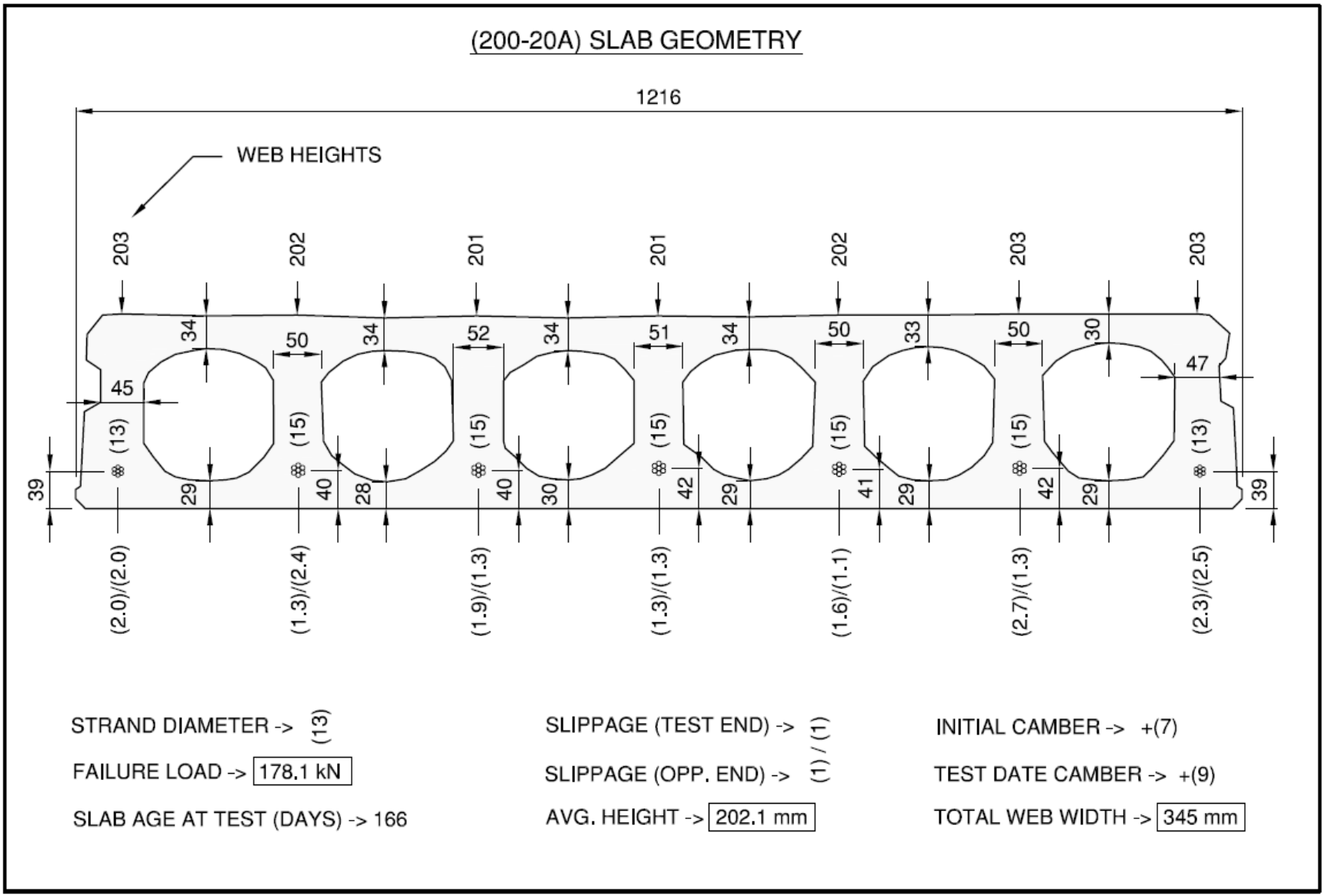

Figure A3: 200-20A Slab Geometry

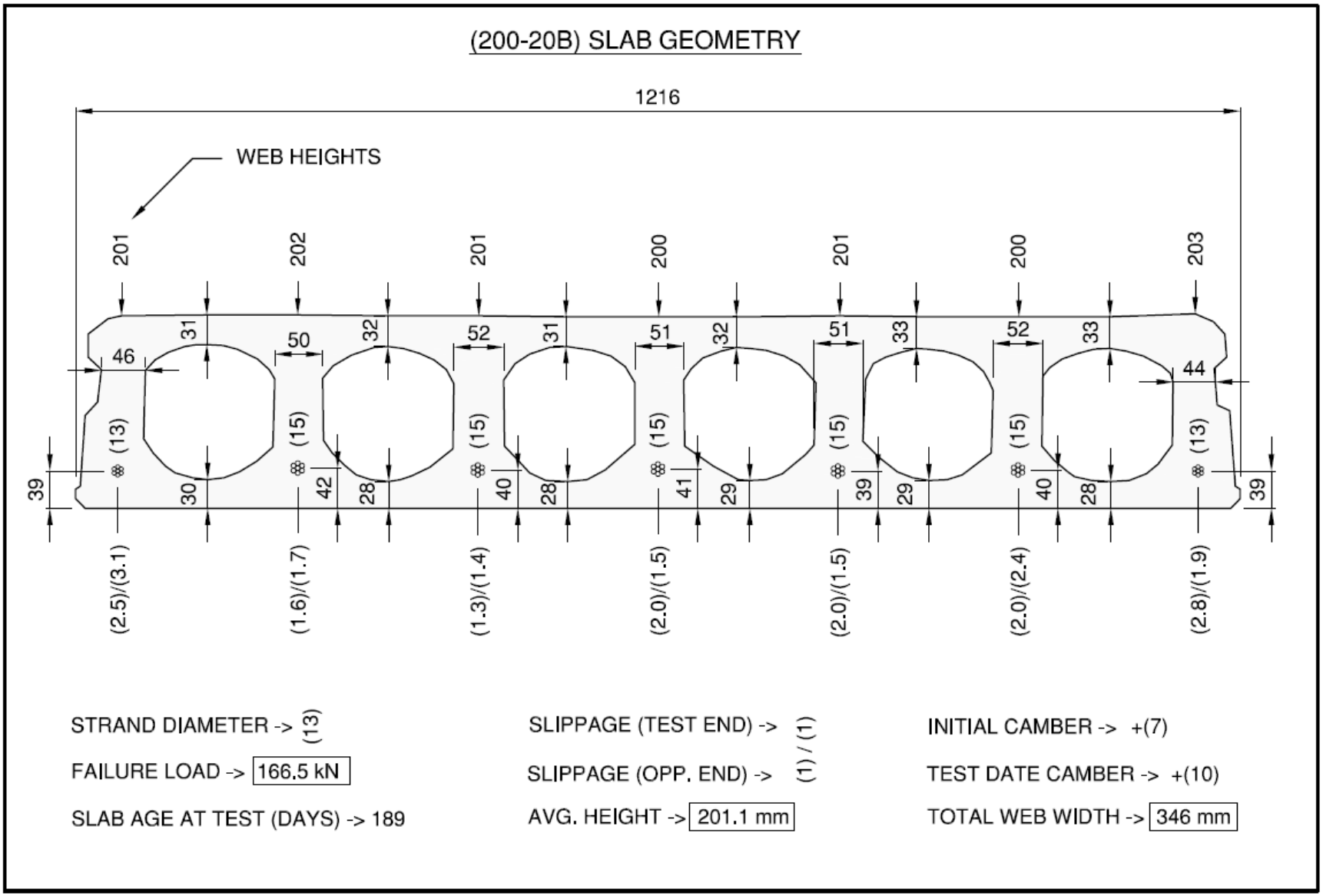

Figure A4: 200-20B Slab Geometry

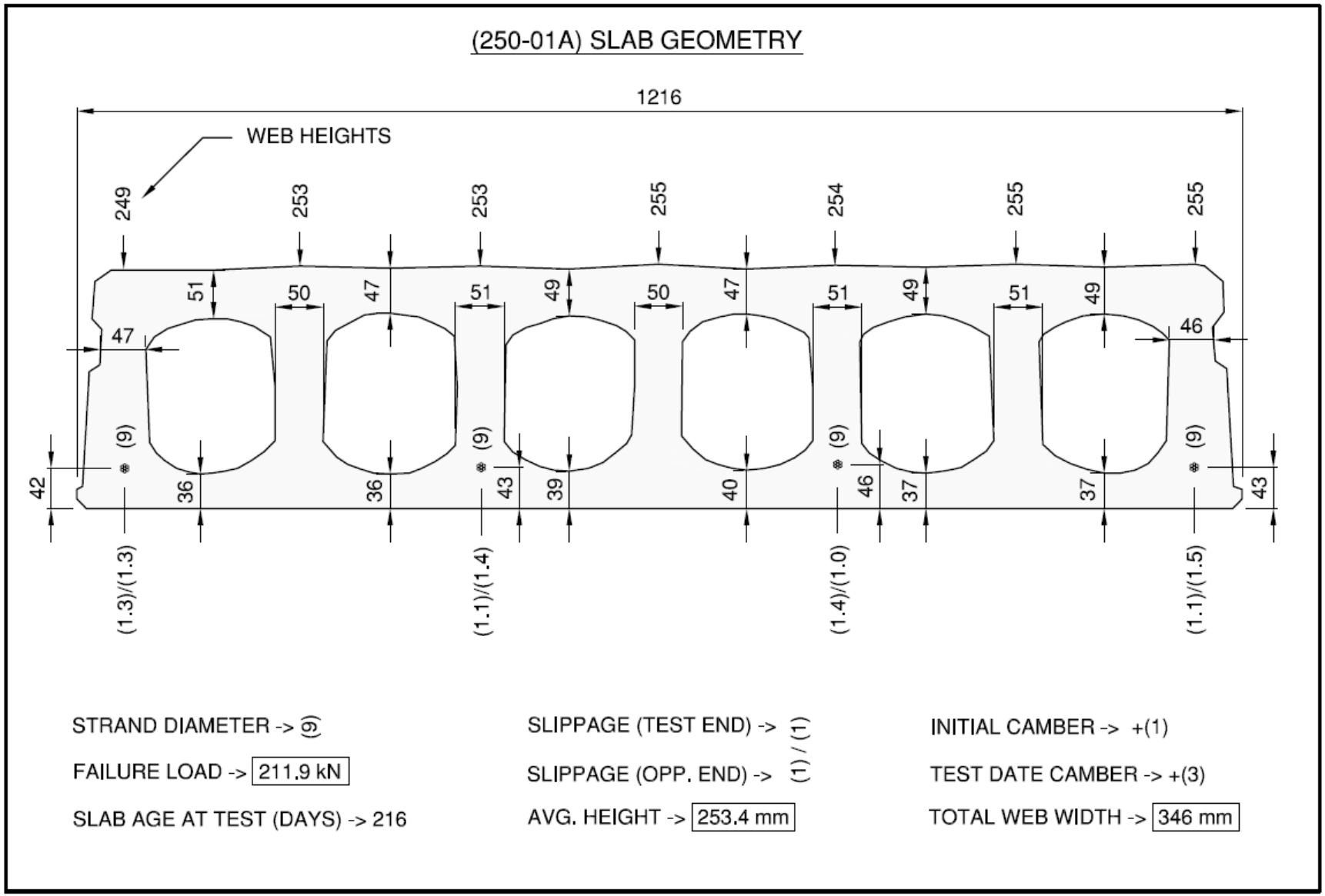

Figure A5: 250-01A Slab Geometry

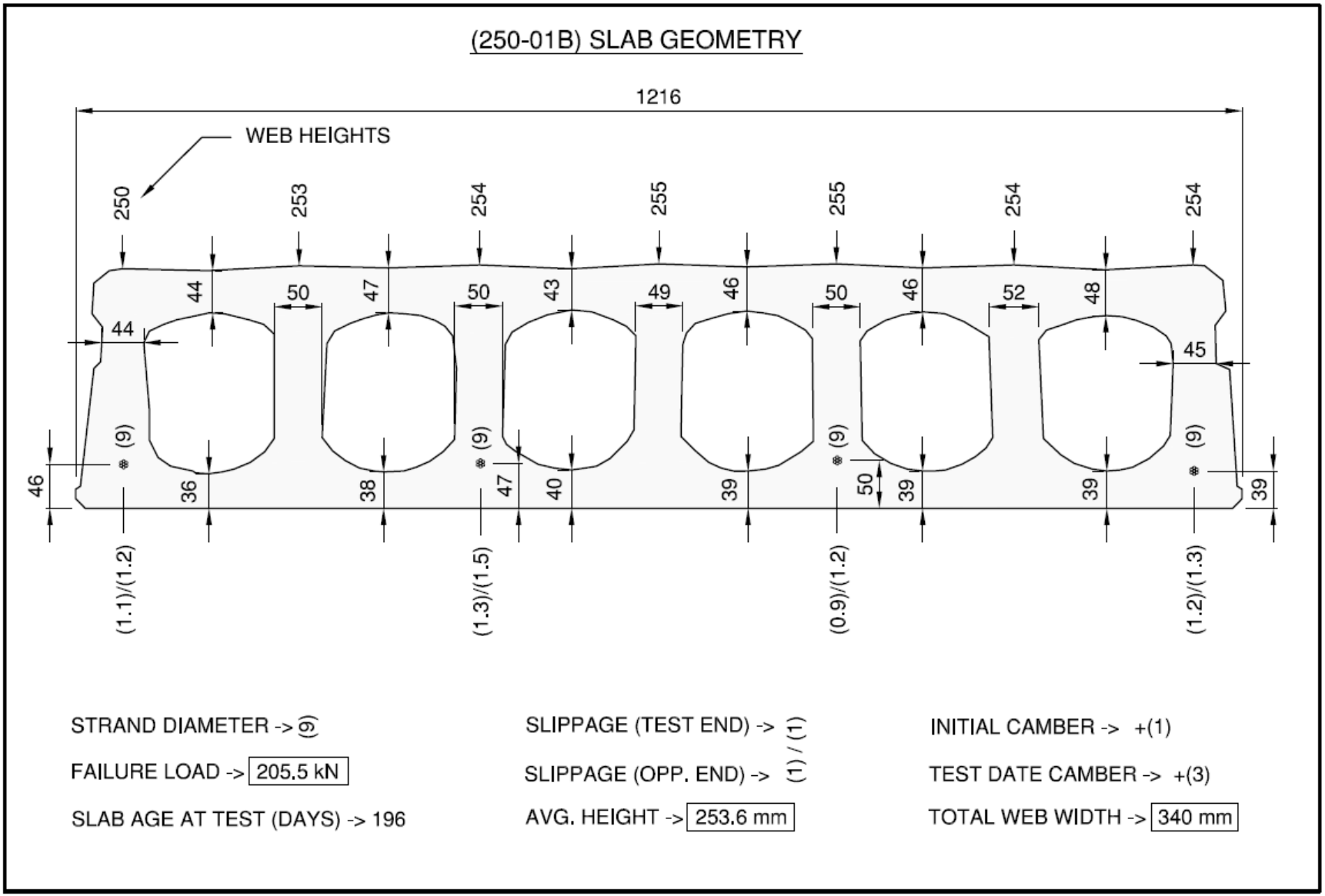

Figure A6: 250-01B Slab Geometry

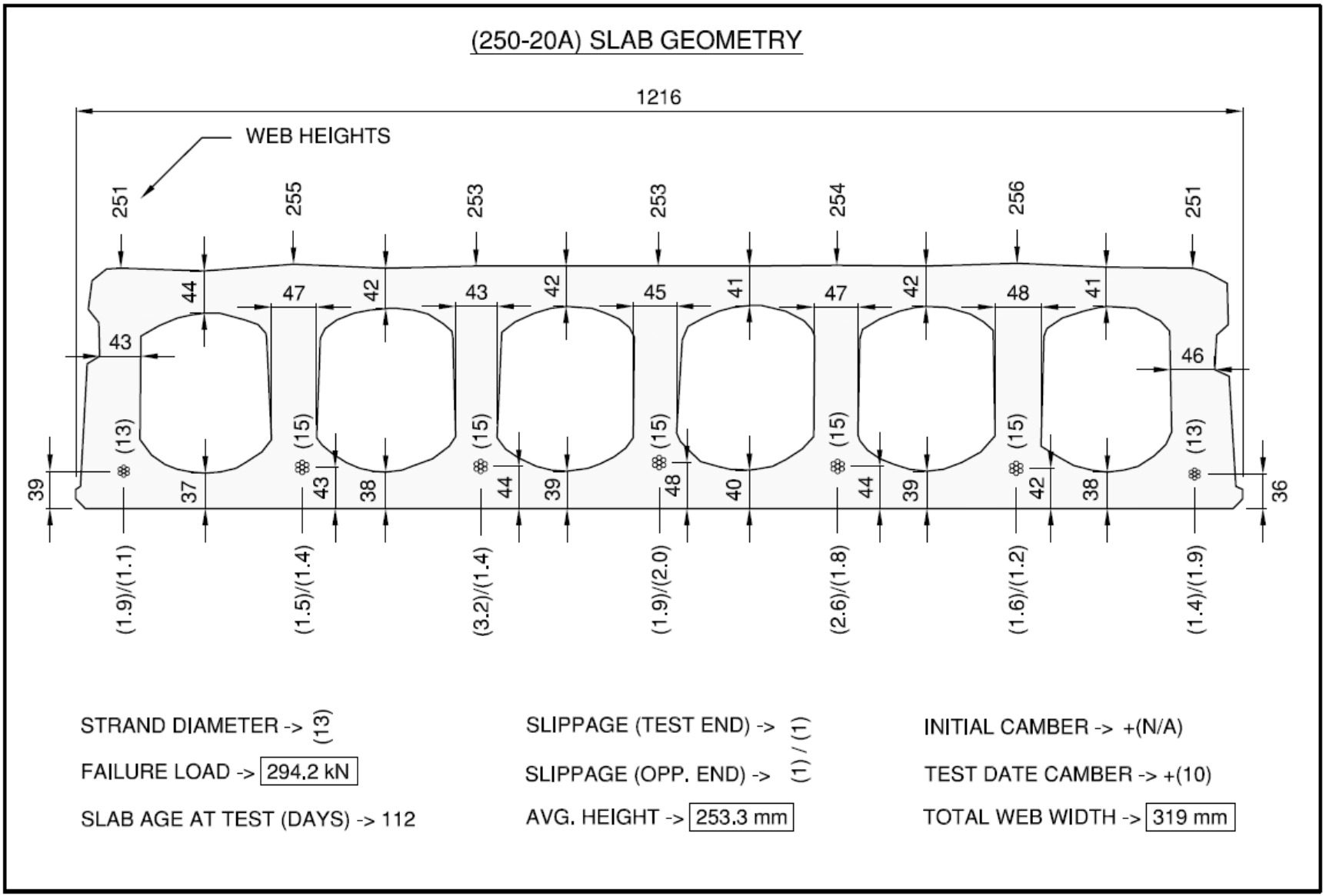

Figure A7: 250-20A Slab Geometry

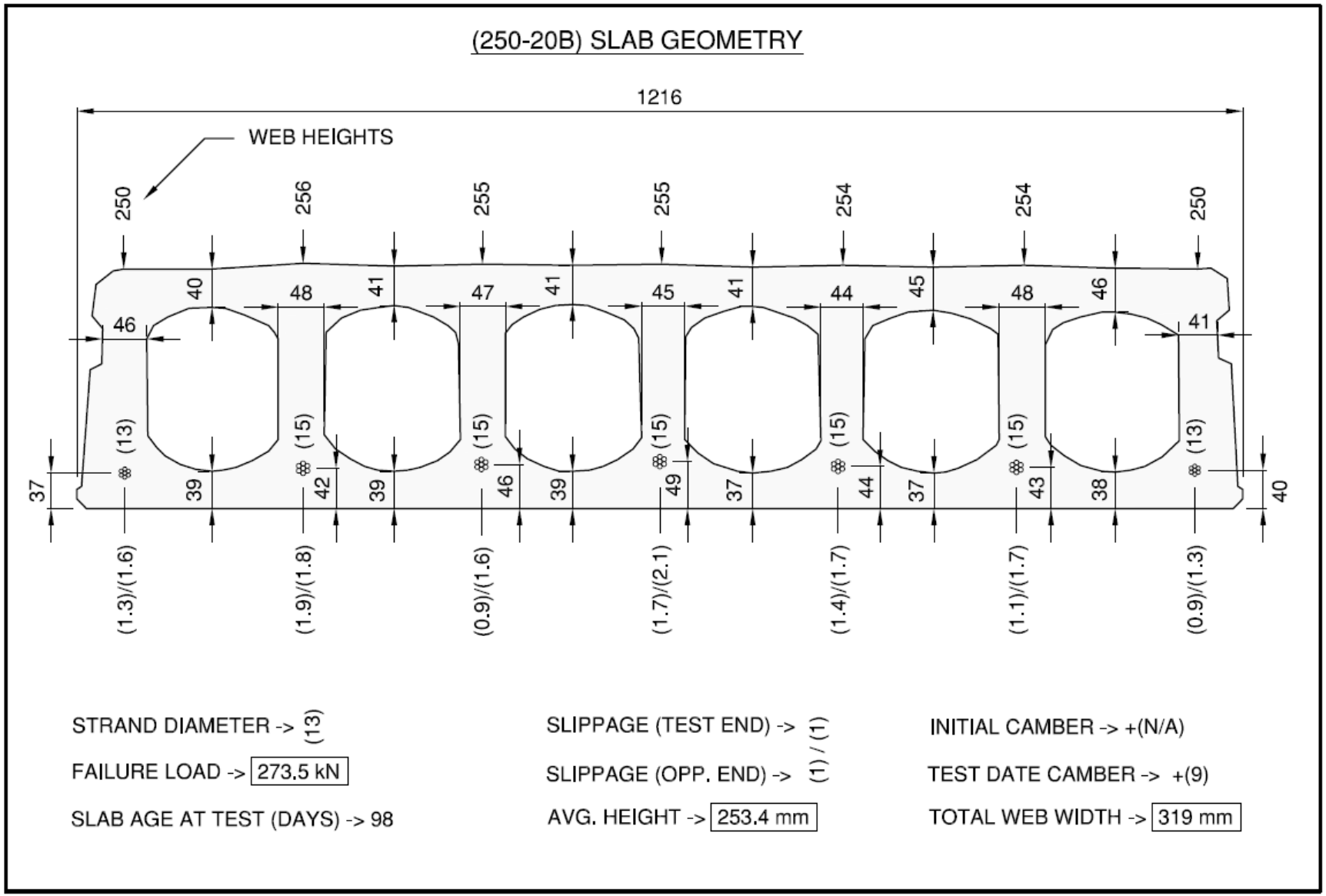

Figure A8: 250-20B Slab Geometry

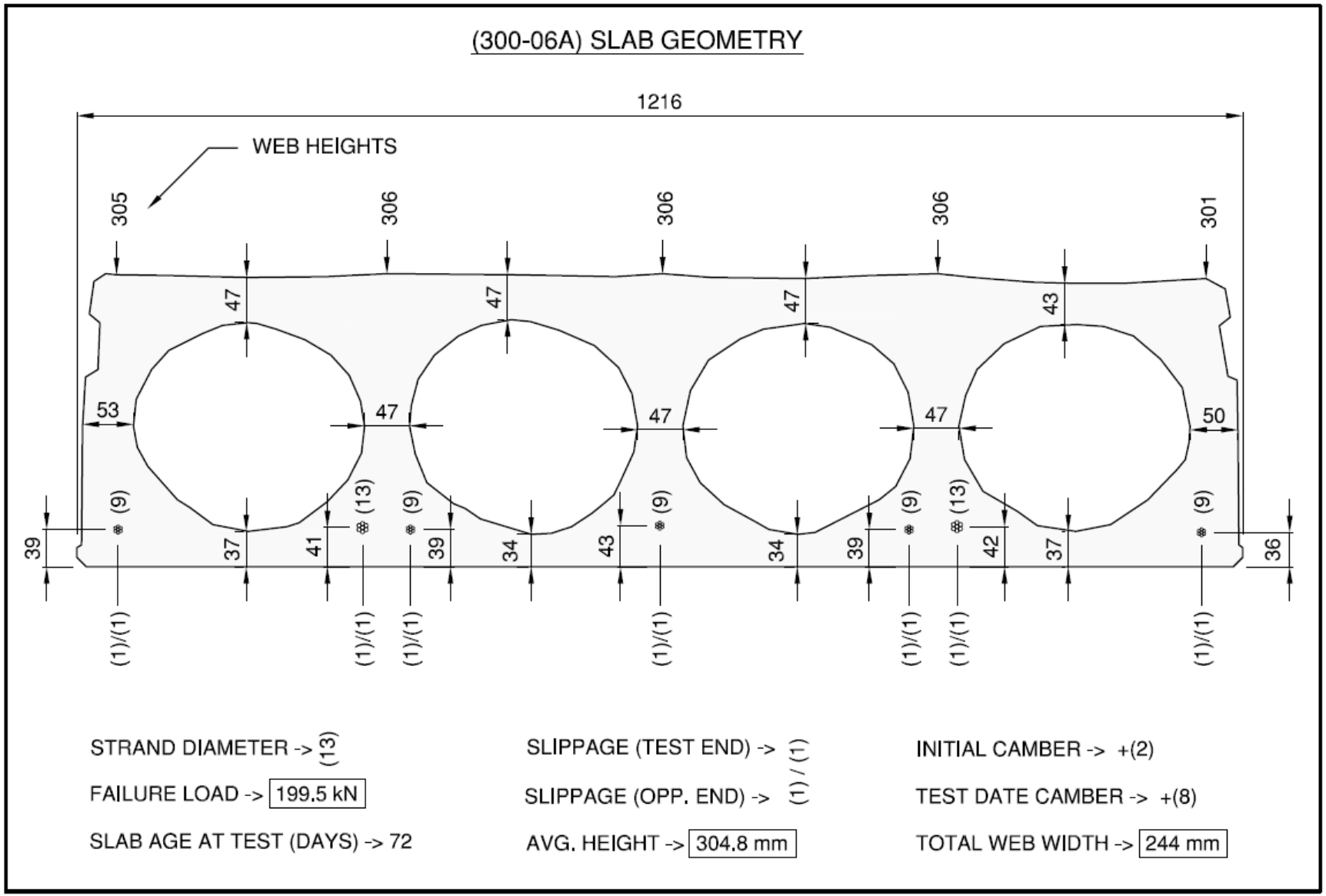

Figure A9: 300-06A Slab Geometry

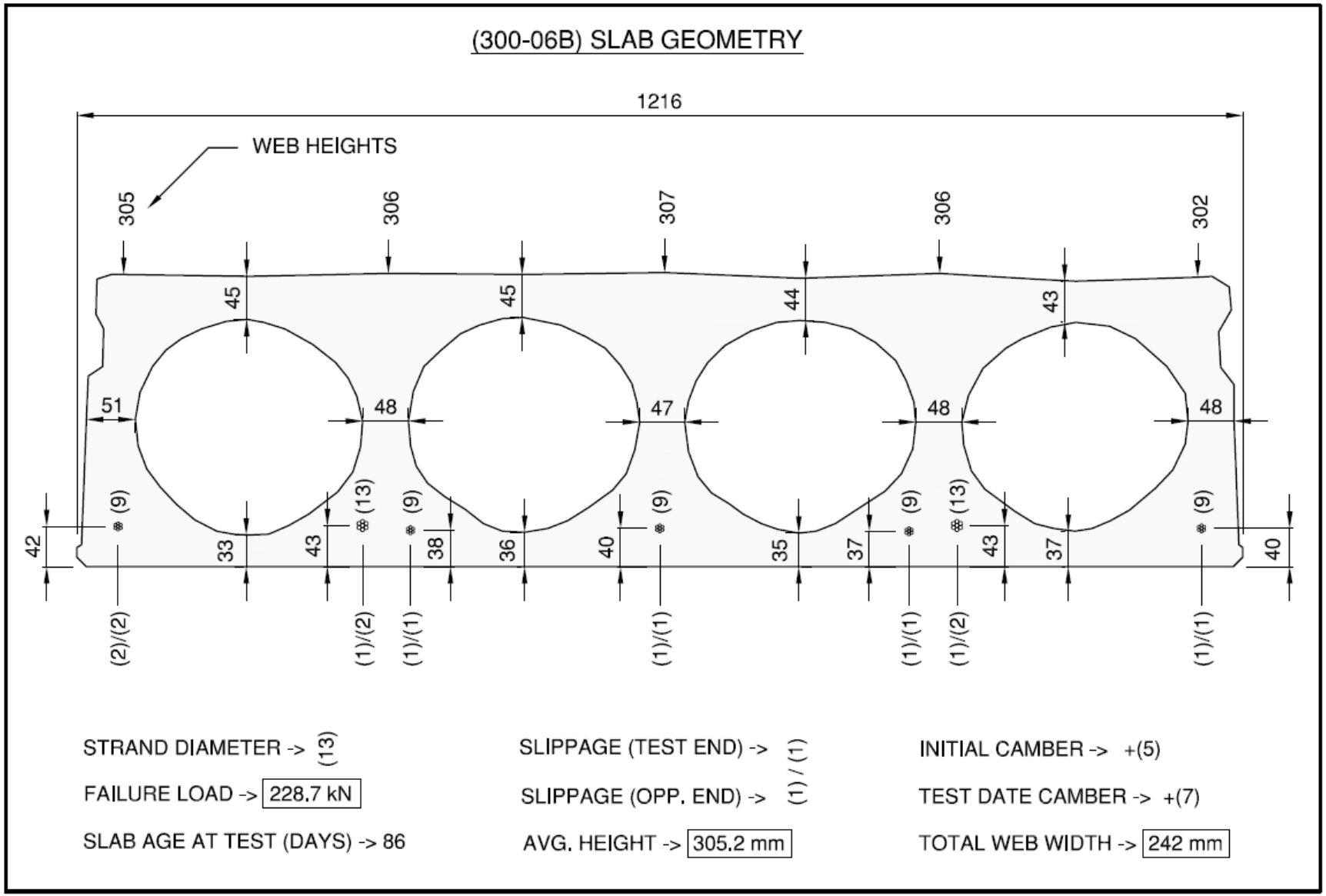

Figure A10: 300-06B Slab Geometry

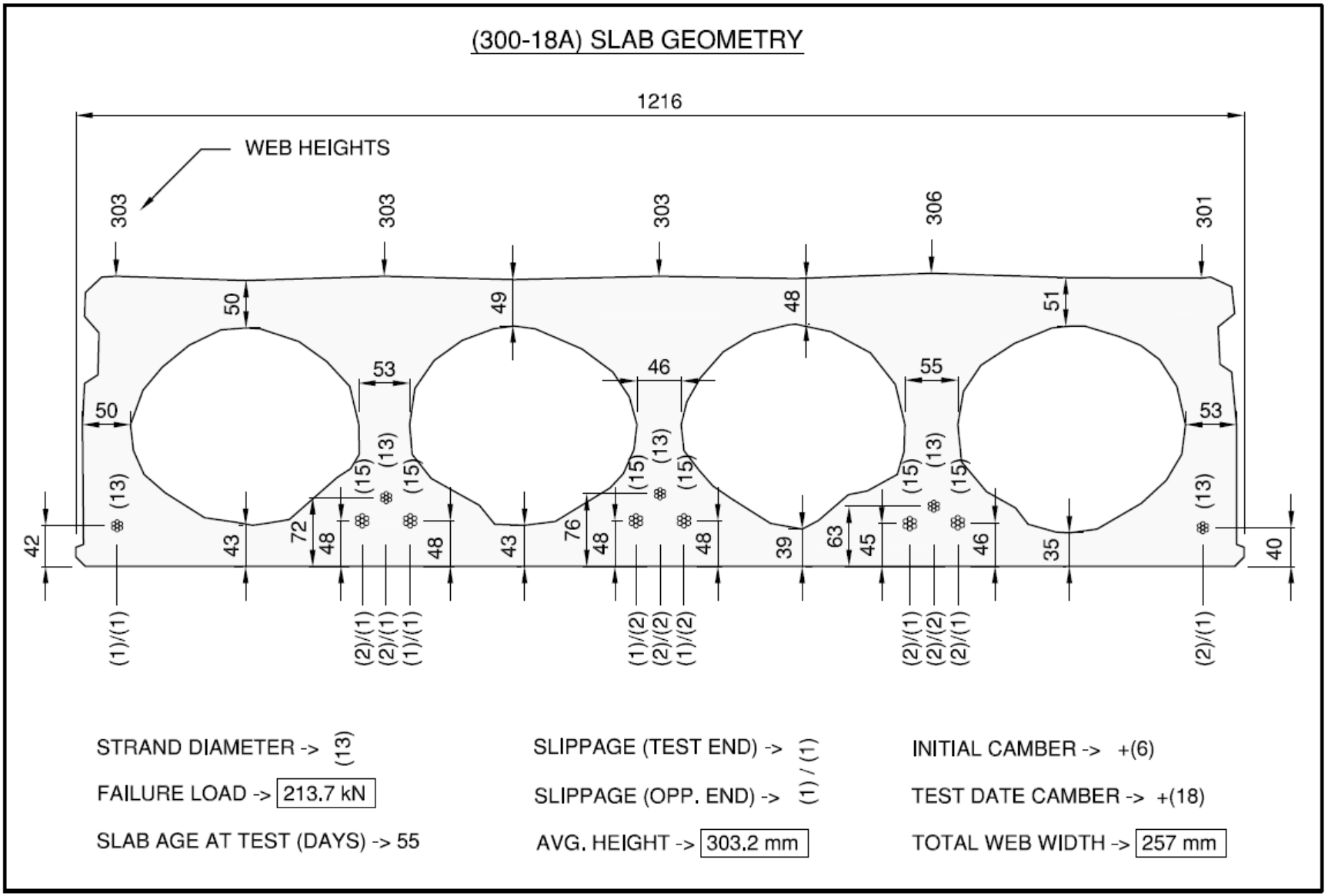

Figure A11: 300-18A Slab Geometry

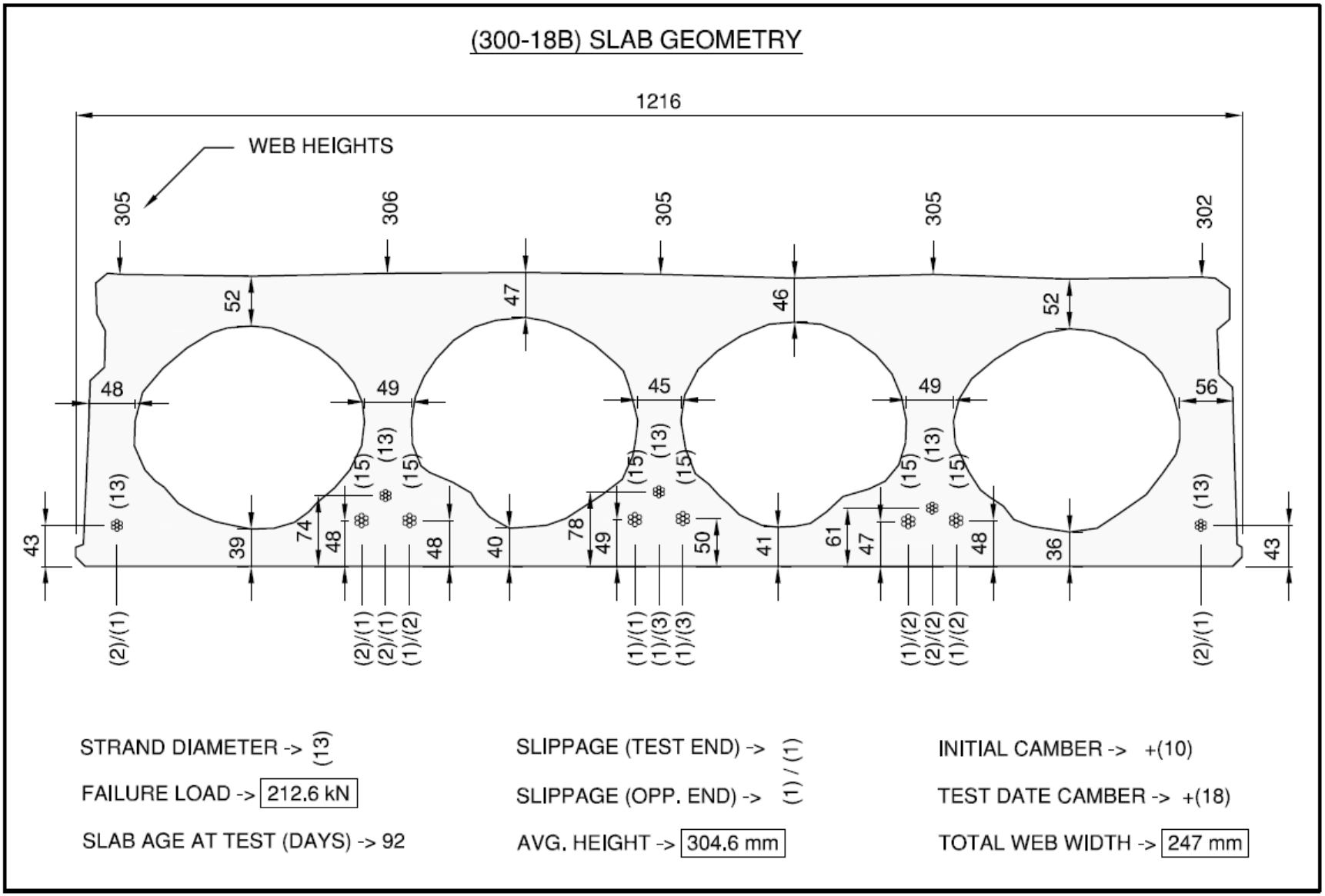

Figure A12: 300-18B Slab Geometry

APPENDIX B

AS-CAST SECTION PROPERTIES

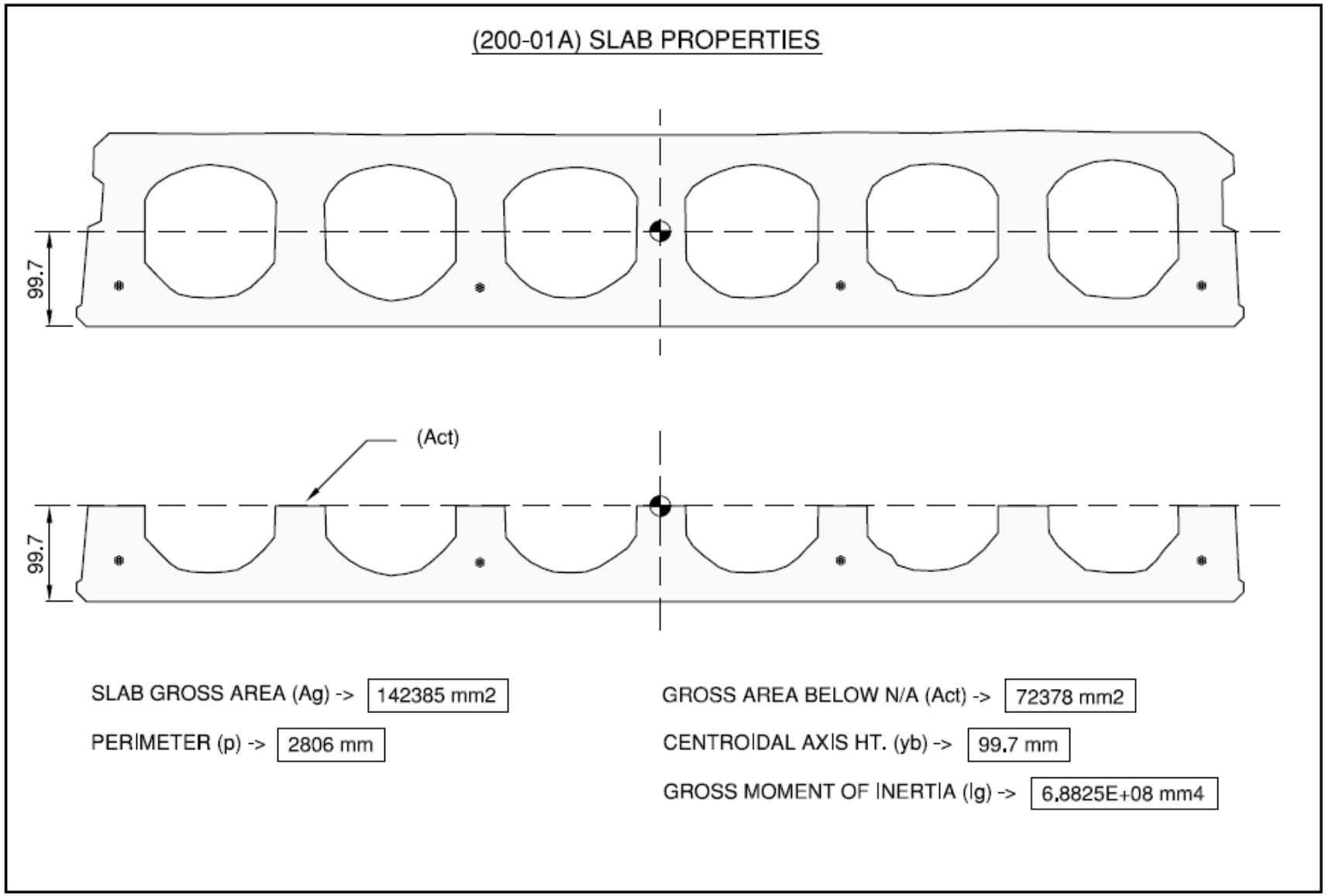

Figure B1: 200-01A Slab Properties

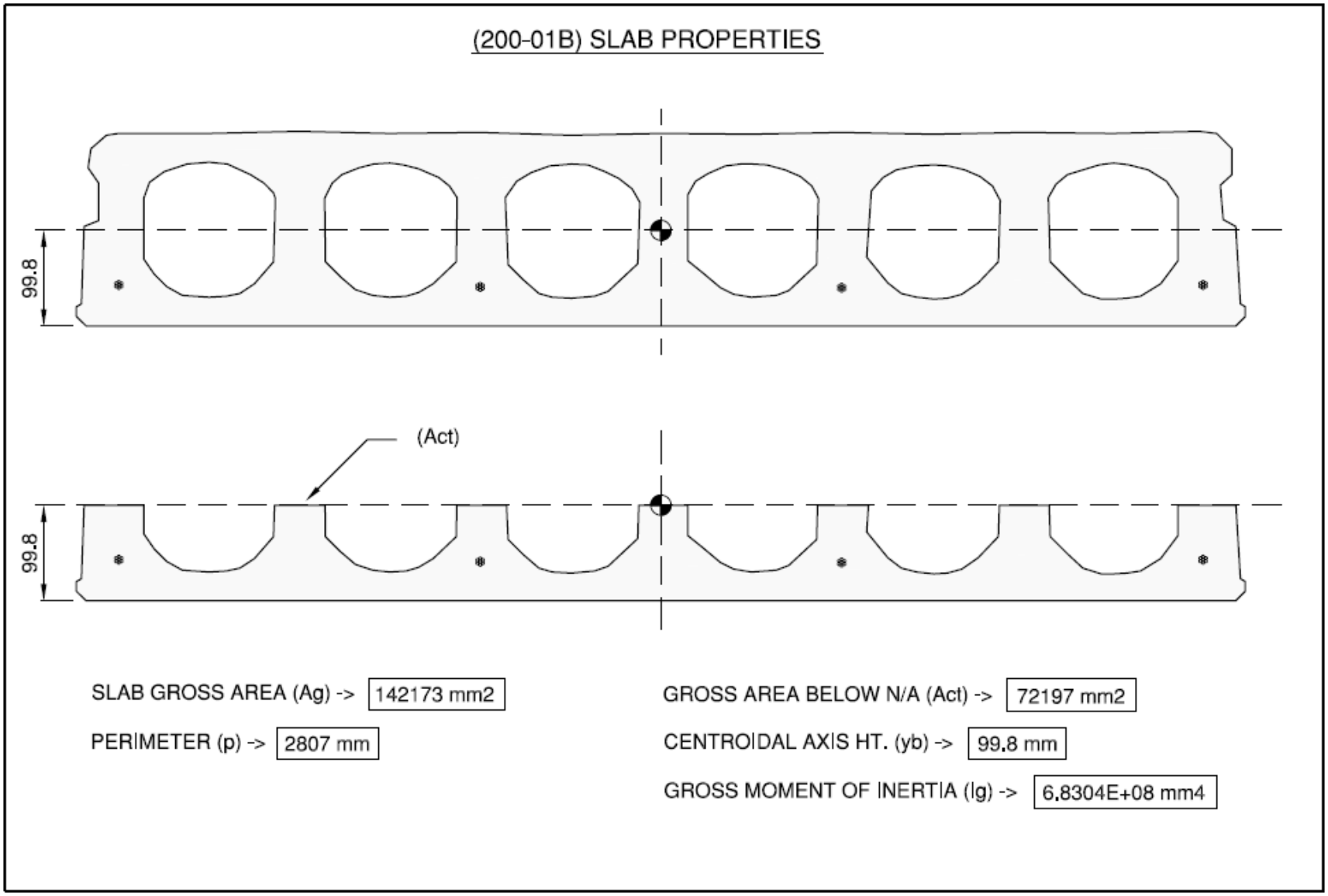

Figure B2: 200-01B Slab Properties

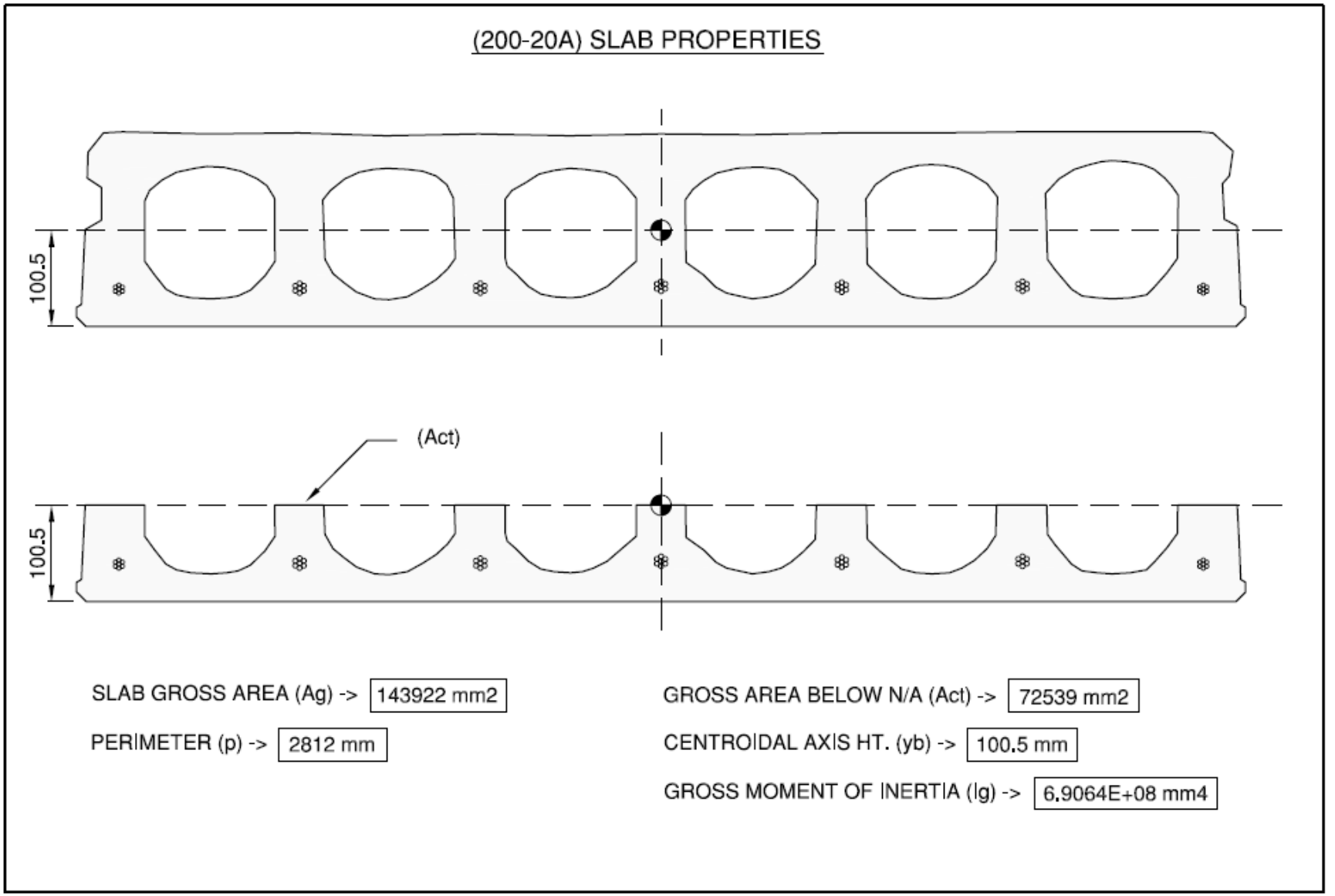

Figure B3: 200-20A Slab Properties

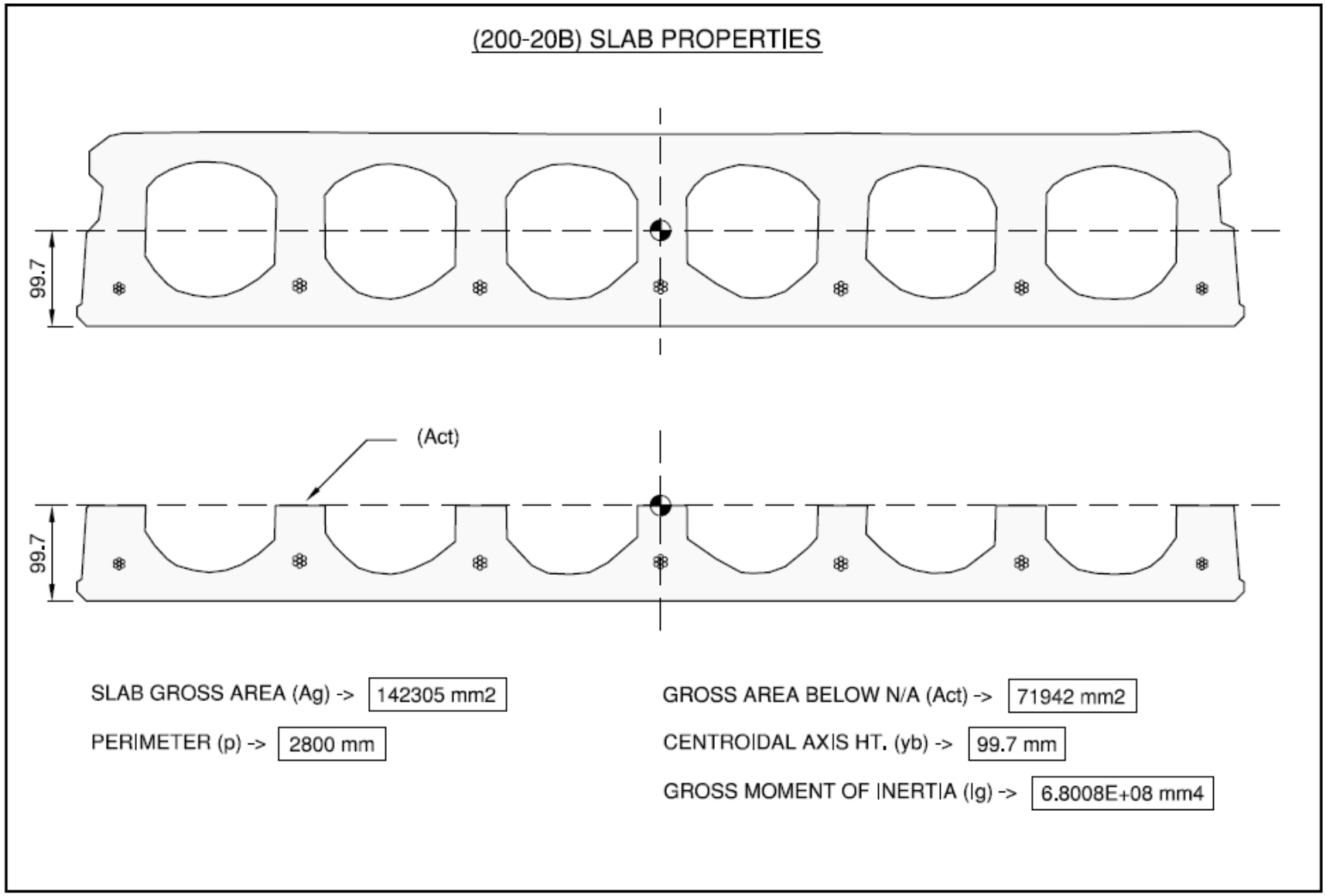

Figure B4: 200-20B Slab Properties

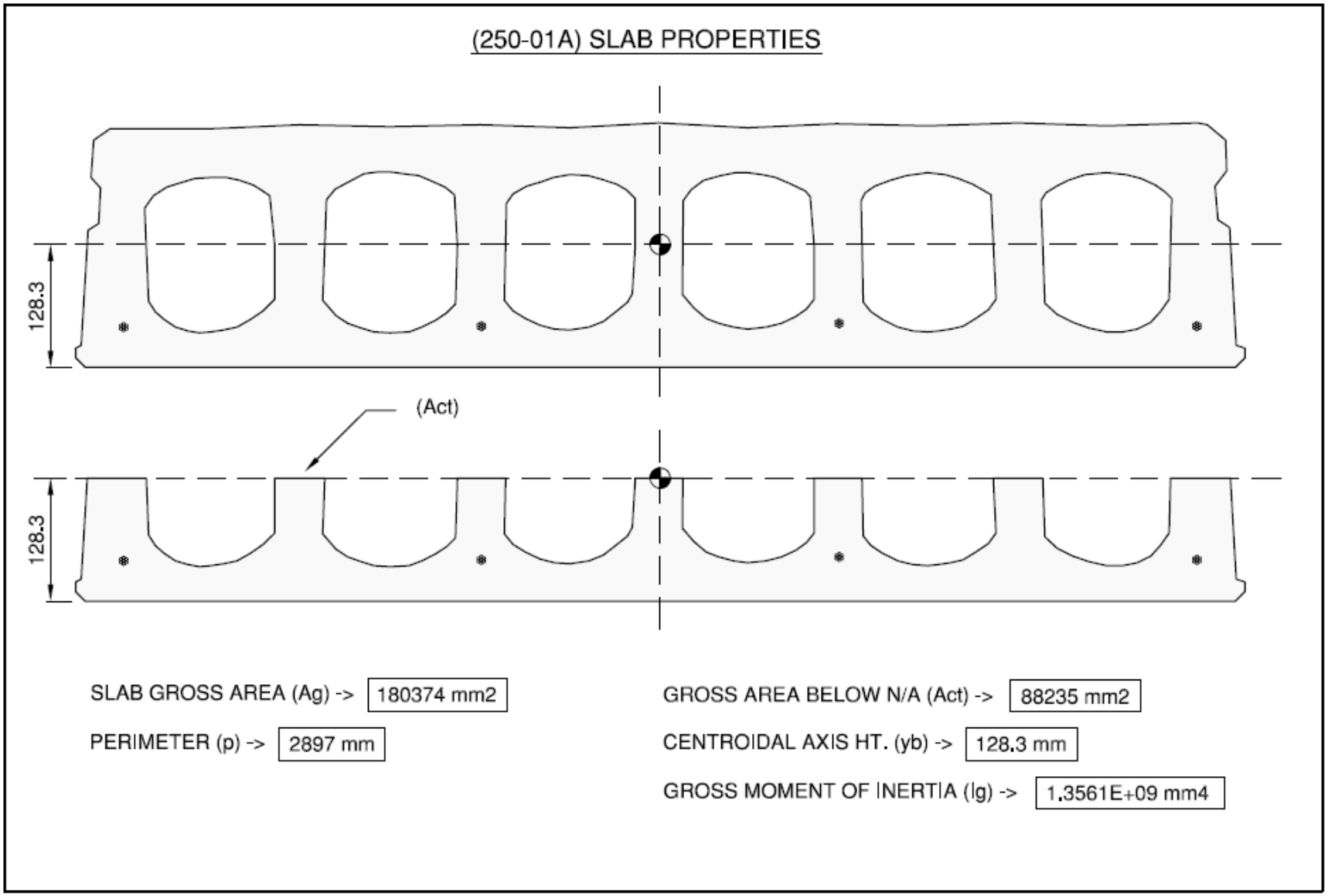

Figure B5: 250-01A Slab Properties

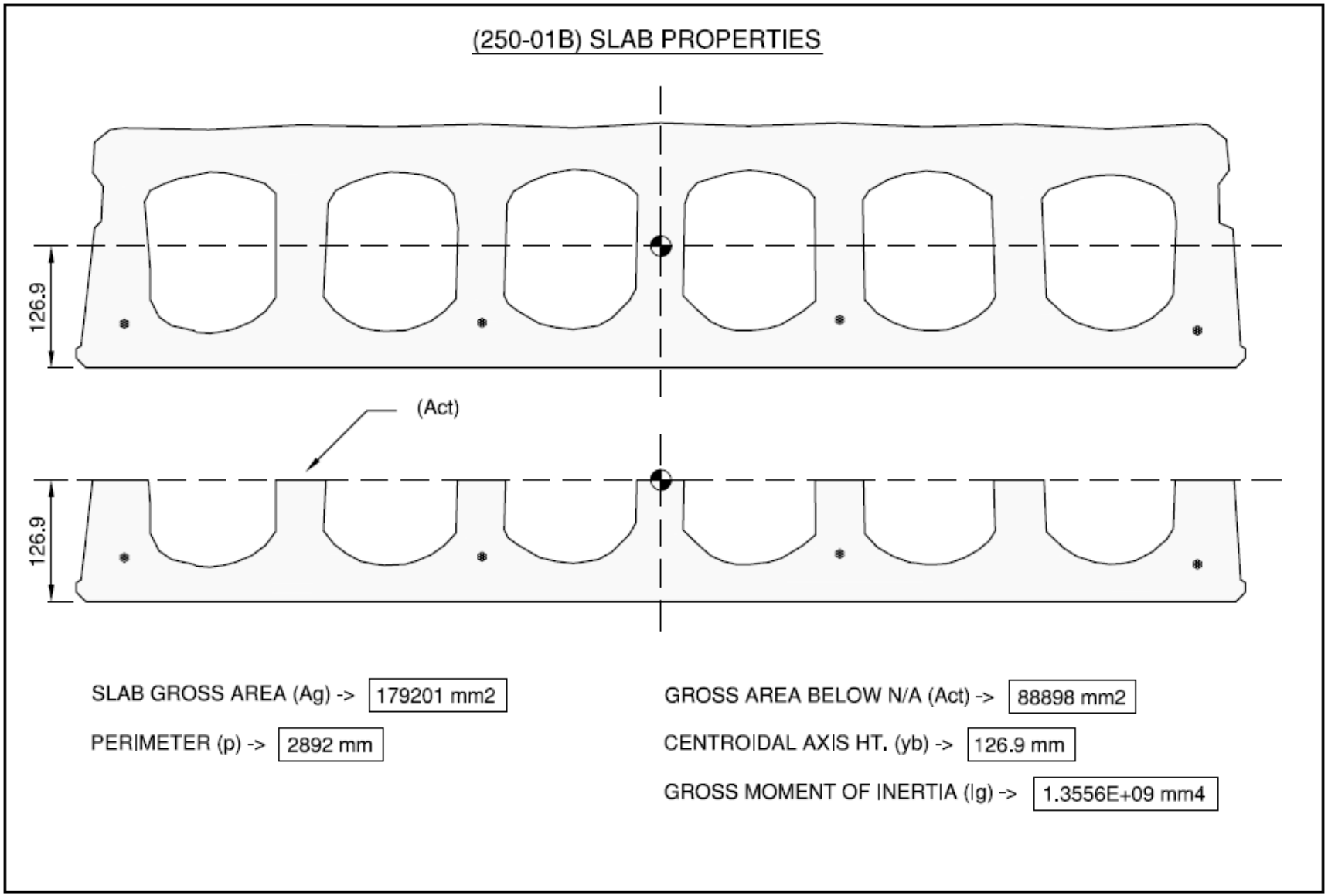

Figure B6: 250-01B Slab Properties

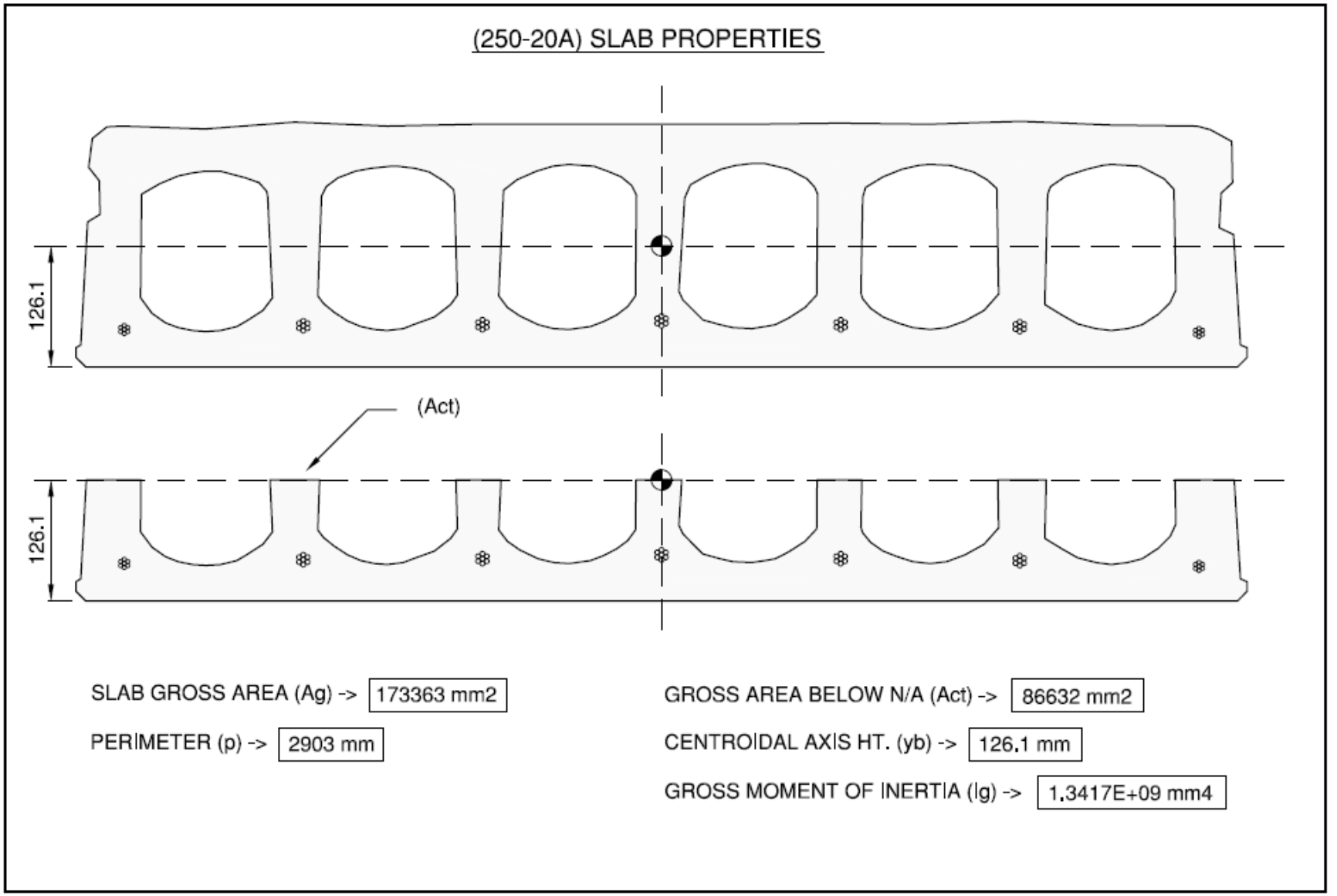

Figure B7: 250-20A Slab Properties

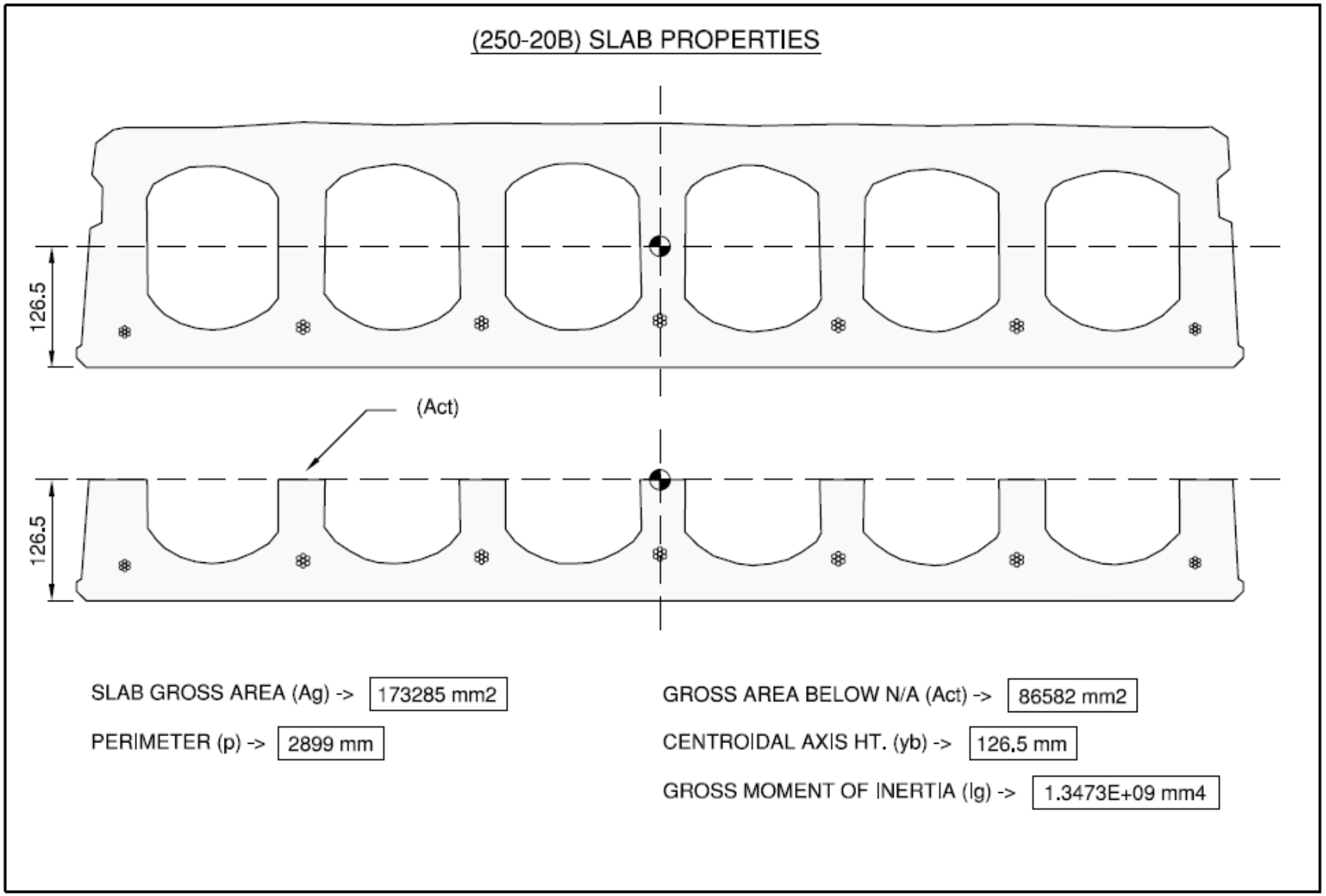

Figure B8: 250-20B Slab Properties

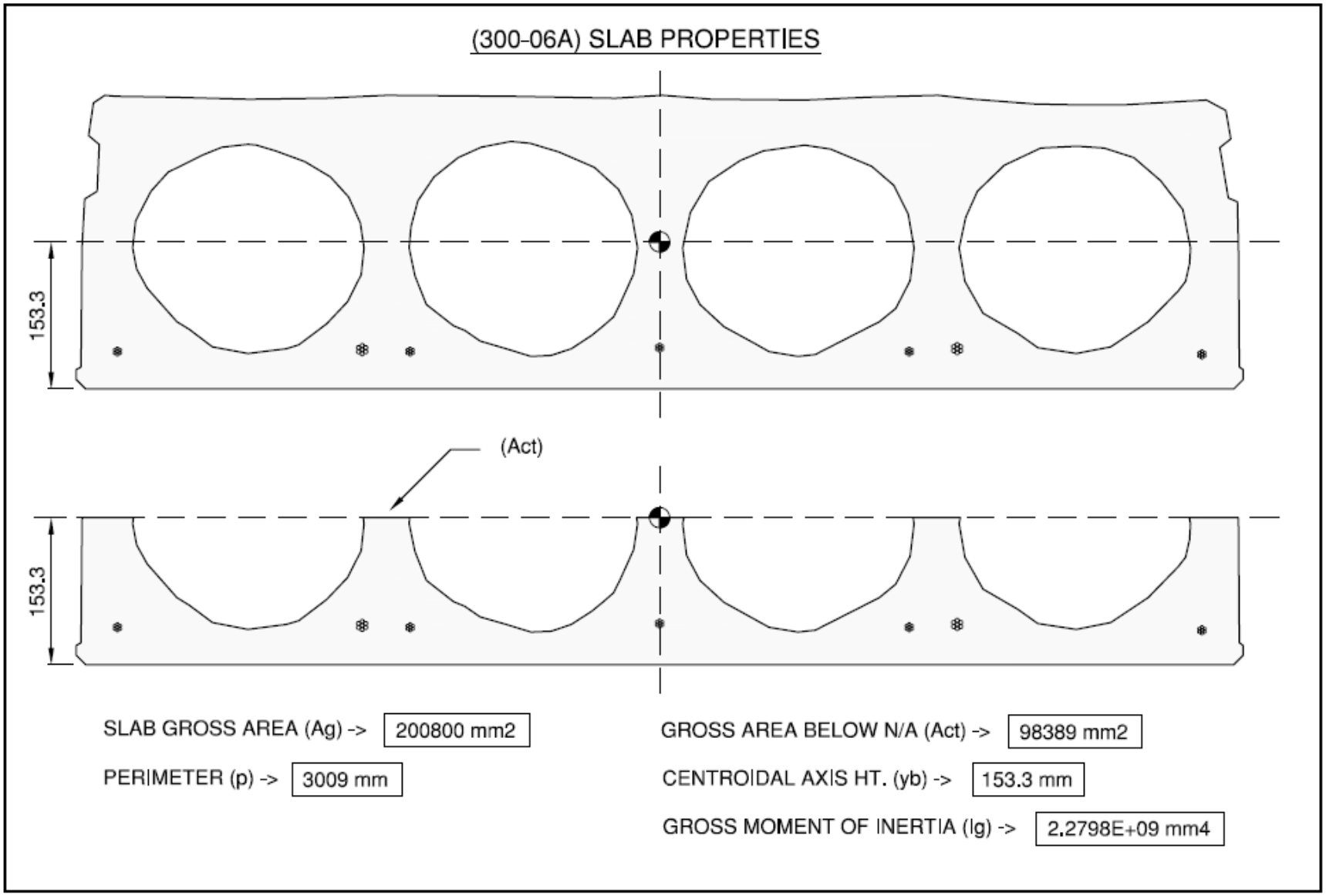

Figure B9: 300-06A Slab Properties

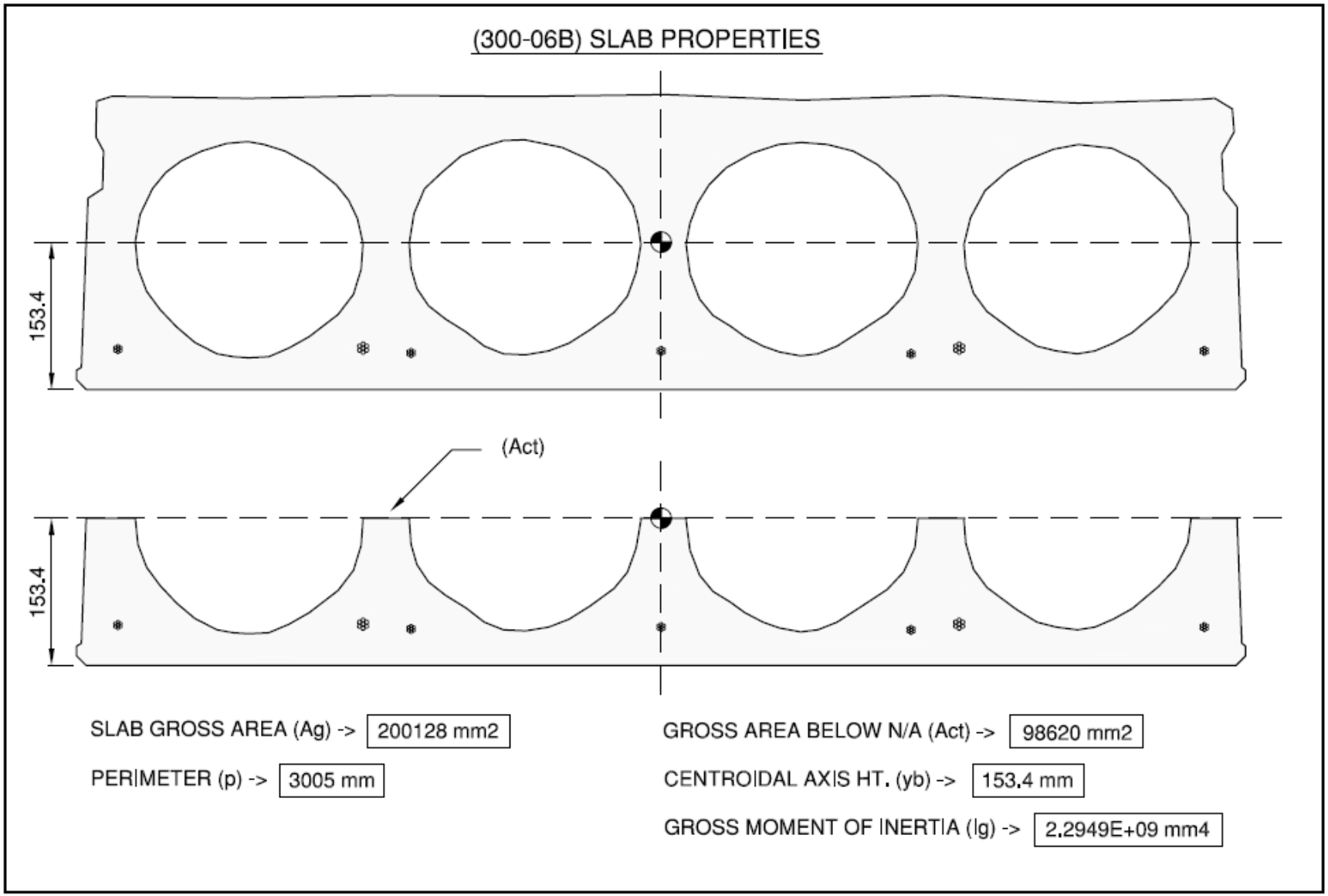

Figure B10: 300-06B Slab Properties

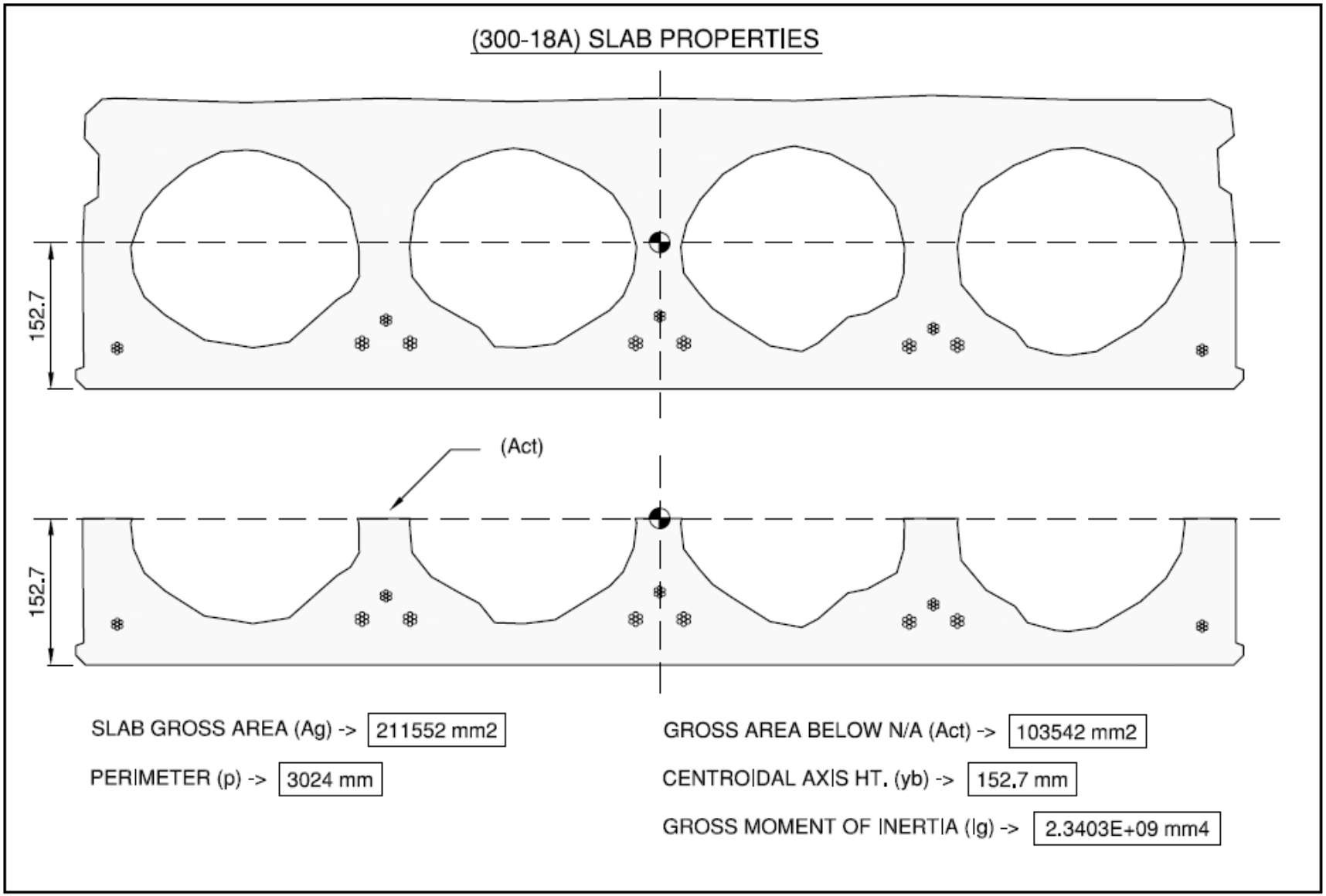

Figure B11: 300-18A Slab Properties

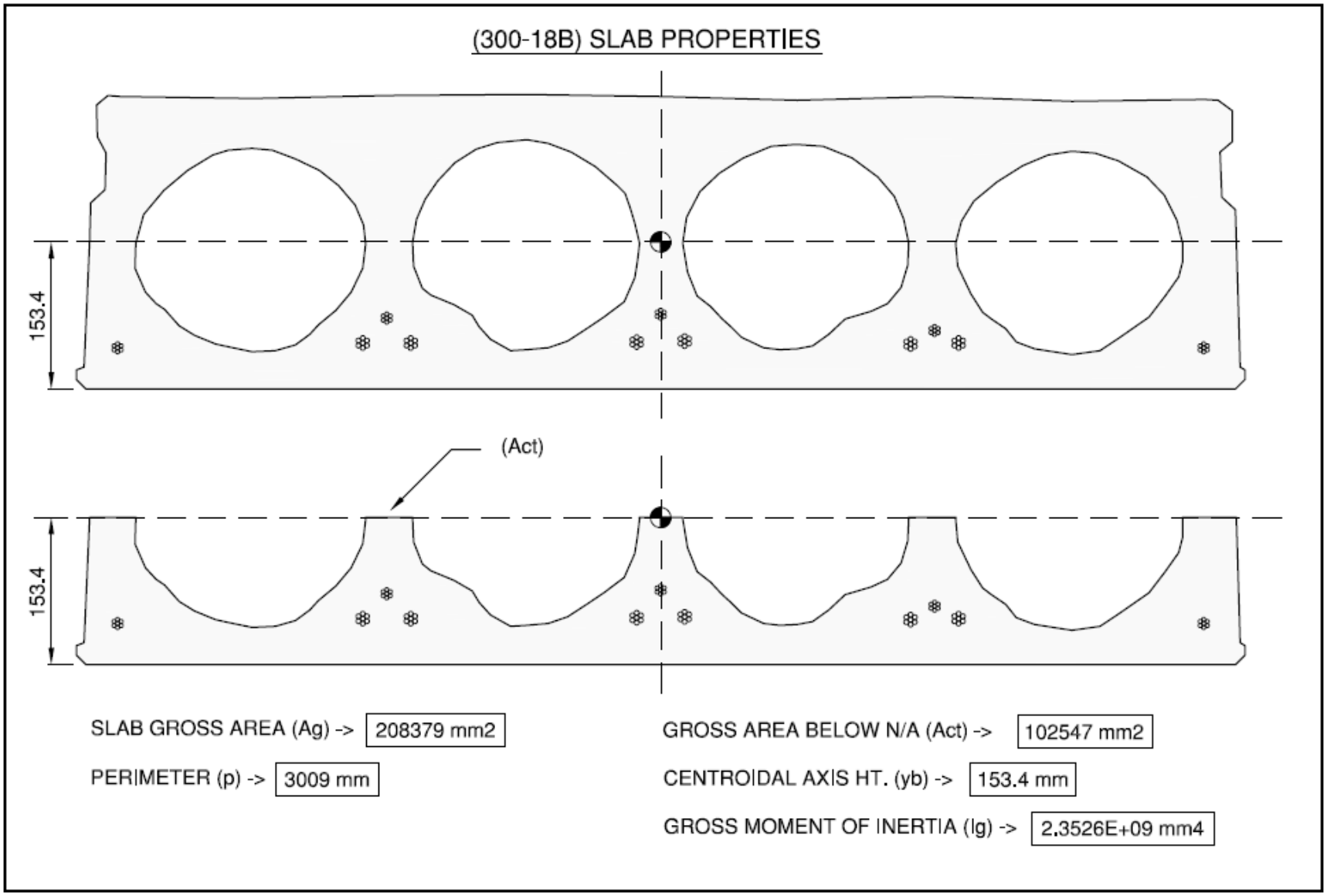

Figure B12: 300-18B Slab Properties

APPENDIX C

CONCRETE PROPERTIES

Table C1: Concrete Strengths for Slabs 200-01A and 200-01B

Concrete Hollowcore Strengths - Phase 1 Test Slabs (2009-2010)

** All strengths listed are in MPa*

** All cylinders and cores were tested using bearing pads (no sulphur caps) at Lafarge unless noted*

** Cylinders tested at University of Manitoba (U of M) used sulphur caps*

Slab Mk# 200-01A / 200-01B (Test Number KARL-8"-1)					
Date Cast:	May 20/09				
Cylinders (19 hrs):	33.9	** Cured in tank*	*Initial Cores (21 hrs):*	38.4	** Cured in tank*
Cylinders (19 hrs):	35.1	** Cured in tank*	*Initial Cores (21 hrs):*	38.4	** Cured in tank*
Cylinders (19 hrs):	34.1	** Cured in tank*	*Initial Cores (21 hrs):*	36.2	** Cured in tank*
Cylinders (19 hrs):	35.7	** Cured in tank*	*Initial Cores (21 hrs):*	36.7	** Cured in tank*
Avg fci' :	34.7	MPa	*Avg fci' :*	37.4	MPa
Cylinders (28 days):	63.7	** Cured in tank*	*Initial Cores (28 days):*	63.2	** Cured in tank*
Cylinders (28 days):	63.0	** Cured in tank*	*Initial Cores (28 days):*	65.5	** Cured in tank*
Cylinders (28 days):	62.9	** Cured in tank*	*Initial Cores (28 days):*	65.3	** Cured in tank*
Cylinders (28 days):	64.2	** Cured in tank*	*Initial Cores (28 days):*	65.4	** Cured in tank*
Average fc' (28 days):	63.5	MPa	*Average fc' (28 days):*	64.9	MPa

Slab Mk# 200-01A	
Date Slab Tested:	Nov 19/09
Slab Age at Test (days):	183

Slab Mk# 200-01B	
Date Slab Tested:	Dec 03/09
Slab Age at Test (days):	197

** Note: Cylinders & Cores were cured in tank until July 09/09*

Date Final Cylinders Tested:	Nov 20/09		*Date Initial Cores Tested:*	Nov 19/09	
Cylinders - U of M (184 days):	87.0	** Cured in tank*	*Initial Cores (183 days):*	89.0	** Cured in tank*
Cylinders - U of M (184 days):	81.2	** Cured in tank*	*Initial Cores (183 days):*	93.4	** Cured in tank*
Cylinders - U of M (184 days):	79.3	** Cured in tank*	*Initial Cores (183 days):*	95.1	** Cured in tank*
Cylinders - U of M (184 days):	82.5	** Cured in tank*	*Initial Cores (183 days):*	94.9	** Cured in tank*
Average fc' (test-cylinder):	82.5	MPa	*Average fc' (test-cores):*	93.1	MPa

Table C2: Concrete Strengths for Slabs 200-20A and 200-20B

Concrete Hollowcore Strengths - Phase 1 Test Slabs (2009-2010)

** All strengths listed are in MPa*

** All cylinders and cores were tested using bearing pads (no sulphur caps) at Lafarge unless noted*

** Cylinders tested at University of Manitoba (U of M) used sulphur caps*

Slab Mk# 200-20A / 200-20B (Test Number KARL-8"-2)

Date Cast:	May 21/09				
Cylinders (18 hrs):	35.1	* Cured in tank	Initial Cores (25 hrs):	44.7	* Cured in tank
Cylinders (18 hrs):	36.4	* Cured in tank	Initial Cores (25 hrs):	42.5	* Cured in tank
Cylinders (18 hrs):	36.3	* Cured in tank	Initial Cores (25 hrs):	41.3	* Cured in tank
Cylinders (18 hrs):	36.6	* Cured in tank	Initial Cores (25 hrs):	41.7	* Cured in tank
Avg fci' :	36.1	MPa	Avg fci' :	42.6	MPa

Cylinders (28 days):	62.8	* Cured in tank	Initial Cores (28 days):	67.5	* Cured in tank
Cylinders (28 days):	63.3	* Cured in tank	Initial Cores (28 days):	65.3	* Cured in tank
Cylinders (28 days):	65.9	* Cured in tank	Initial Cores (28 days):	62.2	* Cured in tank
Cylinders (28 days):	62.9	* Cured in tank	Initial Cores (28 days):	63.5	* Cured in tank
Average fc' (28 days):	63.7	MPa	Average fc' (28 days):	64.6	MPa

Slab Mk# 200-20A	
Date Slab Tested:	Nov 03/09
Slab Age at Test (days):	166

Slab Mk# 200-20B	
Date Slab Tested:	Nov 26/09
Slab Age at Test (days):	189

** Note: Cylinders & Cores were cured in tank until July 09/09*

Date Final Cylinders Tested:	Nov 04/09		Date Initial Cores Tested:	Nov 04/09	
Cylinders - U of M (167 days):	80.8	* Cured in tank	Initial Cores (167 days):	81.4	* Cured in tank
Cylinders - U of M (167 days):	83.0	* Cured in tank	Initial Cores (167 days):	88.2	* Cured in tank
Cylinders - U of M (167 days):	83.2	* Cured in tank	Initial Cores (167 days):	90.8	* Cured in tank
Cylinders - U of M (167 days):	* (71.7)	* Cured in tank	Initial Cores (167 days):	81.7	* Cured in tank
Average fc' (test-cylinder):	82.3	MPa	Average fc' (test-cores):	85.5	MPa

** The value of (71.7) was not included in calc.of above average*

Table C3: Concrete Strengths for Slabs 250-01A and 250-01B

Concrete Hollowcore Strengths - Phase 1 Test Slabs (2009-2010)

** All strengths listed are in MPa*

** All cylinders and cores were tested using bearing pads (no sulphur caps) at Lafarge unless noted*

** Cylinders tested at University of Manitoba (U of M) used sulphur caps*

Slab Mk# 250-01A / 250-01B (Test Number K-10-1)

Date Cast:	July 16/09				
Cylinders (18.25 hrs):	37.3	* Cured with slab	Initial Cores (23.25 hrs):	40.2	* Cured with slab
Cylinders (18.25 hrs):	38.1	* Cured with slab	Initial Cores (23.25 hrs):	42.6	* Cured with slab
Cylinders (20.25 hrs):	40.4	* Cured with slab	Initial Cores (23.25 hrs):	40.9	* Cured with slab
Cylinders (20.25 hrs):	39.1	* Cured with slab	Initial Cores (23.25 hrs):	42.4	* Cured with slab
Avg fci' :	38.7	MPa	Avg fci' :	41.5	MPa

Cylinders (34 days):	70.6	* Cured with slab	Initial Cores (34 days):	63.0	* Cured with slab
Cylinders (34 days):	69.1	* Cured with slab	Initial Cores (34 days):	60.3	* Cured with slab
Cylinders (34 days):	67.2	* Cured with slab	Initial Cores (34 days):	60.0	* Cured with slab
Cylinders (34 days):	70.0	* Cured with slab	Initial Cores (34 days):	63.7	* Cured with slab
Average fc' (34 days):	69.2	MPa	Average fc' (34 days):	61.8	MPa

Slab Mk# 250-01A	
Date Slab Tested:	Feb 17/10
Slab Age at Test (days):	216

Slab Mk# 250-01B	
Date Slab Tested:	Jan 28/10
Slab Age at Test (days):	196

Date Final Cylinders Tested:	Jan 29/10		Date Initial Cores Tested:	Jan 29/10	
Cylinders - U of M (197 days):	65.7	* Cured with slab	Initial Cores (197 days):	92.5	* Cured with slab
Cylinders - U of M (197 days):	67.6	* Cured with slab	Initial Cores (197 days):	92.0	* Cured with slab
Cylinders - U of M (197 days):	69.7	* Cured with slab	Initial Cores (197 days):	96.8	* Cured with slab
Cylinders - U of M (197 days):	*(78.1)	* Cured with slab	Initial Cores (197 days):	89.6	* Cured with slab
Average fc' (test-cylinder):	67.7	MPa	Average fc' (test-cores):	92.7	MPa

** The value of (78.1) was not included in calc.of above average*

Table C4: Concrete Strengths for Slabs 250-20A and 250-20B

Concrete Hollowcore Strengths - Phase 1 Test Slabs (2009-2010)

** All strengths listed are in MPa*

** All cylinders and cores were tested using bearing pads (no sulphur caps) at Lafarge unless noted*

** Cylinders tested at University of Manitoba (U of M) used sulphur caps*

Slab Mk# 250-20A / 250-20B (Test Number K-10-3)

Date Cast:	Oct-15-09				
Cylinders (22 hrs):	38.2	* Cured with slab	Initial Cores (22 hrs):	40.0	* Cured with slab
Cylinders (22 hrs):	38.4	* Cured with slab	Initial Cores (22 hrs):	38.9	* Cured with slab
Cylinders (22 hrs):	37.4	* Cured with slab	Initial Cores (22 hrs):	39.1	* Cured with slab
Cylinders (22 hrs):	38.4	* Cured with slab	Initial Cores (22 hrs):	41.3	* Cured with slab
Avg fci' :	38.1	MPa	Avg fci' :	39.8	MPa

Cylinders (33 days):	61.3	* Cured with slab	Initial Cores (33 days):	67.5	* Cured with slab
Cylinders (33 days):	62.0	* Cured with slab	Initial Cores (33 days):	62.5	* Cured with slab
Cylinders (33 days):	58.7	* Cured with slab	Initial Cores (33 days):	64.6	* Cured with slab
Cylinders (33 days):	60.4	* Cured with slab	Initial Cores (33 days):	65.6	* Cured with slab
Average fc' (33 days):	60.6	MPa	Average fc' (33 days):	65.1	MPa

Slab Mk# 250-20A	
Date Slab Tested:	Feb 04/10
Slab Age at Test (days):	112

Slab Mk# 250-20B	
Date Slab Tested:	Jan 21/10
Slab Age at Test (days):	98

Date Final Cylinders Tested:	Jan 22/10		Date Initial Cores Tested:	Jan 22/10	
Cylinders - U of M (99 days):	61.4	* Cured with slab	Initial Cores (99 days):	90.9	* Cured with slab
Cylinders - U of M (99 days):	61.4	* Cured with slab	Initial Cores (99 days):	88.1	* Cured with slab
Cylinders - U of M (99 days):	63.0	* Cured with slab	Initial Cores (99 days):	88.8	* Cured with slab
Cylinders - U of M (99 days):	60.9	* Cured with slab	Initial Cores (99 days):	85.1	* Cured with slab
Average fc' (test-cylinder):	61.7	MPa	Average fc' (test-cores):	88.2	MPa

Table C5: Concrete Strengths for Slabs 300-06A and 300-06B

Concrete Hollowcore Strengths - Phase 1 Test Slabs (2009-2010)

** All strengths listed are in MPa*

** All cylinders and cores were tested using bearing pads (no sulphur caps) at Lafarge unless noted*

** Cylinders tested at University of Manitoba (U of M) used sulphur caps*

Slab Mk#300-06A / 300-06B (Test Number Karl-12"-1)

Date Cast:	**May 27/09**				
Cylinders (18.25 hrs):	39.3	** Cured in tank*	***Initial Cores (22 hrs):***	39.8	** Cured in tank*
Cylinders (18.25 hrs):	36.7	** Cured in tank*	***Initial Cores (22 hrs):***	39.5	** Cured in tank*
Cylinders (18.25 hrs):	36.8	** Cured in tank*	***Initial Cores (22 hrs):***	38.4	** Cured in tank*
Cylinders (18.25 hrs):	0.0	** Cured in tank*	***Initial Cores (22 hrs):***	39.5	** Cured in tank*
Avg fci' :	**37.6**	**MPa**	***Avg fci' :***	**39.3**	**MPa**
Cylinders (28 days):	62.9	** Cured in tank*	***Initial Cores (28 days):***	67.7	** Cured in tank*
Cylinders (28 days):	62.7	** Cured in tank*	***Initial Cores (28 days):***	65.8	** Cured in tank*
Cylinders (28 days):	69.1	** Cured in tank*	***Initial Cores (28 days):***	67.3	** Cured in tank*
Cylinders (28 days):	66.4	** Cured in tank*	***Initial Cores (28 days):***	61.0	** Cured in tank*
Average fc' (28 days):	**65.3**	**MPa**	***Average fc' (28 days):***	**65.5**	**MPa**

Slab Mk# 300-06A		***Slab Mk# 300-06B***	
Date Slab Tested:	**Aug 07/09**	***Date Slab Tested:***	**Aug 21/09**
Slab Age at Test (days):	**72**	***Slab Age at Test (days):***	**86**

** Note: Cylinders & Cores were cured in tank until July 09/09*

Date Final Cylinders Tested:	**Aug 07/09**		***Date Initial Cores Tested:***	**Aug 10/09**	
Cylinders - U of M (72 days):	66.8	** Cured in tank*	***Initial Cores (75 days):***	82.2	** Cured in tank*
Cylinders - U of M (72 days):	61.9	** Cured in tank*	***Initial Cores (75 days):***	80.7	** Cured in tank*
Cylinders - U of M (72 days):	0.0	** Cured in tank*	***Initial Cores (75 days):***	84.0	** Cured in tank*
Cylinders - U of M (72 days):	0.0	** Cured in tank*	***Initial Cores (75 days):***	81.3	** Cured in tank*
Average fc' (test-cylinder):	**64.4**	**MPa**	***Average fc' (test-cores):***	**82.1**	**MPa**

** Note: Final Cores were cut from failed end of slab.*

Date Final Cores Tested:	**Aug 10/09**		***Date Final Cores Tested:***	**Aug 25/09**	
Final Cores (75 days):	81.3	** Cut from slab*	***Final Cores (90 days):***	84.7	** Cut from slab*
Final Cores (75 days):	74.3	** Cut from slab*	***Final Cores (90 days):***	81.5	** Cut from slab*
Final Cores (75 days):	79.2	** Cut from slab*	***Final Cores (90 days):***	87.2	** Cut from slab*
Final Cores (75 days):	73.9	** Cut from slab*	***Final Cores (90 days):***	81.5	** Cut from slab*
Average fc' (test-cores):	**77.2**	**MPa**	***Final Cores (90 days):***	83.3	
			Average fc' (test-cores):	**83.6**	**MPa**

Table C6: Concrete Strengths for Slabs 300-18A and 300-18B

Concrete Hollowcore Strengths - Phase 1 Test Slabs (2009-2010)

** All strengths listed are in MPa*

** All cylinders and cores were tested using bearing pads (no sulphur caps) at Lafarge unless noted*

** Cylinders tested at University of Manitoba (U of M) used sulphur caps*

Slab Mk#300-18A / 300-18B (Test Number K-12"-2)

Date Cast:	June 02/09	
Cylinders (17 hrs):	33.7	* Cured in tank
Cylinders (17 hrs):	33.0	* Cured in tank
Cylinders (17 hrs):	33.0	* Cured in tank
Cylinders (17 hrs):	34.2	* Cured in tank
Avg fci' :	33.5	MPa

Initial Cores (20 hrs):	36.8	* Cured in tank
Initial Cores (20 hrs):	39.2	* Cured in tank
Initial Cores (20 hrs):	39.2	* Cured in tank
Initial Cores (20 hrs):	37.0	* Cured in tank
Avg fci' :	38.1	MPa

Cylinders (28 days):	66.3	* Cured in tank
Cylinders (28 days):	62.2	* Cured in tank
Cylinders (28 days):	63.8	* Cured in tank
Cylinders (28 days):	61.2	* Cured in tank
Average fc' (28 days):	63.4	MPa

Initial Cores (28 days):	71.3	* Cured in tank
Initial Cores (28 days):	69.1	* Cured in tank
Initial Cores (28 days):	66.3	* Cured in tank
Initial Cores (28 days):	67.3	* Cured in tank
Average fc' (28 days):	68.5	MPa

Slab Mk# 300-18A	
Date Slab Tested:	July 27/09
Slab Age at Test (days):	55

Slab Mk# 300-18B	
Date Slab Tested:	Sept 02/09
Slab Age at Test (days):	92

** Note: Cylinders & Cores were cured in tank until July 09/09*

Date Final Cylinders Tested:	July 28/09	
Cylinders - U of M (56 days):	59.6	* Cured in tank
Cylinders - U of M (56 days):	56.0	* Cured in tank
Cylinders - U of M (56 days):	65.5	* Cured in tank
Cylinders - U of M (56 days):	50.6	* Cured in tank
Average fc' (test-cylinder):	57.9	MPa

Date Initial Cores Tested:	July 28/09	
Initial Cores (56 days):	81.1	* Cured in tank
Initial Cores (56 days):	80.1	* Cured in tank
Initial Cores (56 days):	69.9	* Cured in tank
Initial Cores (56 days):	71.3	* Cured in tank
Average fc' (test-cores):	75.6	MPa

** Note: Final Cores were cut from failed end of slab.*

Date Final Cores Tested:	July 28/09	
Final Cores (56 days):	83.3	* Cut from slab
Final Cores (56 days):	83.3	* Cut from slab
Final Cores (56 days):	88.8	* Cut from slab
Final Cores (56 days):	91.6	* Cut from slab
Average fc' (test-cores):	86.8	MPa

Date Final Cores Tested:	Sept 03/09	
Final Cores (93 days):	90.8	* Cut from slab
Final Cores (93 days):	85.8	* Cut from slab
Final Cores (93 days):	93.0	* Cut from slab
Final Cores (93 days):	78.4	* Cut from slab
Average fc' (test-cores):	87.0	MPa

APPENDIX D

STRAND PROPERTIES

Table D1: Strand Properties for Test Slabs

Hollowcore Shear Testing - Phase 1 Test Slabs (Strands)

Slab Mk #	200-01A	200-01B	200-20A	200-20B	250-01A	250-01B	250-20A	250-20B	300-06A	300-06B	300-18A	300-18B
Date Cast	May 20/09	May 20/09	May 21/09	May 21/09	July 16/09	July 16/09	Oct-15-09	Oct-15-09	May 27/09	May 27/09	June 02/09	June 02/09
Strands												
(9 mm) Strands Pack # 80026-3	4	4	X	X	4	4	X	X	5	5	X	X
(13 mm) Strands Pack # 77584-2	X	X	2	2	X	X	X	X	2	2	5	5
(15 mm) Strands Pack # 20805 06103	X	X	5	5	X	X	X	X	X	X	6	6
(13 mm) Strands Pack # 1450	X	X	X	X	X	X	2	2	X	X	X	X
(15 mm) Strands Pack # 20805 08204	X	X	X	X	X	X	3	3	X	X	X	X
(15 mm) Strands Pack # 20107	X	X	X	X	X	X	2	2	X	X	X	X

Strands	E-Value (x10^6) psi	E-Value (MPa)	Ultimate Load (lbs)	Ultimate Load (kN)	Strand Area (mm2)	Ultimate Strength (MPa)	Design Strength (MPa)
(9 mm) Strands Pack # 80026-3	28.7	197880	25150	111.9	54.8	2041.4	1860.0
(13 mm) Strands Pack # 77584-2	28.1	193743	43330	192.7	98.7	1952.7	1860.0
(15 mm) Strands Pack # 20805 06103	28.4	195811	60810	270.5	140.0	1932.0	1860.0
(13 mm) Strands Pack # 1450	28.1	193743	43366	192.9	98.7	1954.3	1860.0
(15 mm) Strands Pack # 20805 08204	28.4	195811	61150	272.0	140.0	1942.8	1860.0
(15 mm) Strands Pack # 20107	28.4	195811	60399	268.7	140.0	1919.0	1860.0

APPENDIX E

TEST SET-UP ELEVATIONS

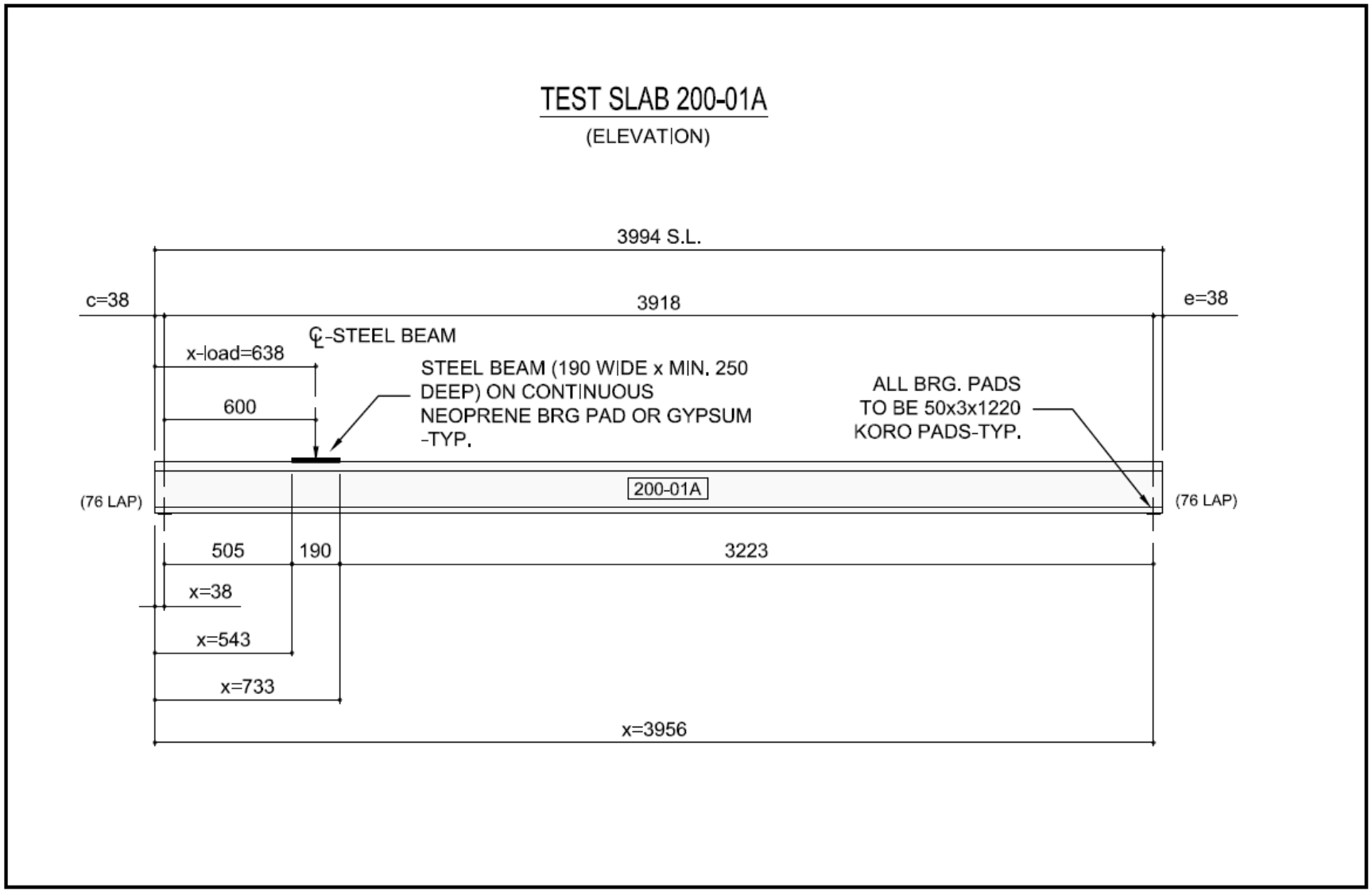

Figure E1: Slab 200-01A Elevation of Test Set-Up

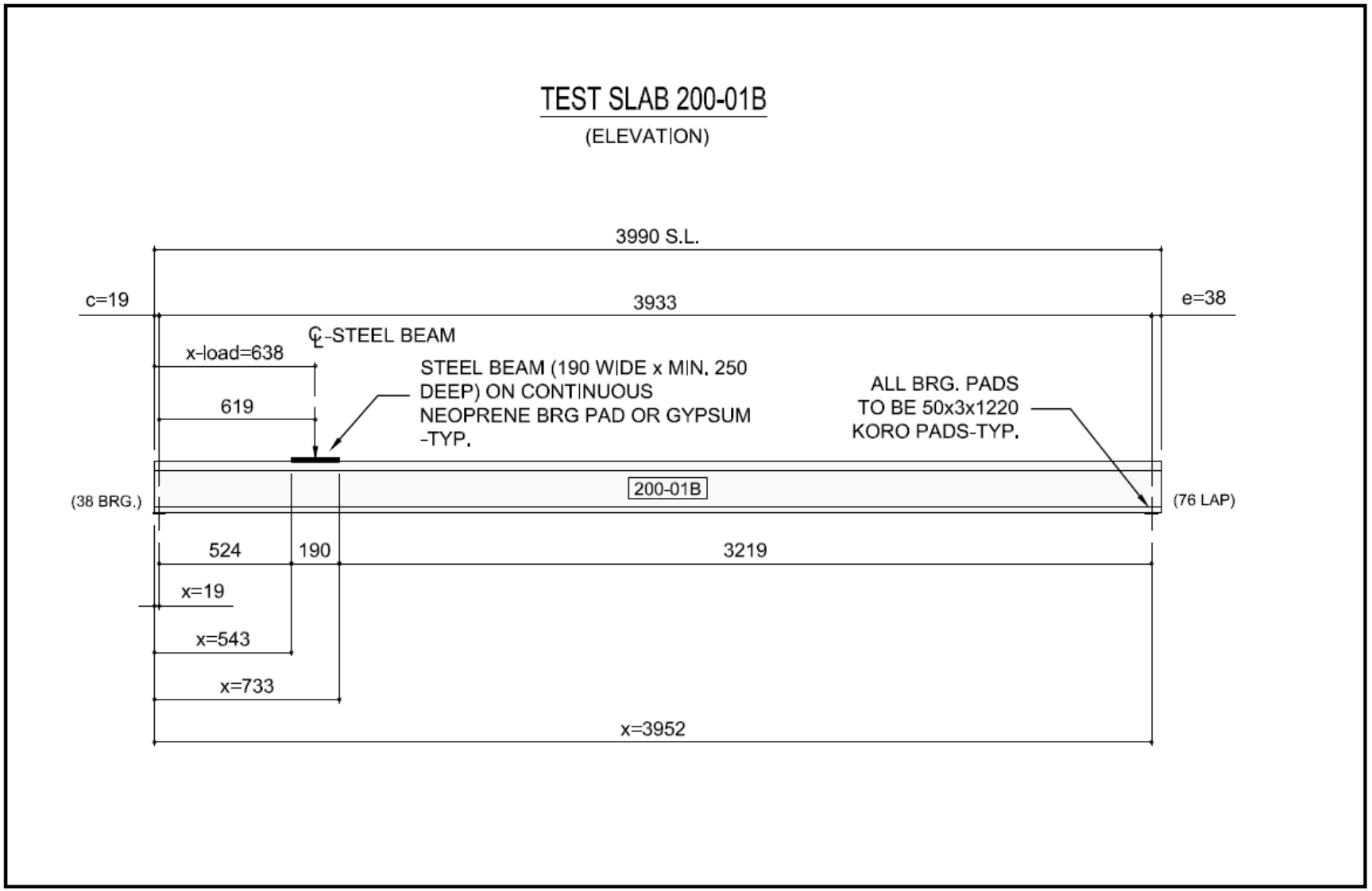

Figure E2: Slab 200-01B Elevation of Test Set-Up

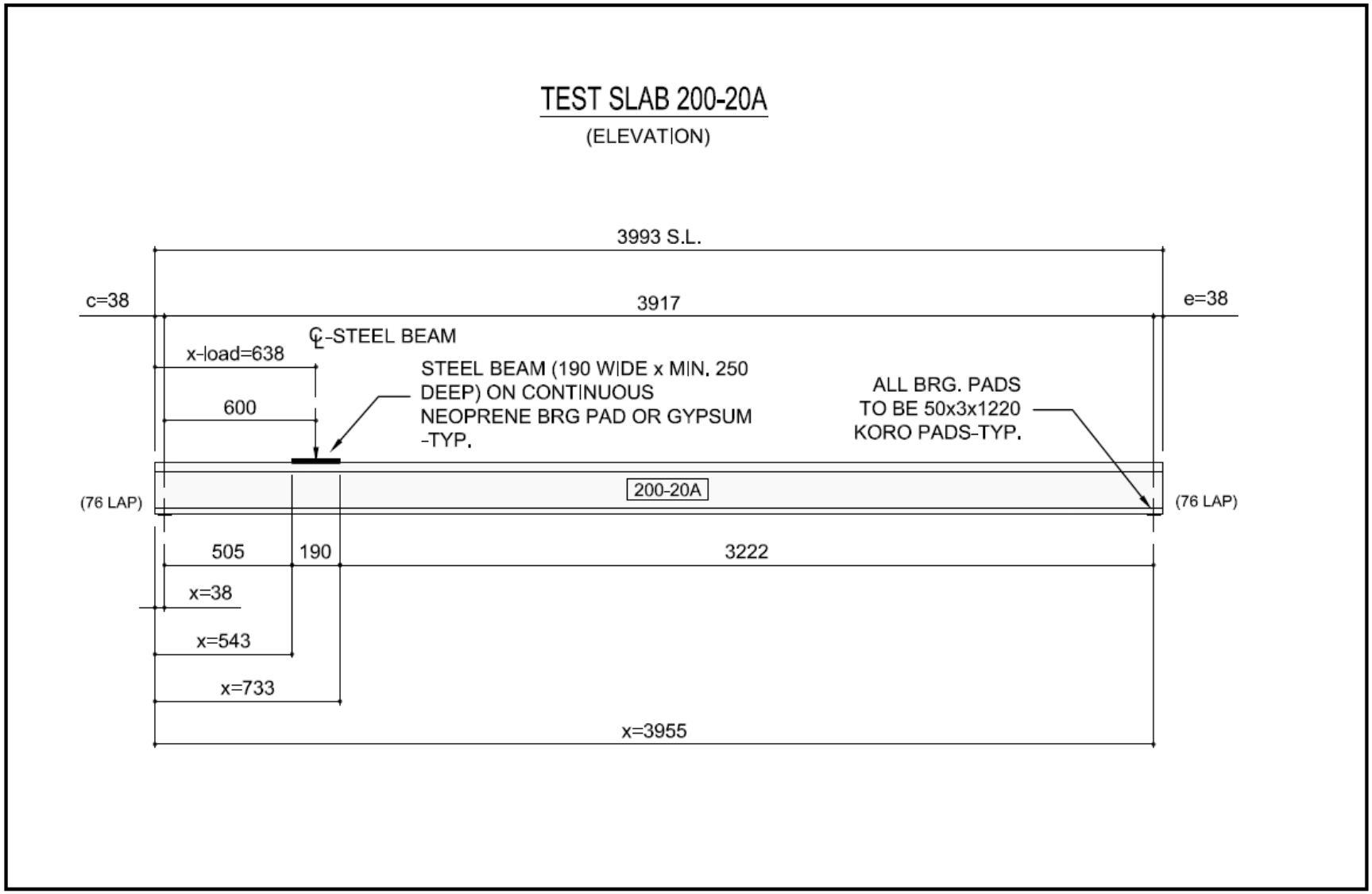

Figure E3: Slab 200-20A Elevation of Test Set-Up

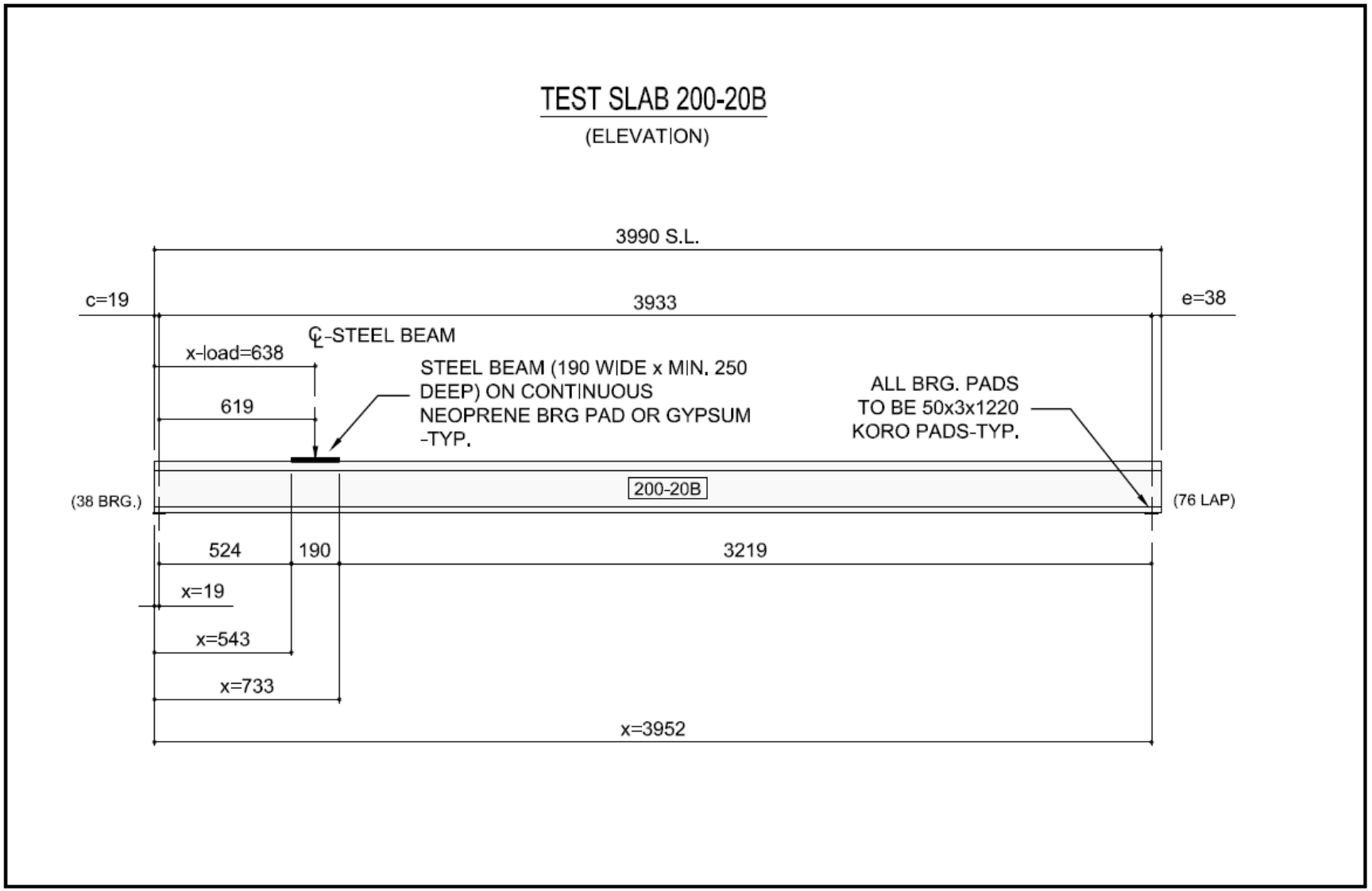

Figure E4: Slab 200-20B Elevation of Test Set-Up

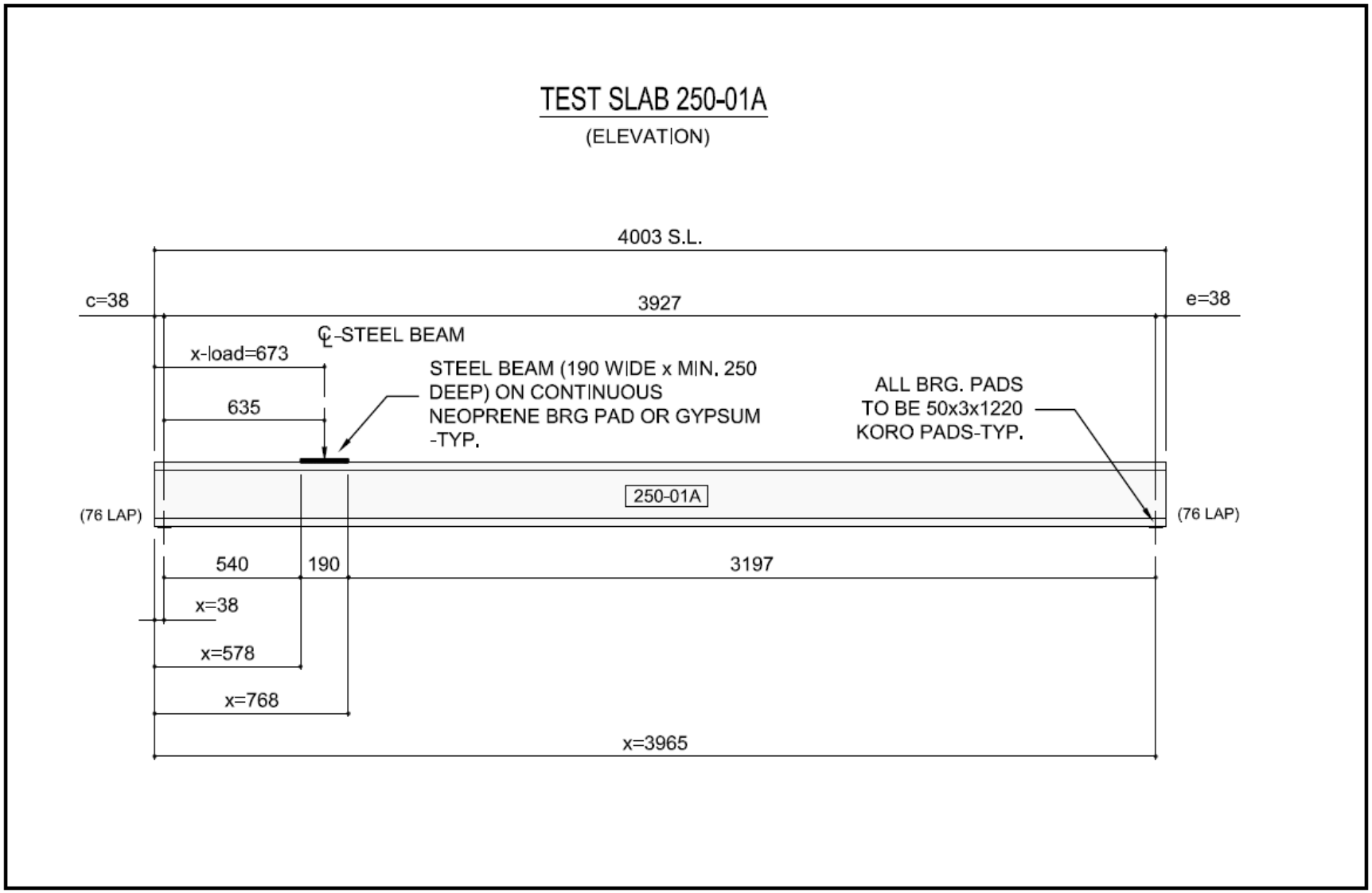

Figure E5: Slab 250-01A Elevation of Test Set-Up

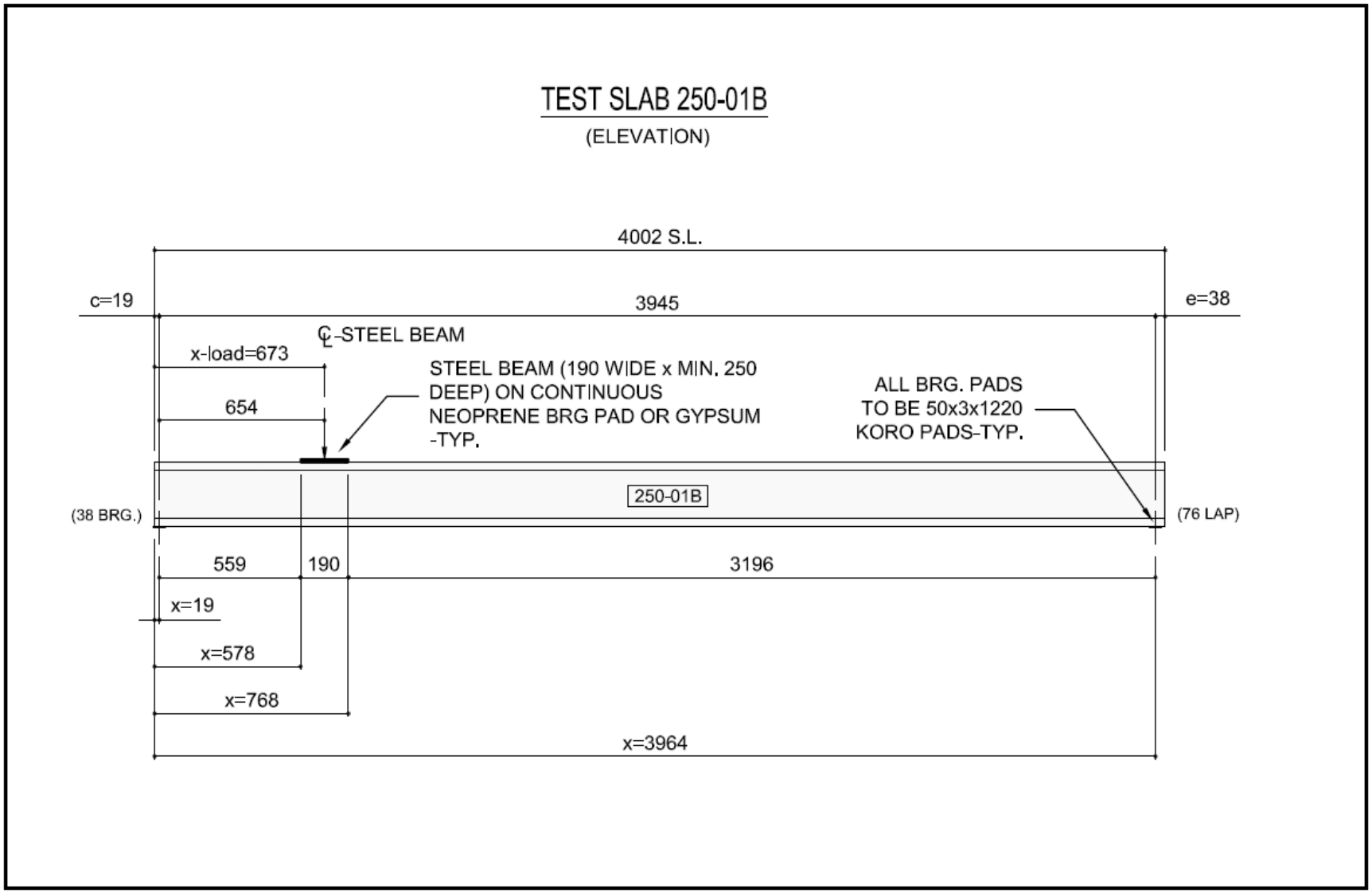

Figure E6: Slab 250-01B Elevation of Test Set-Up

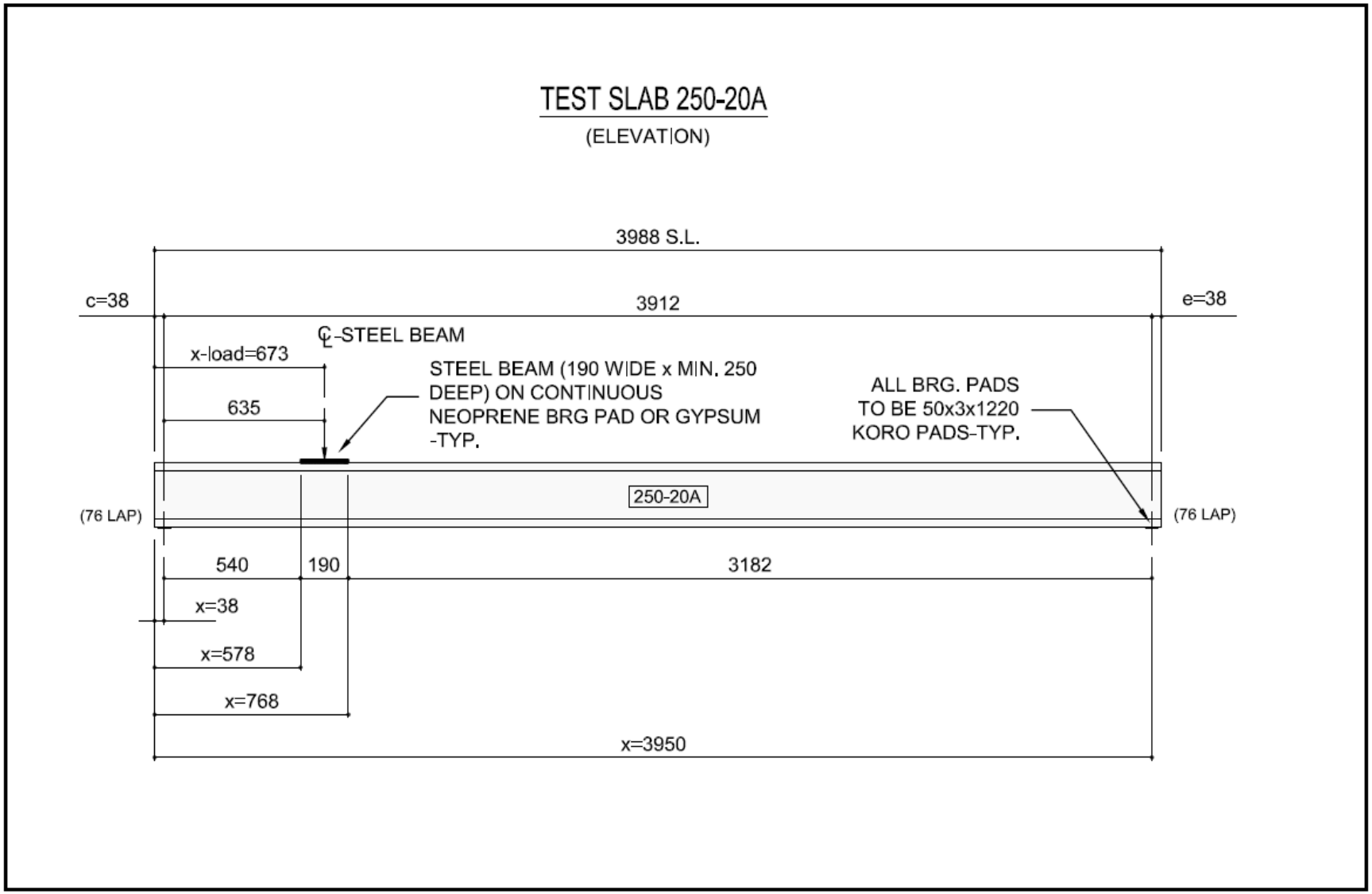

Figure E7: Slab 250-20A Elevation of Test Set-Up

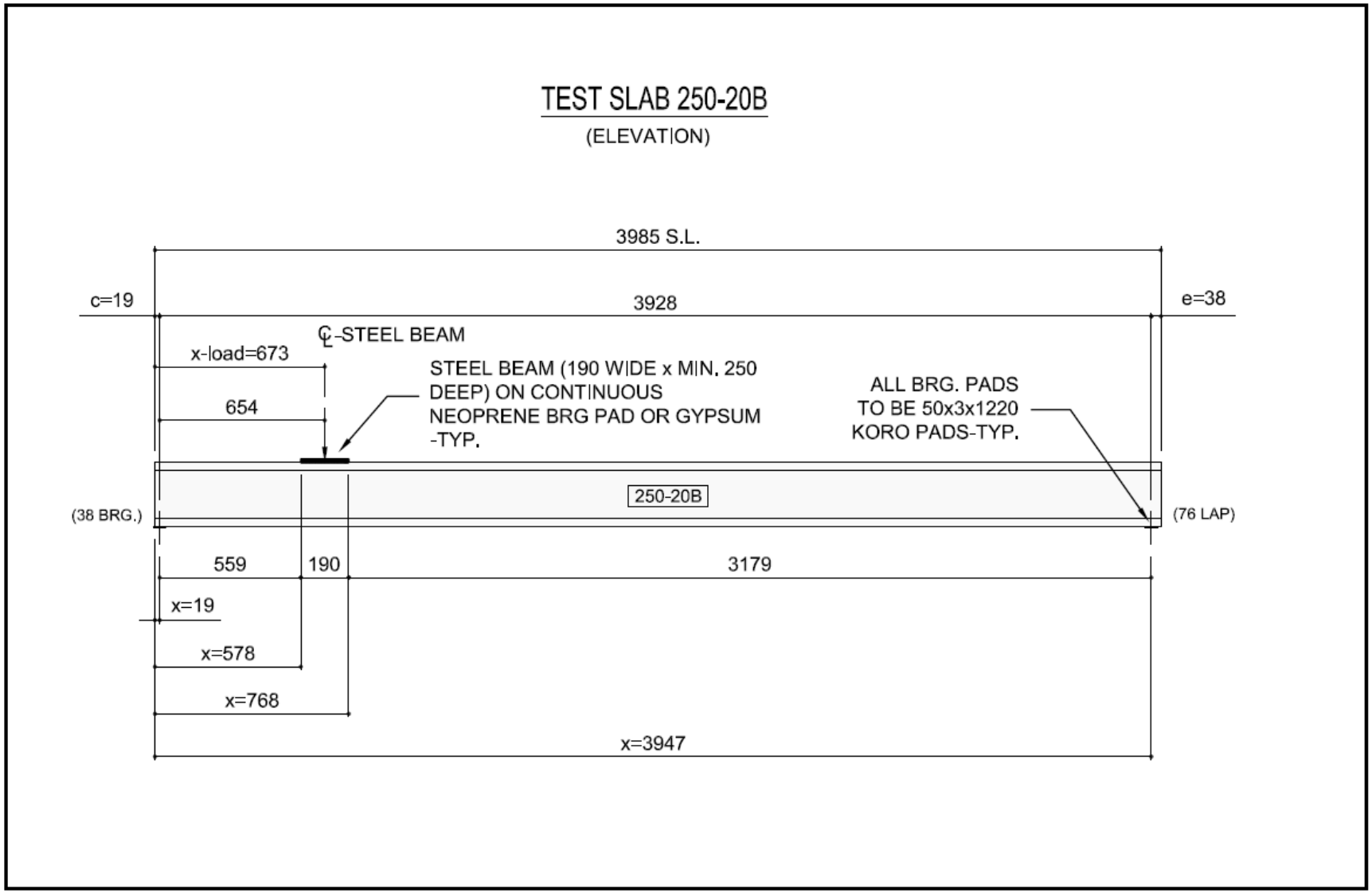

Figure E8: Slab 250-20B Elevation of Test Set-Up

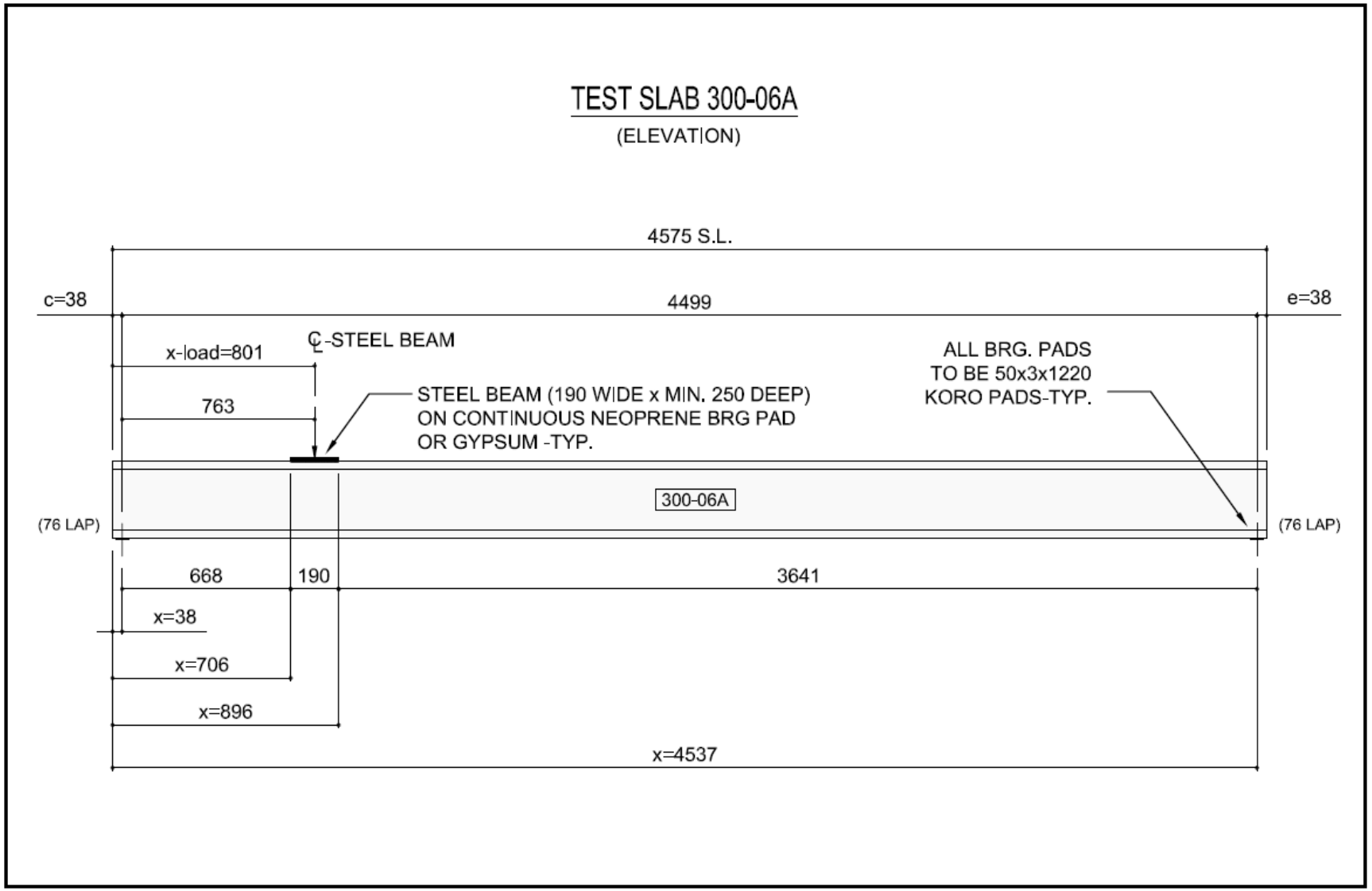

Figure E9: Slab 300-06A Elevation of Test Set-Up

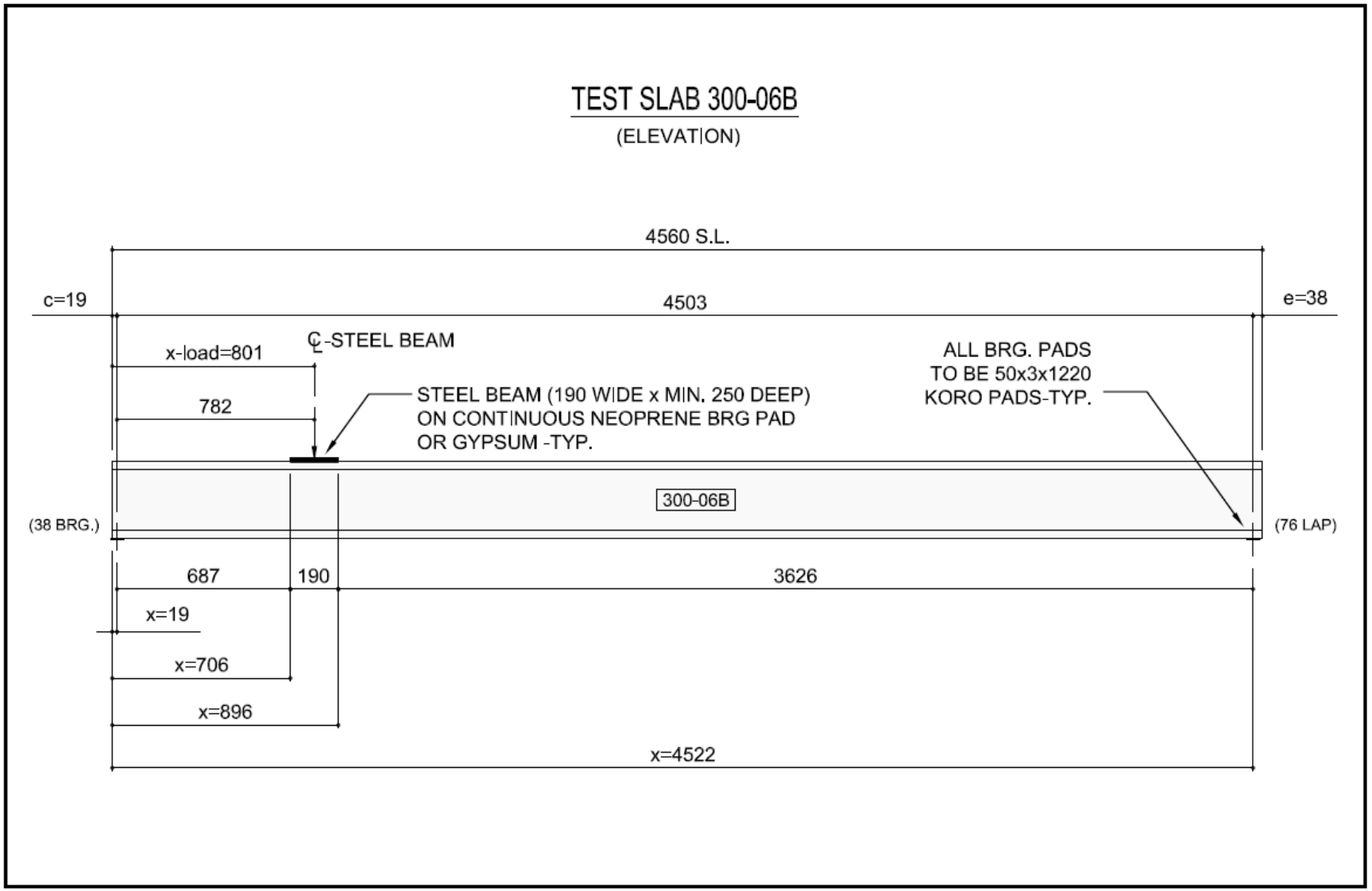

Figure E10: Slab 300-06B Elevation of Test Set-Up

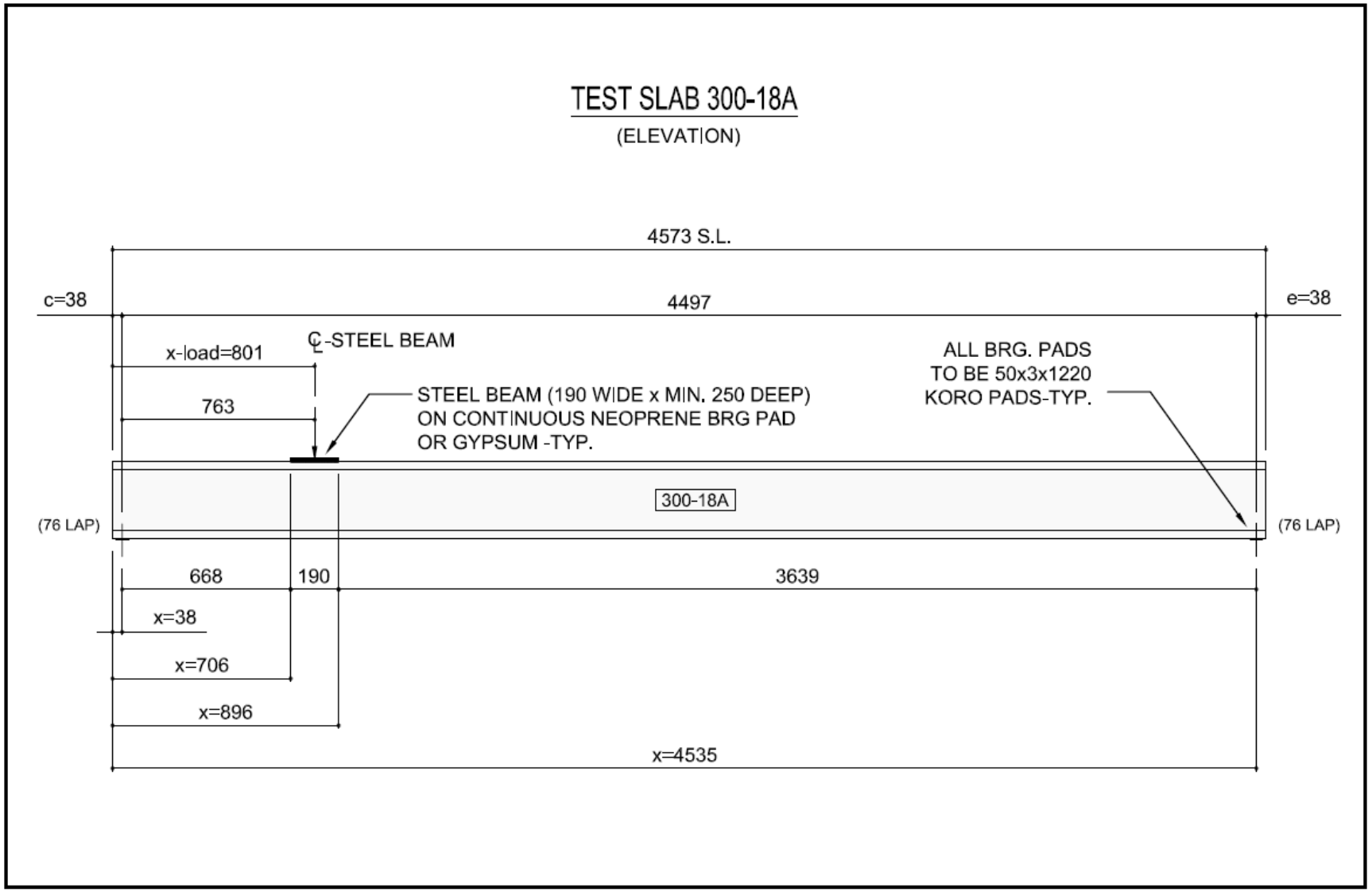

Figure E11: Slab 300-18A Elevation of Test Set-Up

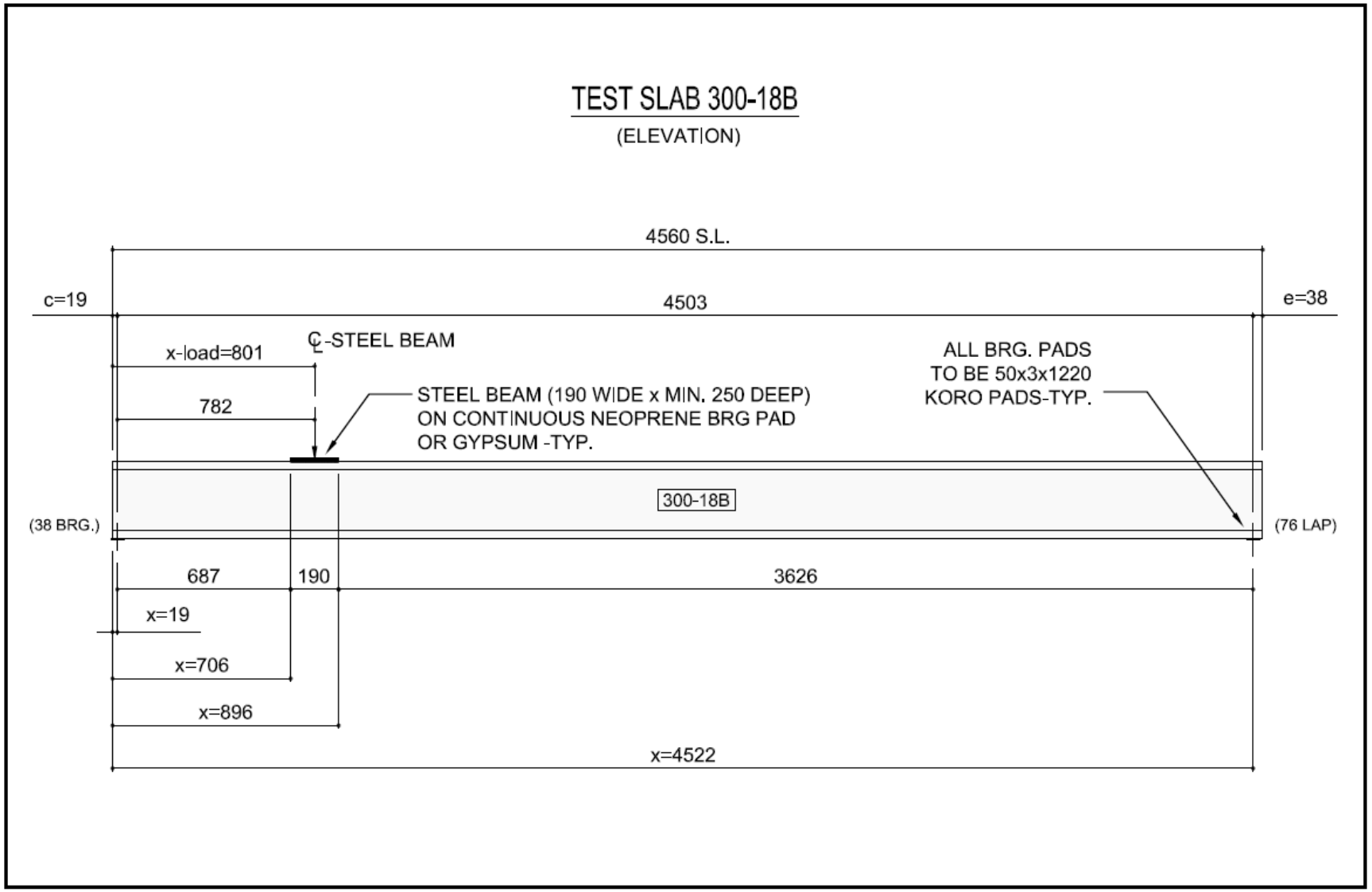

Figure E12: Slab 300-18B Elevation of Test Set-Up

APPENDIX F

SLAB INSTRUMENTATION

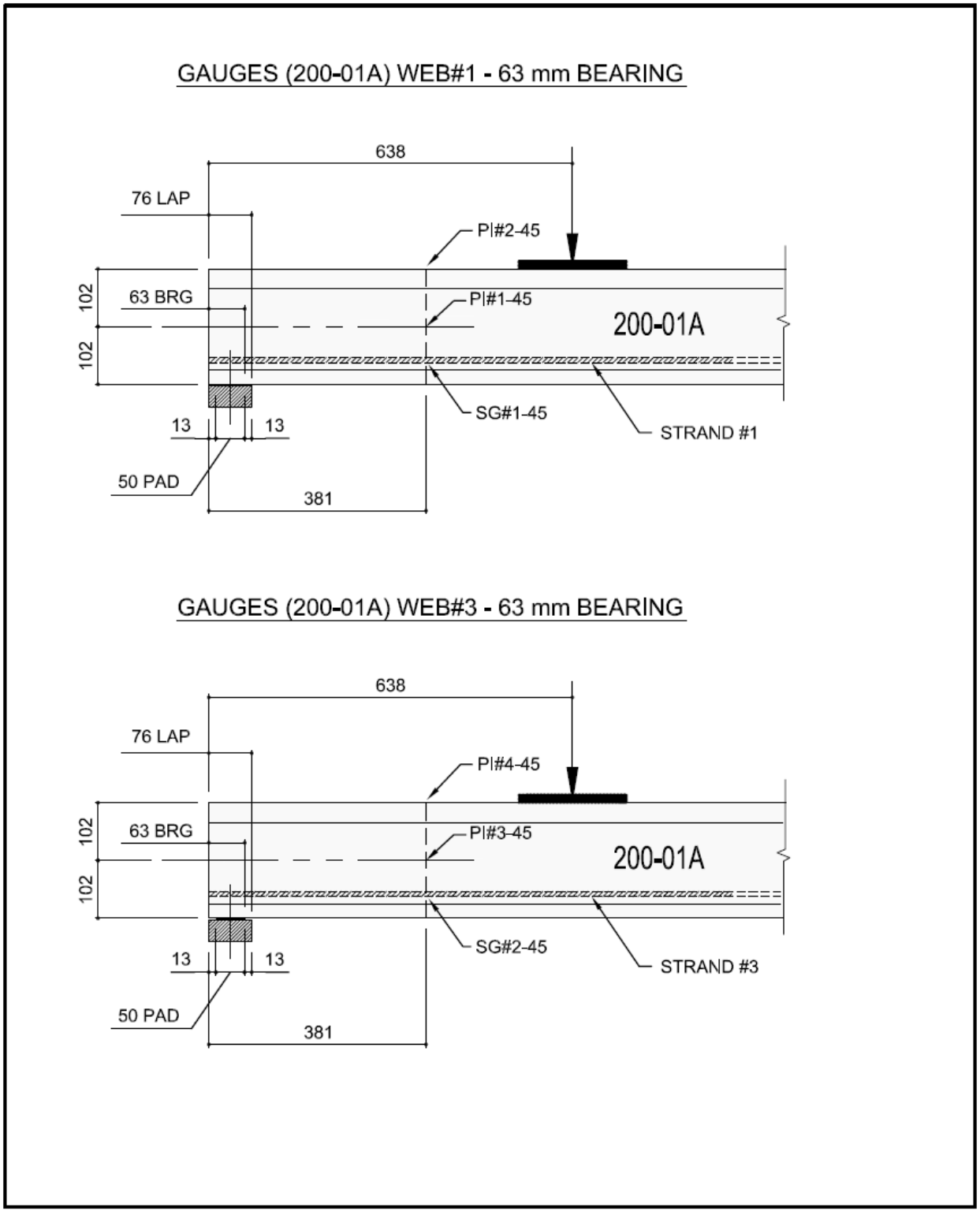

Figure F1: Elevation of Gauges (Slab 200-01A)

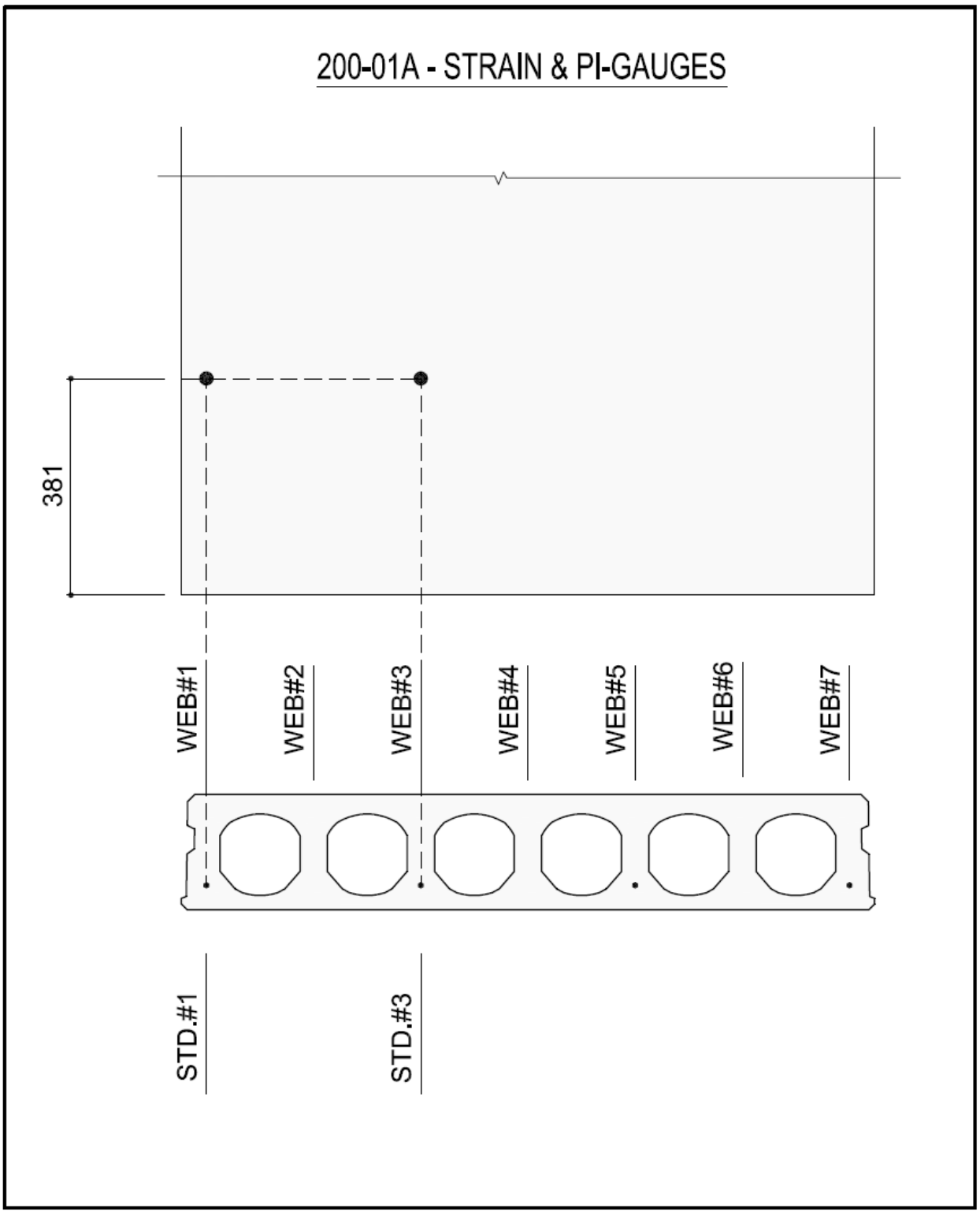

Figure F2: Plan View of Gauges and Crack Profile at Slab Underside (Slab 200-01A)

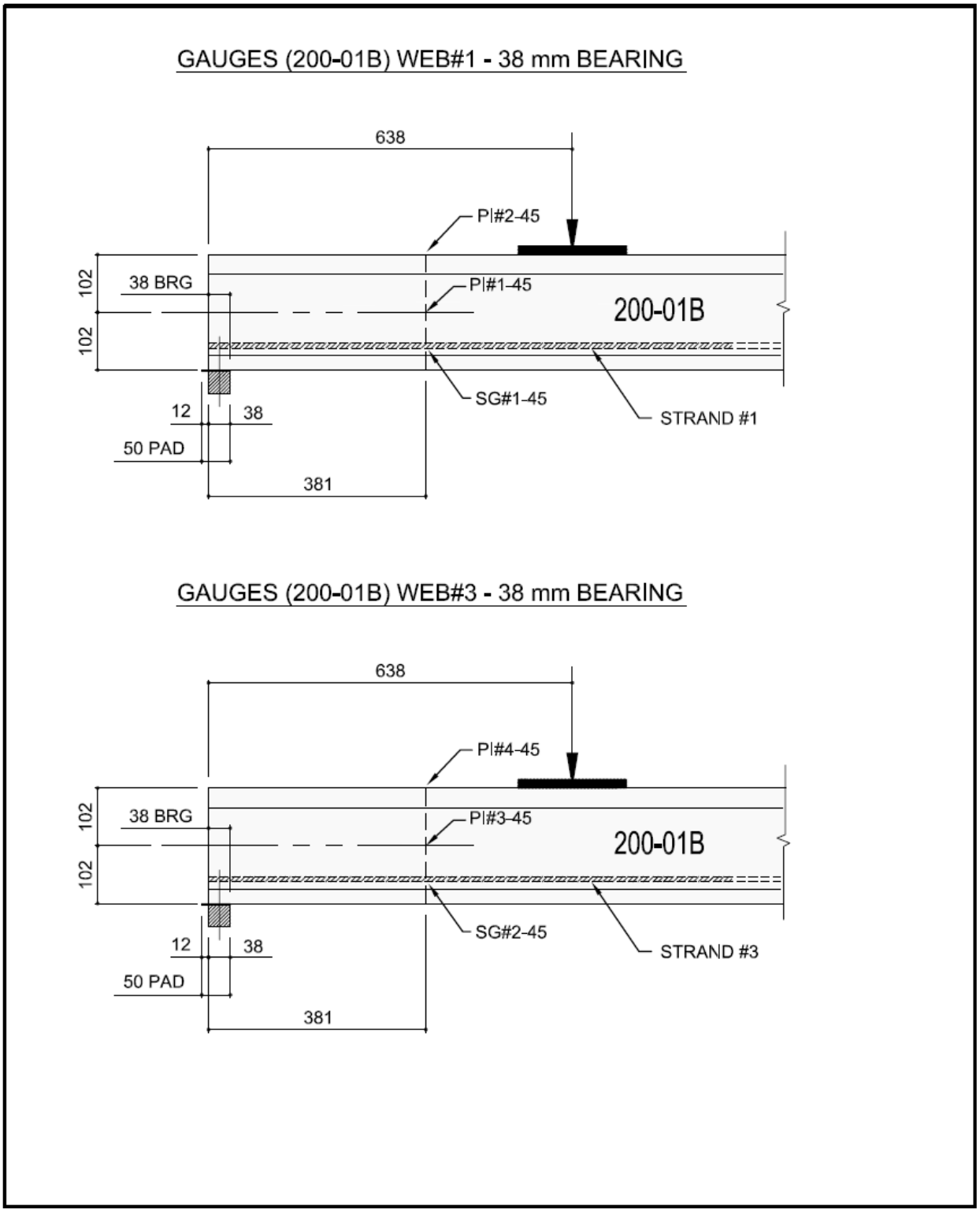

Figure F3: Elevation of Gauges (Slab 200-01B)

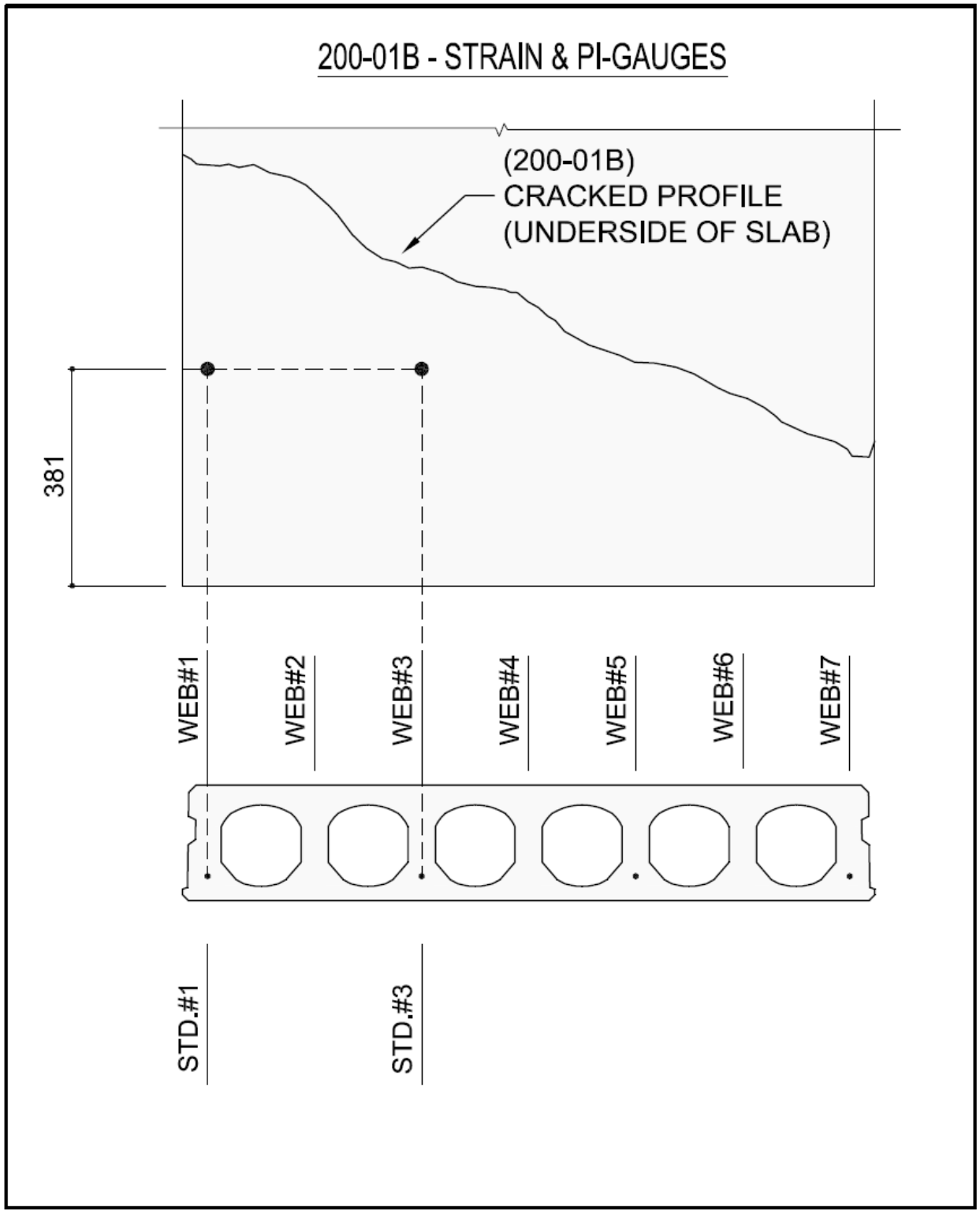

Figure F4: Plan View of Gauges and Crack Profile at Slab Underside (Slab 200-01B)

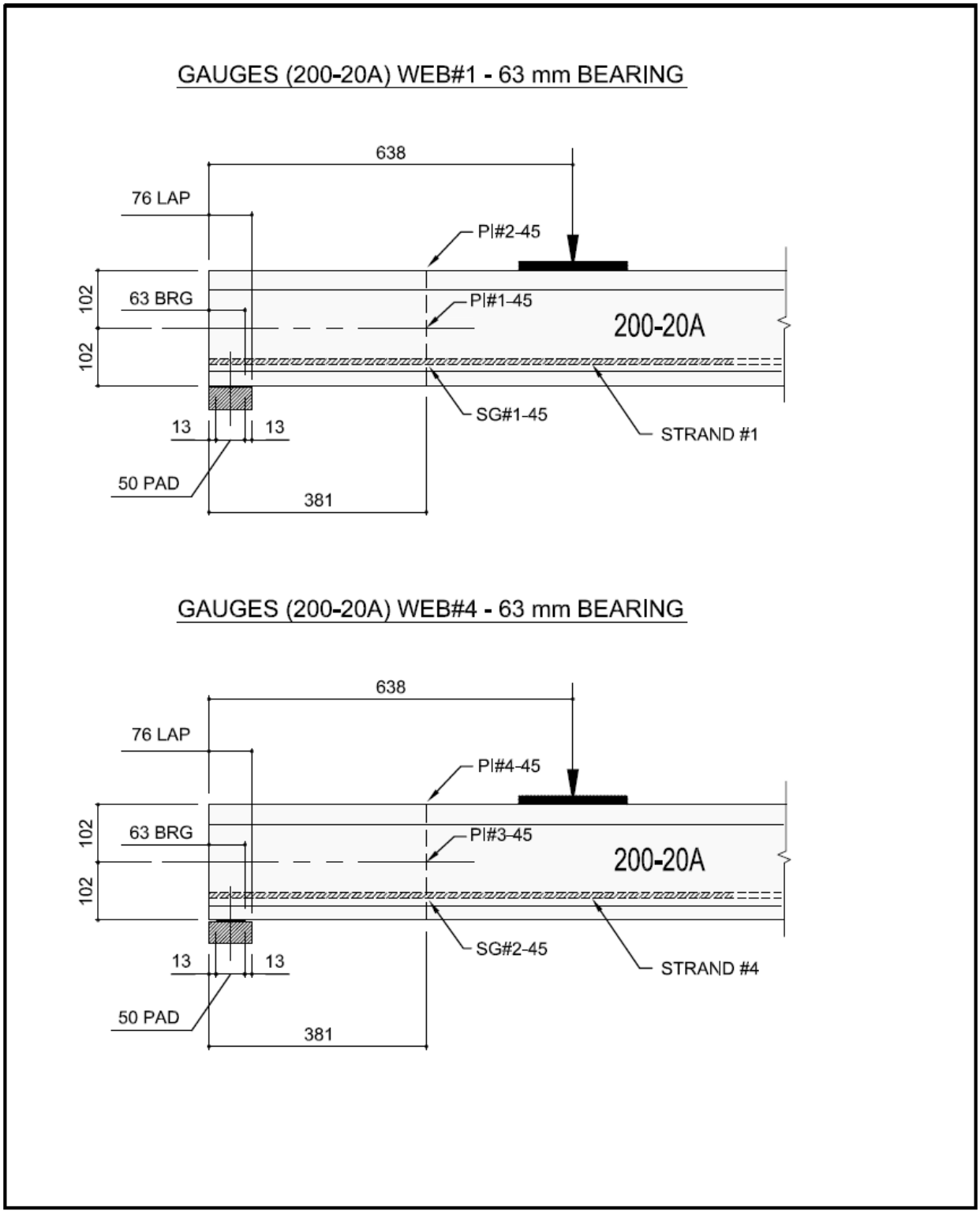

Figure F5: Elevation of Gauges (Slab 200-20A)

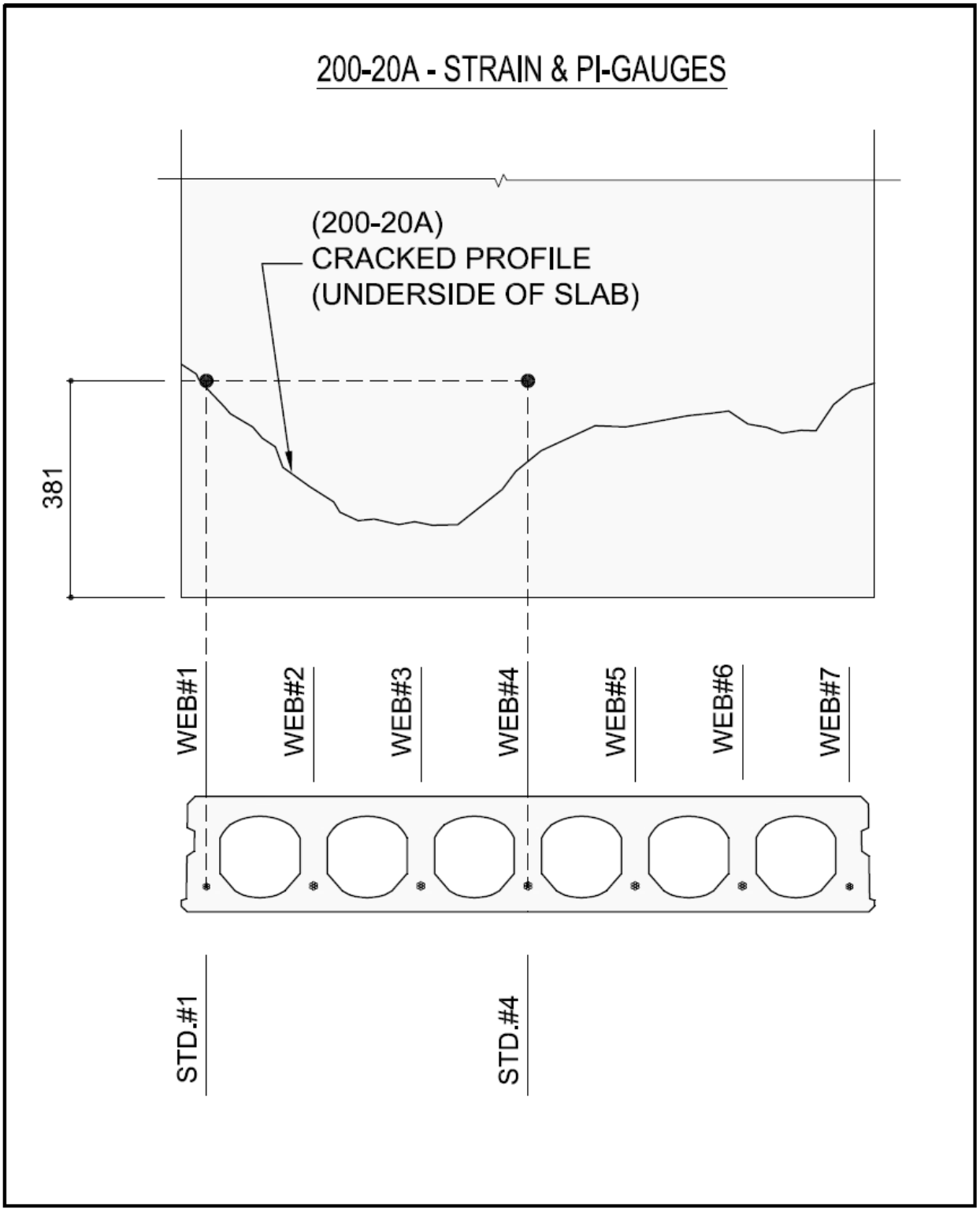

Figure F6: Plan View of Gauges and Crack Profile at Slab Underside (Slab 200-20A)

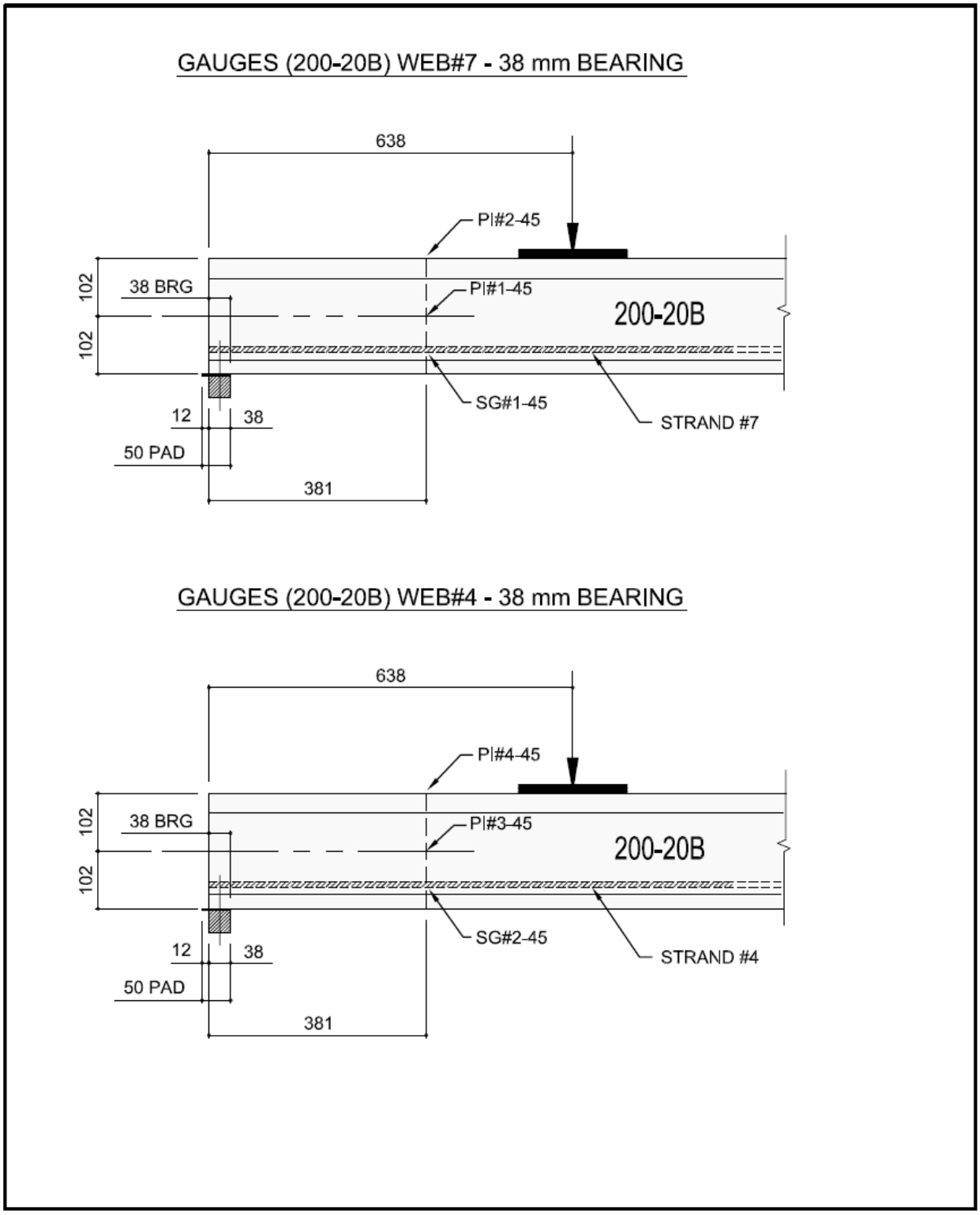

Figure F7: Elevation of Gauges (Slab 200-20B)

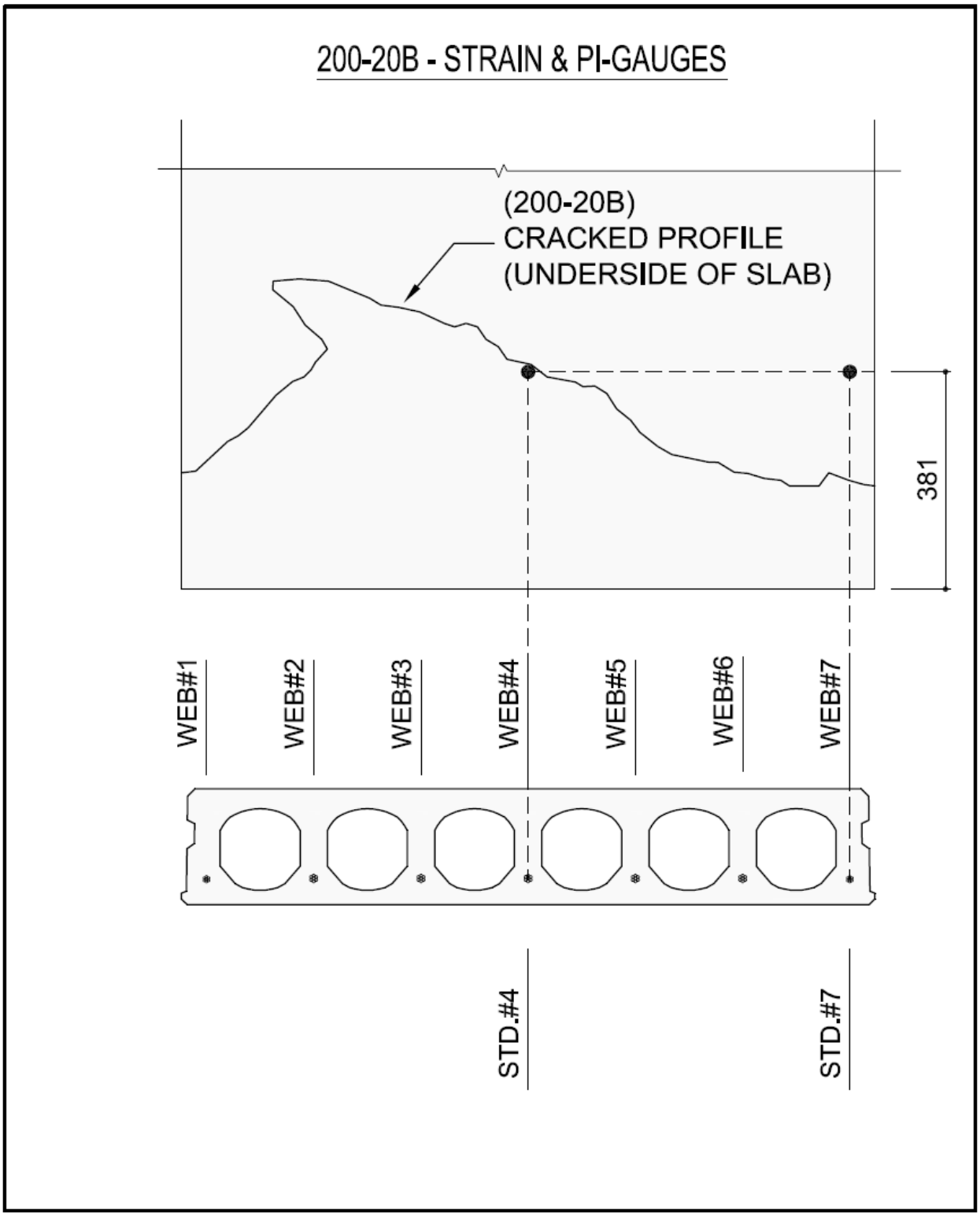

Figure F8: Plan View of Gauges and Crack Profile at Slab Underside (Slab 200-20B)

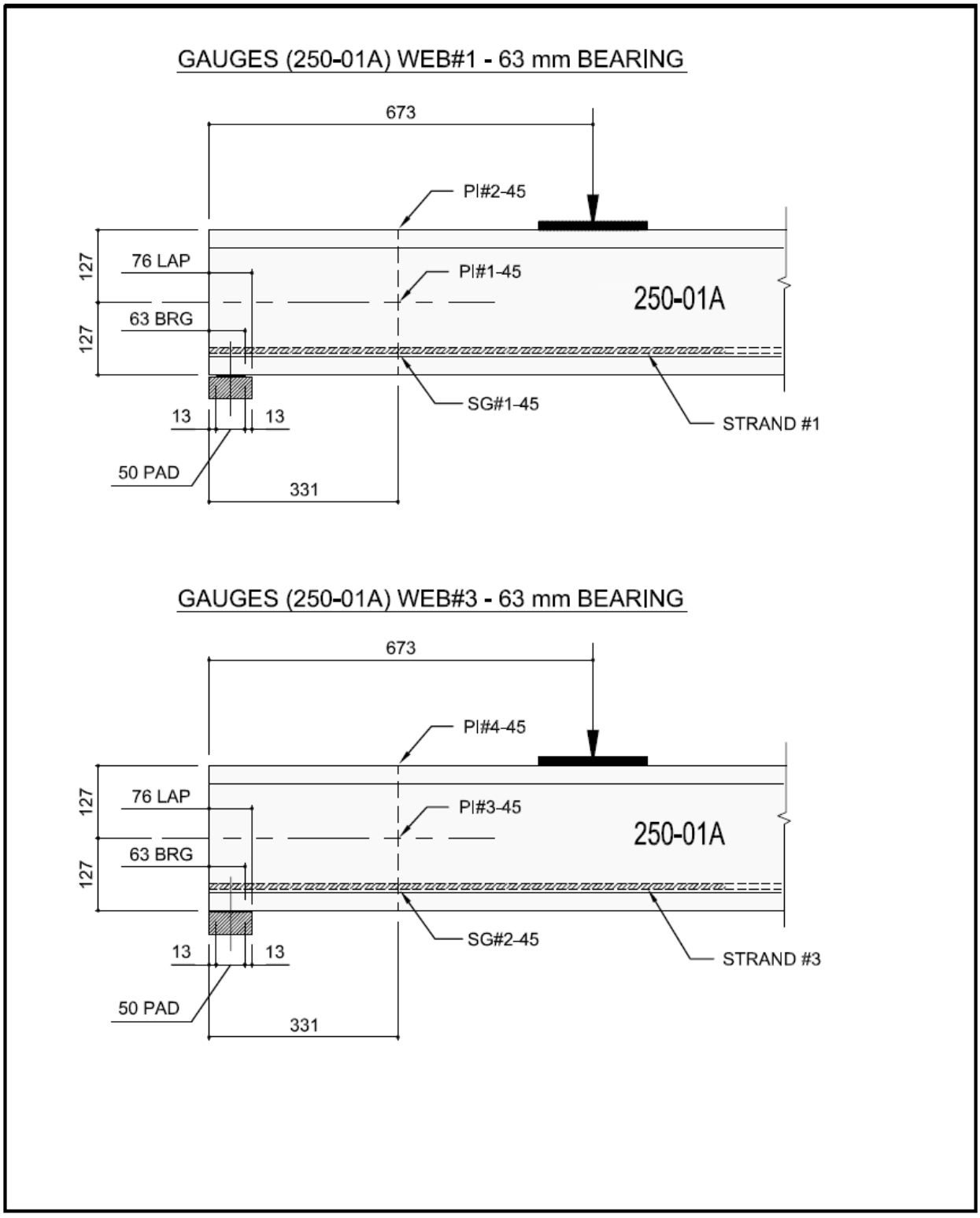

Figure F9: Elevation of Gauges (Slab 250-01A)

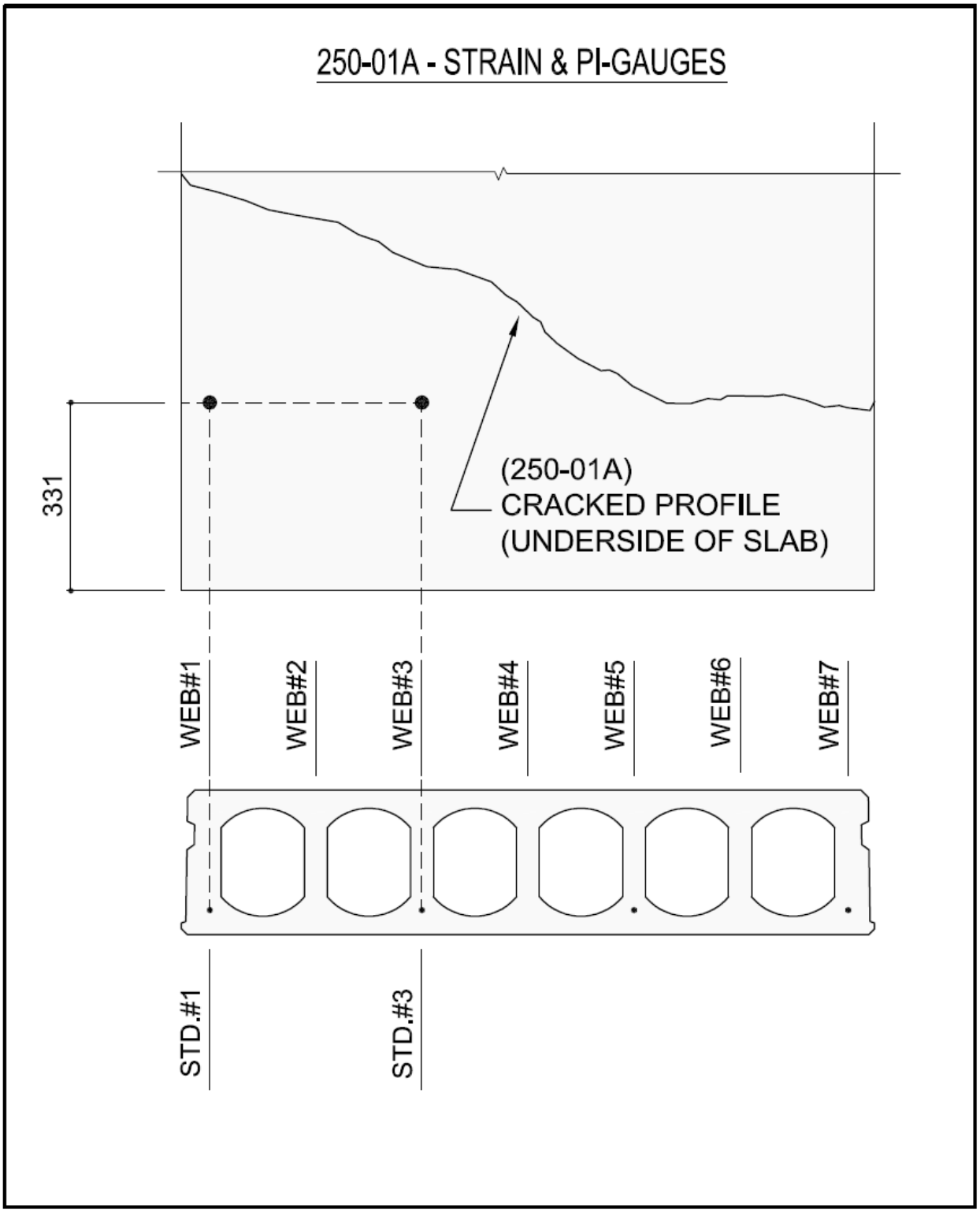

Figure F10: Plan View of Gauges and Crack Profile at Slab Underside (Slab 250-01A)

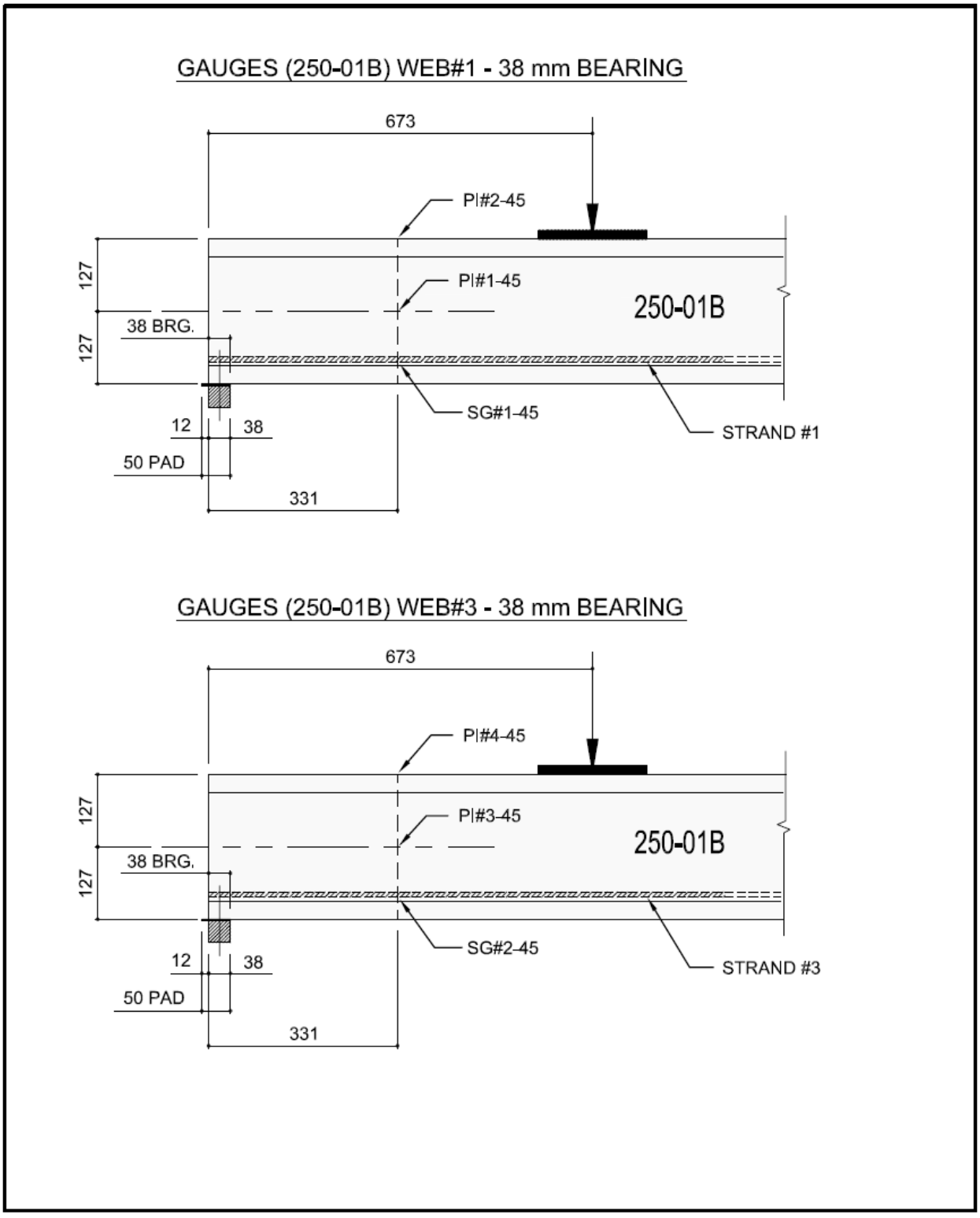

Figure F11: Elevation of Gauges (Slab 250-01B)

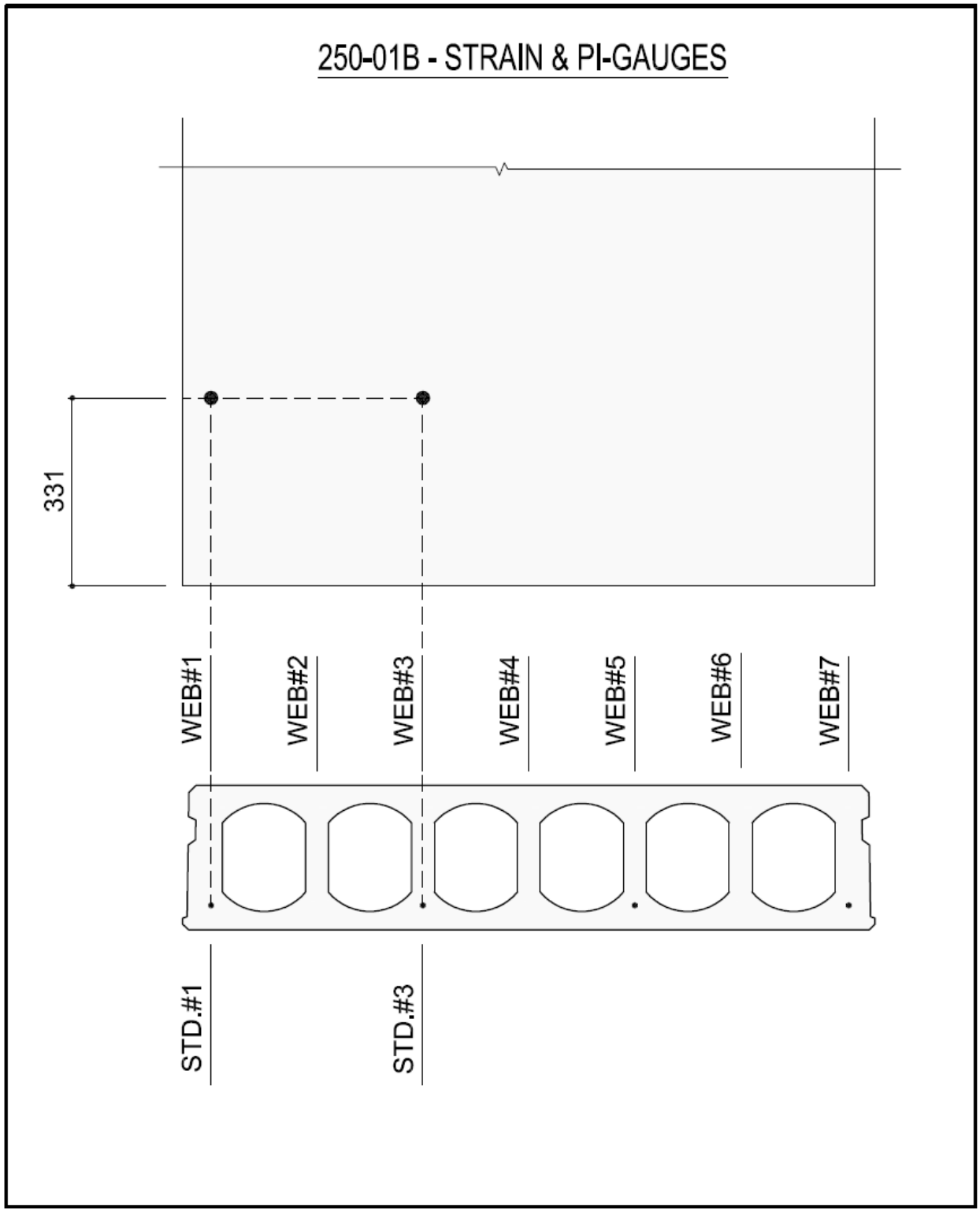

Figure F12: Plan View of Gauges and Crack Profile at Slab Underside (Slab 250-01B)

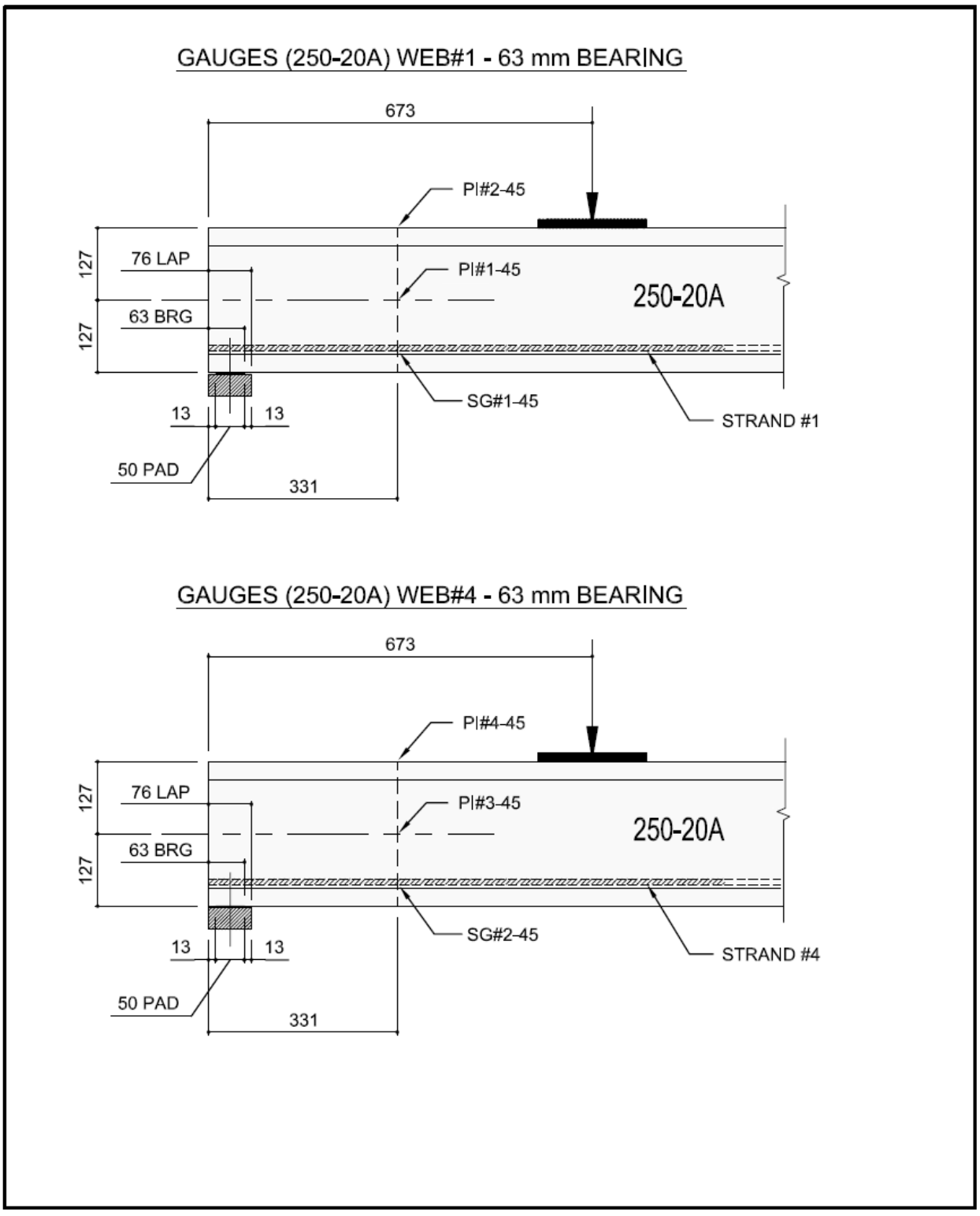

Figure F13: Elevation of Gauges (Slab 250-20A)

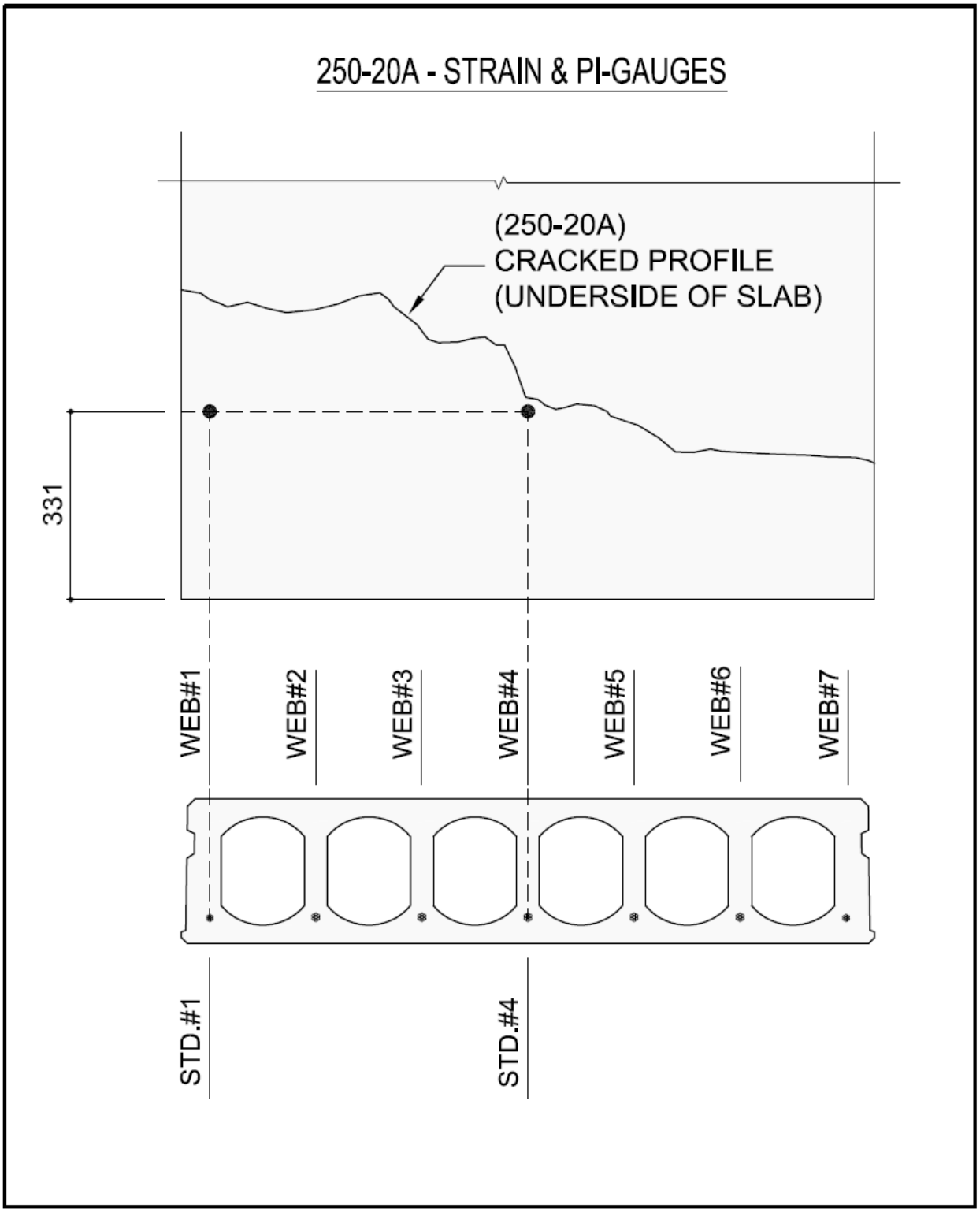

Figure F14: Plan View of Gauges and Crack Profile at Slab Underside (Slab 250-20A)

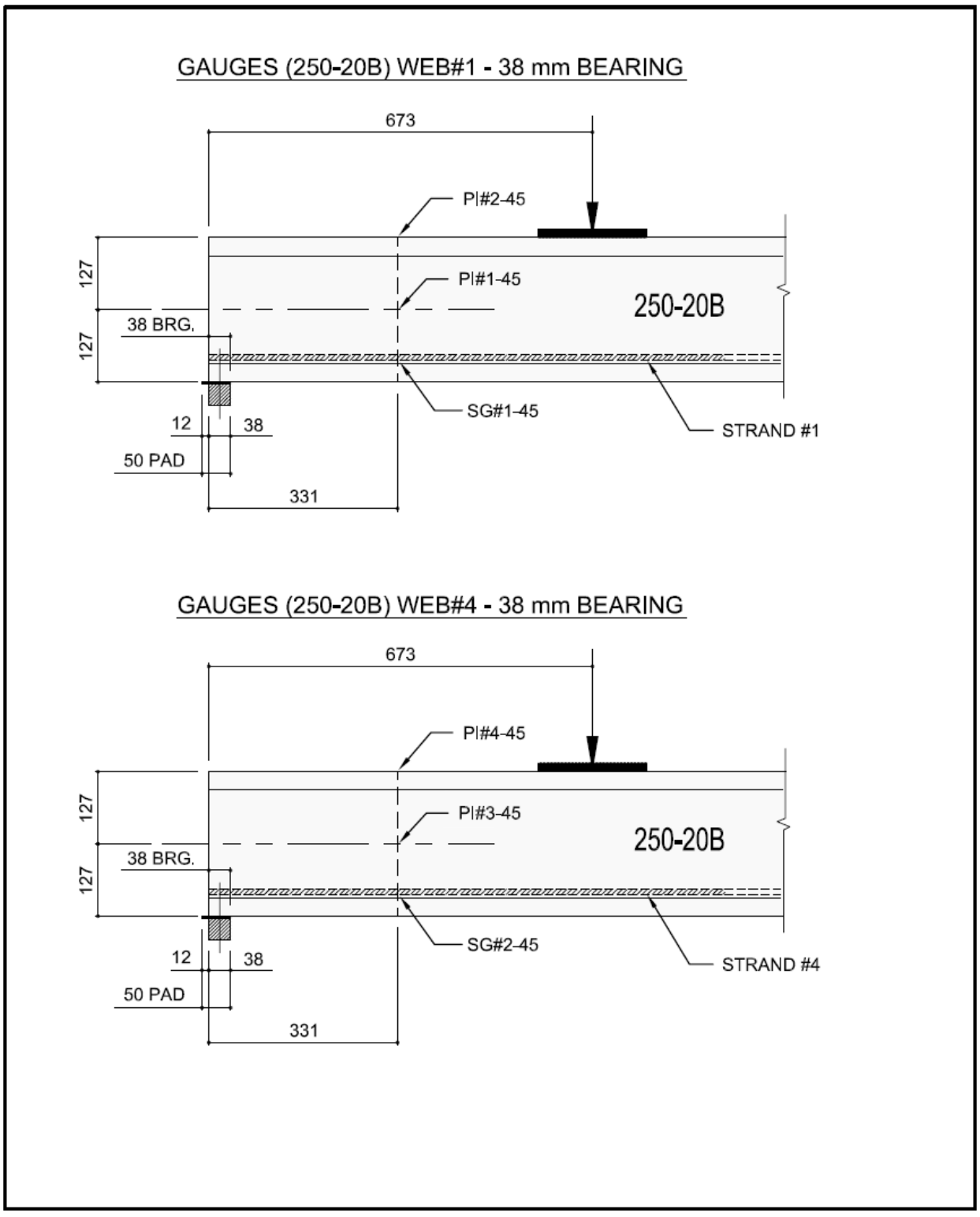

Figure F15: Elevation of Gauges (Slab 250-20B)

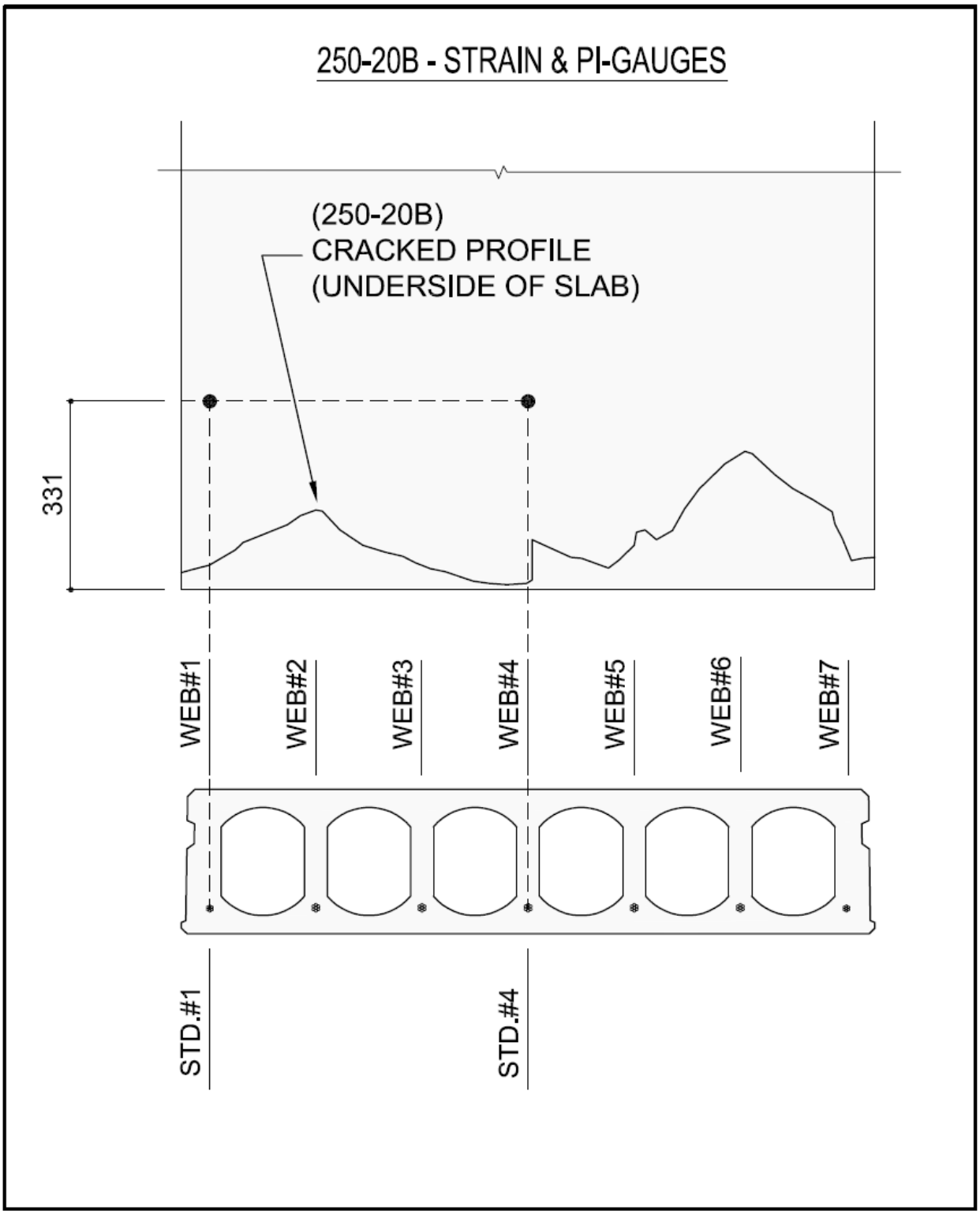

Figure F16: Plan View of Gauges and Crack Profile at Slab Underside (Slab 250-20B)

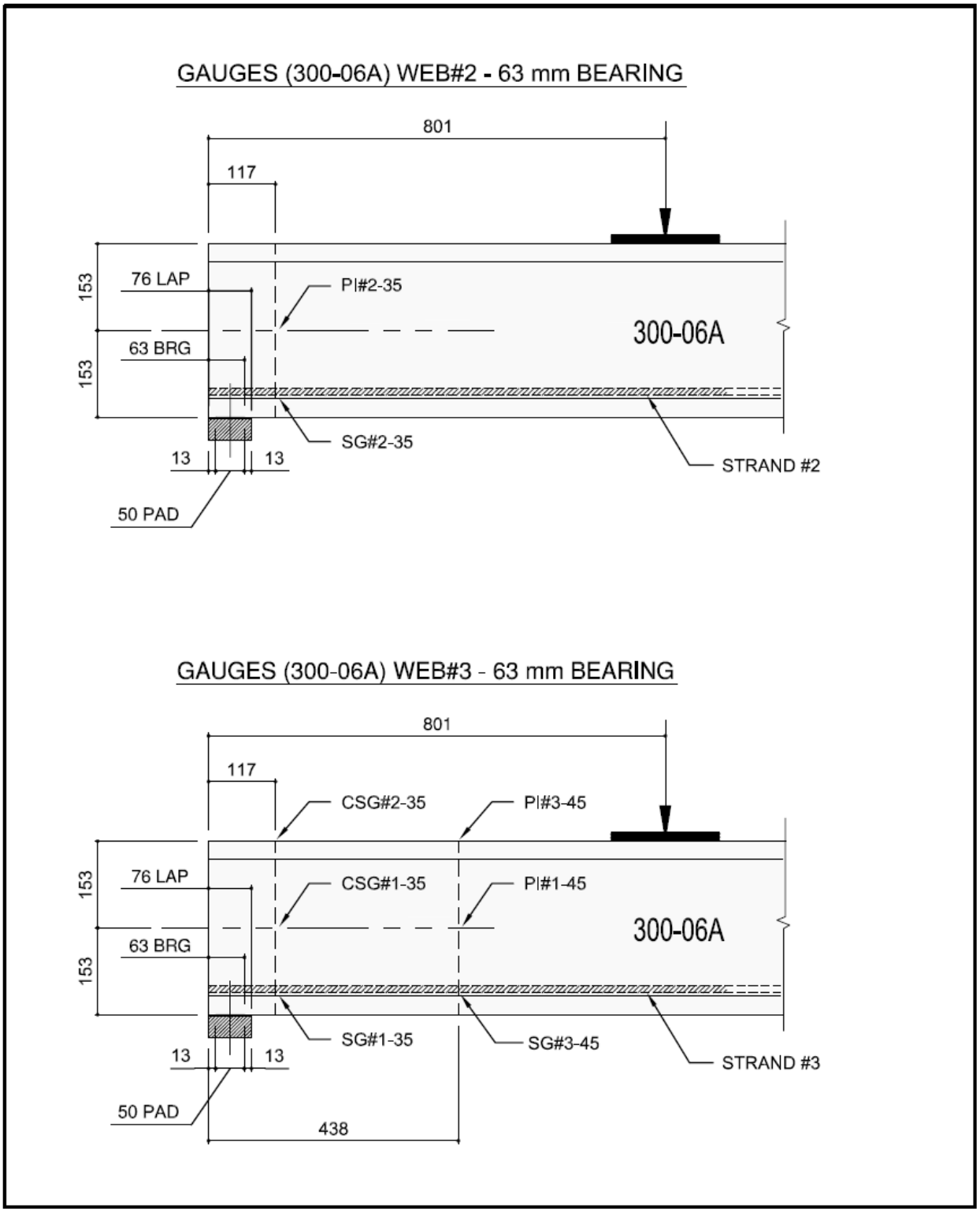

Figure F17: Elevation of Gauges (Slab 300-06A)

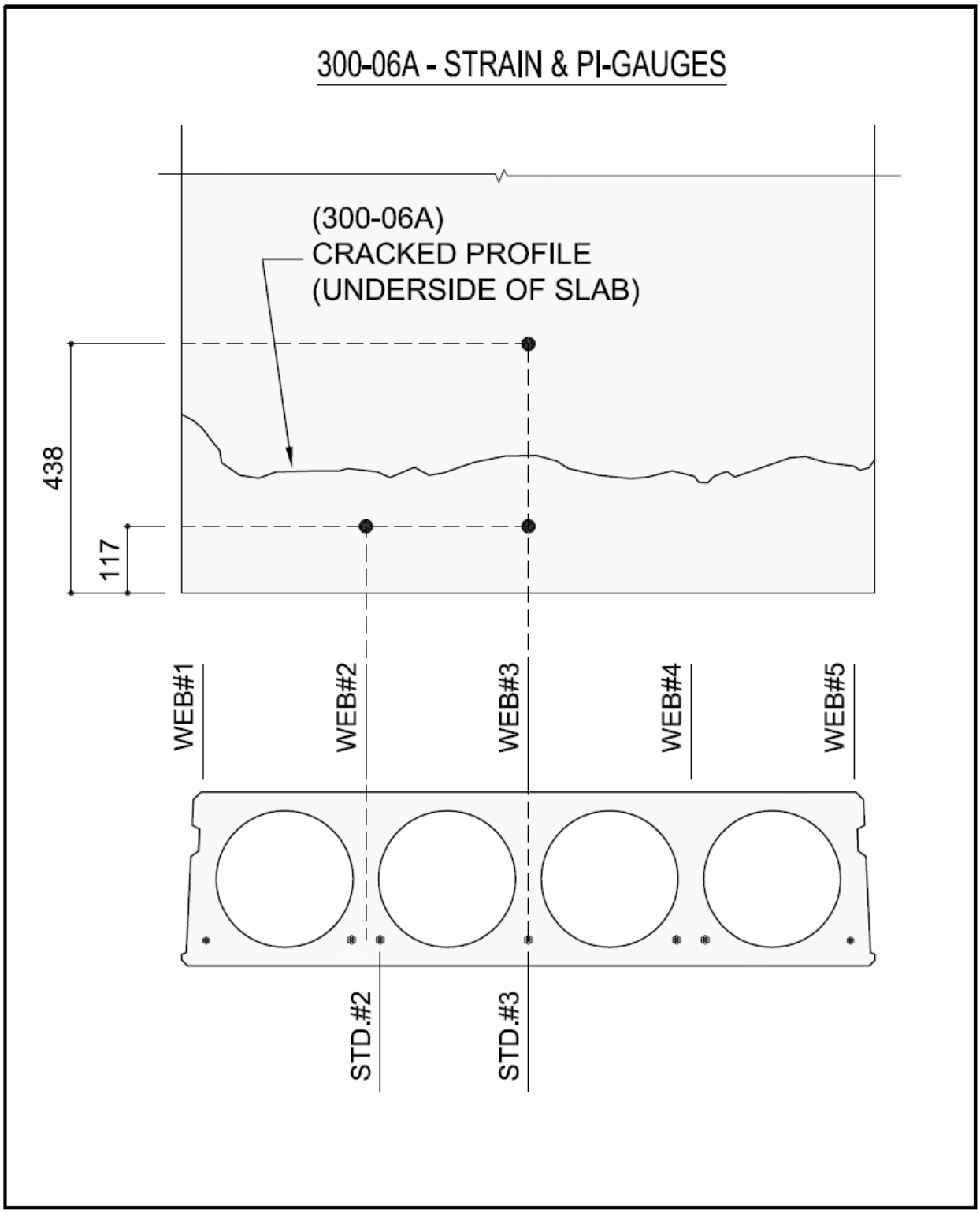

Figure F18: Plan View of Gauges and Crack Profile at Slab Underside (Slab 300-06A)

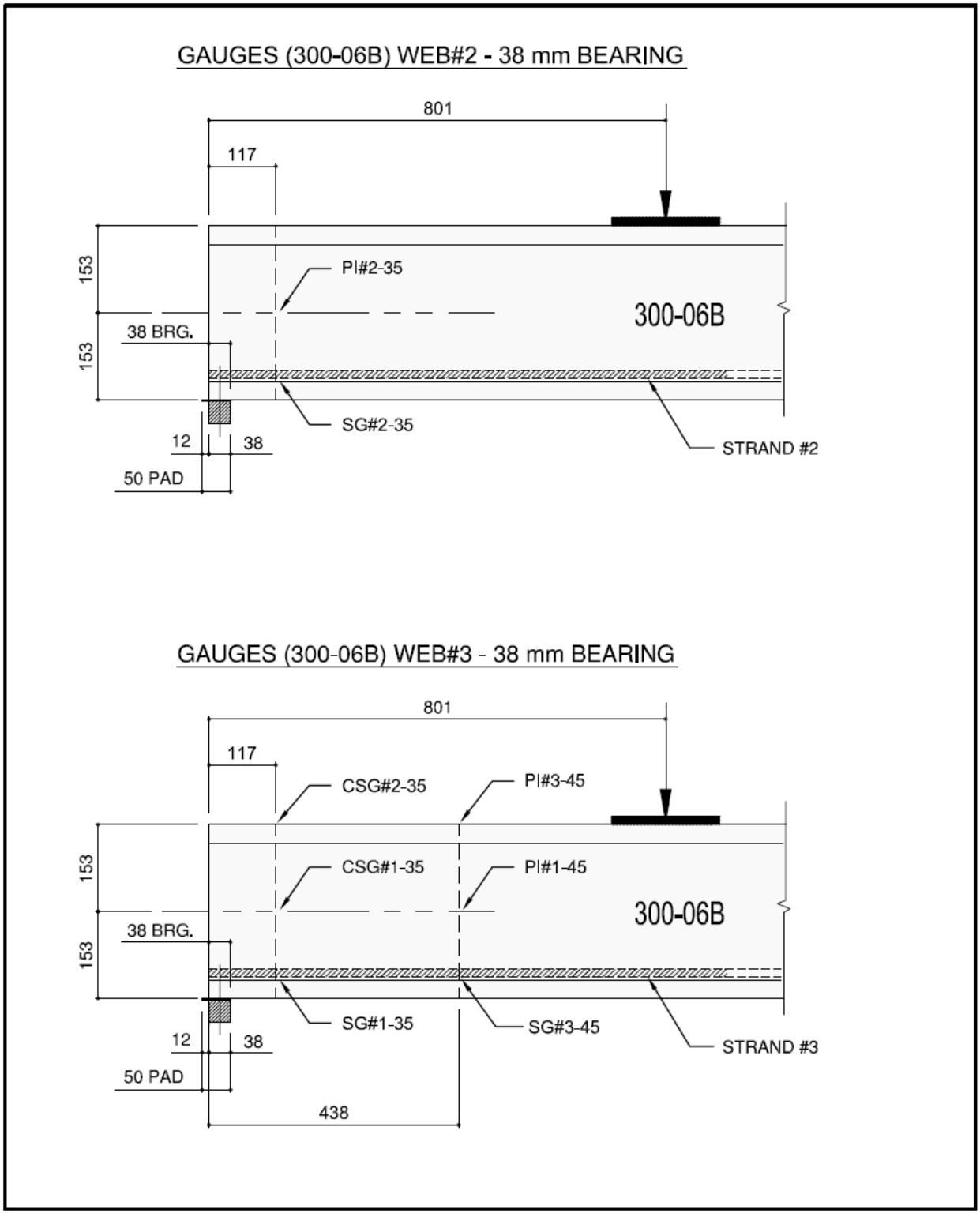

Figure F19: Elevation of Gauges (Slab 300-06B)

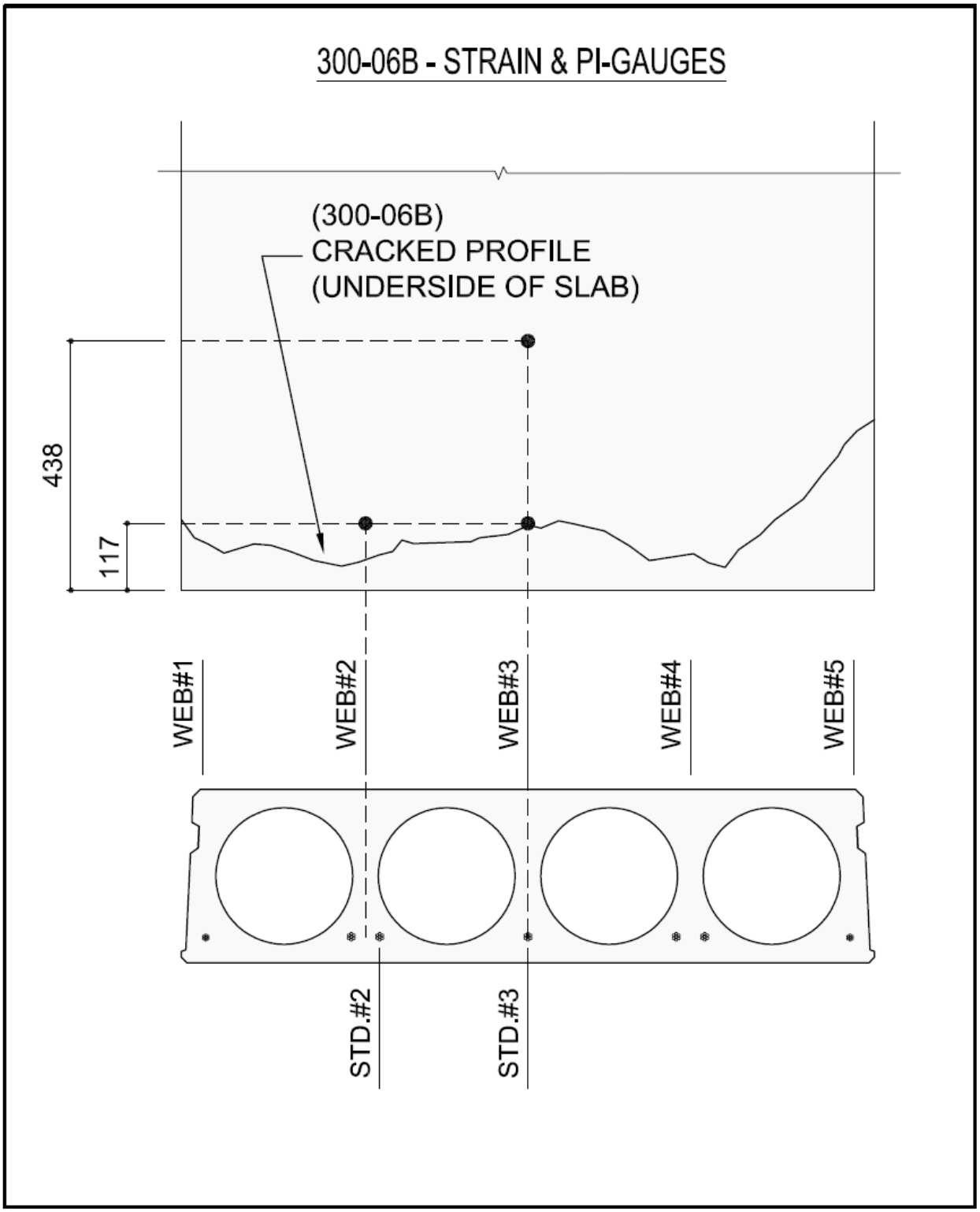

Figure F20: Plan View of Gauges and Crack Profile at Slab Underside (Slab 300-06B)

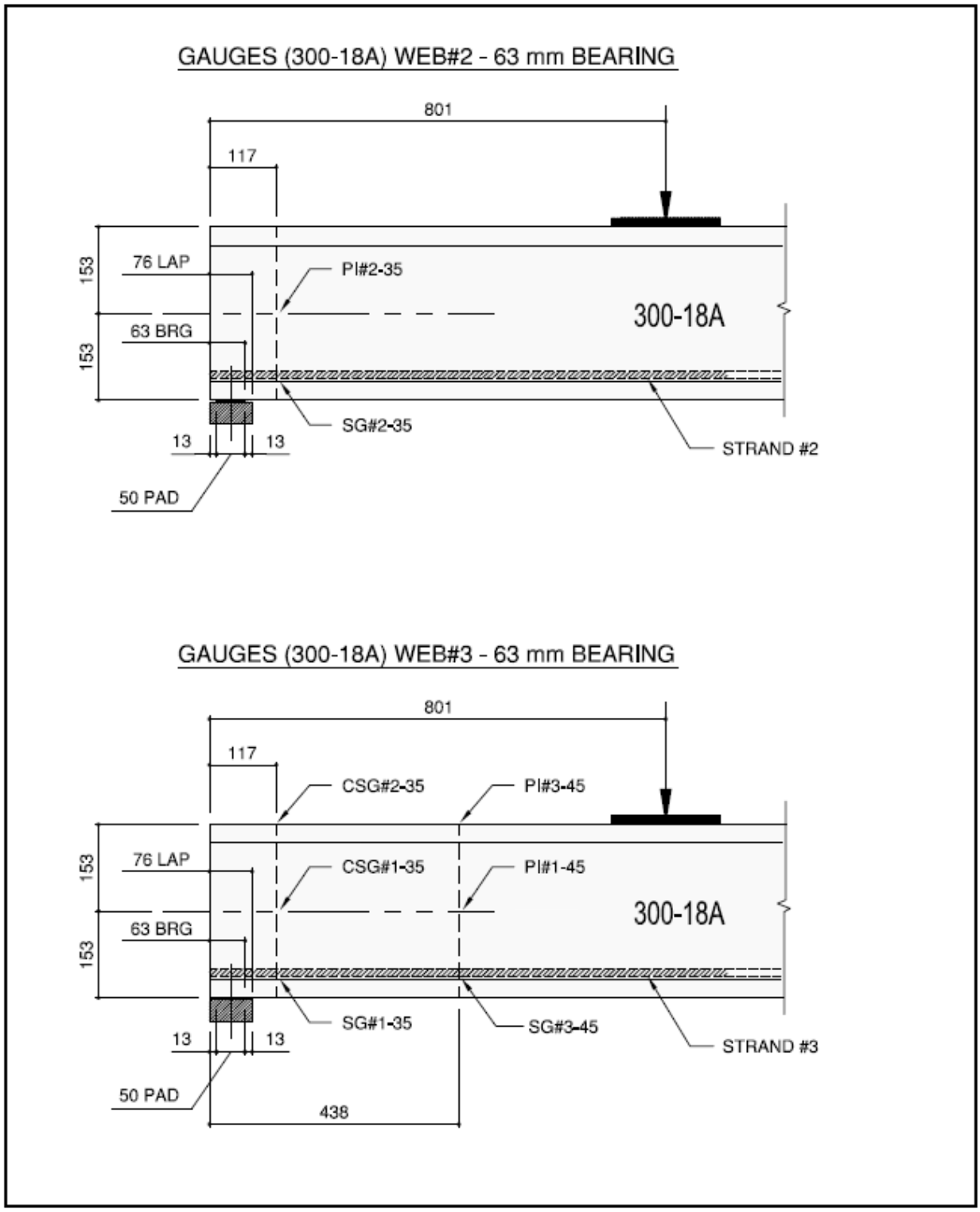

Figure F21: Elevation of Gauges (Slab 300-18A)

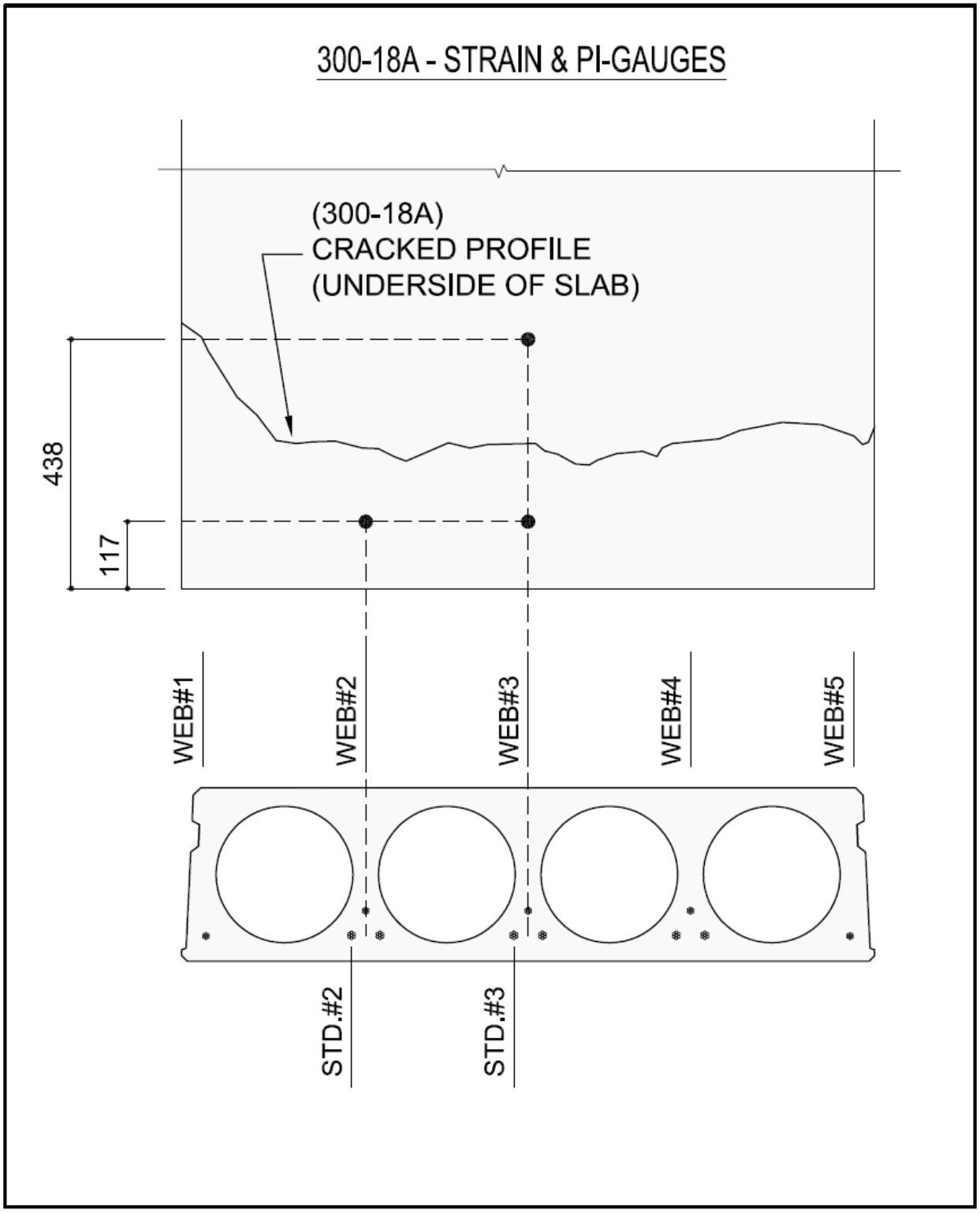

Figure F22: Plan View of Gauges and Crack Profile at Slab Underside (Slab 300-18A)

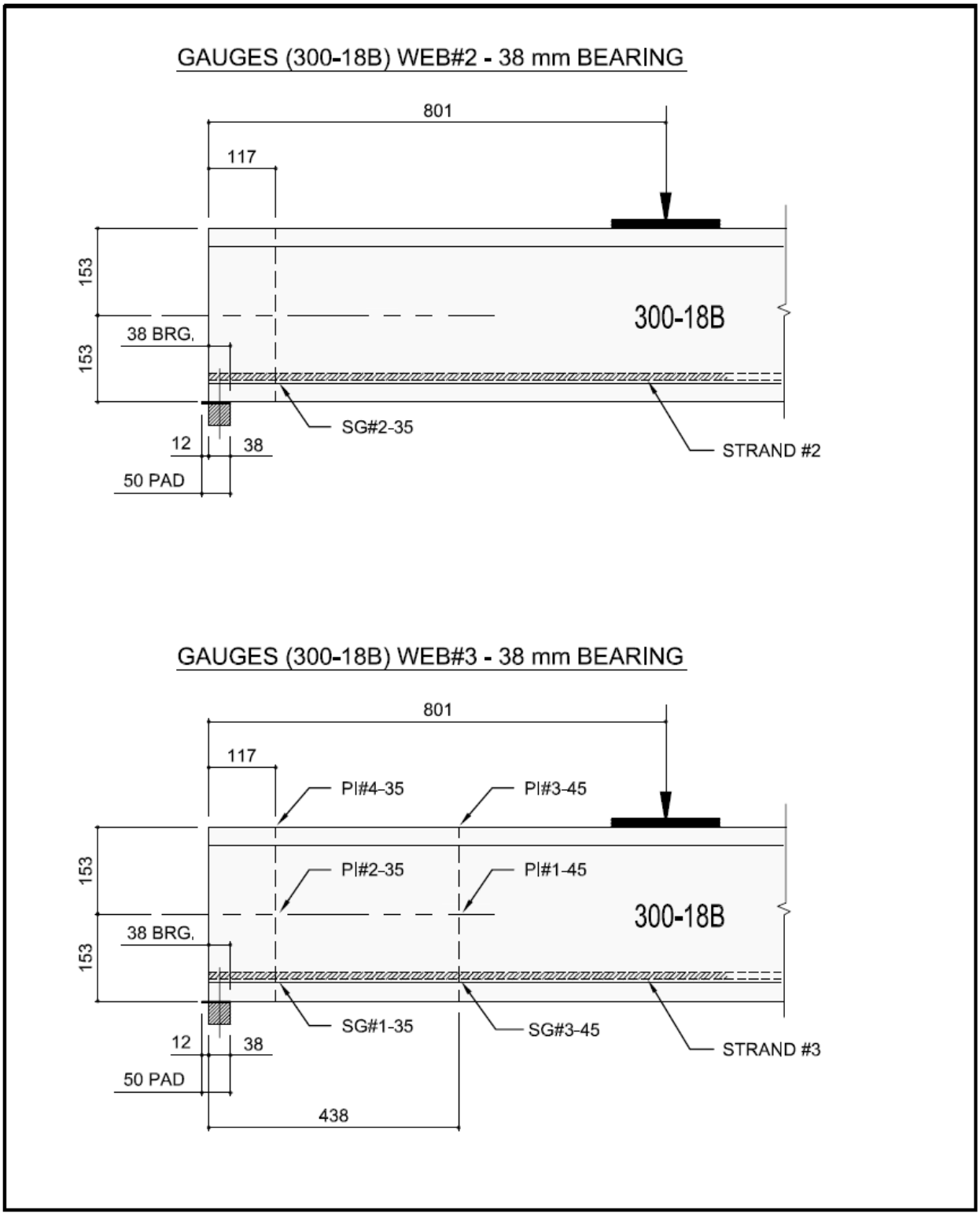

Figure F23: Elevation of Gauges (Slab 300-18B)

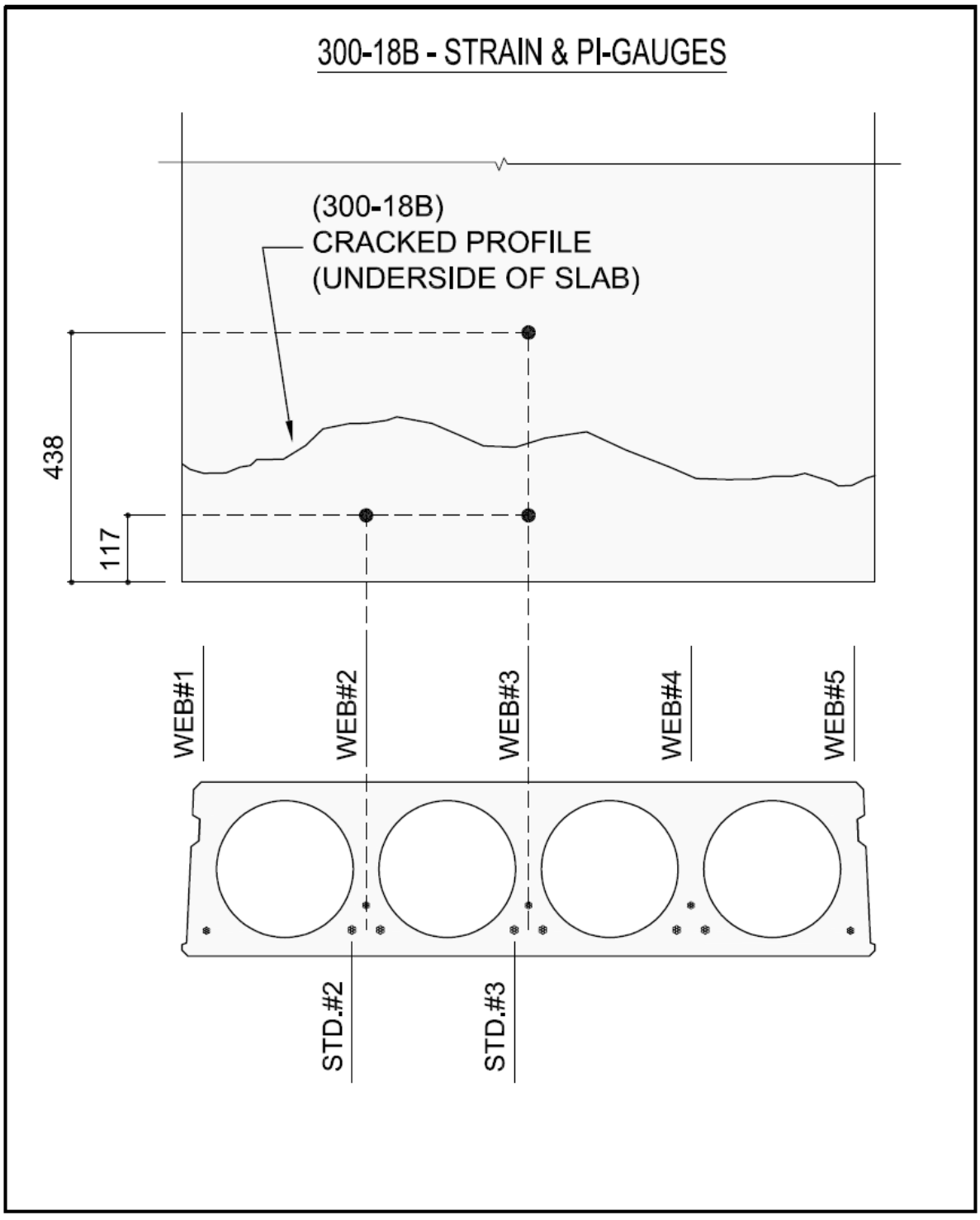

Figure F24: Plan View of Gauges and Crack Profile at Slab Underside (Slab 300-18B)

APPENDIX G

TEST SUMMARIES

Slab 200-01A - Test Summary

Test Notes

- Bearing length (end of slab to face of pad = 63 mm). Small concrete spall adjacent to web #1.
- Some shimming was required due to uneven surface of slab under-side, rubber was added to bearing to even out elevation differences.
- First crack at approximately 143 kN.

Failure Mode

- The slab failure appears to have initiated with the formation of several diagonal flexure-shear cracks at web #1, together with two flexural cracks at web #7, under a peak load of **158.4 kN** (Figures G1 to G2):

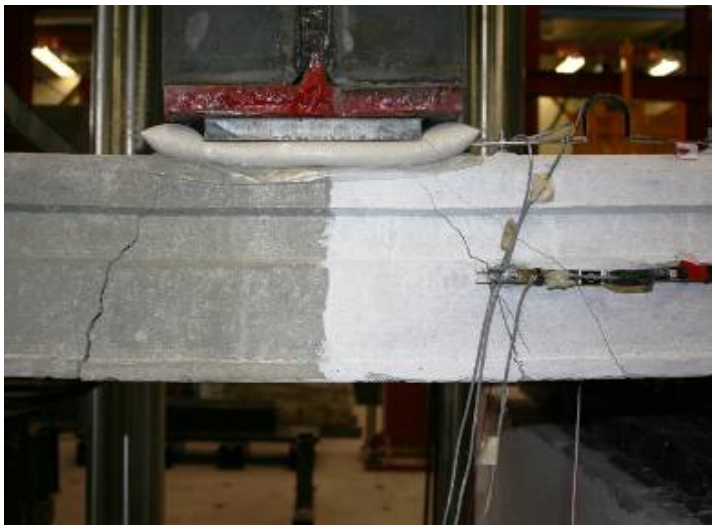

Figure G1: Diagonal Flexure-Shear Cracks at Web #1

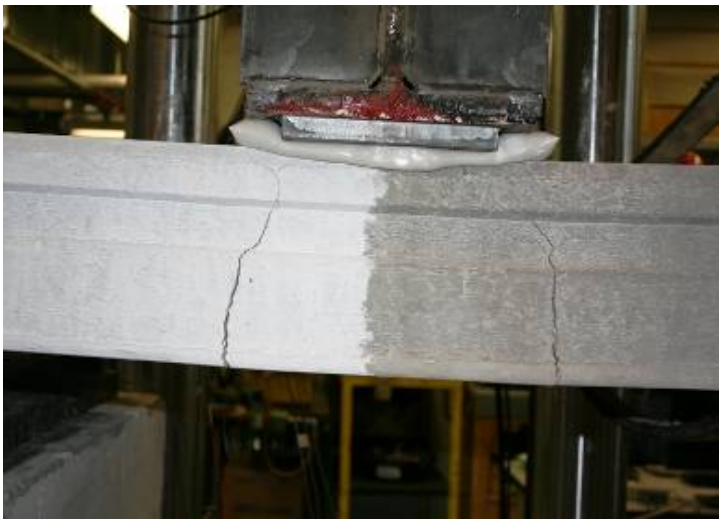

Figure G2: Flexural Cracks at Web #7

- Note that the cracks ran the full width of the slab (Figure G3). Due to the nature of the cracking on either side of the loading beam, no failure profiles were observed for slab 200-01A

Figure G3: Underside of Slab at Web #7

Slab 200-01B - Test Summary

Test Notes

- Bearing length (end of slab to face of pad = 38 mm)
- Spalling of two corners at bottom of slab (at webs #1 and #7)

Failure Mode

- The slab failure initiated with the formation of a vertical flexural crack in web #1, just below the steel beam, at a load of **136.7 kN.** After cracking, the strands in webs #1 and #3 yielded until they ruptured (Figure G4):

Figure G4: Initial Flexural Crack and Ruptured Strand at Web #1

- The crack propagated diagonally across the width of the slab, and transitioned into a flexure-shear failure at web #7 (Figures G5 and G6):

Figure G5: Diagonal Propagation of Crack across Slab Width (Web #1 in Foreground)

Figure G6: Transition from Flexural to Flexure-Shear Failure at Web #7

- Photos of the failure surface are shown in Figures G7 to G10:

Figure G7: Failure Surface – Plan View (Web #1 on Far Right)

Figure G8: Failure Surface – (Web #7 on Far Right)

Figure G9: Failure Surface (Web #1 in Foreground)

Figure G10: Failure Surface (Web #1 & Ruptured Strands in Web #1 and #3 in Foreground)

- Figures G7 to G10 confirm a flexural failure profile for webs #1 and #2, and a flexure-shear profile for webs #3 to #7. It can also be noted that the angle of the flexure-shear failures is fairly steep in webs #3 to #7.

Slab 200-20A - Test Summary

Test Notes

- Bearing length (end of slab to face of pad = 63 mm).
- Some spalling was observed at the corners of web #1 and web #7.

Failure Mode

- During the first load cycle, a diagonal web-shear crack formed in web #1, at approximately 92 kN, which propagated diagonally towards the underside of the slab (Figures G11 and G12).

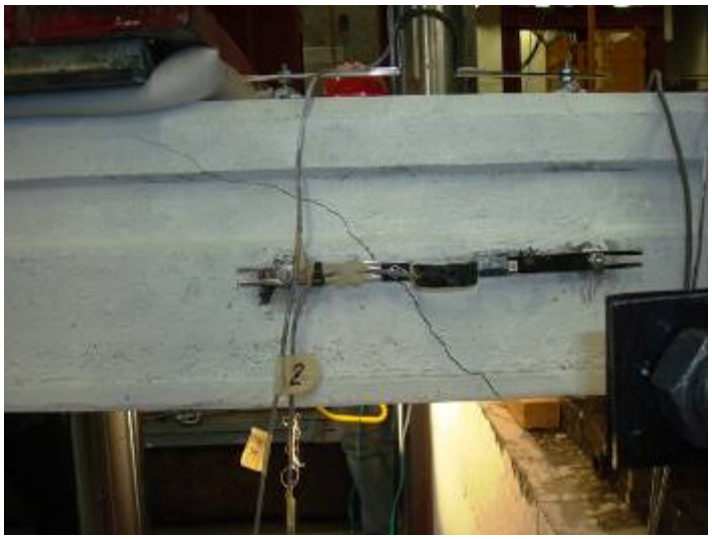

Figure G11: Initial Web-Shear Crack at Web #1 (92 kN)

Figure G12: Initial Web-Shear Crack at Web #1 and Diagonal Crack at Slab Underside (92 kN)

- During the second cycle of load, additional cracks occurred in webs #2 and #3 at approximately 117 kN of load (Figure G13). In addition, at approximately 117 kN, the initial slippage in strand #1 increased from 2.0 mm to 3.1 mm, in strand #2 from 2.4 mm to 3.2 mm and in strand #3 from 1.3 mm to 1.75 mm.

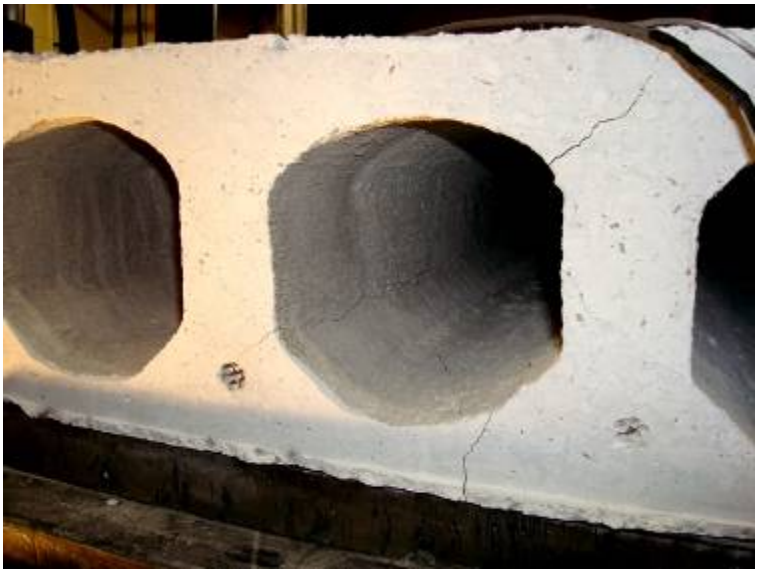

Figure G13: Additional Cracks in Webs #2 and #3 at (117 kN)

- In spite of the formation of significant cracks in the slab during the first two load cycles, the slab carried additional load in the last cycle up to a peak failure load of **178.1 kN**. The final slab failure occurred with a web-shear failure across all webs at the peak load, as shown in Figure G14:

Figure G14: Web-shear Failure across Full Slab Width (Web #7 in Foreground)

- To aid in the viewing of the web profiles, the slab was reloaded again to force the separation of the top half of the slab (Figure G15):

Figure G15: Web-Shear Cracks after Re-Loading Slab (Web #7 in Foreground)

- Photos of the failure surface are shown in Figures G16 to G18:

Figure G16: Failure Surface – Plan View (Web #1 on Far Right)

Figure G17: Failure Surface – Elevation View (Web #7 in Foreground)

Figure G18: Failure Surface (Web #1 in Foreground)

Slab 200-20B - Test Summary

Test Notes

- Bearing length (end of slab to face of pad = 38 mm).
- Some spalling was observed at the corners of web #1 and web #7 and adjacent to the steel loading beam on web #1.

Failure Mode

- Failure appears to have initiated with the formation of a steep web-shear crack under the loading beam (confirmed with a frame-by-frame review of the video at web #1) at a peak load of **166.5 kN**. Immediately after formation of the first web-shear crack, a second shallower diagonal web-shear crack formed adjacent to the support, which rapidly opened up across the slab (Figures G19 and G20).

Figure G19: Diagonal Web-Shear Cracks at Web #1 at Failure

Figure G20: Initial Cracks at Web #1 and Diagonal Crack at Slab Underside

- Figure G21 shows a diagonal web-shear crack, which led to a shear-tension failure of the slab at web #7:

Figure G21: Web-Shear Cracks at Failure (Web #7 in Foreground)

- To aid in the viewing of the web failure profiles, the slab was reloaded again to force the separation of the top half of the slab (Figures G22 and G23). It should be noted that even

after reaching the peak failure load of 166.5 kN and subsequent unloading, the slab was able to be reloaded up to 80 kN, before finally dropping off.

Figure G22: Web-Shear Cracks after Reloading (Web #1 in Foreground)

Figure G23: Web-Shear Cracks after Reloading (Web #7 in Foreground)

- Photos of the failure surface are shown in Figures G24 to G26:

Figure G24: Failure Surface – Plan View (Web #1 on Far Right)

Figure G25: Failure Surface – Elevation View (Web #7 in Foreground)

Figure G26: Failure Surface (Web #1 on Far Left)

Slab 250-01A - Test Summary

Test Notes

- Bearing length (end of slab to face of pad = 63 mm). Slight spalling at corners of web #1 and web #7 at bearing location.
- PI-Gauge #2 (web #1-top) jumped up and didn't come back down (need to adjust).
- Subtract 500 from 2nd and 3rd cycles (see data from first cycle).
- The strain gauge on the strand in web #3 (SG#6) was lost.

Failure Mode

- The slab failure appears to have initiated with the formation of a flexural crack just below the steel beam in web #1, at a peak load of **211.9 kN** (Figure G27):

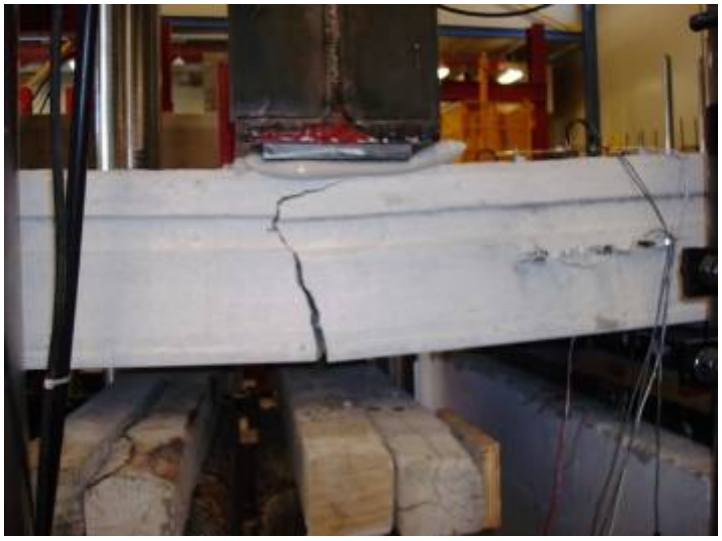

Figure G27: Initial Flexural Crack at Web #1

- The crack then rapidly propagated diagonally across the width of the slab, as shown in Figure G28:

Figure G28: Diagonal Propagation of Crack across Slab Width

- As the crack widened in web #1, the strains in the edge strand rapidly increased beyond the yield point until the edge strand ruptured. The failure mode transitioned from a flexural failure at web #1 to a flexure-shear failure at web #7, initiated by flexure-shear cracking in webs #5, #6 and #7 (Figure G29).

Figure G29: Transition from Flexural to Flexure-Shear Failure (Web #7 in Foreground)

- Photos of the failure surface are shown in Figures G30 to G32:

Figure G30: Failure Surface – Plan View (Web #1 and Ruptured Strand on Far Right)

Figure G31: Failure Surface – Elevation View (Web #7 in Foreground)

Figure G32: Failure Surface (Web #1 & Ruptured Strand in Foreground)

It is evident from Figures G31 and G32 that webs #1, #2 and #3 have a failure profile that is indicative of a flexural failure, whereas webs #5, #6 and #7 have a failure profile matching that of a flexure-shear failure. Web #4 appears to be a transitional failure profile between flexural and flexure-shear.

Slab 250-01B - Test Summary

Test Notes

- Bearing length (end of slab to face of pad = 38 mm)
- Bearing at test end was slightly uneven – shims were placed to correct.
- Some spalling was observed at the corner of web #1.

Failure Mode

- The slab failure initiated with the formation of a nearly vertical flexural crack, adjacent to the steel beam at a peak load of **205.5 kN**. The crack rapidly spread across the full width of the slab, remaining nearly vertical throughout.
- As the crack continued to open, all four strands yielded eventually leading to a complete rupture of all strands. Once the strands ruptured, the slab cracked through the full depth of the member, leading to a complete separation of the slab into 2 pieces.
- Figures G33 to G35 outline the failure surface:

Figure G33: Failure Surface (Web #1 on Far Left)

Figure G34: Failure Surface (Web #7 in Foreground)

Figure G35: Failure Surface (Web #1 in Foreground)

Slab 250-20A - Test Summary

Test Notes

- Bearing length (end of slab to face of pad = 63 mm).
- PI-Gauge #3 initial reading (–) 2600 compression (need to adjust).
- Some spalling was observed at the corners of web #1 and web #7.

Failure Mode

- The slab failure appears to have initiated with the formation of a flexural crack in web #1, just below the beam at a peak load of **294.2 kN**, which then may have travelled diagonally upwards transitioning into a flexure-shear crack and leading to a shear-tension failure in web #1.
- However, it is also possible that a steeply inclined diagonal web-shear crack may have initiated under the beam at the peak load and travelled downwards to the underside of slab. Unfortunately, no video was available for a frame-by-frame study of the cracking on the side of web #1, to confirm the above.
- The cracking in web #1 was followed by a rapid series of successive cracks across the full width of the slab, (Figures G36 to and G37):

Figure G36: Initial Crack and Shear Tension Failure at Web #1

Figure G37: Diagonal Propagation of Crack across Slab Width

- The failure mode transitioned from a steep-angled shear-tension failure at web # 1 to a shallower-angled shear-tension failure at web #7, initiated by web-shear cracking in webs #5, #6 and #7 (Figure G38).

Figure G38: Transition to a Web-Shear Failure (Web #7 in Foreground)

- Photos of the failure surface are shown in Figures G39 and G40:

Figure G39: Failure Surface – Plan View (Web #1 on Far Right)

Figure G40: Failure Surface – Elevation View (Web #7 in Foreground)

- Figure G41 and G42 offer strong evidence that the failure may have in fact originated with a flexural crack in webs #1, #2 and #3 (note the nearly vertical profile on web #3) and transitioned into web-shear cracks, as the cracking extended towards web #7 (note the shallow profiles on webs #4 to #7).

Figure G41: Failure Surface – Elevation View (Web #7 in Foreground)

Figure G42: Failure Surface (Web #1 in Foreground)

Slab 250-20B - Test Summary

Test Notes

- Bearing length (end of slab to face of pad = 38 mm).
- Underside of slab was very level and even – slight surface spall from forklift adjacent to loading beam.

Failure Mode

- The slab failure initiated at a load of **273.5 kN** with the simultaneous formation of a web-shear crack in web #1 and in web #7, running diagonally adjacent to the loading beam. (This was confirmed with a frame-by-frame review of the video – the crack started near the mid-height of the slab, then widened and travelled diagonally from the slab mid-height to the top and bottom of the slab).
- Immediately after initial cracking, two additional web-shear cracks simultaneously formed above the initial cracks; however these cracks were shallower and formed adjacent to the support. (Figures G43, and G44):

Figure G43: Initial and Secondary Web-Shear Cracks at Web #1

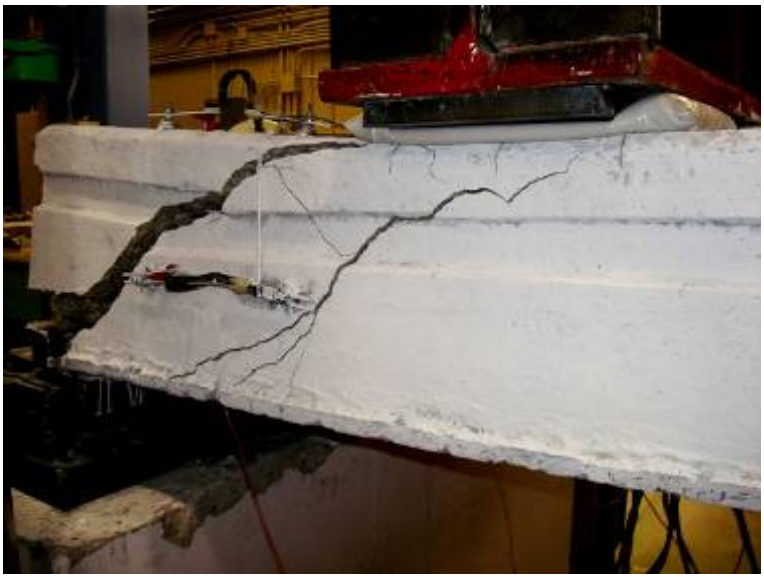

Figure G44: Initial and Secondary Web-Shear Cracks at Web #7

- A rapid shear-tension failure of the entire slab immediately followed the initial cracks (Figures G45 to G47):

Figure G45: Underside of Slab at Web #7

Figure G46: Underside of Slab at Web #1

Figure G47: End View of Slab at Failure

- Photos of the failure surface are shown in Figures G48 to G50. It can be seen in Figures G48 to G50 that the two outside webs (web #1 and web #7) had the secondary shear cracks occur fairly close to the support, while the failure surfaces of the interior webs are all consistently much closer to the loading beam.

Figure G48: Failure Surface – Plan View (Web #1 on Far Right)

Figure G49: Failure Surface – Elevation View (Web #7 in Foreground)

Figure G50: Failure Surface (Web #1 in Foreground)

Slab 300-06A - Test Summary

Test Notes

- Bearing length (end of slab to face of pad = 63 mm).
- Spall at corner of web #5 at bearing.

Failure Mode

- During the first load cycle, a diagonal web-shear crack formed adjacent to the loading beam in web #1, at a load of approximately 113 kN. The web-shear crack then propagated diagonally across the underside of the slab. In addition, some cracks also formed in the flanges between webs #1 and #2 (Figures G51 and G52).

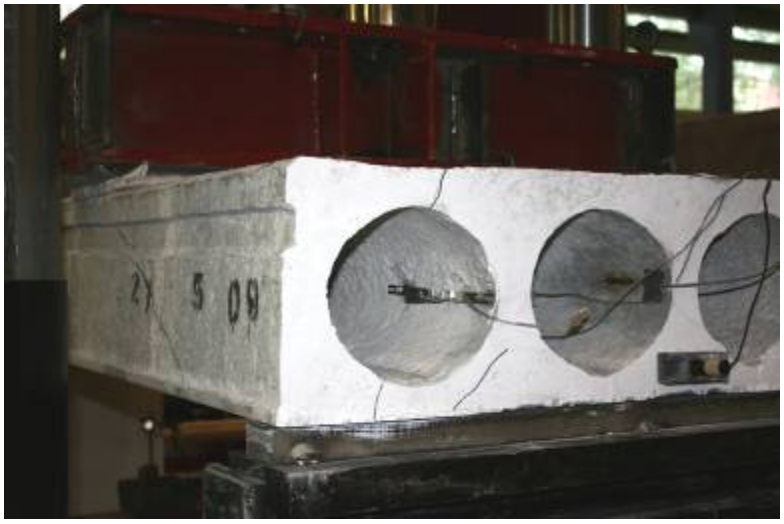

Figure G51: Initial Cracking at Web #1 (113 kN)

Figure G52: Diagonal Crack at Slab Underside (113 kN) – (Web #1 on Far Right)

- In spite of the formation of significant cracks in the slab during the first two load cycles, the slab carried additional load in the last cycle up to a peak failure load of **199.5 kN**. The final slab failure occurred with a web-shear failure across all webs at the peak load, resulting in a shear-tension failure as shown in Figures G53 to G55:

Figure G53: Shear-Tension Failure across Full Slab Width (Web #1 on Far Left)

Figure G54: Shear-Tension Failure across Full Slab Width (Web #1 on Far Left)

Figure G55: Shear-Tension Failure across Full Slab Width (Web #1 on Far Left)

- Photos of the failure surface are shown in Figures G56 to G58:

Figure G56: Failure Surface – Plan View (Web #1 on Far Right)

Figure G57: Failure Surface – Elevation View (Web #1 on Far Left)

Figure G58: Failure Surface (Web #5 in Foreground)

Slab 300-06B - Test Summary

Test Notes

- Bearing length (end of slab to face of pad = 38 mm).
- Spalling at corners of web #1 and #5 at bearing.

Failure Mode

- Prior to the first load cycle, the full weight of the hydraulic bulkhead (approximately 150 kN) was accidentally released onto the slab, leading to extensive cracking the flanges and in the outer webs. (Figures G59 to G62).

Figure G59: Initial Cracking at Web #1

Figure G60: Cracking at Slab Underside – (Web #1 on Far Right)

Figure G61: Initial Cracking at Web #5

Figure G62: Cracking at Slab Underside – (Web #5 on Far Left)

- In spite of the formation of significant cracks in the slab prior to the final load cycle, the slab carried additional load up to a peak failure load of **228.7 kN**. The final slab failure occurred with a web-shear failure across all webs at the peak load, resulting in a shear-tension failure as shown in Figures G63 to G65:

Figure G63: Shear-Tension Failure across Full Slab Width (Web #1 on Far Left)

Figure G64: Shear-Tension Failure (Web #1 in Foreground)

Figure G65: Shear-Tension Failure (Web #5 in Foreground)

- Photos of the failure surface are shown in Figures G66 to G68:

Figure G66: Failure Surface – Elevation View (Web #5 on Far Right)

Figure G67: Failure Surface – End View (Web #5 on Far Right)

Figure G68: Failure Surface (Web #5 on Far Right)

Slab 300-18A - Test Summary

Test Notes

- Bearing length (end of slab to face of pad = 63 mm).

Failure Mode

- No cracks appeared in the slab during the first two load cycles. In the final load cycle, the slab carried a peak load of **213.7 kN**, after which web-shear cracks formed successively in all webs, leading to a shear-tension failure (Figures G69 to G72).

Figure G69: Shear-Tension Failure across Full Slab Width (Web #5 on Far Right)

Figure G70: Shear-Tension Failure across Full Slab Width (Web #1 on Far Left)

Figure G71: Shear-Tension Failure (Web #1 in Foreground)

Figure G72: Shear-Tension Failure (Web #5 in Foreground)

- Photos of the failure surface are shown in Figures G73 to G75:

Figure G73: Failure Surface – Plan View (Web #1 on Far Right)

Figure G74: Failure Surface – Elevation View (Web #5 on Far Right)

Figure G75: Failure Surface – End View (Web #1 on Far Left)

Slab 300-18B - Test Summary

Test Notes

- Bearing length (end of slab to face of pad = 38 mm).
- Small spalling at corners of web #1 and web #5 at bearing, some tearing in web #2.

Failure Mode

- No cracks appeared in the slab during the first two load cycles. In the final load cycle, the slab carried a peak load of **212.6 kN**, after which web-shear cracks formed successively in all webs, leading to a shear-tension failure (Figures G76 to G80).

Figure G76: Shear-Tension Failure across Full Slab Width (Web #5 on Far Right)

Figure G77: Shear-Tension Failure across Full Slab Width (Web #5 on Far Right)

Figure G78: Shear-Tension Failure across Full Slab Width (Web #5 on Far Right)

Figure G79: Shear-Tension Failure (Web #1 in Foreground)

Figure G80: Shear-Tension Failure (Web #5 in Foreground)

- Photos of the failure surface are shown in Figures G81 to G82:

Figure G81: Failure Surface – Elevation View (Web #5 on Far Right)

Figure G82: Failure Surface – Elevation View (Web #1 on Far Left)

APPENDIX H

CRACK PROFILES

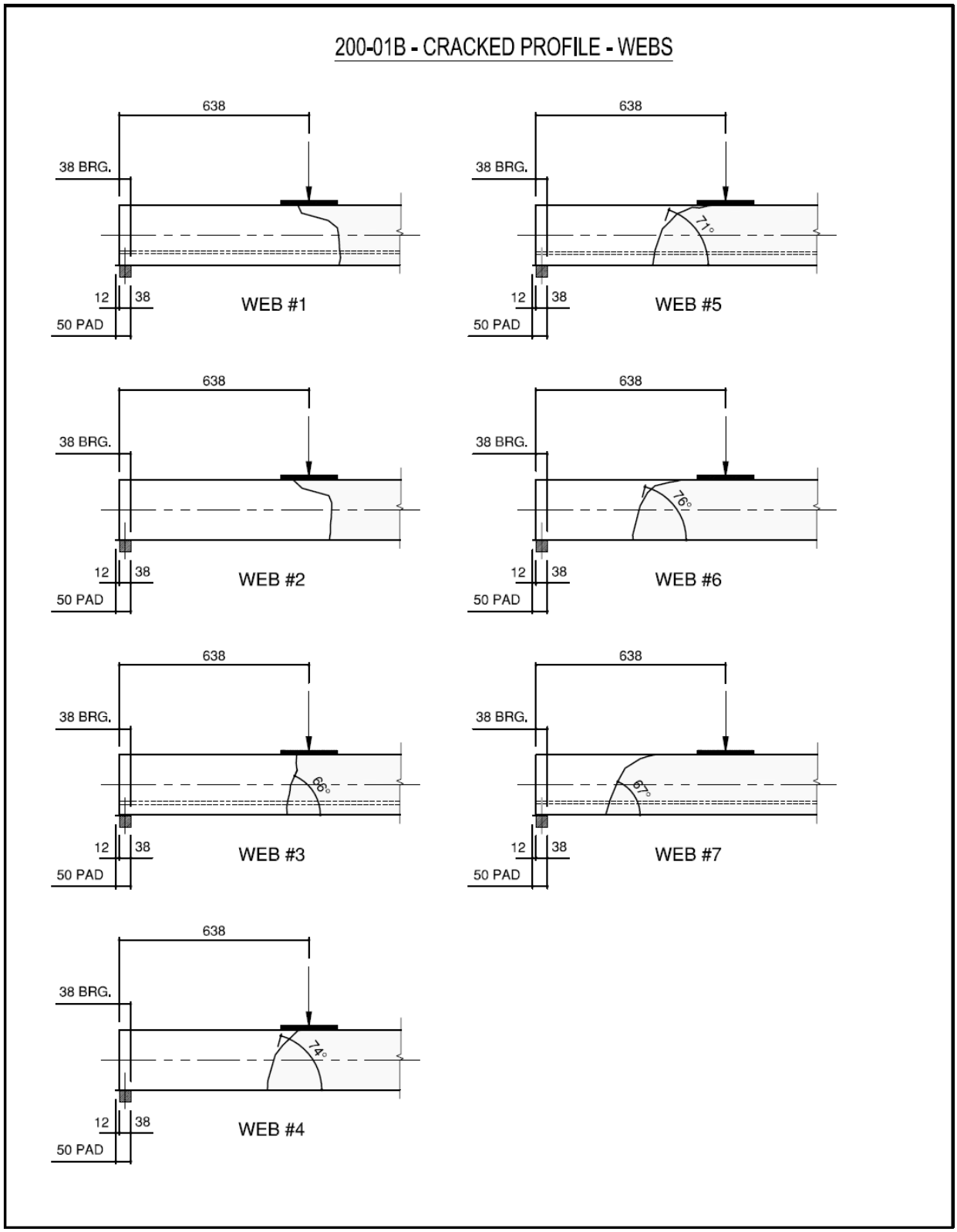

Figure H1: Slab 200-01B Cracked Profile - Webs

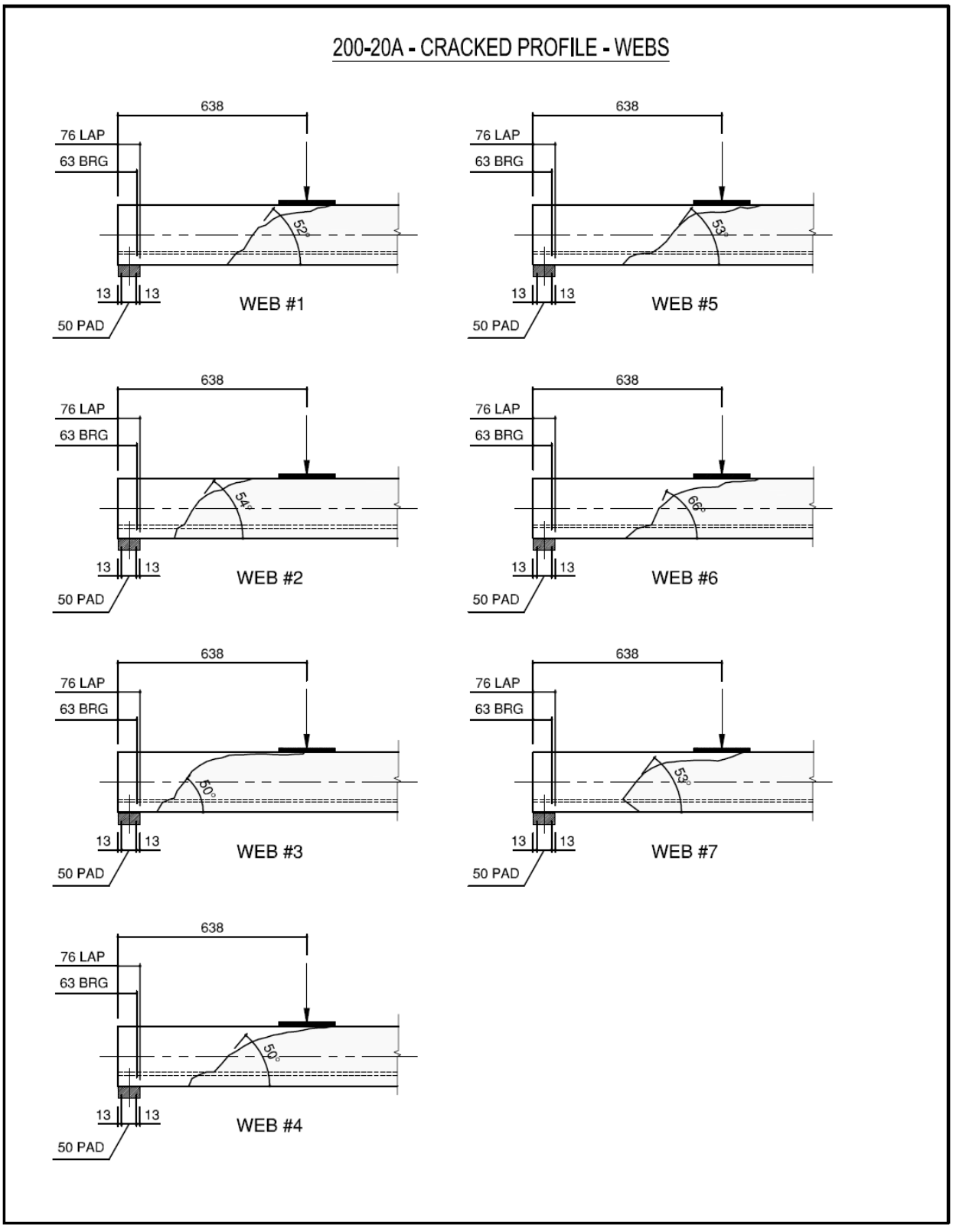

Figure H2: Slab 200-20A Cracked Profile - Webs

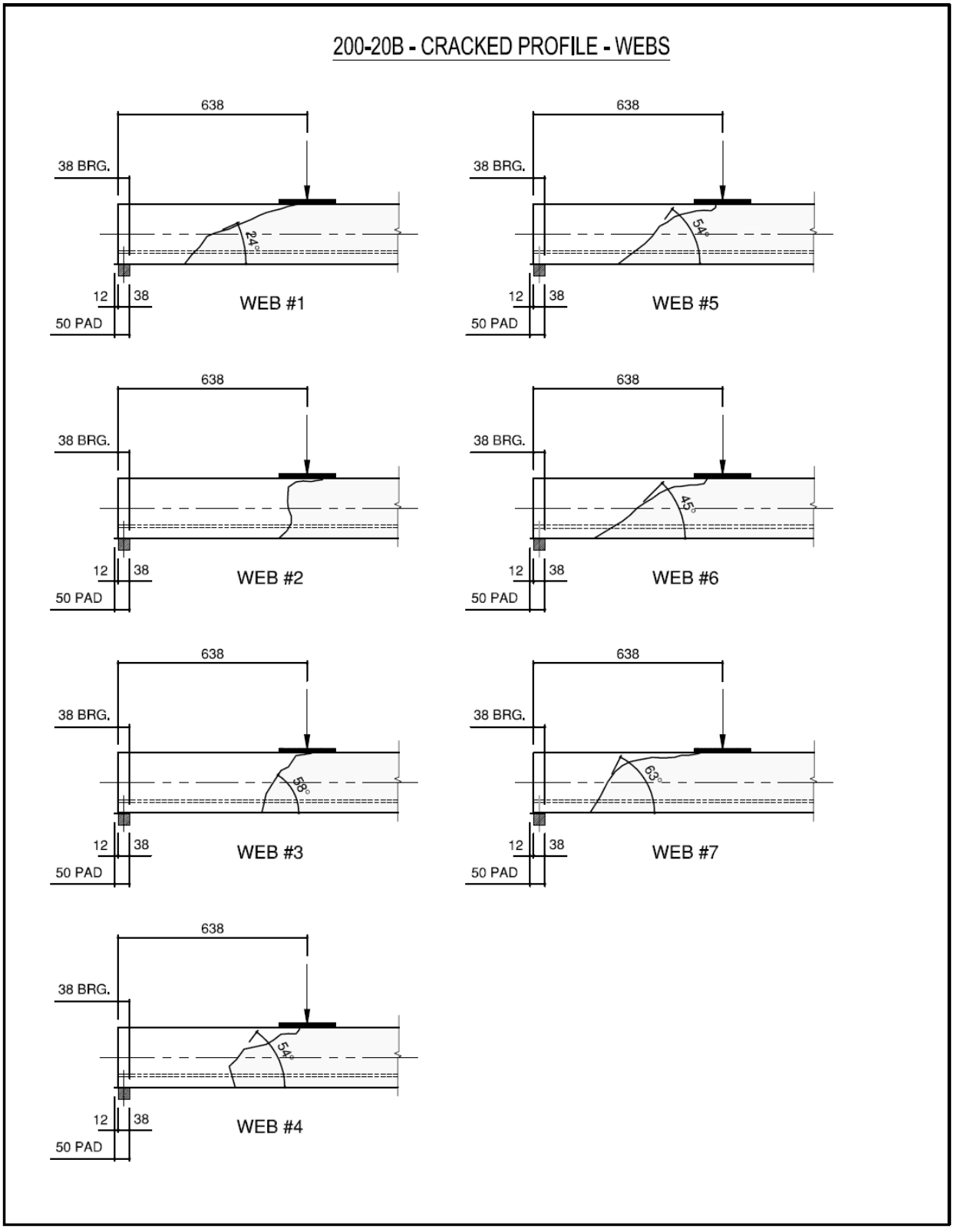

Figure H3: Slab 200-20B Cracked Profile - Webs

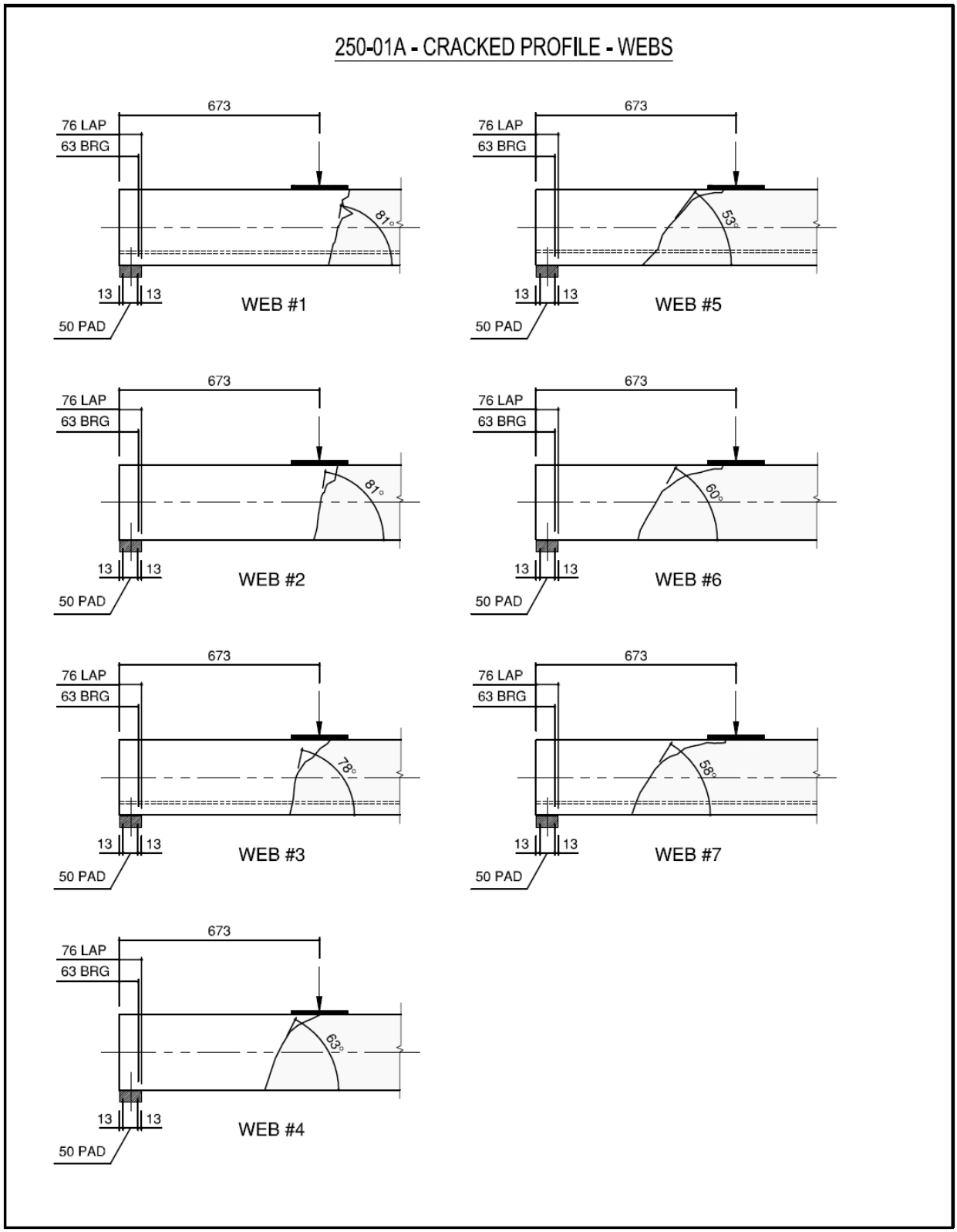

Figure H4: Slab 250-01A Cracked Profile - Webs

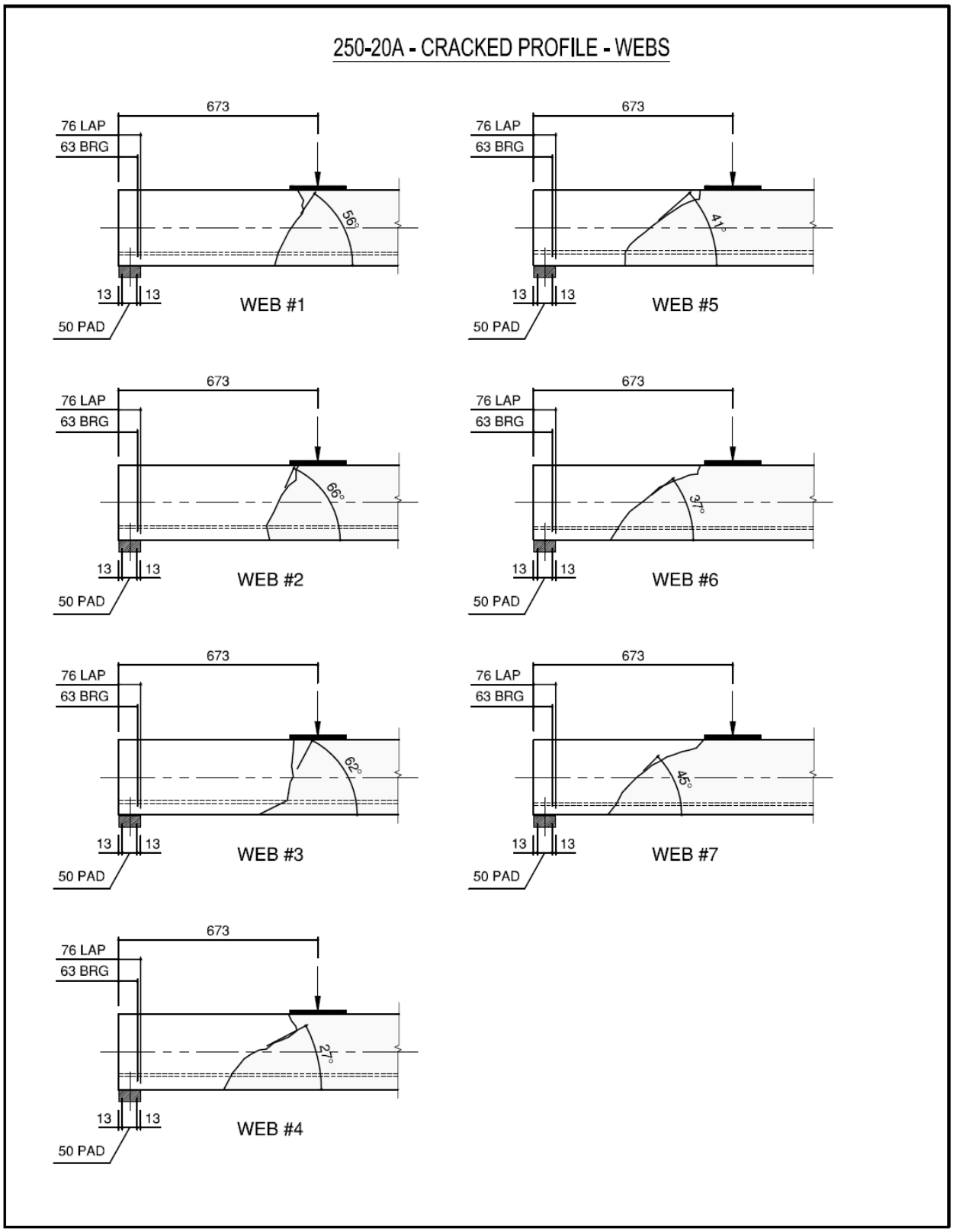

Figure H5: Slab 250-20A Cracked Profile - Webs

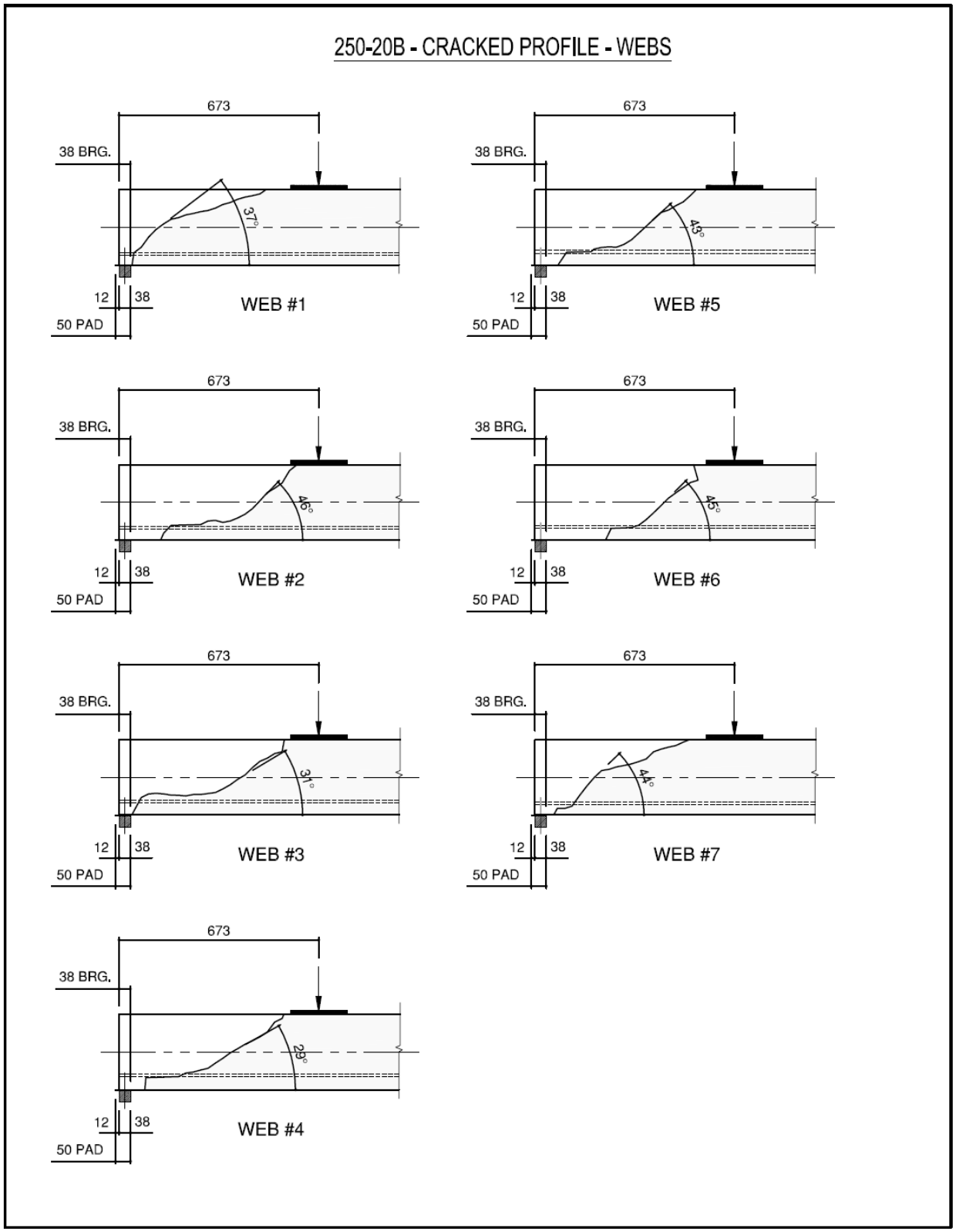

Figure H6: Slab 250-20B Cracked Profile - Webs

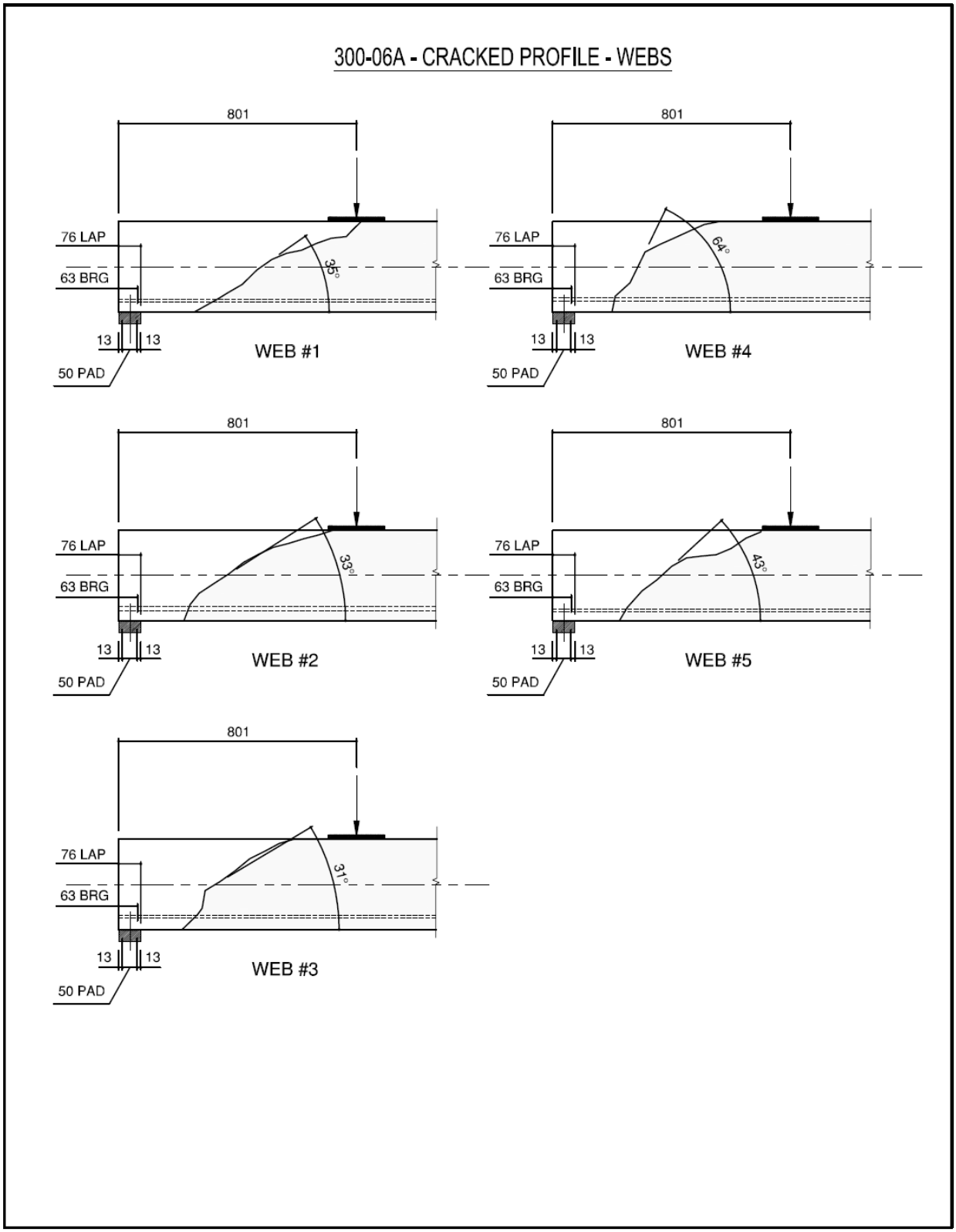

Figure H7: Slab 300-06A Cracked Profile - Webs

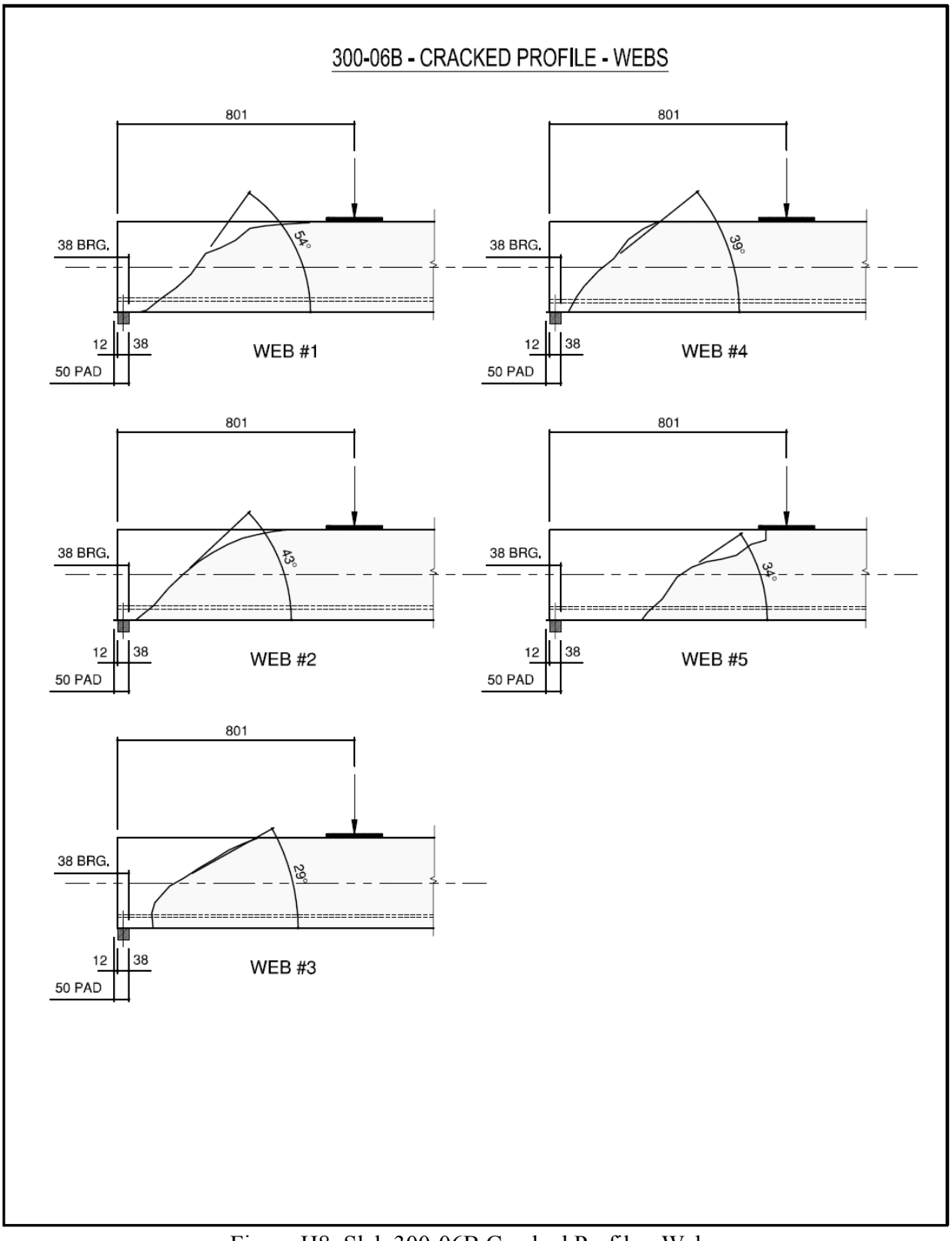

Figure H8: Slab 300-06B Cracked Profile - Webs

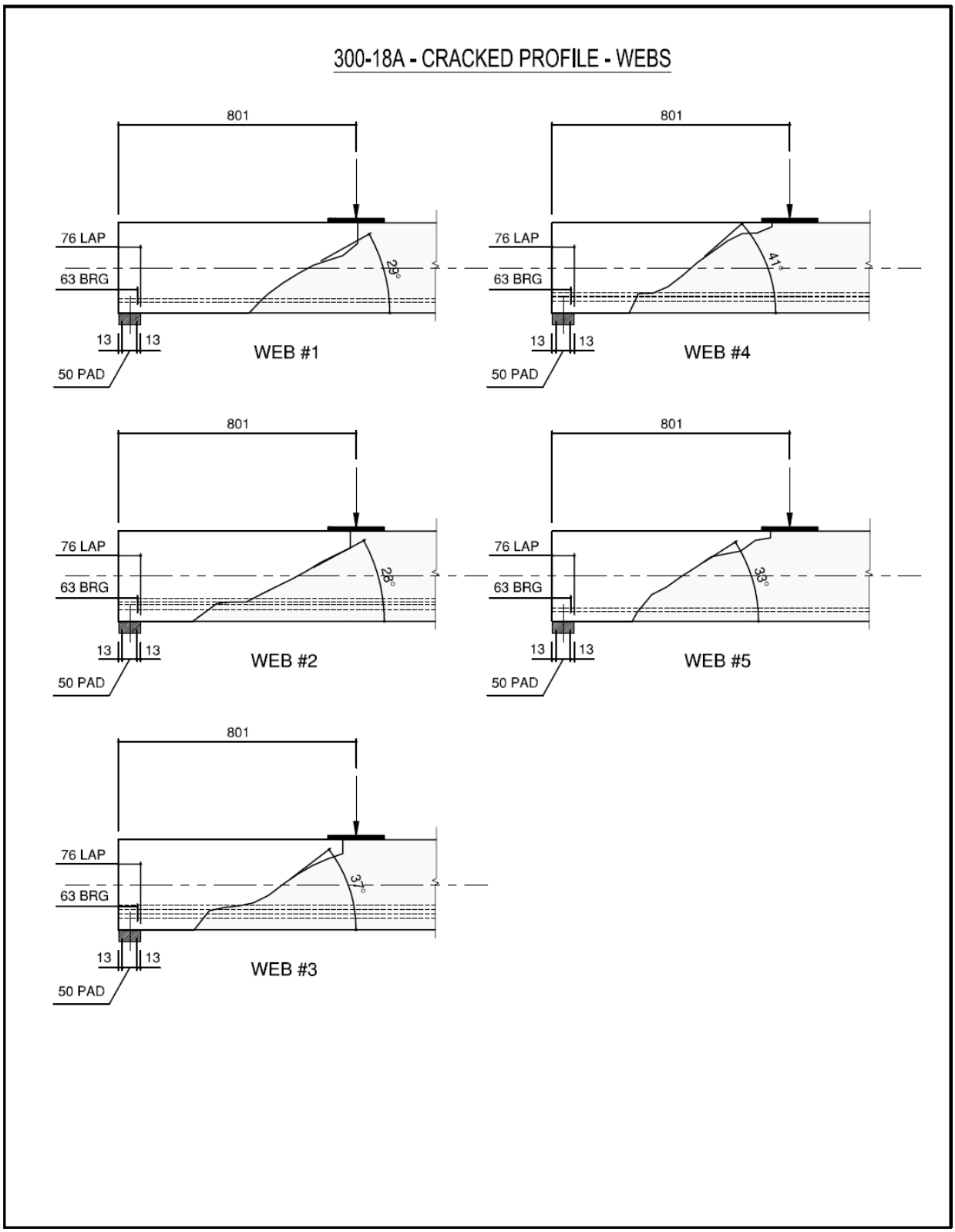

Figure H9: Slab 300-18A Cracked Profile - Webs

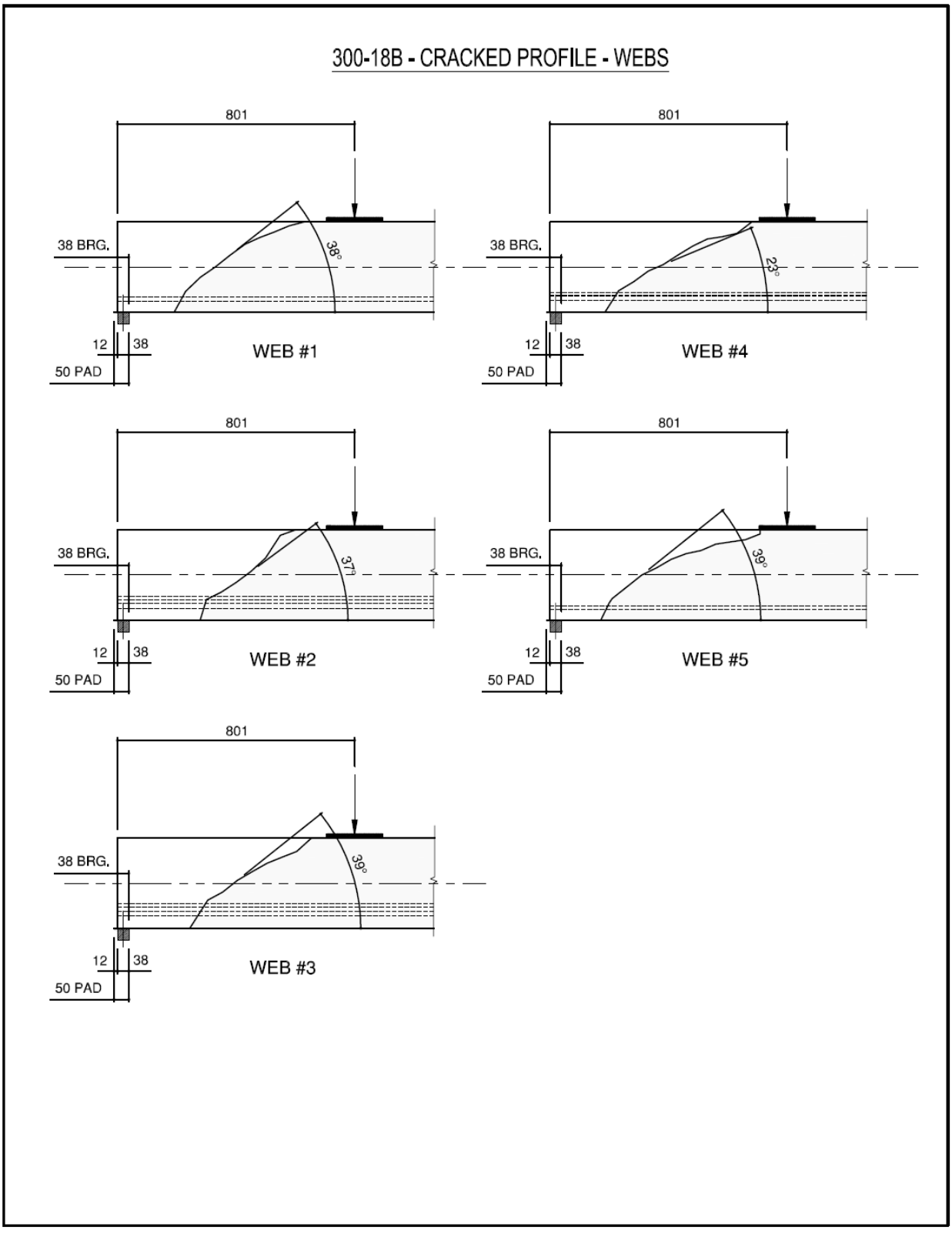

Figure H10: Slab 300-18B Cracked Profile - Webs